Matrix Assisted Laser Desorption/Ionisation Time-of-Flight Mass Spectroscopic Analysis of Synthetic Polymers

Marten Francis Snel

Presented for the degree of PhD

The University of Edinburgh

1999

To Alison

Abstract

Matrix assisted laser desorption/ionisation time-of-flight mass spectrometry was used to mass analyse a range of synthetic polymers. Synthetic polymers with average molecular weights of up to 20000 Da were investigated. The polymers studied included polyglycols, polystyrene and poly(methyl methacrylate). Information on the repeat units, endgroups and average molecular weights was obtained.

A detailed study of novel copolymers was made, in which the end-group masses and the repeat unit masses of the polymers were determined. From this information combined with information of the polymer synthesis it was possible to propose detailed structures for the polymers studied.

An improved sample preparation technique was developed. This technique used an aerosol spray to deposit the matrix and analyte onto the sample holder. The new sample preparation technique made it possible to collect a large number of mass spectra with good reproducibility.

The stability of metal ion/polymer adducts was studied for poly(ethylene glycol) (PEG), poly(propylene glycol) (PPG) and poly(methyl methacrylate) (PMMA) adducts of lithium, sodium, potassium and rubidium, as well as the silver ion adduct of polystyrene. No post source decay (PSD) was seen for the lithium and sodium adducts of PEG, PPG and PMMA, however potassium and rubidium adducts of these polymers did undergo PSD. Rubidium adducts were seen to decay more readily than the potassium adducts.

Pulsed-field delayed ion extraction experiments were carried out. These experiments suggest that gas-phase reactions contribute comparatively little to the cation adduct formation of synthetic polymers. Further experiments showed that the ratio between salt and matrix in the sample did not affect the ionisation behaviour.

During the course of this work several improvements were made to the mass spectrometer used. The length of the time-of-flight mass analyser was increased and an in-line detector was fitted to the existing instrument. The addition of the second detector made it possible to operate the instrument in a linear mode. A mass gate was added to make it possible to avoid detector saturation by low-mass ions.

Acknowledgements

Great thanks go to Robert Donovan whose enthusiastic encouragement and guidance have been a great help to me. I would also like to thank John Monaghan for his support and help over the past four years. The instrumental side of things would have been very much more daunting and less fun without the support of Robert Maier. Ian Mowat has been great for helping me to get started and for the many discussions.

I am also very grateful to Andy Cormack for writing me some extremely useful programs which saved me a great deal of time. I also would like to thank Annette and Mags for their friendly help.

The other 'mass spec' people, Alan, Brian, Angela Alison Michel, Mike and Pat all deserve a big thank you for the many chats (not all mass spec) and the occasional borrowed spanner.

Thanks to Mike, Paul and Sandy and all the rest of the coffee room crowd you all have been and always will be great friends to me.

A special thank you goes to Alison for her loving support throughout this work and beyond. My parents also have my deepest gratitude for all their support over the years.

I would also like to thank Franz Haaf for turning me onto chemistry.

Finally I would like to thank The University of Edinburgh and Procter and Gamble Ltd for financial support.

There are many more people that have been there for me and I am sorry that I haven't been able to name them all in person. Thanks.

Table of contents

List of figures

List of tables

List of abbreviations

2,5-DHB	2,5-dihydroxy benzoic acid
CID	collision induced dissociation
GPC	gel permeation chromatography
HABA	2-(4-hydroxyphenylazo) benzoic acid
IAA	3-β-indole acrylic acid
MALDI	matrix assisted laser desorption/ionisation
M_n	number averaged molecular weight
M_p	most probable molecular weight
MS	mass spectrometry
M_w	weight averaged molecular weight
PEG	poly(ethylene glycol)
PMMA	poly(methyl methacrylate)
PPG	poly(propylene glycol)
PS	polystyrene
PSD	post-source decay
SEC	size exclusion chromatography
THF	tertahydrofuran
TOF	time-of-flight

List of poster presentations

22nd Meeting of the British Mass Spectrometry Society (BMSS), University of Wales Swansea, Swansea, September 1996

Autumn Meeting and Pre-Doctoral Symposium of The Royal Society of Chemistry, University of Aberdeen, Aberdeen September 1997

1998 National Congress and Young Researchers' Meeting of The Royal Society of Chemistry, University of Durham, Durham April 1998

Chapter 1 – Introduction

1.1 Introduction to MALDI mass spectrometry

The last sixteen years have seen a revolution in the mass analysis of high molecular mass species [1]. The effective mass-spectrometric analysis of very large molecules with minimal fragmentation has been made possible by the introduction/development of two soft ionisation techniques namely electrospray ionisation (ESI) [2] and matrix assisted laser desorption/ionisation (MALDI) [3,4]. The work presented in this dissertation focuses on MALDI.

MALDI, as the name suggests, was developed from laser ablation techniques. Unlike conventional laser desorption, the molecules to be analysed are dispersed through a matrix during sample preparation. The matrix is usually solid, consisting of small organic molecules, although various liquid matrix systems have been reported [4,5]. In order to produce molecular ions, with MALDI, only one pulsed laser focused on the sample is required. The most commonly used lasers are the nitrogen laser [6] and frequency tripled [7] and quadrupled [8] Nd:YAG lasers, both emitting ns pulses of UV radiation. However IR MALDI has also been reported [9,10]. Positive and negative analyte species can both be produced by MALDI. In positive ion experiments quasi-molecular analyte ions are the most common analyte species detected. These usually take the form of proton or cation complexes usually

referred to as adducts [11]. Negative ion experiments tend to yield ions formed by the loss of a proton [12].

Since its advent, MALDI has been used to study a number of different types of large molecules, including proteins, peptides [11], oligosaccharides [13], nucleic acids [14] and synthetic polymers [15]. The focus of this work is on the synthetic polymer mass analysis by MALDI. A detailed discussion of polymer MALDI experiments follows in section 1.5.

1.2 Time-of-flight mass analysis

The most commonly used mass analyser in conjunction with MALDI is the time-of-flight (TOF) mass analyser. Some experiments have been reported where other mass analysers such as sector instruments [16] and Fourier-transform ion cyclotron resonance mass spectrometers (FTICR-MS) [17] have been used. Time-of-flight mass analysers have several features that make them ideal for use with MALDI sources. Possibly the most important of these is that, in principle, TOF analysers have no upper mass limit. Another desirable attribute of a TOF analyser is the detection of all ions with every laser shot.

Michael Guilhaus's recently published tutorial on the principles of and instrumentation in time-of-flight mass spectrometry gives a good background to this technique [18]. The basic principle behind TOF mass separation is that ions moving in the same direction with roughly the same kinetic energy will have a distribution of

velocities inversely proportional to the square root of *m/z*. The origin of this relationship can be illustrated using the example of a simple linear time-of-flight mass spectrometer. A schematic diagram of such an instrument is shown in figure 1.1. The ions are generated by a laser pulse hitting the sample mounted in the source. In this example a high voltage is applied to the backplate of the source. For positive ion detection a positive voltage is applied to the backplate and for negative ions a negative voltage is applied to the backplate. The source region is separated from the drift region by grounded ion optics. The drift region is field free. The ions are accelerated out of the source region by the electric field they experience. The amount of energy imparted to the ions is given by the following equation:

$$E_q = zeV \qquad \textbf{1.1}$$

where E_q is the electrical energy, z is the number of charges on the ion, e is the elementary charge and V is the applied voltage. Assuming that all the kinetic energy of the ion stems from the acceleration, the following relationship can be derived:

$$\tfrac{1}{2}mv^2 = zeV \qquad \textbf{1.2}$$

where m is the mass of the ion and v is the ion velocity. This equation can be rearranged to show that:

$$\frac{m}{z} = \frac{2eV}{v^2} \qquad \textbf{1.3}$$

The spread in velocities of a population of ions of different masses can be used for mass analysis by measuring the time taken by an ion to cover a known distance D. In the case of the linear time-of-flight mass spectrometer in figure 1.1, D is the length of the drift region. The ion velocity v can be expressed in terms of the time-of-flight (t_D) and the drifttube length (D) using the following expression:

$$v = \frac{D}{t_D} \qquad \textbf{1.4}$$

Hence m/z can be expressed as a function of t_D:

$$\frac{m}{z} = \frac{2eVt_D^{\,2}}{D^2} \qquad \textbf{1.5}$$

Therefore, in principle, it is possible to calculate m/z from the time of flight of the ion and some instrumental parameters using equation 1.5. In practice t_D can not easily be measured accurately. Instead, the observed time-of-flight t_{obs} is measured, which is given by:

$$t_{obs} = t_D + t_0 + t_a + t_d \qquad \textbf{1.6}$$

where t_0 is the time after the start of recording data when the ions begin to accelerate, t_a is the time taken by the ion to accelerate to v and t_d is the response time of the

detection system. In practice it is therefore easiest to convert time-of-flight information into *m/z* using the following equation:

$$\frac{m}{z} = At_{obs}^{\ 2} + Bt_{obs} + C \qquad \textbf{1.7}$$

where A, B and C are instrument constants that can be determined by calibration of the mass spectrometer with ions of known mass.

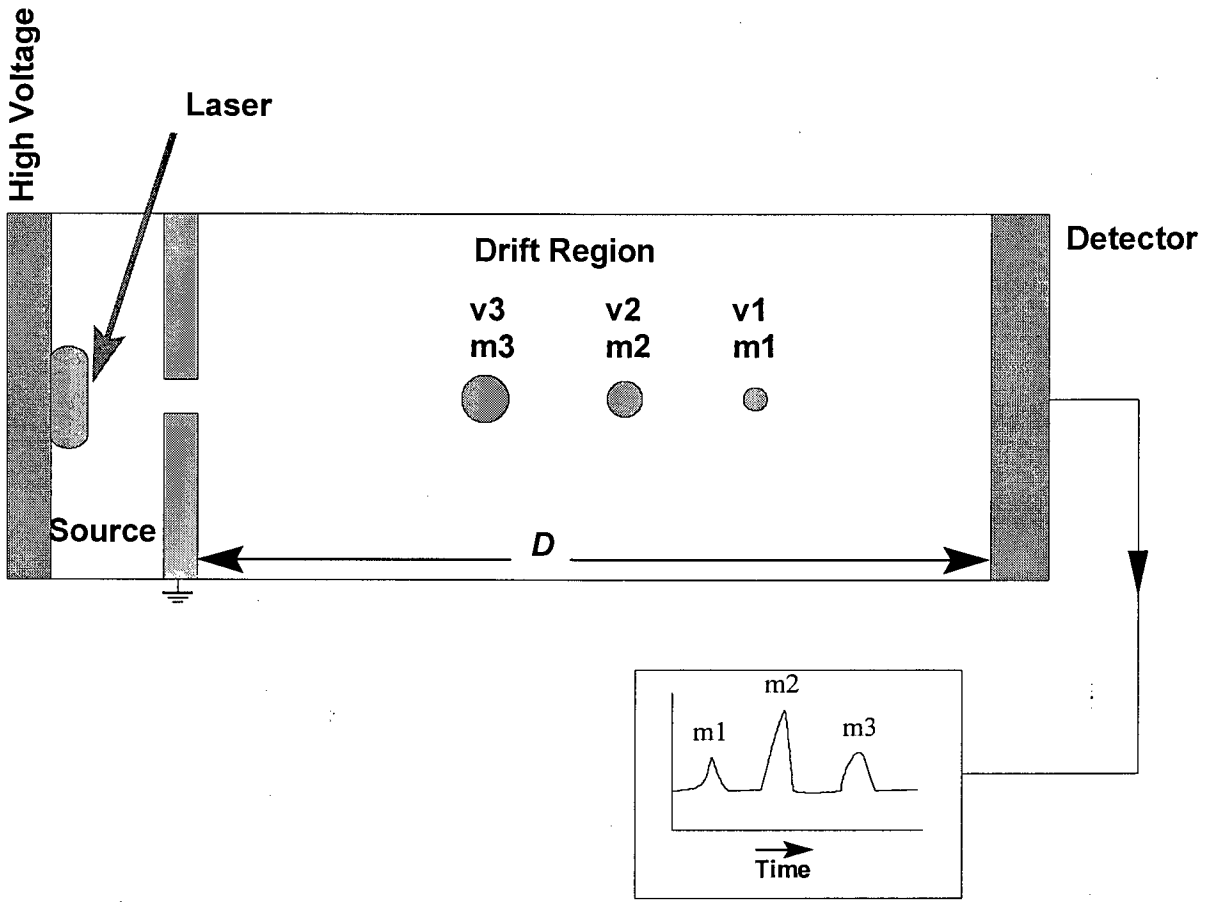

Figure 1.1 Schematic representation of a linear time-of-flight mass spectrometer.

1.2.1 Instrumental strategies for enhancing the resolution of time-of-flight mass analysers

The resolution of linear time-of-flight instruments used with MALDI sources is limited by the kinetic energy spread of ions produced by MALDI [19]. Two techniques are widely used for the correction of the kinetic energy spread. One is the use of an ion mirror, usually referred to as a reflectron and the other technique is delayed extraction or time-lag focusing.

Reflectrons are probably the most widely used method for improving the resolution of time-of-flight mass spectrometers. Reflectrons are essentially ion mirrors which reverse the direction of travel of the ion [20]. A detailed description of the coaxial reflectron used in this work is given in Chapter 2. The small difference in ion velocity between ions of the same mass is compensated for by the reflectron, as ions with higher kinetic energy penetrate more deeply and therefore take longer to be reflected, similarly ions with lower kinetic energy penetrate the reflecting field less deeply and hence are reflected more quickly.

Delayed extraction is based on the idea of time-lag focusing, which was originally proposed by Wiley and McLaren [21]. Delayed extraction has been shown to be an effective method for improving the resolution of MALDI TOF systems.[22,23,24,25] In delayed extraction experiments, there is a time delay between the laser hitting the sample and the acceleration of the ions out of the source region of the mass spectrometer. The ions are allowed to spread out in space before

the acceleration potential is applied. As the ions have reached different positions in the source at the time of acceleration, they will receive differing amounts of kinetic energy from acceleration. With the right delay time, it is largely possible to compensate for the kinetic energy spread of ions and hence bring about an improvement in resolution.

1.3 Ionisation and desorption in MALDI

Although MALDI is a technique that is widely used in commercial laboratories, the MALDI process(es) is/are as yet not completely understood. However, a great deal of work has gone into furthering the understanding of matrix assisted laser desorption and matrix assisted laser ionisation. The next two sections give an overview of this area. For simplicity's sake desorption and ionisation are discussed separately.

1.3.1 Desorption mechanism

Matrix assisted laser desorption (MALD) is believed to be brought about by rapid local heating of the matrix leading to vaporisation of the matrix [26]. As the hot matrix material expands away from the sample surface it takes with it analyte species. Although the matrix is heated rapidly little fragmentation is seen of the analyte molecules. This has been accounted for by modelling studies showing that the matrix to analyte molecule energy transfer is limited [27].

1.3.2 Ionisation mechanism

Cation-molecule complexes are the most commonly detected species in positive ion MALDI. The ion formation mechanisms are still largely unknown. Ions may exist as pre-formed species in the solid state or may be formed by ion-molecule reactions initiated by the laser shot or, most probably, ions are formed by a combination of these two processes [28]. The matrix is believed to play an important part in the ionisation processes in MALDI [29].

Several possible protonation and sodiation mechanisms were proposed by Liao and Allison [30]. The proposed mechanisms are outlined below. In these mechanisms, mH represents the matrix, M the analyte and X a metal (the mechanisms were generalised from the sodium case to encompass all possible metal ion adducts).

$$mH + h\nu \rightarrow mH^{*} \qquad (1.1a)$$

$$mH^{*} + M \underset{(mH^{*})}{\rightarrow} m^{-} + [M + H]^{+} \qquad (1.1b)$$

$$mH^{*} + mH \underset{(mH^{*})}{\rightarrow} m^{-} + [mH + H]^{+} \qquad (1.1c)$$

Mechanism 1.1: excited-state acid-base chemistry

$$mH + nh\nu \rightarrow mH^{+\bullet} + e^{-} \qquad (1.2a)$$

$$mH^{+\bullet} + M \rightarrow m^{\bullet} + [M + H]^{+} \qquad (1.2b)$$

$$mH^{+\bullet} + mH \rightarrow m^{\bullet} + [mH + H]^{+} \qquad (1.2c)$$

Mechanism 1.2: proton transfer following matrix photoionisation

$$mH + nh\nu \rightarrow mH^{+\bullet} + e^- \qquad (1.3a)$$

$$mH^{+\bullet} + mH \rightarrow m^{\bullet} + [mH + H]^+ \qquad (1.3b)$$

$$[mH + H]^+ + M \rightarrow mH + [M + H]^+ \qquad (1.3c)$$

Mechanism 1.3: proton transfer sequence following matrix photoionisation

$$mH + h\nu \rightarrow mH^{*} \qquad (1.4a)$$

$$nmH^{*} + M \rightarrow nmH + M^{+\bullet} + e^- \qquad (1.4b)$$

$$M^{+\bullet} + mH \rightarrow m^{\bullet} + [M + H]^+ \qquad (1.4c)$$

Mechanism 1.4: H-atom transfer following photoionisation

$$mX + h\nu \rightarrow mX^{*} \qquad (1.5a)$$

$$mX^{*} + M \rightarrow [M + X]^+ + m^- \qquad (1.5b)$$

Mechanism 1.5: excited-state 'salt' chemistry

$$mH^{*}, mH^{+} \text{ or } [mH + H]^+ + \{M - H + X\} \rightarrow$$

$$[\{M + X\} + H]^+ + \text{side product(s)} \qquad (1.6)$$

Mechanism 1.6: protonation of the metal salt of the analyte

$$X^+ (g) + M(g) \rightarrow [M + X]^{+\bullet} (g) \qquad (1.7a)$$

$$[M + X]^{+\bullet} \rightarrow [M + X]^+ + h\nu \qquad (1.7b)$$

$$[M + X]^{+\bullet} + Y \rightarrow [M + X]^+ + Y^{*} \qquad (1.7c)$$

Mechanism 1.7: gas-phase capture of X^+ ions by the analyte (Y is a third body)

Evidence of gas phase reactions such as the ones described by mechanism 1.7 has been provided by delayed extraction experiments and by layered sample preparation experiments [31,32,33]. Two delayed extraction studies have been reported, one on small peptides and the other on synthetic polymers. Both experiments showed that the analyte cation adduct signal intensity in MALDI mass spectra increased if the extraction of the ions was delayed in time with respect to the laser shot. Wang *et al.* carried out an experiment, where gas-phase Na ions were introduced separately by laser ablation from a NaI surface perpendicular to the MALDI sample holder. Mass spectra obtained when Na-ions were introduced prior to the MALDI process showed a large increase in the signal intensity of sodium adduct peaks of the analyte, suggesting gas-phase adduct formation. In the layer experiments performed by Hoberg *et al.* a sandwich of two salt layers containing a matrix analyte layer was prepared. The analyte was poly(methyl methacrylate) (PMMA) and the matrix used was 1,8,9-trihydroxyanthracene (dithranol). Two different salts, LiCl and RbCl, were used for the top and the bottom salt layer with both combinations being used. The interesting outcome of this experiment was that only the cation present in the bottom salt layer formed adducts with PMMA. This observation was rationalised as evidence for gas-phase cation adduction. The assumption was made that metal ions move away from the surface more quickly than the larger PMMA molecules and hence the metal ions produced from the top layer have a far smaller chance to interact with the PMMA than the bottom layer ions. The rapid separation of metal ions from PMMA neutrals in the high field gradient in the MALDI source region would mean that ion molecule reaction would have to occur near the surface in the gas plume.

Evidence for an ionisation process analogous to mechanism 1.1 was reported by Knochenmuss *et al.* [34]. This work suggests that the reactions 1.1b and 1.1c only occur when at least two $mH^{\bullet}$ species are present. The evidence for this mechanism is that MALDI mass spectra can be obtained from samples with low matrix concentrations in which no matrix signal is seen, the so called matrix suppression effect. Matrix suppression is thought to occur when the matrix concentration is so low that when two photoexcited matrix molecules are nearest neighbours in the solid they are always in close proximity to an analyte molecule. If reaction 1.1b is strongly favoured over reaction 1.1c, little or no cationised matrix species will be formed as the proton available would be used to form an analyte adduct [34]. It can be seen from mechanism 1.1 that when no positive matrix species are produced negative matrix ions, m^-, should be produced. Knochenmuss and co-workers did observe a strong m^- signal in negative ion mass spectra obtained from samples that showed matrix suppression in the positive ion mode. The same group illustrated the requirement for two photoexcited matrix molecules to bring about successful ionisation by diluting 2,5-dihydroxybenzoic acid (DHB) with CsI. It was noted that at a mole ratio of CsI to DHB higher than 1:2, the DHB signal became very weak which was interpreted as being due to the low likelihood of two photoexcited DHB molecules being nearest neighbours.

In this section a number of ionisation mechanisms have been described. It is not yet possible to say with certainty which mechanism(s) play(s) the most important role in the ionisation mechanism in MALDI.

1.4 Introduction to polymer chemistry

A good introduction to polymer chemistry can be found in most university chemistry textbooks [35,36]. The word polymer is derived from the Greek words 'poly' meaning many and 'meros' meaning part. A polymer is a macromolecule that is made up of a large number of smaller components known as monomers. The term, polymer, covers a wide range of very different compounds. Polymers can be split into two main categories; these are the biopolymers and the synthetic polymers. Biopolymers include proteins, peptides, polysaccharides and nucleic acids. Polythene, polystyrene, silicones and dendrimers are all examples of synthetic polymers. This introduction will focus on synthetic polymers.

The first synthetic polymers to gain commercial importance were the phenol-formaldehydes. They were discovered in the early 1890s by G. T. Morgan. However, it was not until 1910 when Leo Bakeland founded the General Bakelite Company that these compounds were used commercially. Despite the fact that synthetic polymers were being manufactured the concept of macromolecules was only introduced in 1920 by Hermann Staudinger. The macromolecular hypothesis finally became established through the work of Wallace Carothers who set out in 1929 to synthesise polymers of definite structure using conventional organic reactions. His work successfully demonstrated the relationship between structure and properties for a number of polymers. He also invented polymers of great commercial importance such as the nylons.

Synthetic polymers consist of long linear or branched chains of monomers forming one molecule. Simple linear polymers may be written as X-(A)$_n$-Y, where n is an integer, A is the monomer or repeat unit and X and Y are endgroups. All man-made polymeric materials consist of molecules with a range of different values of n; moreover it is very difficult to isolate molecules with one discrete n value. The abundance of molecules with a particular n value in a given polymer follows a statistical distribution, which is affected by the reaction conditions used during the synthesis of the polymer.

There are two distinct polymerisation mechanisms, which are known as chain and step polymerisation, respectively. During chain polymerisation the monomer concentration decreases steadily with time and high molar mass polymers are formed throughout the course of the polymeristaion reaction [35]. The molar mass of the polymers that are formed varies little as the reaction proceeds [35]. Typically chain polymerisation involves the addition reaction of unsaturated monomers. An example is shown in figure 1.2. Chain polymerisation yields only linear and slightly branched polymers.

$$n\ CH_2{=}CH_2 \rightarrow [\text{-}CH_2\text{-}CH_2\text{-}]_n$$

Figure 1.2 The formation of polyethylene, as an example of chain polymerisation.

Step polymerisation can be characterised by the following reaction conditions. The monomer concentration decreases rapidly and the polymer molar mass rises steadily throughout the reaction [35]. In order to obtain polymers with a

high molar mass long reaction times are required. It is possible to produce a range of different polymer morphologies, from linear polymers to highly crosslinked polymers, depending on the number of functional groups on the monomer units. Step growth polymers are often produced using condensation type reactions (see figure 1.3).

$$n\ H_2N(CH_2)_6NH_2 + n\ HOOC(CH_2)_8COOH \rightarrow H_2N[(CH_2)_6NHCO(CH_2)_8CO]_n + (n\text{-}1)\ H_2O$$

Figure 1.3 The reaction to form nylon 6,10, as an example of a typical step polymerisation mechanism.

Polymers with more than one type of monomer are referred to as copolymers. An example of a copolymer is nylon 6,10 (see figure 1.3).

1.5 Polymer mass distributions

The molar mass of a polymer is an important quantity to know as it yields significant information about the physical properties of the polymeric material. As discussed previously, because of the way polymers are synthesised more than one different chain length is generally present in a polymer sample. It is not practically possible, or indeed necessary, in order to produce useful materials, to isolate polymers of one chain length. It is therefore convention to look at average or most probable molecular masses for polymer samples. There are several generally accepted definitions of the average molecular weight of polymers. The most commonly used of these are the number-averaged molecular weight (M_n) and the

weight-averaged molecular weight (M_W) [35]. M_n is given by the following equation:

$$M_n = \frac{\sum N_i M_i}{\sum N_i} \qquad \textbf{1.8}$$

where M_i is the molar mass of the molecular species i and N_i is the number of molecules of i in the sample. The weight-averaged molar mass on the other hand is given by:

$$M_w = \frac{\sum N_i M_i^2}{\sum N_i M_i} \qquad \textbf{1.9}$$

M_n gives greater weighting to the lower molecular mass polymers in a polymer sample, whereas M_W gives greater emphasis to the higher molecular mass part of a polymer sample. The ratio of M_W to M_n is known as the polydispersity and is often used as an indication of the spread of masses within a polymer sample. When polymer samples have a very narrow spread of masses $M_W/M_n \approx 1$ these polymer mass distribution are referred to as monodisperse. Similarly, if $M_W/M_n > 1$, the polymer sample has a wider spread of masses and is said to be polydisperse.

1.6 Polymer mass analysis by MALDI mass spectrometry

Traditional means of determining polymer mass information include size exclusion chromatography (SEC), light scattering and viscometry [35]. These techniques can yield accurate information on the average molecular weight and polydispersity of polymers. They are however limited in that they do not provide structural information on polymers. SEC also requires calibration using well defined molecular weight standards, which means that molecular weights obtained using this technique are relative to the standard [37].

MALDI is one of the most promising techniques for synthetic polymer analysis. MALDI does not only give information on the average molecular weight of polymers but can also provide end-group masses and repeat unit information. A range of suitable matrix compounds for use in synthetic polymer analysis has been identified. The number of different synthetic polymers that can be analysed by MALDI is continuously increasing. Problem areas in the MALDI analysis of polymers, such as the analysis of highly polydisperse polymers and the analysis of hydrocarbon polymers have recently been addressed. Several reviews of synthetic polymer MALDI have been published, which provide a good introduction to this area of research [38,39].

1.6.1 The range of polymers be analysed by MALDI

A wide range of polymers can be analysed using MALDI MS. The capacity of MALDI to yield detailed structural information, such as repeat unit mass and

endgroup mass, has meant that it is becoming an increasingly widely used tool for the mass analysis of low molecular weight polymers in commercial laboratories [40]. The most commonly used synthetic polymers in MALDI experiments are poly(ethylene glycol) (PEG) and poly(propylene glycol) (PPG), polystyrene (PS) and poly (methyl methacrylate) (PMMA). These particular polymers are used as model systems. Samples whose average molar masses and polydispersity are well characterised by means of other techniques are readily available, as these compounds are often used to calibrate gel permeation chromatography systems [41]. They also lend themselves particularly well to MALDI analysis [15]. Some of the studies in which PMMA, PEG, PPG and PS have been used will be discussed in sections 1.6.3 and 1.6.4. A list of other polymers studied by means of MALDI mass spectrometry is given in table 1.1, with a brief description of the reaction conditions used. This table is intended as a quick reference guide for suggested matrix and salt selection for the analysis of the listed or similar polymers (for details on sample preparation see chapter 3).

Polymer	**Matrix and/or salt used**	**Comment**	**Ref.**
α,ω-macrozwitterionic block copolymers of styrene and isoprene	dithranol	Analytical technique	42
2-hydroxyethyl acrylate polymers	*trans*-3-indoleacrylic acid, $NaCF_3CO_2$	Analytical technique	43
4-alkyl substituted phenol-formaldehyde novalac type resins	dithranol, LiBr	Analytical technique	44
aromatic and non-aromatic polyesters	2,5-DHB, *trans*-3-indoleacrylic acid	Analytical technique	45
aromatic polyester dendrimers	2,5-DHB, Na^+, K^+	Analytical technique	46, 47
bisphenol A-epichlorohydrin resisns	2,5-DHB, Na^+	Analytical technique	48
cyclic polyesters	2,5-DHB	Analytical technique	49

cyclic(arylene ether) oligomers	dithranol	Analytical technique	50
dendritic-linear block-copolymers	*trans*-3-indoleacrylic acid, $AgCF_3CO_2$	Analytical technique	51
fatty alcohol ethoxylate	2,5-DHB	HPLC pre-treatment	64
fluorinated phosphazine	various solid matrices		52
high T_g macrocyclic oligomers	dithranol, $AgCF_3CO_2$	Analytical technique	53
ionic and non-ionic surfactants	2,5-DHB, ethylene bis[3-(2-naphthyl) acrylate]	positive and negative spectra, MALDI and LDI	54
macrocyclic aryl ether oligomers	dithranol, LiCl	Analytical technique	55
nylon 6	HABA, Na^+, K^+	Demonstration of calibration technique	62
phenylacetylene hydrocarbon dendrimers	retinoic acid, 1,4-diphenyl-1,3-butadiene, Ag^+	FTICR and TOF MALDI	56
poly(β-hydroxybutyrate-co-β-hydroxyvalerate)	2,5-DHB	Analytical technique	57
poly(1,2-dihydroxybenzene phthalates)	HABA	Analytical technique	58
poly(12-hydroxy stearic acid)	*trans*-3-indoleacrylic acid	Introduction of new matrices	59
poly(acrylic acid)	Sinapinic acid	Demonstration of technique	83
poly(aryl ether) dendrimers	dithranol, $AgCF_3CO_2$	Analytical technique	60
poly(bisphenol A carbonate)	HABA	Analytical technique	63
poly(butyl methacrylate)	*trans*-3-indoleacrylic acid, Na^+	Analytical technique, comparison with GPC and LALLS	61
poly(butyleneadipate)	HABA, Na^+, K^+	Demonstration of calibration technique	62
poly(caprolactone)	HABA	Analytical technique	63
poly(caprolactone)	2,5-DHB, Na^+, K^+	GPC pre-treatment	64
poly(D,L)lactide	2,5-DHB, HABA	Analytical technique	65
poly(decamethyl adipate)	2,5-DHB, Na^+	HPLC pre-treatment	64
poly(dimethylsiloxane)	a range of liquid matrices	Demonstration of the use of liquid matrices	66

poly(dimethylsiloxane)	2,5-DHB	combination of GPC with MALDI	67
poly(ethylene terephthalate)	2,5-DHB, Trishydroxyactephenone, Na^+, K^+	Analytical technique	68
poly(ethylene terephthalate)	2,4,6-trihydroxy acetophenone	Analytical technique	69, 70
poly(methyl methacrylate)/ poly(methyl α-phenylacrylate) copolymer	2,5-DHB, LiCl	Analytical technique	71
poly(N-vinylpyrrolidone/ vinyl acetate)	*trans*-3-indoleacrylic acid	Introduction of new matrices	59
poly(oxyethylene) bis(acetaminophen)	HABA, Na^+	Demonstration of time-lag focusing	72
poly(oxyethylene) bis(ephidrene)	HABA, Na^+	Demonstration of time-lag focusing	72
poly(oxypropylene)/ poly(oxyethylene) block copolymer	2,5–DHB	MALDI FTICR	73
poly(vinyl acetate)	2,5-DHB	Introduction of new matrices	59
poly(vinyl chloride)	*trans*-3-indoleacrylic acid, HABA	Introduction of new matrices	59
poly[(R)-3-hydroxybutanone]	2,5-DHB	Analytical technique	74
polybisphenol A carbonate resin	all-*trans*-retinoic acid, *trans*-3-indoleacrylic acid	SEC/MALDI interface development	75
polybutadiene	dithranol, Ag^+	demonstration of technique	79
polybutadiene	all-*trans*-retinoic acid, Cu(II) nitrate	demonstration of technique	76
polybutadiene	2,5-DHB, $AgNO_3$	demonstration of technique	77
polycarbonate	*trans*-3-indoleacrylic acid, HABA	Introduction of new matrices	59
polycyclic phosphonate resins	dithranol, LiBr	Analytical technique	78
polydimethylsiloxane	dithranol, Ag^+	demonstration of technique	79
polyisoprene	dithranol, Ag^+	demonstration of technique	79
polyisoprene	all-*trans*-retinoic acid, Cu(II) nitrate	demonstration of technique	76
polyisoprene	2,5-DHB, $AgNO_3$	demonstration of technique	77
poly-N,N-diethylacrylamide	2,5-DHB, Na^+, K^+	Analytical technique	80

polyorganometallic ferrocene derivative	Dithranol, quinizarin, HABA, 9-nitroanthracene	Analytical technique	81
polysilabutane	2,5-DHB	Analytical technique	82
polystyrene sulphonic acid	Sinapinic acid	Demonstration of technique	83
polystyrene/ poly(α-methylstyrene) block copolymer	*trans*-3-indoleacrylic acid, silver acetylacetonate	Analytical technique	84
polystyrene-oligothiophene-polystyrene triblock copolymer		Analytical technique	85
polyvinyl pyrrolidone	2,5-DHB	MALDI FTICR	86
triazine based polyamines	2,5-DHB in formic acid	Analytical technique	87
triblock ethyleneoxide/propyleneoxide copolymer	2,5-DHB, Li^+	Critical point LC pre-treatment	64

Table 1.1 List of polymers analysed by MALDI with the matrix and/or salt used

1.6.2 Matrices used in polymer MALDI

As with all MALDI experiments, the choice of an appropriate matrix is an important factor in successful MALDI mass analysis of synthetic polymers. The most commonly used matrices for polymer mass analysis are shown in figure 1.4. In the early polymer MALDI experiments, matrices commonly used for the analysis of biomolecules were employed for polymer mass analysis. Hillenkamp *et al.* used 2,5-dihydroxybenzoic acid to analyse PEG, PPG and PMMA [88] and sinapinic acid was used by Danis and Karr to mass analyse polystyrene sulphonic acid and polyacrylic acid [89]. These matrix compounds worked well for polar polymers; however, non-polar polymers showed poor miscibility with these matrices.

New less polar matrices were introduced which were more suited to the analysis of polymers which are frequently non-polar. A matrix that is extensively used for polymer analysis is 2-(-4 hydroxyphenylazo) benzoic acid (HABA) [90,91]. It was first introduced by Costello and co-workers, who used it to analyse peptides and PEG [92]. Costello *et al.* also introduced dithranol, another important matrix for polymer analysis by MALDI [91]. *Trans*-3-indoleacrylic acid was introduced as a matrix by Danis and Karr [93].

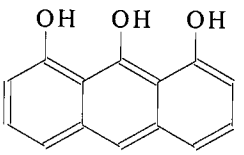

1,8,9-anthracenetriol (dithranol)

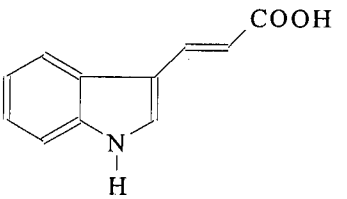

***trans*-3-indoleacrylic acid (IAA)**

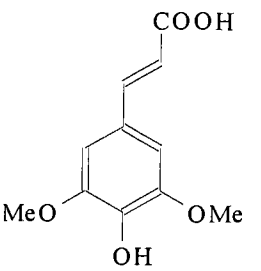

3,5-dimethoxy-4-hydrocinnamic acid (sinapinic acid)

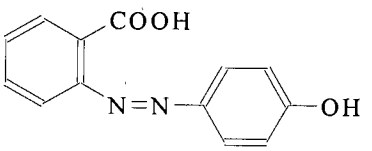

2-(4-hydroxyphenylazo) benzoic acid (HABA)

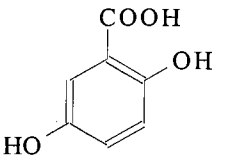

2,5-dihydroxybenzoic acid (DHB)

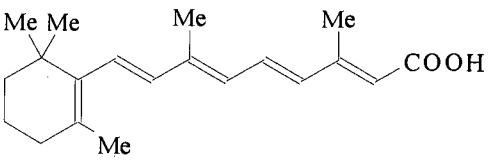

***all-trans*-retinoic acid**

Figure 1.4 Typical matrix compounds employed in polymer mass analysis by MALDI

1.6.3 MALDI mass analysis of polydisperse polymers

It has been noted that there can be discrepancies between average molecular mass values obtained by MALDI and those obtained by other techniques [94]. There is generally good agreement between MALDI and other techniques in the mass analysis of monodisperse polymer samples [95]; however, mass discrimination has been observed in the mass analysis of polydisperse polymer by MALDI in comparison with other techniques. Several studies of the mass discrimination phenomenon have been reported [94,96,97,98,99]. Perhaps the most complete and extensive of these is the work published by Schriemer and Li [100,101]. Their work examined sample preparation and desorption/ionisation [100] issues as well as instrumental issues [101]. Some of the most significant factors in the analysis of polydisperse polymer samples by MALDI appear to be the lack of high-mass sensitivity of most commonly used detector systems [100] and more efficient desorption of lower-mass polymers. Longer chain length polymers are more likely to dimerise which leads to loss of signal intensity of the monomer [101].

1.6.3.1 Solutions to the polydisperse polymer analysis problem

The most commonly used method for overcoming the problems of polydisperse MALDI analysis is chromatographic pre-treatment of the polymer sample [102]. The separation technique of choice is usually size exclusion chromatography (SEC), also called gel permeation chromatography (GPC). In experiments of this type eluent samples are taken at various elution times and MALDI mass analysed [103,104,105]. These eluent samples consist of a virtually

monodisperse polymer distribution. In this way MALDI can be used as an absolute mass detector for GPC. More traditional GPC detection systems need to be calibrated with model polymer compounds and can therefore only give relative molecular weight information. Furthermore, MALDI mass spectrometry can also yield repeat-unit and endgroup mass information. The combination of MALDI with GPC therefore is a powerful analytical tool which overcomes some of the main weaknesses of the two constituent techniques, *i.e.* MALDI's difficulty in coping with polydisperse samples and GPC's reliance on model compounds for calibration. Current developments are focusing on automating the interface between the two techniques [75,106,107].

1.6.4 Other polymer MALDI studies

A noteworthy demonstration of the high-mass analysis capacity of MALDI was recently given by Schriemer and Li, when they mass analysed monodisperse polystyrene samples of up to 1.5 MDa using MALDI time-of-flight mass spectrometry [108]. The same group also used polystyrene mass analysis to demonstrate the mass resolving power of a time-lag focusing mass spectrometer, with polystyrene oligomers being resolved at masses over 50 kDa [72].

An area of polymer mass analysis that has generated considerable interest is the attachment of metal ions to polymers to form adducts [109,110,111]. Metal ion attachment issues will be discussed in some detail in chapters 5 and 6.

1.7 References

[1] F. Hillenkamp, *Int. J. Mass Spectrom. Ion Proc.*, **169**, R9-R11 (1997)
[2] M. Yamashita and J. B. Fenn, *J. Phys. Chem.*, **88**, 4451-4459 (1984)
[3] F. Hillenkamp and M. Karas, *Anal. Chem.*, **60**, 2299-2301 (1988)
[4] K. Tanaka, H. Waki, Y. Ido, S. Akita, Y. Yoshida and T. Yoshida, *Rapid Commun. Mass Spectrom.*, **2**, 151-153 (1988)
[5] J. B. Williams, A. I. Gusev and D. M. Hercules, *Macromolecules*, **29**, 8144-8150 (1996)
[6] M. R. Chevrier and R. J. Cotter, *Rapid Commun. Mass Spectrom.*, **5**, 611-617 (1991)
[7] R. C. Beavis and B. T. Chait, *Rapid Commun. Mass Spectrom.*, **3**, 436-439 (1989)
[8] R. C. Beavis and B. T. Chait, *Rapid Commun. Mass Spectrom.*, **3**, 233-237 (1989)
[9] S. Berkenkamp, C. Menzel, M. Karas and F. Hillenkamp, *Rapid Commun. Mass Spectrom.*, **11**, 1399-1406 (1997)
[10] M. Sadeghi, Z. Olumee, X. D. Tang, A. Vertes, Z. X. Jiang, A. J. Henderson, H. S. Lee and C. R. Prasad, *Rapid Commun. Mass Spectrom.*, **11**, 393-397 (1997)
[11] R. C. Beavis and B. T. Chait, *Anal. Chem.*, **62**, 1836-1840 (1990)
[12] R. Knochenmuss, V. Karbach, U. Wiesli, K. Breuker and R. Zenobi, *Rapid Commun. Mass Spectrom.*, **12**, 529-534 (1998)
[13] B. Stahl, M. Steup, M. Karas and F. Hillenkamp, *Anal. Chem.*, **63**, 1463-1466 (1991)
[14] B. Spengler, Y. Pan and R. J. Cotter, *Rapid Commun. Mass Spectrom.*, **4**, 99-102 (1990)
[15] U. Bahr, A. Deppe, M. Karas and F. Hillenkamp, *Anal. Chem.*, **64**, 2866-2869 (1992)
[16] V. S. K. Kolli and R. Orlando, *Rapid Commun. Mass Spectrom.*, **10**, 923-926 (1997)
[17] C. G. de Koster, M. C. Duursma, G. J. v. Rooij, R. M. A. Heeren and J. J. Boon, *Rapid Commun. Mass Spectrom.*, **9**, 957-962 (1995)
[18] M. Guilhaus, *J. Mass Spectrom.*, **30**, 1519-1532 (1995)
[19] A. Ingendoh, M. Karas, F. Hillenkamp and U. Giessmann, *Int. J. Mass Spectrom. Ion Proc.*, **131**, 345-354 (1994)
[20] B. A. Mamyrin, *Int. J. Mass Spectrom. Ion Proc.*, **131**, 1-19 (1994)
[21] W. C. Wiley and I. H. McLaren, *Rev. Sci. Instrum.*, **67**, 1150-1157 (1955)
[22] M. L. Vestal, P. Juhasz and S. A. Martin, *Rapid Commun. Mass Spectrom.*, **9**, 1044-1050 (1995)
[23] R. M. Whittal and L. Li, *Anal. Chem.*, **67**, 1950-1954 (1995)
[24] S. M. Colby, T. B. King and J. P. Reilly, *Rapid Commun. Mass Spectrom.*, **8**, 865-868 (1994)

[25] R. S. Brown and J. J. Lennon, *Anal. Chem.*, **67**, 1998-2003 (1995)
[26] A. Bencsura and A. Vertes, *Chem. Phys. Lett.*, **247**, 142-148 (1995)
[27] A. Bencsura, V. Navali, M. Sadeghi and A. Vertes, *Rapid Commun. Mass Spectrom.*, **11**, 679-682 (1997)
[28] E. Lehmann, R. Knochenmuss and R. Zenobi, *Rapid Commun. Mass Spectrom.*, **11**, 1483-1492 (1997)
[29] H. Ehring, M. Karas and F. Hillenkamp, *Org. Mass Spectrom.*, **27**, 472-480 (1992)
[30] P. -C. Liao and J. Allison, *J. Mass Spectrom.*, **30**, 408-423 (1995)
[31] I. A. Mowat, R. J. Donovan and R. R. Maier, *Rapid Commun. Mass Spectrom.*, **11**, 89-90 (1997)
[32] B. H. Wang, K. Dreisewerd, U. Bahr, M. Karas and F. Hillenkamp, *J. Am. Soc. Mass Spectrom.*, **4**, 393-398 (1993)
[33] A. -M. Hoberg, D. Haddleton and P.J. Derrick, *Eur. Mass Spectrom.*, **3**, 471-473 (1997)
[34] R Knochenmuss, F. Dubois, M. J. Dale and R. Zenobi, *Rapid Commun. Mass Spectrom.*, **10**, 871-877 (1996)
[35] J. W. Nicholson, *The Chemistry of Polymers*, The Royal Society of Chemistry, Cambridge, UK (1991)
[36] R. T. Morrison and R. N. Boyd, *Organic Chemistry*, 5th Ed., Allyn and Bacon Inc., Massachusetts, USA (1987)
[37] Transcript of product presentation by Viscotek (Unit 2, Lennox Mall, Lister Road, Basingstoke, Hampshire, RG22 4DF UK), April 1998
[38] K. J. Wu and R. W. Odom, *Anal. Chem.*, **70**, 456 A-461 A (1998)
[39] C. A. Jackson and W.J. Simonsick, *Current Opinion in Solid State and Materials Science*, **2**, 661-667 (1997)
[40] B. Thomson, K. Suddaby, A. Rudin and G. Lajoie, *Eur. Polym. J.*, **32**, 239-256 (1996)
[41] Polymer Laboratories Ltd, Church Stretton, Shropshire, UK.
[42] V. Schädler, J. Spickermann, H. J. Räder and U. Wiesner, *Macromolecules*, **29**, 4865-4870 (1996)
[43] S. Coca, C. B. Jasieczek, K. L. Beers and K. Matyjaszewski, *J. Polym. Sci. Part A*, **36**, 1417-1424 (1998)
[44] H. Mandal and A. S. Hay, *Polymer*, **38**, 6267-6271 (1997)
[45] J. C. Blais, M. Tessier, G. Bolbach, B. Remaud, L. Rozes, J. Guittard, A. Brunot, E. Maréchal and J. C. Tabet, *Int. J. Mass Spectrom. Ion Proc.*, **144**, 131-138 (1995)
[46] H. S. Sahota, P. M. Lloyd, S. G. Yeates, P. J. Derrick, P. C. Taylor and D. M. Haddleton, *J. Chem. Soc., Chem. Commun.*, 2445-2446 (1994)
[47] P. J. Derrick, D. M. Haddleton, P. Lloyd, H. Sahota, P. C. Taylor and S. G. Yeates, *Abs. Papers. Am. Chem. Soc.*, **208**, No. Pt2, 271-Poly (1994)
[48] H. Pasch, R. Unvericht and M. Resch, *Angew. Makromol. Chem.*, **212**, 191-200 (1993)
[49] S. C. Hamilton, J. A. Semlyen and D. M. Haddleton, *Polymer*, **39**, 3241-3252 (1998)

[50] Y. Ding and A. S. Hay, *J. Polym. Sci. Part A*, **36**, 5019-5026 (1998)
[51] M. R. Leduc, W. Hayes and J. M. J. Frechet, *J. Polym. Sci. Part A*, **36,** 1-10 (1998)
[52] L. Latourte, J. C. Blais and J. C. Tabet, *Anal. Chem.*, **69**, 2742-2750 (1997)
[53] Y. F. Wang, M. Paveni, K. P. Chan, A. S. Hay, *J. Polym. Sci., Part A*, **34** 2135-2138 (1997)
[54] B. Thomson, Z. Wang, A. Paine, A. Rudin and G. Lajoie, *J. Am. Oil Chem. Soc.*, **72**(1), 11-15 (1995)
[55] Y. F. Wang, M. Paventi and A. S. Hay, *Polymer*, **38**, 469-482 (1997)
[56] K. L. Walker, M. S. Kahr, C. L. Wilkins, Z. Xu and J. S. Moore, *J. Am. Soc. Mass Spectrom.*, **5**, 731-739 (1994)
[57] R. Abate, A. Ballistreri, G. Montaudo, D. Garozzo, G. Impallomeni, G. Critchley and K. Tanaka, *Rapid Commun. Mass Spectrom.*, **7**, 1033-1036 (1993)
[58] E. Scamporrino, D. Vitalini and P. Mineo, *Macromolecules*, **29**, 5520-5528 (1996)
[59] P. O. Danis and D. E. Karr, *Org. Mass Spectrom.*, **28**, 923-925 (1993)
[60] C. A. Martinez and A. S. Hay, *J. Polym. Sci. Part A*, **35,** 1781-1798 (1997)
[61] P. O. Danis, D. E. Karr, W. J. Simonsick Jr. and D. T. Wu, *Macromolecules,* **28**, 1229-1228 (1995)
[62] G. Montaudo, M. S. Montaudo, C. Puglisi and F. Samperi, *Rapid Commun. Mass Spectrom.*, **8,** 981-984 (1994)
[63] G. Montaudo, M. S. Montaudo, C. Puglisi and F. Samperi, *Anal. Chem.*, **66**, 4366-4369 (1994)
[64] H. Pasch and K. Rode, *J. Chrom. A*, **699**, 21-29 (1995)
[65] G. Montaudo, M. S. Montaudo, C. Puglisi, F. Samperi, N. Spassky, A. LeBorgne and M. Wisniewski, *Macromolecules,* **29**, 6461-6465 (1996)
[66] J. B. Williams, A. I. Gusev and D. M. Hercules, *Macromolecules*, **29**, 8144-8150 (1996)
[67] G. Montaudo, M. S. Montaudo, C. Puglisi and F. Samperi, *Rapid Commun. Mass Spectrom.,* **9**, 1158-1163 (1995)
[68] St. Weidner, G. Kühn and U. Just, *Rapid Commun. Mass Spectrom.*, **9**, 697-702 (1995)
[69] S. Weidner, G. Kuehn, R. Decker, D. Roessner and J. Friedrich, *J. Polym. Sci. Part A*, **36,** 1639-1648 (1998)
[70] S. Weidner, G. Kuehn, B. Werthmann, H. Schroeder, U. Just, R. Borowski, R. Decker, B. Schwarz, I. Schmuecking and I. Seifert, *J. Polym. Sci. Part A*, **35** 2183-2192 (1997)
[71] W. Mormann, J. Walter, H. Pasch and K. Rode, *Macromolecules*, **31**, 249-255 (1998)
[72] R. M. Whittal, D. C. Schriemer and L. Li, *Anal. Chem.*, **69**, 2734-2741 (1997)
[73] G. J. van Rooij, M. C. Duursma, C. G. de Koster, R. M. A. Heeren, J. J. Boon, P. J. W. Schuyl and E. R. E. van der Hage, *Anal. Chem.*, **70**, 843-850 (1998)
[74] H. M. Bürger, H.-M. Müller, D. Seebach, K. O. Börnsen, M. Schär and H. M. Widmer, *Macromolecules*, **26**, 4783-4790 (1993)

[75] M. W. F. Nielen, *Anal. Chem.*, **70**, 1563-1568, (1998)
[76] T. Yalcin, D. C. Schriemer and L. Li, *J. Am. Soc. Mass Spectrom.*, **8**, 1220-1229 (1997)
[77] S. J. Pastor and C. L. Wilkins, *J. Am. Soc. Mass Spectrom.*, **8**, 225-233 (1997)
[78] H. Mandal and A. S. Hay, *J. Polym. Sci. Part A*, **36,** 1911-1918 (1998)
[79] A. M. Belu, J. M. Desimone, R. W. Linton, G. W. Lange and R. M. Friedman, *J. Am. Soc. Mass Spectrom.*, **7**, 11-24 (1996)
[80] M. Eggert and R. Freitag, *J. Polym. Sci. A, Polym. Chem.*, **32**, 803-813 (1994)
[81] P. Juhasz and C. E. Costello, *Rapid Commun. Mass Spectrom.*, **7,** 343-351 (1993)
[82] K. Matsumoto, H. Shimazu, H. Yamaoka, *J. Polym. Sci. Part A*, **36,** 225-231 (1998)
[83] P. O. Danis, D. E. Karr, F. Mayer, A. Holle and C. H. Watson, *Org. Mass Spectrom.*, **27**, 843-845 (27)
[84] G. Wilczek-Vera, P. O. Danis and A. Eisenberg, *Macromolecules*, **29**, 4036-4044 (1996)
[85] M. A. Hempenius, B. M. W. Langeveld-Voss, J. A. E. H. van Haare, R. A. J. Janssen, S. S. Sheiko, J. P. Spatz, M. Moller and E. W. Meijer, *J. Am. Chem. Soc.*, **120**, 2798-2804 (1998)
[86] G. J. van Rooij, M. C. Duursma, R. M. A. Heeren, J. J. Boon and C. G. de Koster, *J. Am. Soc. Mass Spectrom.*, **7**, 449-457 (1996)
[87] D. Braun, R. Grahary and H. Pasch, *Polymer*, **37**, 777-783 (1996)
[88] U. Bahr, A. Deppe, M. Karas and F. Hillenkamp, *Anal. Chem.*, **64**, 2866-2869 (1992)
[89] P. O. Danis, D. E. Karr, F. Mayer, A. Holle and C. H. Watson, *Org. Mass Spectrom.*, **27**, 843-845 (1992)
[90] G. Montaudo, M. S. Montaudo, C. Puglisi and F. Samperi, *Rapid Commun. Mass Spectrom.*, **8,** 1011-1015 (1994)
[91] P. Juhasz and C. E. Costello, *Rapid Commun. Mass Spectrom.*, **7**, 343-351 (1993)
[92] P. Juhasz, C. E. Costello and K. Biemann, *J. Am. Soc. Mass Spectrom.*, **4,** 399-409 (1993)
[93] P. O. Danis and D. E. Karr, *Org. Mass Spectrom.*, **28**, 923-925 (1993)
[94] K. Martin, J. Spickermann, H. J. Rader and K. Mullen, *Rapid Commun. Mass Spectrom.*, **10**, 1471-1474 (1996)
[95] P. M. Lloyd, K. G. Suddaby, J. E. Varney, E. Scrivener, P. J. Derrick and D. M. Haddleton, *Eur. Mass Spectrom.*, **1**, 293-300 (1995)
[96] J. Axelsson, E. Scrivener, D. M. Haddleton and P. J. Derrick, *Macromolecules*, **29**, 8875-8882 (1996)
[97] R. S. Lehrle and D. S. Sarson, *Rapid Commun. Mass Spectrom.*, **9**, 91-92 (1995)
[98] B. C. Guo, H. Chen, H. Rashidzadeh and X. Liu, *Rapid Commun. Mass Spectrom.*, **11**, 781-785 (1997)
[99] H. Rashidzadeh and B. C. Guo, *Anal. Chem.*, **70**, 131-135 (1998)
[100] D. C. Schriemer and L. Li, *Anal. Chem.*, **69**, 4169-4175 (1997)

[101] D. C. Schriemer and L. Li, *Anal. Chem.*, **69**, 4176-4183 (1997)
[102] K. K. Murray, *Mass Spectrom. Reviews*, **16**, 283-299 (1997)
[103] M. S. Montaudo, C. Puglisi, F. Samperi and G. Montaudo, *Macromolecules*, **31** 3839-3845 (1998)
[104] M. W. Nielen and S. Malusha, *Rapid Commun. Mass Spectrom.*, **11**, 1194-1204 (1997)
[105] M. S. Montaudo, C. Puglisi, F. Samperi, G. Montaudo, *Rapid Commun. Mass Spectrom.*, **12**, 519-528 (1998)
[106] C. E. Kassis, J. M. DeSimone, R. W. Linton, E. E. Remsen, G. W. Lange and R. M. Friedmann, *Rapid Commun. Mass Spectrom.*, **11**, 1134-1138 (1997)
[107] X. Fei and K. K. Murray, *Anal. Chem.*, **68**, 3555-3560 (1996)
[108] D. C. Schriemer and L. Li, *Anal. Chem.*, **68**, 2721-2725 (1996)
[109] I. A. Mowat and R. J. Donovan, *Rapid Commun. Mass Spectrom.*, **9**, 82-90 (1995)
[110] M. J. Deery, K. R. Jennings, C. B. Jasieczek, D. M. Haddleton, A.T. Jackson, H. T. Yates and J. H. Scrivens, *Rapid Commun. Mass Spectrom.*, **11**, 57-62 (1997)
[111] C. K. L. Wong and T. W. D. Chan, *Rapid Commun. Mass Spectrom.*, **11**, 513-519 (1997)

Chapter 2 – Instrumentation

2.1 Introduction

The experimental aspects of the research carried out will be discussed in two chapters. The first chapter will deal with the instrumental set-up used and the second chapter will deal with sample preparation.

The mass spectrometer described in this report was designed and constructed in the Chemistry Department at The University of Edinburgh [1,2]. The instrument was originally designed as a MALDI time-of-flight mass spectrometer, equipped with a coaxial linear reflectron and a microchannel plate detector [1,2]. The original design of the MALDI TOF mass spectrometer is illustrated in figure 2.1. Over the course of the work described here, a number of changes were made to the mass spectrometer. The overall length of the flight tube was extended from 50 cm to 83 cm. The flight tube extension brought several advantages, improving mass separation and allowing the installation of an in-line detector in addition to the original reflectron detector. The addition of the in-line detector greatly enhanced the versatility of the instrument, extending the mass range that could be studied and making the study of metastable decay possible [3,4].

Another improvement to the mass spectrometer was the addition of a pulsed deflection plate, allowing the removal of intense low-mass signals and therefore

improving sensitivity at higher masses. A schematic diagram of the extended mass spectrometer is provided in figure 2.2.

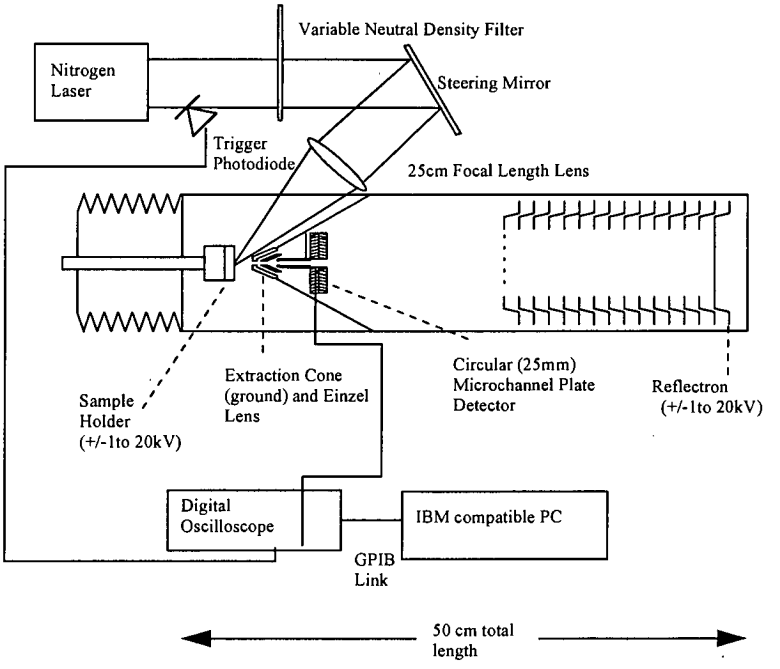

Figure 2.1 Full diagram of the apparatus prior to modification

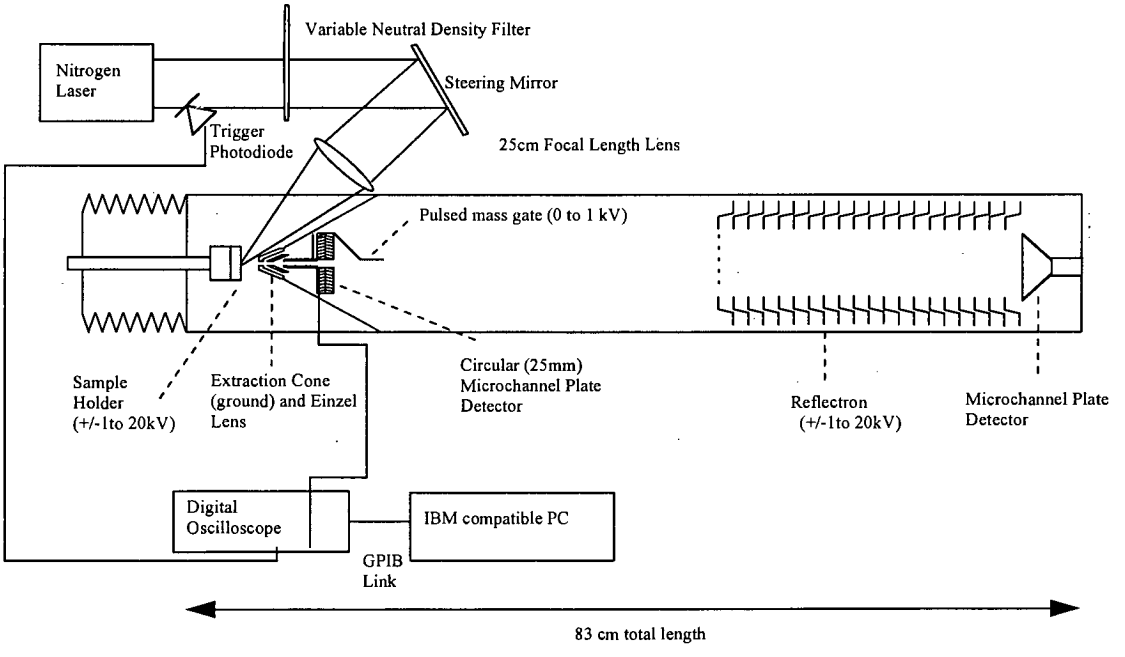

Figure 2.2 Full diagram of the experimental apparatus after the extension of the flight tube and the addition of a new detector and a mass gate.

The components of the instrument will be described in separate sections and any further changes that were made during this work will be mentioned in the appropriate sections.

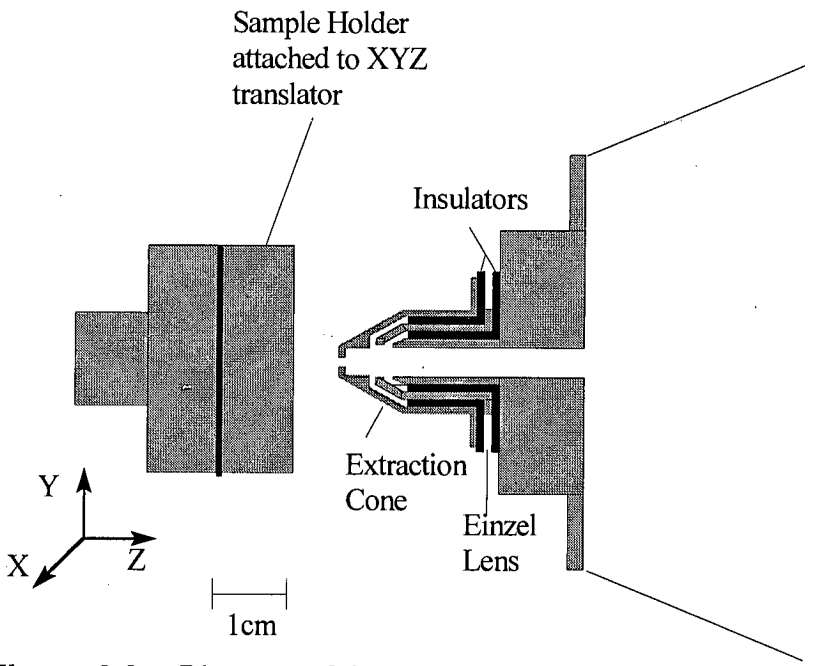

Figure 2.3 Diagram of the ion extraction optics

2.2 The ion source

A schematic representation of the ion source region is given in figure 2.3. The sample holder consists of a 2 cm-diameter removable stainless steel disk on which the sample was deposited. The sample holder could be moved by means of XYZ translators (Mitutoyo, Japan). The distance between the sample holder and the front of the extraction cone was maintained at 6 mm for all experiments. Moving the sample holder in the XY plane made it possible to move any part of the sample holder into the focus of the laser beam. The laser set-up is described in detail in section 2.6. Stepper motors were attached to the XYZ translators and allowed the

sample holder to be moved under computer control. For qualitative experiments, the XY translators were moved manually. For quantitative experiments, on samples produced by the aerosol method, (see section 3.3) the sample holder was moved by the stepper motors, which were computer controlled. The stepper motors were interfaced to a PC (XT, IBM) by means of an "isel" 3 axis steppermotor controller fitted with an "isel" interface card (Isert-electronic, Eiterfeld, Germany). The software for controlling the stepper motors was written in-house [5]. The sample holder also acted as the repeller plate by means of which the ions were accelerated. Two different high voltage power supplies to supply the repeller were used during the course of this work, depending on the experiment. For work requiring low extraction potentials, and delayed extraction experiments, a PS350 power supply (Stanford Research Systems Inc.) with a maximum output voltage of 5 kV was used. For all other experiments a home built power supply capable of delivering up to 20 kV was used. Either positive or negative ions could be extracted. For positive ion extraction, the repeller was held at a positive potential while for negative ion extraction the repeller voltage had to be negative. The extraction cone and the Einzel lens of the ion optics were grounded for all experiments described in this thesis.

2.3 Time-of-flight mass analyser

The simplest time-of-flight mass analyser is a linear time-of-flight tube with a detector at one end and an ion source at the other. The extreme simplicity, and hence low cost and robustness, is one of the factors that make time-of-flight mass analysis an attractive technique. Other factors are the theoretically unlimited mass range and, more specifically to MALDI, the fact that it is ideally suited to coupling with a

pulsed ion source. A drawback of time-of-flight analysis is its comparatively low resolution. The problems with resolution are exacerbated in MALDI by the fact that ions may be produced with a considerable energy spread [6,7,8]. The spread of kinetic energy of ions produced by MALDI leads to a spread in ion velocity and hence peak broadening in time-of-flight spectra. Several strategies have been developed to compensate for the kinetic energy spread. The most commonly used strategies are delayed ion extraction [9] or the use of a reflectron [10]. The principles behind delayed extraction and reflectrons are laid out in detail in chapter 1. Initially the instrument used for the work in this thesis was 50 cm long and equipped with a reflectron and a microchannel plate detector (see fig. 2.4). Later, the flight tube was extended by 33 cm and a second detector was added at the end of the reflectron section, allowing the instrument to function both as a linear and as a reflectron time-of-flight mass spectrometer (see figure 2.5).

2.3.1 Reflectron Design

Both of the reflectrons used were simple one stage gridded reflectrons. The reflectron originally used and the reflectron installed during the flight tube extension are shown in figure 2.6 and figure 2.7, respectively. The gridded front face of the reflectron was grounded. The voltage to each lens element was increased, through a resistor chain, up to a maximum voltage at the rear of the reflectron that exceeded the voltage of the repeller in the source. The back plate in the original reflectron design (fig. 2.6) was a solid plate. The redesigned back-plate consisted of a grid, which was necessary to allow operation of the instrument in the linear mode. For operation in the linear mode no voltage was supplied to the reflectron, allowing ions to travel

through the reflectron region without being impeded. The voltage to the reflectron was either supplied by a Stanford Research PS 350 high voltage power supply (Stanford Research Systems Inc) or by the homebuilt power supply, used to supply the repeller, through a voltage divider.

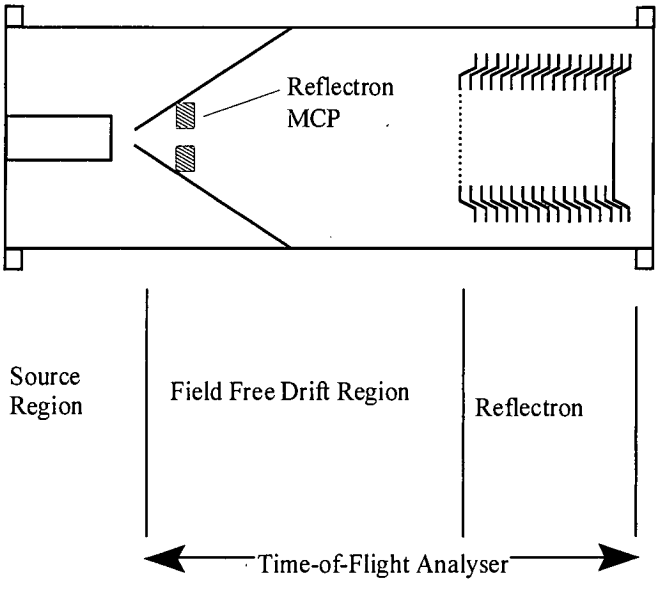

Figure 2.4 Schematic diagram of the time-of-flight mass spectrometer, prior to modification

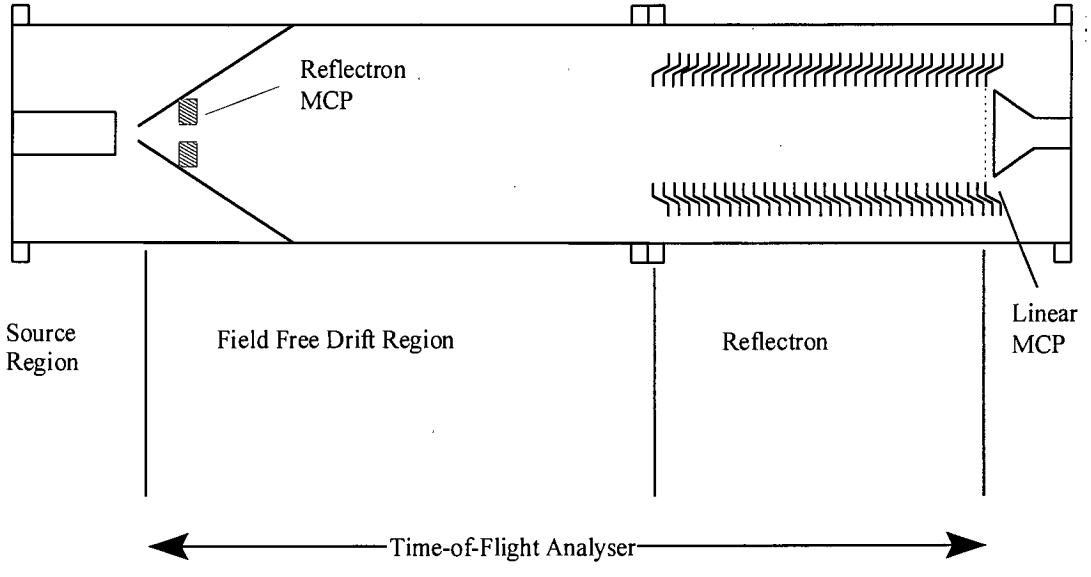

Figure 2.5 Schematic diagram of the time-of-flight mass spectrometer after the flight tube extension

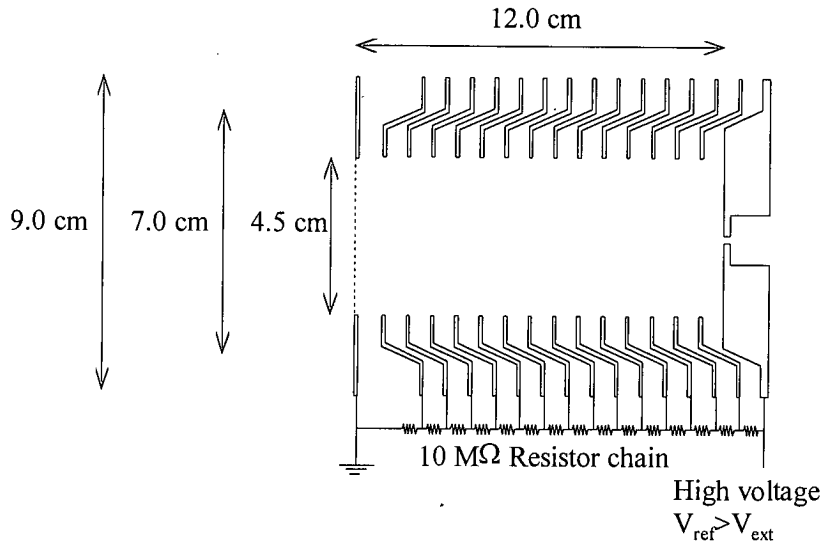

Figure 2.6 Original reflectron design

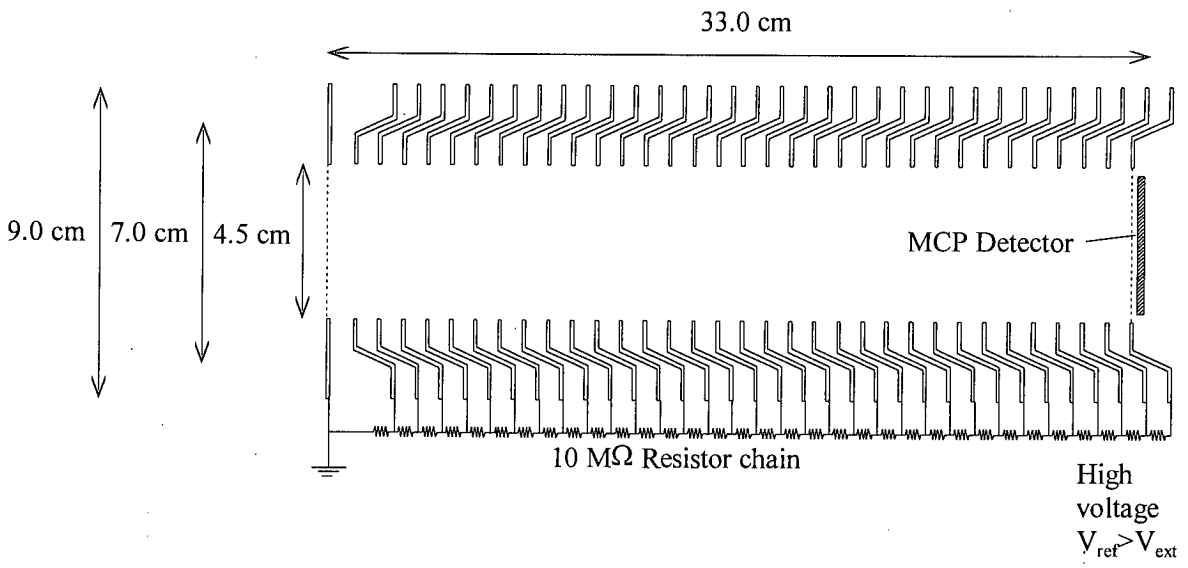

Figure 2.7 Modified reflectron used after flight tube extension

2.4 Detectors and data analysis

The detection systems used were based around microchannel plate (MCP) detectors that were interfaced to a LeCroy 9310M digital oscilloscope. Unless otherwise stated, the oscilloscope was triggered by a fast photodiode, which was exposed to the laser beam. In order to improve the signal to noise ratio, summed average spectra over 50-100 laser shots were produced. Data recorded using the oscilloscope could be transferred to a PC via a GPIB interface. Further data analysis was carried out on the PC using Microcal Origin software [11].

The mountings and circuit diagrams for the reflectron MCP are shown in figures 2.8 and 2.9. The reflectron MCP (Galileo Electro-Optics Corp.) was mounted directly on the back of the ion optics. The central hole in the detector allowed ions to pass through the detector into the time-of-flight mass analyser. The detector could be used both for positive and for negative ion detection. The linear detector was mounted on the back flange of the instrument as shown in figure 2.5. The circuit diagrams for positive and negative ion detection using the linear detector are shown in figure 2.10.

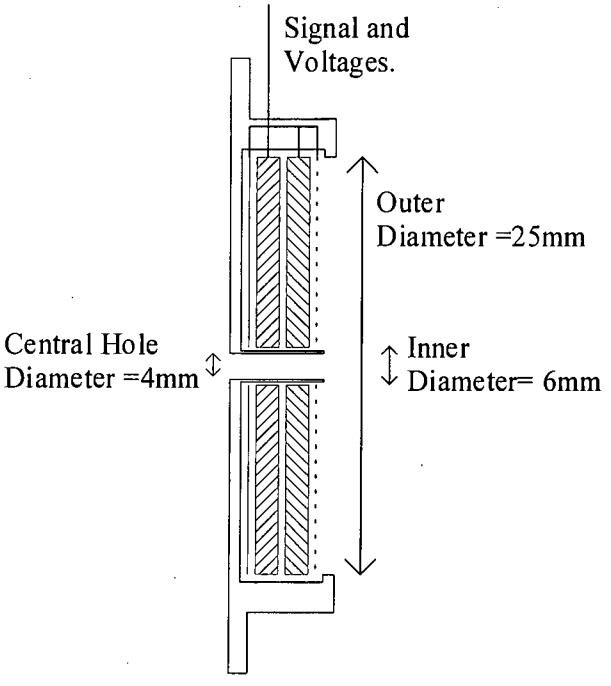

Figure 2.8 Mounting for the reflectron detector

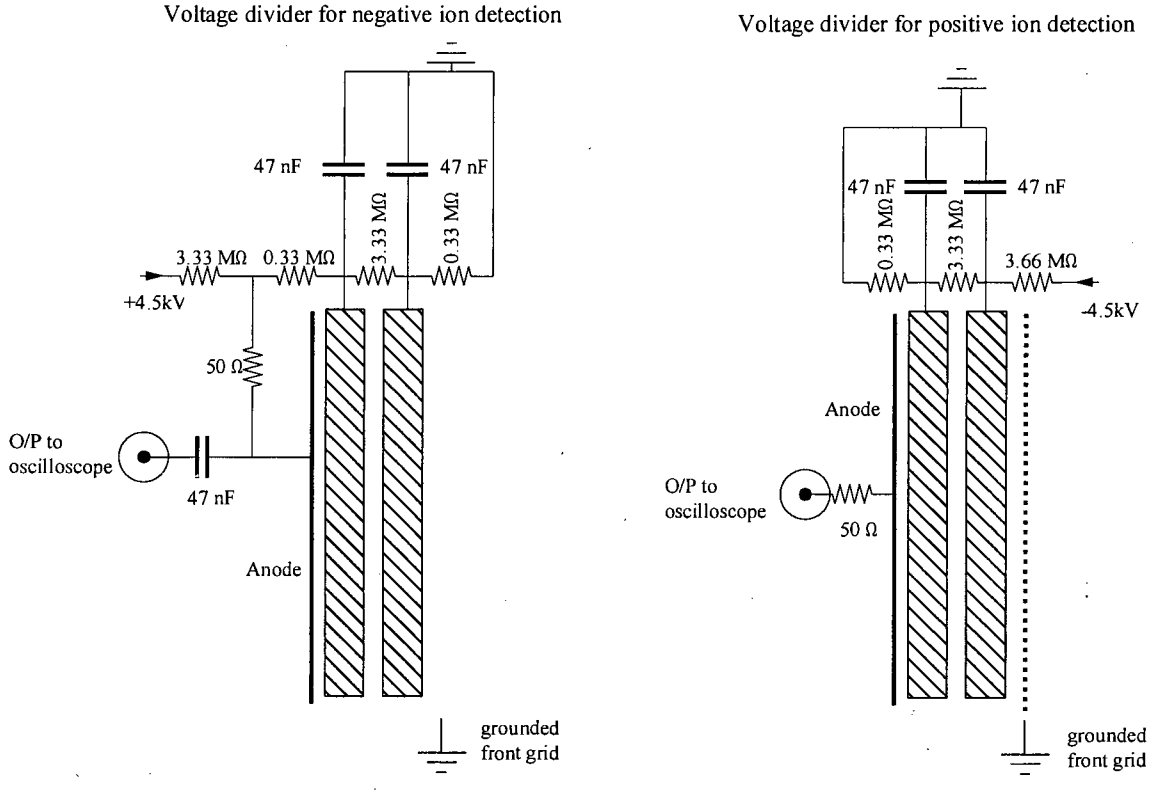

Figure 2.9 Voltage dividers for the reflectron detector

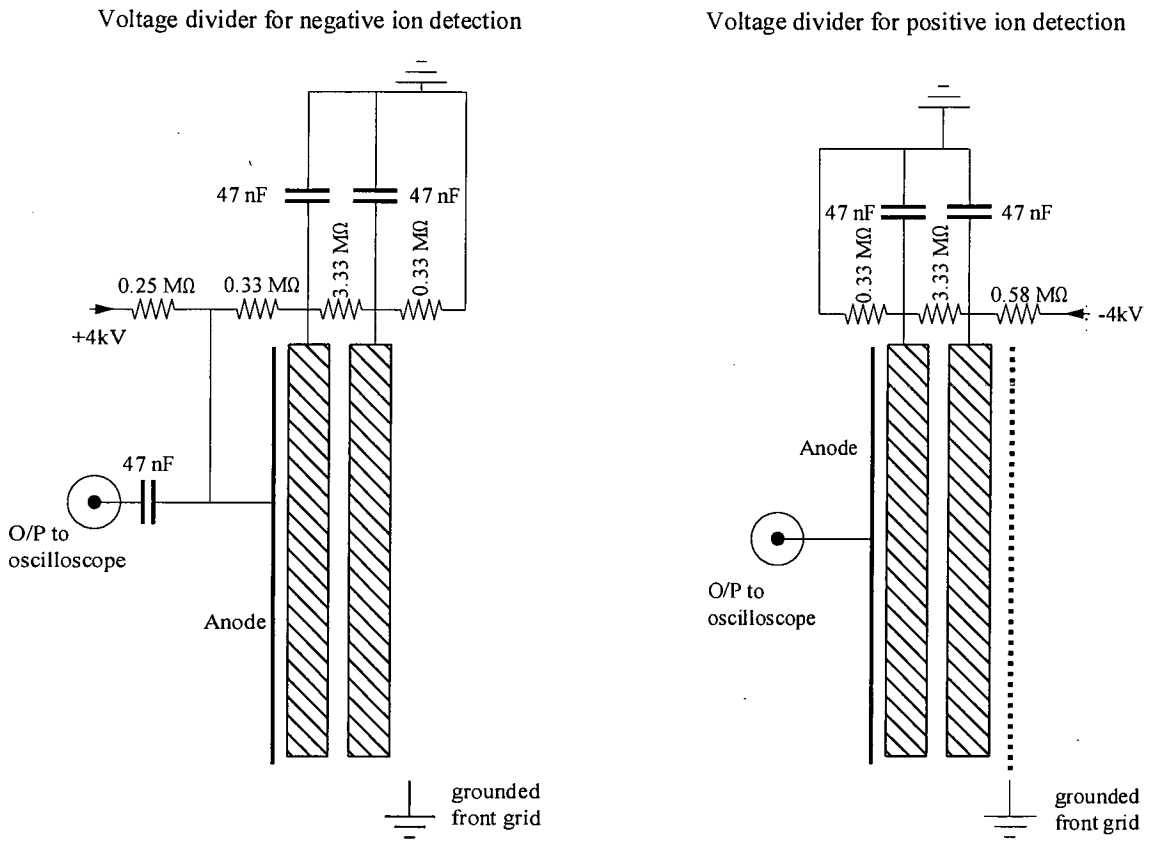

Figure 2.10 Voltage dividers for the linear detector

2.5 The Mass Gate

A characteristic of microchannel plate detectors is that they can suffer from saturation effects when a large number of ions, particularly fast ions, impact on them [12]. The greater the velocity of the particle impacting on the MCP detector, the greater the initial yield of electrons and hence the stronger the signal. As light particles are accelerated to the highest velocities, these are the particles most likely to induce MCP saturation. After saturation, detection efficiency of the detector can be seriously reduced. The nature of MALDI experiments means that in the process of producing analyte ions a large number of matrix ions are also produced. Matrix ions are usually considerably smaller than the analyte ions. Matrix ions will consequently

hit the detector before the analyte ions do and will also hit the detector at a higher velocity. Furthermore, the larger the analyte, the higher the matrix to analyte ratio needs to be, in order to efficiently transfer ions into the gas-phase [13]. Consequently the number of matrix ions produced increases. Hence detector saturation is more likely to occur when analysing heavier analytes. Problems with detecting high-mass analytes are further compounded by the fact that they will not be accelerated to a high enough velocity to be detected efficiently. Probably the best solution to high-mass detection problems would be the development of a new type of detector [14]. Although work on this issue is ongoing, a detection system, which is economically viable and has the required resolution, has not yet been developed [15,16,17,18].

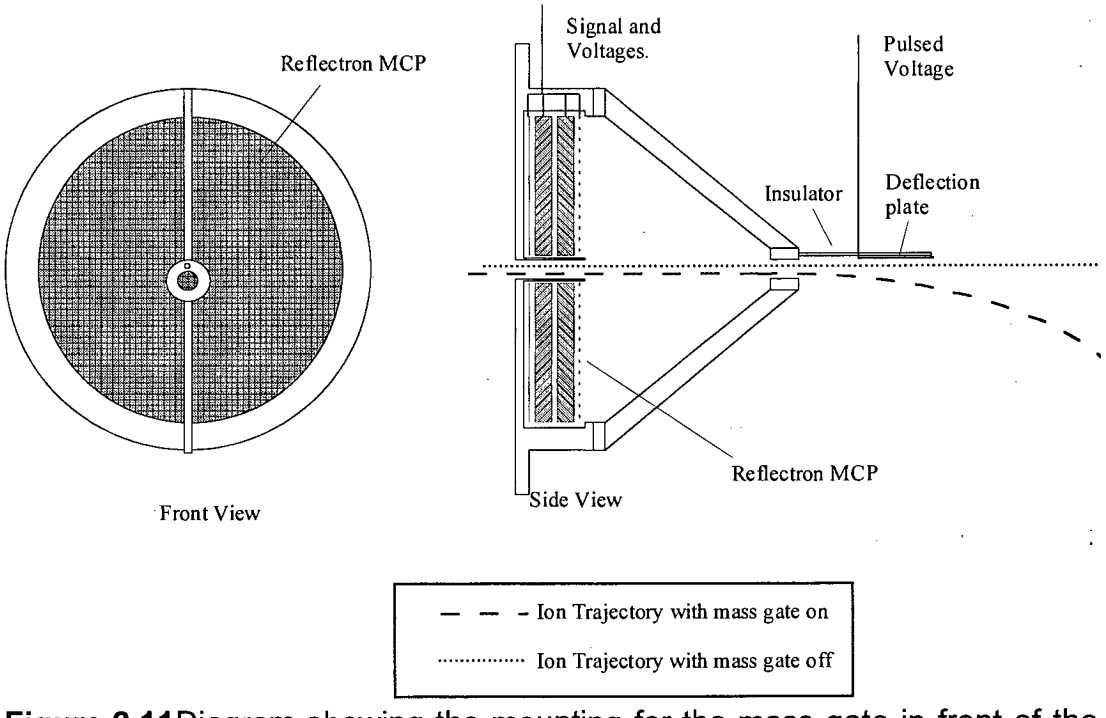

Figure 2.11 Diagram showing the mounting for the mass gate in front of the reflectron detector.

Detector saturation caused by low-mass ions can be overcome by the use of a mass gate. A mass gate is a device that deflects ions of a selected mass but allows other ions to pass unhindered. The simplest mass gates consist of a deflection plate or a pair of deflection plates, mounted parallel to the ion flight path in the field free drift region of the mass spectrometer. As the ions that are to be deflected approach the deflection plate a potential is applied to the plate; consequently the ion packet is pushed onto a different trajectory. This change in direction results in a collision with the sides of the flight tube. When an ion packet that is to be detected approaches the deflector plates, the plates are switched to ground, allowing the ions to continue without deflection. The simple deflector plate mass gate is very effective as a means of removing low-mass signals from a time-of-flight spectrum and hence improving detection efficiency of higher mass ions. More sophisticated ion gates have been designed and used for the selection of ions of a single mass, such as the Bradbury-Nielsen type ion gate [19]. These more elaborate devices are required where an ion of a single mass needs to be selected *e.g.* when conducting tandem mass spectrometry experiments. For the purposes of the work conducted in this research, namely to extend the mass range over which the instrument could efficiently be used, a simple deflector plate assembly was sufficient. The addition of an ion gate capable of selecting a single mass peak would be a worthwhile avenue to explore in future work on this instrument.

The mass gate used was a single deflector plate, to which a high voltage pulse was applied. The deflector plate was mounted in the field free drift region of the mass spectrometer, as illustrated in figure 2.11. The high voltage switch and pulse generator were built in-house. The high voltage switch was triggered by the pulse

generator, which in turn was triggered from the synchronous output of the laser. The high voltage was supplied by a Brandenburg power supply (model 475R) and was typically +500 V. The high voltage pulse produced had a rise time of less than 50 ns. The power to the pulser and high voltage switch was provided by a dual tracking dc power supply (Topward Electric Instruments Co., Ltd, model tps-4000).

2.5.1 Illustration of the effectiveness of the mass gate

In order to demonstrate the performance of the mass gate several experiments were carried out. A poly(propylene glycol) (PPG) sample (average molecular weight *ca* 1000 Da) was prepared with dithranol as the matrix and LiCl as the doping salt. The sample was made up using the aerosol method described in section 3.3.3. The effects of different gate voltages and gate pulse lengths were investigated. The gate pulse length is taken as the duration of the high voltage pulse applied to the deflection plate of the mass gate. The high voltage pulse was triggered on the synchronous output of the laser and was timed so that the high voltage was applied at the same time as the laser struck the sample holder. It was determined, that a pulse voltage of +500 V was sufficient to deflect low-mass ions. The results of two experiments are presented in figures 2.12 and 2.13.

The traces shown in figure 2.12 were recorded using a source repeller voltage of 12 kV. The spectrum shown in figure 2.12 (d) was obtained without the use of the mass gate. All peaks with flight times above 12 μs are due to lithium adducts of PPG oligomers. The peaks below 12 μs are due to matrix species and metal ions. The signal below 2 μs is due to noise pick up from the firing of the laser. The group of

peaks at 7.5 μs is due to protonated and lithiated matrix. Further investigation showed that the matrix peaks in the spectrum recorded without the mass gate were off scale and are actually *ca* 50 to 100 times as intense, as they appear. The use of the mass gate can be seen to remove low-mass ions from time-of-flight spectra (see figures 2.12 (a) to (c)). In all spectra recorded with the mass gate on, the low-mass peaks below 5 μs are no longer seen. By increasing the length of time that the gate is left on, ions of increasingly larger masses are deflected and hence fewer peaks appear in the mass spectra.

Little difference in the signal intensity of the polymer ions is seen whether the mass gate is switched on or off. This is best illustrated by comparing figure 2.12 (d) with figure 2.12 (c). The fact that the polymer signal intensity only increase a little when the mass gate is employed shows that under the experimental conditions employed little or no detector saturation occurred.

It is noteworthy, that a large peak is observed at 7.5 μs in figures 2.12 (a) and 2.12 (b), despite the fact that other ions in that mass region have been deflected. The species that are not affected by the mass gate are neutrals formed from the lithium and sodium adducts of the matrix. The neutral nature of the species detected at 7.5 μs in figs 2.12 (a) and 2.12 (b) was confirmed, by switching on the reflectron and using the linear detector to observe what passed through the reflectron. Only uncharged species could pass through the reflectron. With the reflectron on, only the peak at 7.5 μs was detected. The generation of neutrals under MALDI conditions will be further discussed in chapter 5.

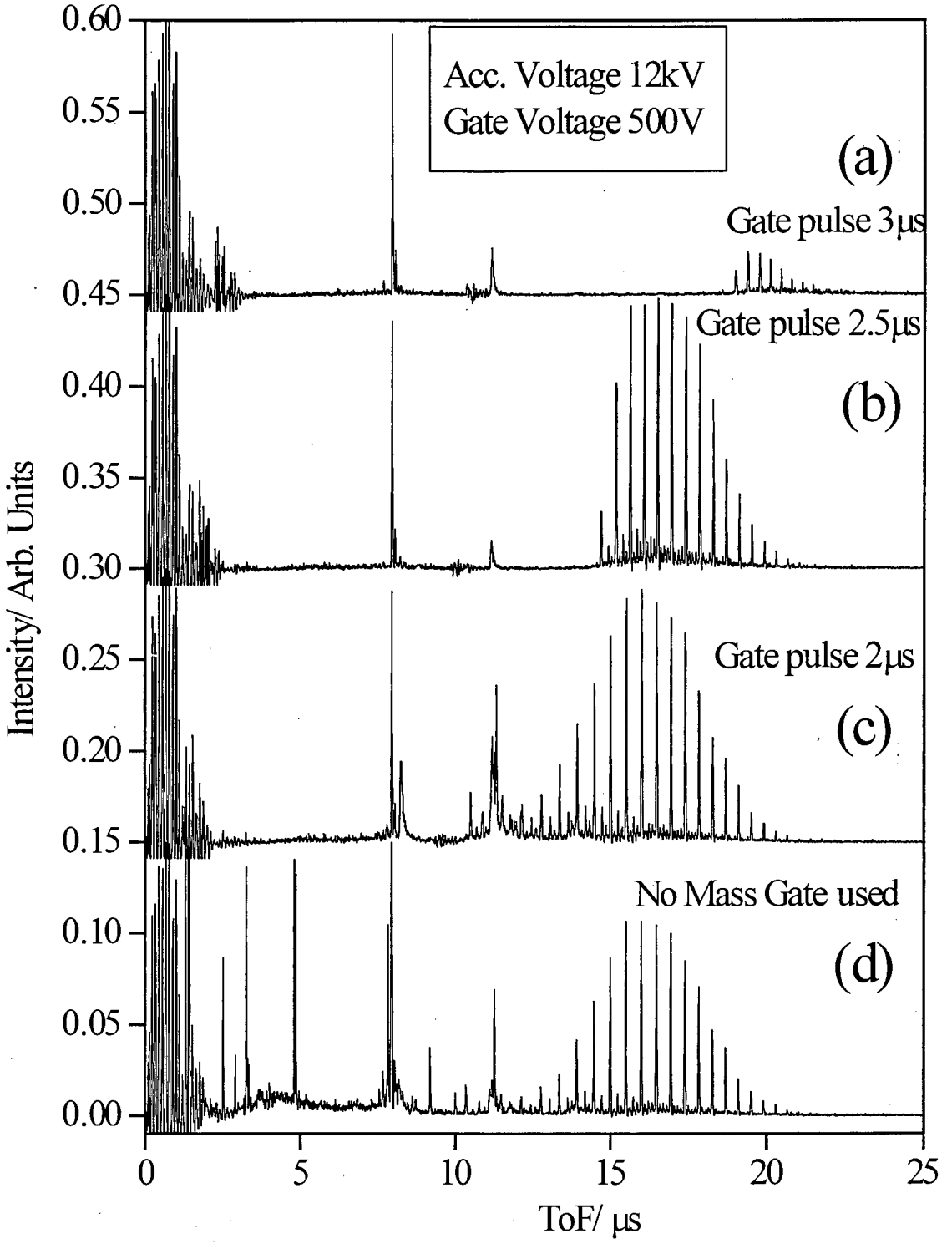

Figure 2.12 The effect of the use of the mass gate on the time-of-flight spectrum of PPG 1000. An extraction voltage of 12kV was used and the period of time for which the mass gate was left on was varied as shown ((a) to (c)). The mass gate was not used for the time-of-flight spectrum shown in (d).

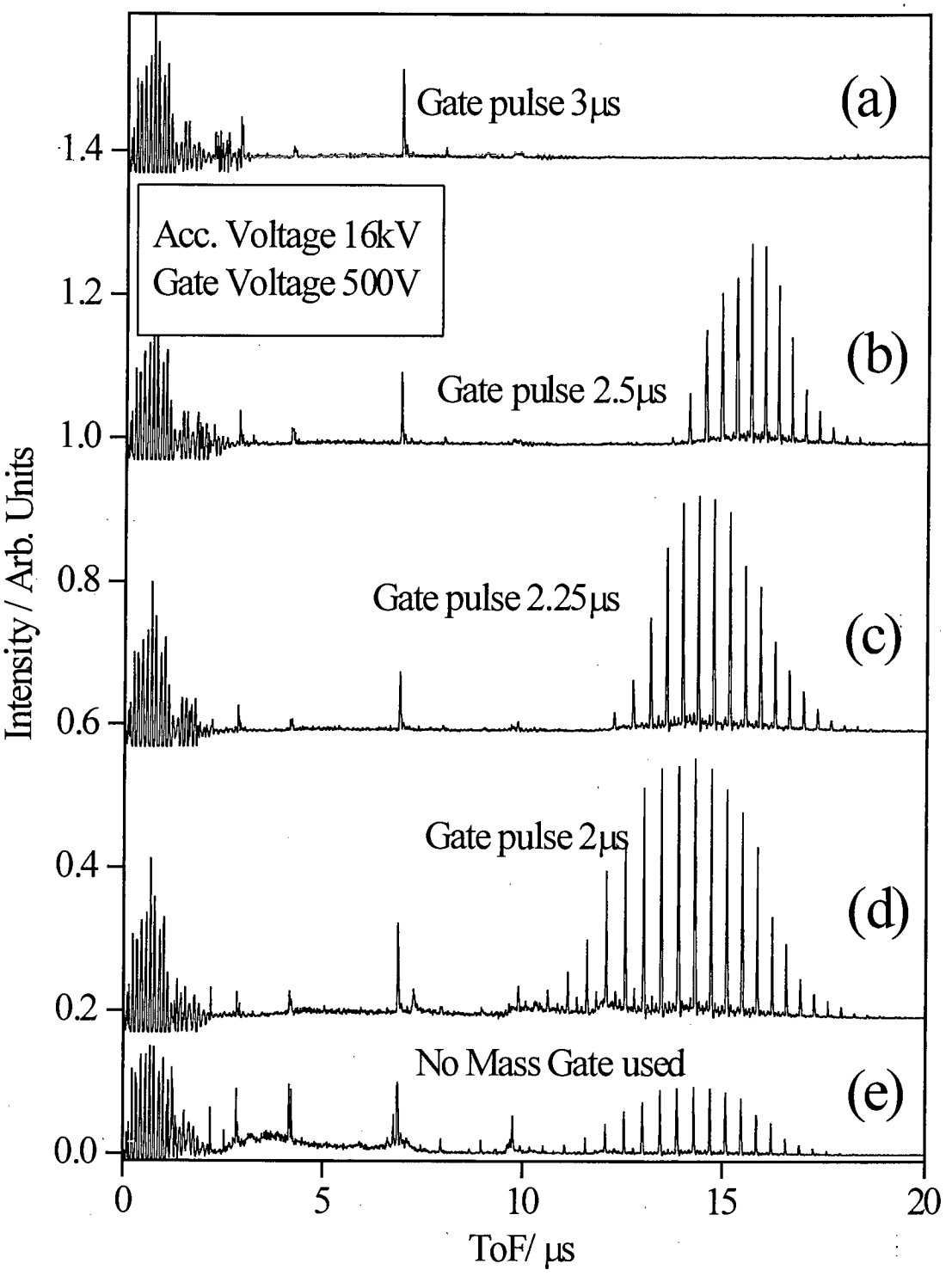

Figure 2.13 The effect of the use of the mass gate on the time-of-flight spectrum of PPG 1000. An extraction voltage of 16kV was used and the period of time for which the mass gate was left on was varied as shown ((a) to (d)). The mass gate was not used for the time-of-flight spectrum shown in (e).

Figure 2.13 shows the results of a similar experiment to that illustrated in figure 2.12, the only difference being the extraction voltage used (*i.e.* 16 kV for figure 2.13). The most notable difference between the two figures is the considerable increase in signal intensity for the polymer adduct peaks (flight times between 10 μs and 20 μs) in the spectra recorded with the mass gate in operation with an accelerating potential of 16 kV (figure 2.13). The difference in signal intensity is clearly demonstrated when comparing figure 2.13 (d), where the mass gate was used, with figure 2.13 (e), where the mass gate was not employed. The large increase in signal intensity is observed because at the accelerating voltage used, 16 kV, saturation of the detector occurs. At higher source voltages low-mass ions have higher kinetic energies and therefore produce a greater yield of electrons when impacting on the detector.

As well as testing the mass gate in the linear mode, it was also tested for use in the reflectron mode. The sample was again made up using the aerosol method. The polymer investigated was poly(ethylene glycol) (average molecular weight 2000 Da) using dithranol as the matrix and NaCl as the cation donor. A lower deflection voltage (100 V) was required to deflect low-mass ions in the reflectron experiments, compared with linear experiments (500 V). The lower voltage required was expected, as the flight-path of ions was increased considerably by the use of the reflectron. Therefore, even a small deviation from the correct flight path would lead to collision of the ions with the walls of the mass spectrometer and hence the ions would not be detected.

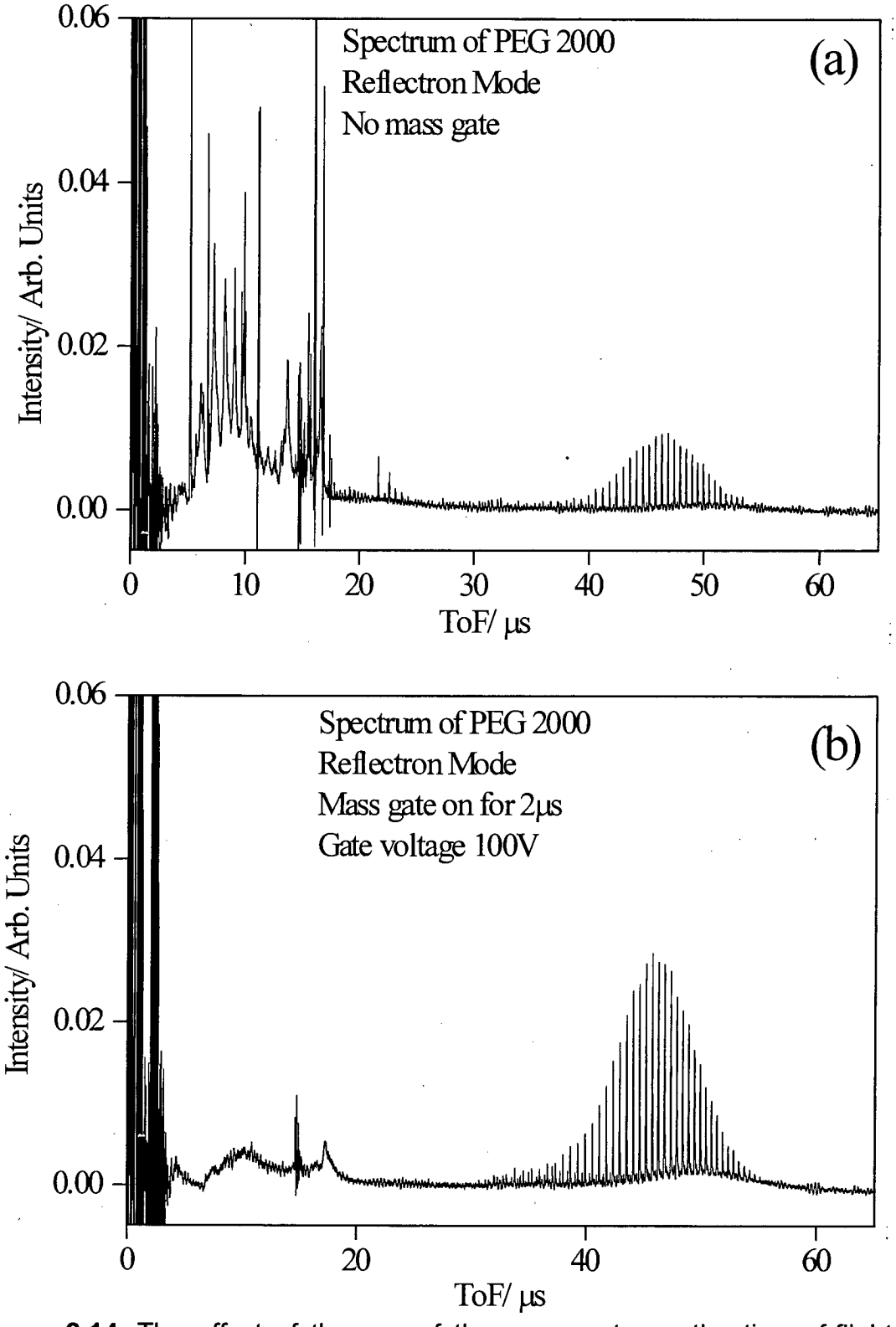

Figure 2.14 The effect of the use of the mass gate on the time-of-flight spectrum of PEG 2000 recorded in the reflectron mode. Spectrum (a) was recorded with the mass gate switched off. When spectrum (b) was recorded the mass gate was left on for 2 μs at 100 V.

The results for the reflectron mass gate experiment are shown in figure 2.14. An obvious difference between the reflectron and linear mode experiments is the lower abundance of peaks in the low-mass region in the spectra recorded with the mass gate on. In the reflectron experiment (figure 2.14 (b)) only two broad humps centred at 10 μs and 17 μs, respectively, can be seen. The most likely origin of these features is the detection of matrix ions, which were not deflected sufficiently to avoid detection. The sharper feature observed in figure 2.14 (b), with a time-of-flight of 15 μs, is switching noise from the high voltage switch of the mass gate.

Again, the analyte spectrum is enhanced by the use of the mass gate, as saturation effects have been avoided.

2.6 Laser System

The laser used for all experiments in this thesis was a Lambda Physik EMG 102 (Göttingen, Germany) excimer laser, running as a nitrogen laser. The gas fill used was a mixture of 60 mbar of nitrogen with 940 mbar of helium. The laser output produced from a 30 kV discharge was a 5 mJ pulse with a pulsewidth of 3.5 ns at a repetition rate of 6 Hz. The lasing wavelength was 337.1 nm. The beam produced was steered into the source region of the mass spectrometer by two mirrors. Owing to the large divergence of the beam only *ca* 25% of the light actually reached the instrument. However, 1.2 mJ was still far in excess of the energy required for MALDI experiments and the beam was further attenuated using a circular neutral density filter. The use of the neutral density filter made it possible to adjust the laser

energy smoothly. After attenuation the beam was focused onto the sample holder in the source region of the instrument using a 25 cm focal length quartz lens. The angle of incidence of the laser on the sample holder was 45°. The laser spot size and shape on the sample holder was estimated using UV sensitive paper to be a teardrop shape with a main axis length of *ca* 500 μm and a short axis length of *ca* 150-200 μm.

2.7 Pumping system

The whole mass spectrometer was pumped using one oil diffusion pump (Edwards Diffstak 160) with a cryotrap. Edwards L9 diffusion pump fluid was used. The diffusion pump was backed by a rotary pump (Edwards Speedivac ES200). The diffusion pump could be isolated from the mass spectrometer by the use of a butterfly valve. To accomplish the removal of the sample holder stage, the whole instrument had to be brought up to atmospheric pressure which involved isolating the instrument from the pumping system and gradually bringing it up to atmospheric pressure by bleeding in nitrogen. Nitrogen was used to avoid the influence of water vapour and thus facilitate the pumping down after sample loading. After sample loading, the sample holder stage was refitted to the mass spectrometer and the system was pumped down to operating pressure. Before the mass spectrometer could be pumped by the diffusion pump, the system needed to be brought to a pressure of less than $5*10^{-2}$ mbar, using the rotary pump. When the rotary pump was used as a roughing pump for the mass spectrometer, the diffusion pump was isolated. The base pressure attainable using the diffusion pump was $5*10^{-8}$ mbar. Experiments could be performed at a maximum pressure of $2*10^{-6}$ mbar. It took *ca* 20 min for the system

to pump down to operating pressure after sample loading. The pressure in the instrument was monitored using three pressure gauges. A Pirani gauge (Edwards PRL10) monitored the backing pressure of the diffusion pump. The pressure in the mass spectrometer was measured by a Pirani gauge (Edwards PRL10) and a Penning gauge (Edwards CP25EK). All gauges were controlled via a Pirani Penning 1005 pressure gauge controller (Edwards).

2.8 Conclusion

This chapter has given a description of the instrumentation employed, in the experimental work for this thesis. Changes made to the experimental set-up have been discussed, including a detailed discussion of the introduction of a low-mass gate for eliminating low-mass ions from mass spectra.

2.9 References

[1] I. A. Mowat and R. J. Donovan, *Rapid Commun. Mass Spectrom.*, **9**, 82-90 (1995)

[2] I. A. Mowat, R. J. Donovan and R. R. Maier, *Rapid Commun. Mass Spectrom.*, **11**, 89-90 (1997)

[3] S. Della-Negra and Y. Le Beyec, *Anal. Chem.*, **57**, 2035-2040 (1985)

[4] R. Kaufmann, D. Kirsch and B. Spengler, *Int. J. Mass Spectrom. Ion Proc.*, **131**, 355-385 (1994)

[5] Program written in QuickBasic by M. F. Snel and L. Hogg, not published.

[6] V. Bokelmann, B. Spengler and R. Kaufmann, *Eur. Mass Spectrom.*, **1**, 81-93 (1995)

[7] Y. Pan and R. J. Cotter, *Org. Mass Spectrom.*, **27**, 3-8 (1992)

[8] R. C. Beavis and B. T. Chait, *Chem. Phys. Lett.*, **181**, 479-484 (1991)

[9] W. C. Wiley and I. H. McLaren, *Rev. Sci. Instrum.*, **67**, 1150-1157 (1955)

[10] B. A. Mamyrin, *Int. J. Mass Spectrom. Ion Proc.*, **131**, 1-19 (1994)

[11] MicroCal Software Inc., One Roundhouse Plaza, Northampton, MA 01060, USA

[12] A. Westman, G. Brinkmalm and D. F. Barofsky, *Int. J. Mass Spectrom. Ion Proc.*, **169,** 79-87 (1997)

[13] D. C. Schriemer and L. Li, *Anal. Chem.*, **68**, 2721-2725 (1996)

[14] D. C. Schriemer and L. Li, *Anal. Chem.*, **69**, 4176-4183 (1997)

[15] F. Dubois, R. Knochenmuss and R. Zenobi, *Int. J. Mass Spectrom. Ion Proc.*, **169,** 89-98 (1997)

[16] U. Bahr, U. Rohling, C. Lautz, K. Strupat, M. Schurenberg and F. Hillenkamp, *Int. J. Mass Spectrom. Ion Proc.*, **153,** 9-21 (1996)

[17] G. C. Hilton, J. M. Martinis, D. A. Wollman, K. D. Irwin, L. L. Dulcie, D. Gerber, P. M. Gillevet and D. Twerenbold, *Nature*, **391**, 672-675 (1998)

[18] D. C. Imrie, J. M. Pentney and J. S. Cottrell, *Rapid Commun. Mass Spectrom.*, **9**, 1293-1296 (1995)

[19] C. W. Stoermer, S. Gilb, J. Friedrich, D. Schooss and M. M. Kappes, *Rev. Sci. Inst.*, **69**, 1661- 1664 (1998)

Chapter 3 – Sample preparation

3.1 Introduction

Sample preparation is of key importance for successful MALDI mass analysis. Without due attention being paid to sample preparation the results become very scattered and irreproducible [1]. It has recently been shown that, through careful sample preparation, narrow molecular fractions of polystyrene with average molecular weights of up to 1.5 MDa can be mass analysed [2]. It is also known that the resolution of mass spectra can be affected by sample preparation. In the analysis of synthetic polymers, even the molecular weight distribution observed can vary with different sample preparation regimes [3].

The work presented here has focused on the mass analysis of synthetic polymers and this chapter will therefore deal with sample preparation for synthetic polymers. For synthetic polymer mass analysis samples usually consist of a mixture of three components, namely the polymer, a salt and the matrix. In this mixture, the polymer is the analyte. The matrix absorbs the laser radiation which facilitates transition of the analyte into the gas phase and plays a role in the ionisation process. Polymers are usually detected in the form of metal cation polymer adducts and the salt is added as a cation source for adduct formation with the polymer [4,5]. The ratios between the three sample constituents are determined empirically and are dependent on the nature of the sample constituents.

A problem that has been reported and that was also observed in this work was poor shot to shot reproducibility of signal intensity [1]. This posed a significant problem when quantitative studies were carried out. An example of an experiment requiring good reproducibility is one in which the variation of one experimental parameter is investigated, such as laser energy, extraction potential, *etc.* The work described in this chapter details the development of a method of sample preparation that improves shot to shot reproducibility and hence facilitates quantitative experiments. This chapter is also intended to give a practical guide to sample preparation for polymer MALDI.

3.2 Choice of matrix and salt

Over the years, many new MALDI matrices have been introduced, some of which are very well suited to polymer analysis. Several matrices were used successfully during this research. The matrices most commonly used are summarised in Table 3.1. For the analysis of new types of polymers, all the matrices were tried and the best one chosen for further work. A molar ratio of matrix to polymer of between 40:1 and 500:1 was used for polymers with average molecular weights of up to 20 kDa. Dithranol was used very successfully for low-mass polymers up to *ca* 7000 Da. 2-(4-hydroxyphenylazo) benzoic acid (HABA) [6,7] and 3-β-indole acrylic acid (IAA) [8] were both used for analysing higher mass polymers and copolymers. HABA and IAA gave rise to large signals from matrix species, including multimers extending up to 1500 Da, making them a less suitable choice for

low mass polymer analysis. All-*trans*-retinoic acid was used exclusively for polystyrene analysis [9].

Name of Matrix	Suitable Solvents	Concentration Range / g L^{-1}	Comments
1,8,9-anthracenetriol (Dithranol)	THF	5-20	Good all round polymer matrix very good for low mass polymers
2-(4-hydroxyphenylazo) benzoic acid (HABA)	acetone, 1,4-dioxane	5-20	Good for higher mass polymers >8kDa. Large signal associated with matrix multimers
3-β-indole acrylic acid (IAA)	acetone	5-20	Suitable for polymer and copolymer analysis
all-*trans*-retinoic acid	THF	20-50	Very good matrix for polystyrene analysis

Table 3.1 Summary of some commonly used matrices for polymer mass analysis

For all experiments conducted, salt was added to the sample, to provide a source of cations for attachment to the polymers. A variety of salts was used. Although no hard and fast rules can be made as to which cation attaches most efficiently it was found that for most polymers alkali metal-ions were suitable. Of the alkali metals, lithium tended to give the most intense mass spectra. Although alkali metal ions worked very well in most cases, other metal ions were also used for polymer MALDI. Polystyrene, for example, forms adducts most readily using silver or other transition metal ions [4,10]. The salts used in this work were the chlorides of the alkali metals and $AgCF_3CO_2$ or $AgNO_3$ as a silver ion source. The trifluoroacetate of silver was chosen for two reasons; first it contains silver in the 1+ oxidation state and, second, this salt is readily soluble in tetrahydrofuran, which facilitates the mixing of salt solution with matrix and polymer solutions. The amount of salt added changed significantly for different sample preparation schemes and will be dealt with in the following sections on sample deposition.

3.3 Sample deposition

Three different sample deposition methods were employed during this work. The first method will be referred to as the droplet method, where a micropipette was used for depositing the sample on the sample holder [11]. The other two methods involved using spray techniques for sample deposition. These will be referred to as the electrospray and the aerosol method, respectively. For the electrospray method, a fine spray was produced by drawing the sample through a hypodermic needle by means of an applied electrical potential. In the case of the aerosol method, the sample was deposited using an aerosol spray-gun. A summary of the advantages and disadvantages of the droplet method and the two spray techniques is given in table 3.2.

Techniques that rely on depositing droplets of sample solution onto the sample holder are the most commonly used MALDI sample preparation methods. The droplet method is useful as a qualitative technique, best suited to analysing a large number of samples quickly or for finding the correct ratio between matrix, salt and polymer. The droplet method was, however, found to be less suitable for detailed quantitative work. The limitations of this type of sample preparation have been recognised by several groups and alternative sample preparation techniques have been suggested [1,12]. The primary problems with the sample spots produced by the droplet method are the uneven surface and the limited size of the sample spot. One of the factors giving rise to an inhomogeneous sample surface is that the solvent evaporates more quickly at the edges of the droplet than at the centre. This can lead

to 'edge effects' *i.e.* different results being obtained from the edge of a sample spot compared with the centre.

Table 3.2 Summary of the advantages and disadvantages of different sample preparation techniques

Droplet method		**Electrospray method**		**Aerosol spray method**	
Advantages	Disadvantages	Advantages	Disadvantages	Advantages	Disadvantages
Fast sample prep. A number of different samples per sample holder Well suited to screening large numbers of samples and/or different matrix analyte combinations	Not well suited to the systematic investigation of experimental variables Small sample spot and only a few spectra from each sample spot	Large sample spot allowing very large numbers of single shot spectra from one sample holder Excellent reproducibility Well suited to the systematic investigation of the variation of experimental variables Useful for the analysis of samples that give a weak signal and require the averaging of large numbers of spectra Potential for coupling of liquid chromatography systems to MALDI MS	Time consuming Only 1 sample per sample holder Spray settings need to be adjusted to the solvent system used making two stage sample deposition very difficult	Large sample spot allowing very large numbers of single shot spectra from one sample holder Excellent reproducibility Well suited to the systematic investigation of the variation of experimental variables Useful for the analysis of samples that give a weak signal and require the averaging of large numbers of spectra Potential for coupling of liquid chromatography systems to MALDI MS Not sensitive to the solvent system used Salt and polymer/ matrix can easily be sprayed separately	Time consuming Only 1 sample per sample holder

Derrick *et al.* proposed a sample preparation technique in which the matrix analyte mixture was deposited on the sample holder using an electrospray method [1]. This work was repeated at The University of Edinburgh and it was found to work well for samples where the matrix polymer and salt could be dissolved in the same solvent. However, it was difficult to use two-stage sample deposition where first a salt solution and then a matrix/analyte solution was sprayed onto the sample holder. Problems arose when adjustments had to be made to the spray conditions after the salt layer was sprayed, owing to the different physical properties of the aqueous salt solution, compared with the organic solvent used for the matrix and analyte. It was difficult to optimise spray conditions for both layers, and this led to poor sample quality. It was also an extremely time consuming method.

An alternative approach was developed. A spray-gun was used to coat the sample holder first with a salt layer and then with the sample/matrix mixture. The spray-gun technique was found to be less solvent dependent than the electrospray technique. Using a spray-gun was also more straightforward, as it did not require the design and construction of specific apparatus, unlike the electrospray technique.

The strength of the spray techniques was in quantitative work, for instance, when the ratios of the sample components were kept constant, and other experimental parameters, such as laser energy or the ion extraction field strength, were varied. As a large sample spot with an even sample surface was produced it became possible to collect a large number of spectra from the same sample holder, using a fresh section of the sample for each laser shot. Each of these methods is discussed in some detail below.

3.3.1 The droplet method

The droplet method is a very simple technique for MALDI sample preparation. It involves depositing a small droplet of sample solution on the sample holder and leaving the solvent to evaporate. Most MALDI experiments described in the literature involve this method of sample preparation.

A micropipette (Socorex, Switzerland) was used to spot the sample onto the sample holder. The sample holder consisted of a 2 cm diameter stainless steel disk, which had been thoroughly cleaned and polished. Sample deposition could be a one or a two-stage process depending on the matrix and polymer used.

For the one-stage droplet deposition method, solutions were prepared of salt, polymer and matrix and these were combined prior to sample deposition. A 0.5 to 2 μL droplet of the polymer, analyte and salt mixture was then spotted straight onto the sample holder by means of the micropipette, and the solvent was left to evaporate. The quality of the sample spot that was produced using this method varied, depending mostly on the surface tension of the solvents used. Droplets of solutions with low surface tension spread out quickly over the sample holder and the solvent evaporated very quickly, leading to an uneven sample surface and poor reproducibility of MALDI mass spectra. However, it was often still possible to obtain mass spectra from these sample spots from which valuable qualitative information could be obtained.

The two-stage droplet method involved the deposition of a 0.5 – 4 μL droplet of aqueous salt solution on the sample holder. A 0.5 - 4 μL aliquot of a 1:1 by volume mixture of matrix and polymer solutions was then injected into the salt droplet. As soon as the polymer/matrix mixture was injected into the salt droplet, crystal formation could be observed. The sample spot was allowed to air dry. The dry sample spot typically had a diameter of 5 mm. The two-stage sample preparation technique had the advantage that the sample spot was confined to the area taken up by the initial salt solution droplet. Also, it was easy to make up aqueous solutions of salts, whereas salts are in general poorly soluble in the organic solvents, which are often needed to dissolve the matrix and the polymer. A summary of typical sample compositions is given in table 3.3.

Matrix	**Matrix conc.**	**Polymer conc.**	**Salt conc.**	**Method**	**matrix:polymer:salt v/v/v**
dithranol	50 mM in THF or acetone	1-10 mM	10 mM in H_2O	2 stage	from 1:1:0.25 to 1:1:8
HABA	50 mM in 1,4 dioxane or acetone	1 mM	Saturated in MeOH	1 stage	90:10:1
IAA	50 mM in THF or acetone	1 mM	Saturated in MeOH	1 stage	90:10:1
all *trans* retinoic acid	150 mM in THF	1 mM in THF	Saturated in MeOH	1 stage	90:10:1

Table 3.3 Typical sample compositions for polymer MALDI

It should be noted that although the droplet method is very useful for obtaining qualitative information such as molecular weight distributions of polymers it is of limited use in experiments where signal intensity comparisons are made between mass spectra. The variation in signal intensity is regularly more than 50% between mass spectra.

3.3.2 Electrospray sample deposition

The apparatus used for electrospray sample deposition is shown in figure 3.1. For safety reasons, the whole apparatus was housed in an interlocked safety cage (not shown). The solution to be sprayed, was loaded into the Luer fitting of a 26 gauge blunt tipped hypodermic needle (Cooper's Needle Works Ltd, Birmingham). The Luer fitting of the needle was large enough to hold 100 μL of solution. The rate at which the solution ran through the needle could easily be adjusted by inserting a length of wire part way down the top of the needle. The solution could be seen to slowly drip out of the end of the needle. When a positive potential was applied to the needle, a fine spray was produced. The higher the voltage applied to the needle, the more divergent the spray. A lens (ring electrode) was used to focus the spray onto the sample holder. The optimum spray conditions were found to be at a needle potential of 6 kV, with the tip of the needle being 6 cm from the top of the sample holder. The thickness of the layer that was deposited could most easily be controlled by changing the length of the spray time. The spray time was regulated by the use of a shutter, which was opened at the beginning of spraying and shut to end the spray. The use of a shutter had another advantage, namely that it stopped drops of solution falling from the needle onto the sample holder, when no potential was applied. An example of typical spray conditions for polystyrene analysis would be 22 mm of wire being inserted into the needle and a spray time of 120 s. Over this time period, 60 μL of solution were sprayed producing a 1 cm diameter sample spot. A typical sample solution consisted of a mixture of equal volumes of polystyrene (1 g L^{-1} in THF), dithranol (10 g L^{-1} in THF) and silver trifluoroacetate (1 g L^{-1} in THF) solutions. The thickness of the sample was the same as for an equivalent sample produced using the droplet method. Samples produced in this way showed a very even sample surface.

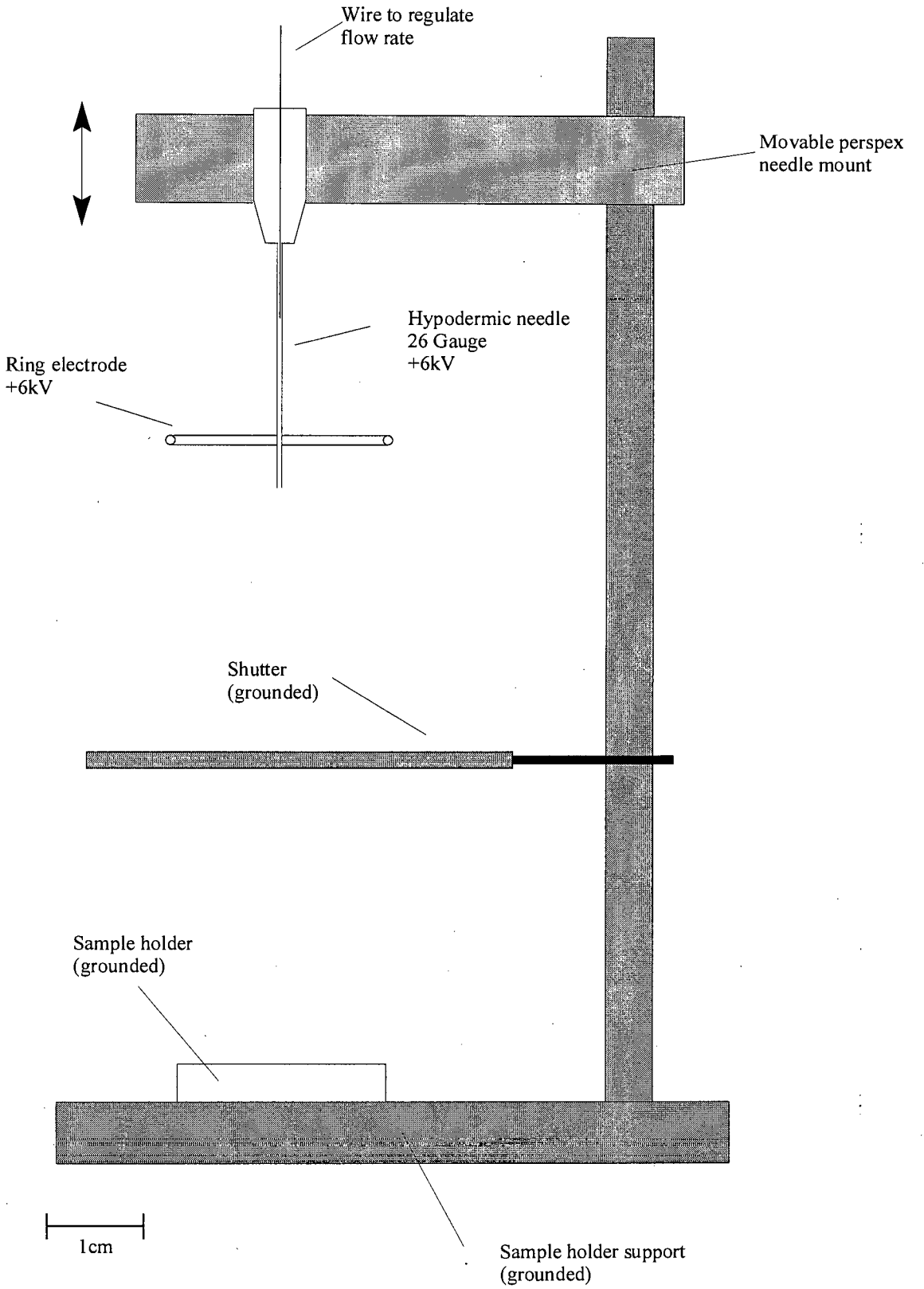

Figure 3.1 Electrospray sample preparation apparatus

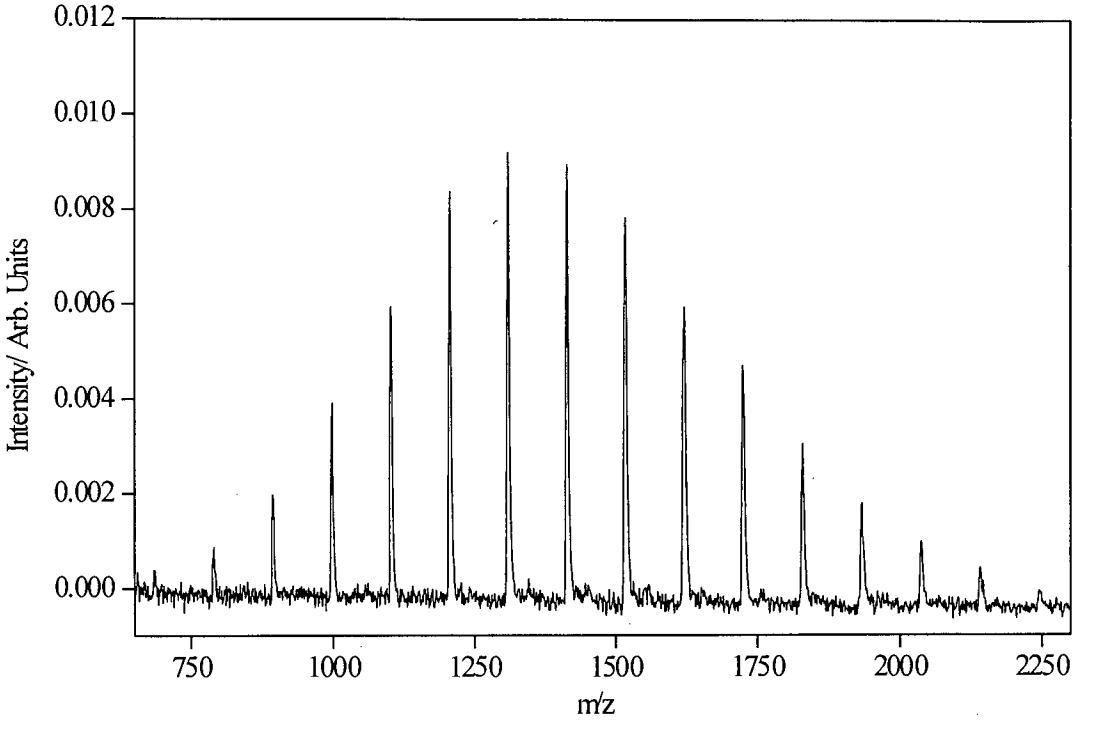

Figure 3.2 Example of polystyrene mass spectrum produced using the electrospray sample preparation method. Dithranol was used as the matrix and $AgCF_3CO_2$ as the salt.

The reproducibility across samples was studied by collecting a series of spectra from a sprayed sample. Polystyrene samples were used with an average molecular weight of 1340 Da. A typical mass spectrum is shown in figure 3.2. In the reproducibility experiment presented here, 13 spectra were collected. All spectra were the summed averages of 50 single shot spectra. During data acquisition, the sample holder was moved at a constant speed of 60 $\mu m\ s^{-1}$ relative to the laser by means of computer controlled stepper motors. This ensured that every laser pulse hit a previously unused spot. The data were evaluated by making a comparison of the area under the 12-mer peak of polystyrene in each spectrum collected. The normalised results are presented in figure 3.3. As can clearly be seen, quite good

reproducibility was achieved, with all peak areas recorded falling within 25% of the mean peak area.

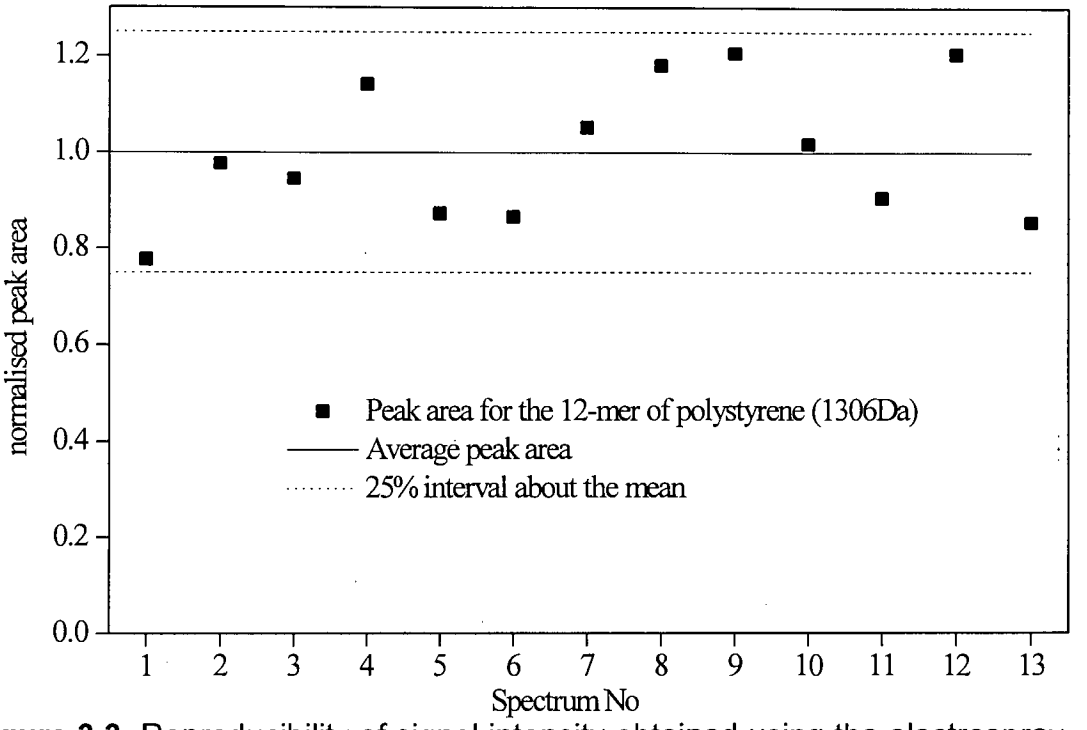

Figure 3.3 Reproducibility of signal intensity obtained using the electrospray method. The variation in normalised peak areas of the 12-mer peak of polystyrene from a series of spectra collected from the same sample holder is shown.

Although the electrospray method was very successful for producing reproducible data from samples that lend themselves to one-stage sample deposition, the same was not found for two-stage sample preparation, owing to problems encountered in switching spray conditions between the salt solution and the matrix/analyte solution. Another drawback of the electrospray technique was the comparatively complex procedure required for optimising spray conditions and the necessity of working with high voltages. For these reasons, another spray technique was developed.

3.3.3 The aerosol method

The spray gun used in these experiments was a modified thin layer chromatography (TLC) spray gun. The solvent reservoir of the spray gun was replaced with a 7 mL glass sample vial. The vial was attached to the spray gun by means of the vial's plastic lid, which had been punctured to allow a tube, which was attached to the spray gun nozzle, to be inserted into the vial. Compressed air was used to produce the aerosol. As with the droplet technique, both single and two-stage sample deposition could be used.

For two-stage sample preparation, 1.5 mL of salt solution (0.01 M in deionised water) was sprayed onto a heated sample holder. The sample holder was heated to aid the evaporation of the water. The total area sprayed was a circle of *ca* 5 cm diameter. The sample holder was at the centre of the spray circle and measured 2 cm in diameter. A uniform dry salt layer was deposited over the full area of the sample holder. The sample holder was then allowed to cool to room temperature. Once the sample holder had cooled, the second solution was sprayed onto the sample holder. The solution sprayed consisted of 0.75 mL matrix solution (*e.g.* 10 g L^{-1} dithranol in THF) mixed with 0.75 mL of polymer solution (1 mM solution). The matrix/polymer solution could be seen to wet the previously deposited salt layer before the solvent evaporated, ensuring good mixing between all three sample components. It was essential that the sample holder should be cold, as decomposition/reaction of polymer molecules has been observed as a result of spraying the second coat onto a hot substrate. The sample produced had a very

homogenous surface and it was shown that a large number of spectra could be recorded with very reproducible peak intensities (a spread of *ca* 25% around the average). During data acquisition the sample holder was moved by stepper motor at a speed of 60 $\mu m\ s^{-1}$, ensuring that every single shot spectrum was collected from a fresh part of the sample.

The reproducibility of the aerosol technique was tested in the same way as the electrospray technique. The results are shown in figure 3.4. It should be noted that, with this experiment, a two-stage sample preparation technique was used. As can be seen, reasonable reproducibility was obtained, with all values falling within 25% of the mean.

The aerosol technique was extremely robust and easy to use. It gave good reproducibilty both for one and two-stage sample deposition. During the course of this work, the aerosol technique was used for most experiments that required good reproducibility. The technique also proved to be a useful tool when analysing samples that only produced weak signal intensity as, owing to the large size of the sample spot, it was possible to produce spectra averaged over several thousand laser shots, with each single shot hitting a previously unused part of the sample surface. By averaging over such a large number of shots, the signal-to-noise ratio could be improved.

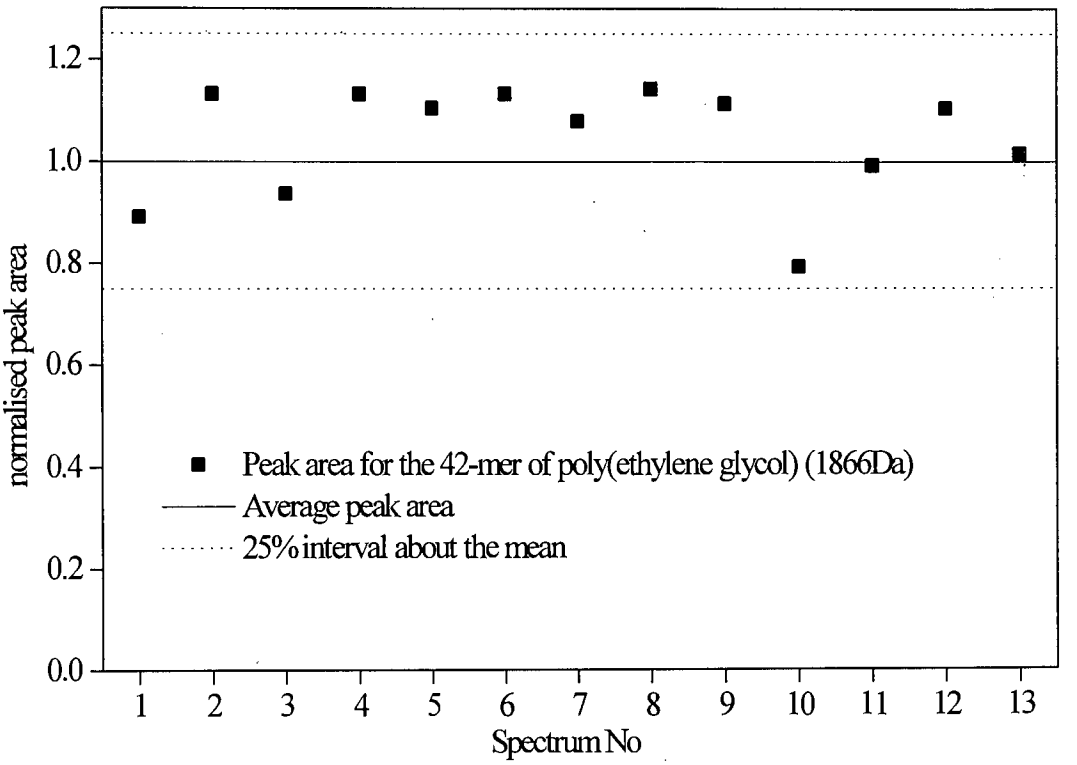

Figure 3.4 Reproducibility of signal intensity obtained using the aerosol method. The variation in normalised peak areas of the 42-mer peak of poly(ethylene glycol) from a series of spectra collected from the same sample holder is shown.

3.4 Conclusions

This chapter has provided an overview of sample preparation for polymer MALDI. Several aspects of sample preparation, such as choice of matrix and addition of salt were addressed.

Three different methods of sample deposition were described and the advantages and disadvantages of each technique were discussed. The droplet method was found to be most useful in the analysis of large numbers of different samples. It

was, however, limited in its use for experiments requiring good shot-to-shot reproducibility of signal intensity.

Two spray techniques were investigated, namely an electrospray and an aersosol spray technique. The spray techniques were both seen to produce large sample spots with very homogeneous sample surfaces. The reproducibilty of signal intensity was shown to be good for both techniques. The good reproducibility meant that these techniques are well suited as sample deposition techniques, when conducting experiments where quantitative data are required. Both spray techniques were useful for depositing samples in a one-stage approach. However, the electrospray technique was found to be difficult to use for two-stage sample deposition, whereas the aerosol technique was not subject to this restraint. The aerosol technique was also found to be easier to use and more robust than the electrospray technique. However, spray techniques may be too time consuming to be used for the routine analysis of large numbers of samples.

3.5 References

[1] J. Axelson, A. Hoberg, C. Waterson, P. Myatt, G. L. Shield, J. Varney, D. M. Haddleton and P. J. Derrick, *Rapid Commun. Mass Spectrom.*, **11**, 209-213 (1997)

[2] D. C. Schriemer and L. Li, *Anal. Chem.*, **68**, 2721-2725 (1996)

[3] D. C. Schriemer and L. Li, *Anal. Chem.*, **69**, 4169-4175 (1997)

[4] I. A. Mowat and R. J. Donovan, *Rapid Commun. Mass Spectrom.*, **9**, 82-90 (1995)

[5] H. Rashidezadeh and B. C. Guo, *J. Am. Soc. Mass Spectrom.*, **9**, 724-730 (1998)

[6] G. Montaudo, M. S. Montaudo, C. Puglisi and F. Samperi, *Rapid Commun. Mass Spectrom.*, **8**, 1011-1015 (1994)

[7] P. Juhasz and C. E. Costello, *Rapid Commun. Mass Spectrom.*, **7**, 343-351 (1993)

[8] P. O. Danis and D. E. Karr, *Org. Mass Spectrom.*, **28**, 923-925 (1993)

[9] K. L. Walker, M. S. Kahr, C. L. Wilkins, Z. Xu and J. S. Moore, *J. Am. Soc. Mass Spectrom.*, **5**, 731-739 (1994)

[10] M. J. Deery, K. R. Jennings, C. B. Jasieczek, D. M. Haddleton, A.T. Jackson, H. T. Yates and J. H. Scrivens, *Rapid Commun. Mass Spectrom.*, **11**, 57-62 (1997)

[11] Ian A. Mowat, PhD Thesis, The University of Edinburgh (1995)

[12] R. R. Hensel, R. C. King and K. G. Owens, *Rapid Commun. Mass Spectrom.*, **11**, 1785-1793 (1997)

Chapter 4 – Analysis of high-mass polymers

4.1 Introduction

One of the aims of this research was to extend the mass range over which the existing mass spectrometer was usable. Previously, the instrument was only effective up to *ca* 5 kDa, for polymer analysis.

This chapter describes the results obtained for high-mass polymers. Improvements in sample preparation technique and instrumental design required for higher mass detection are discussed. For this work, high-mass is defined as being any polymer of mass over 10 kDa. The average molecular weights obtained by MALDI are compared with average molecular weights quoted by the manufacturers, which were obtained by different techniques such as size exclusion chromatography. Issues that need to be considered for high-mass detection in MALDI are discussed.

4.2 Detection Systems

Possibly the major limiting factor in MALDI time-of-flight mass spectrometery for the analysis of high-mass molecules is the detection system [1,2]. The most commonly described detector systems used for laser time-of-flight mass

spectrometers are based around microchannel plate (MCP) or electron multipliers. The detector used in this work was MCP based. The detection efficiency of MCPs and electron multipliers is approximately proportional to the velocity of the ion impacting on the detector [3]. A detailed study of the relationship between ion velocity and detection efficiency of MCP detectors for ions of up to 1000 Da in mass was carried out by MacFarlane and Geno [3]. Their work clearly shows a large drop off in detection efficiency with decreasing ion velocity. Ions hitting the detector at velocities less than 20 km s^{-1} have detection probabilities below 5%. Figure 4.1 shows the relationship between ion velocity and ion mass at three different accelerating potentials. This clearly illustrates the rapid decrease in ion velocities with increasing mass, so that even at the highest accelerating voltage of 30 kV, the ion velocity drops below 20 km s^{-1} at a mass of only 15000 Da.

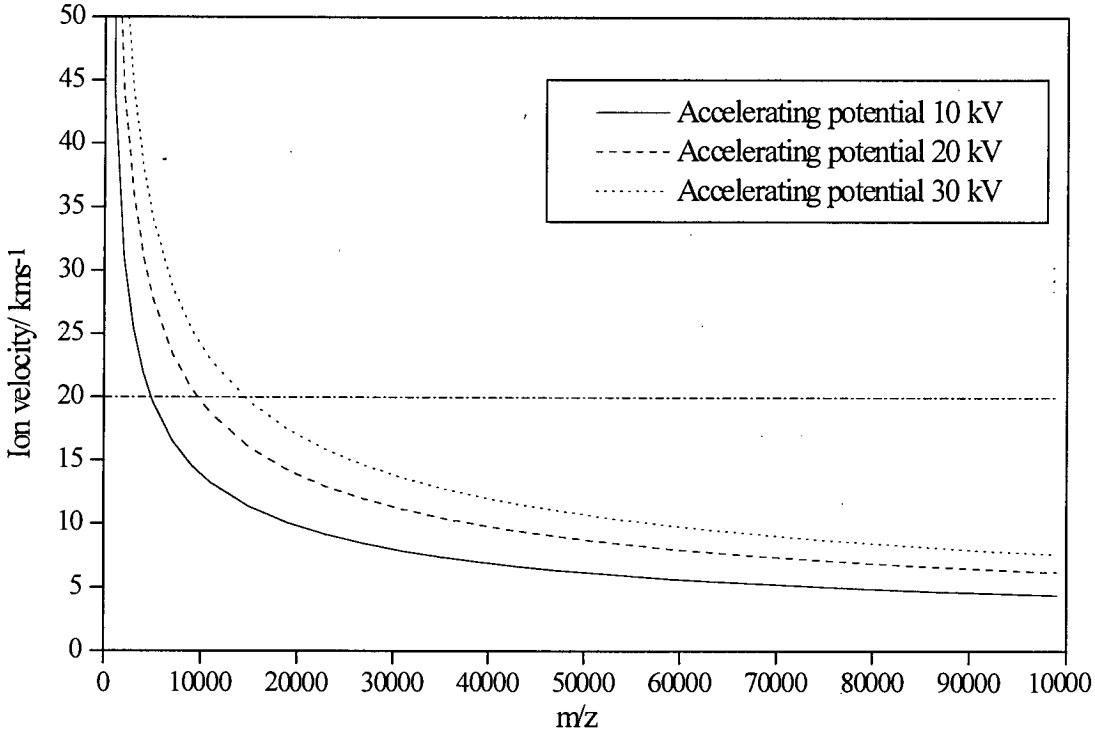

Figure 4.1 Change in ion velocity with ion mass

In MCP based detectors, like the one used for this research, saturation effects linked to low mass ions are often observed [4]. In order to detect high-mass ions high accelerating potentials are used, which leads to very fast low mass ions hitting the detector before the high-mass ions. The fast low mass ions can produce large electron currents which often lead to detector saturation. In order to overcome the saturation problems, a gated deflection plate was installed in the field free drift region of the mass spectrometer (discussed in detail in section 2.5).

4.3 Sample preparation for high-mass polymers

Sample preparation is of key importance in MALDI. In a recent paper, Li *et al.* showed that with the proper choice of matrix and cationising agent, and with careful sample preparation, it was possible to mass analyse monodisperse polystyrene samples with average molecular weights up to 1.5 MDa, using a commercial MALDI mass spectrometer [5]. These impressive results show that, even when using conventional MALDI equipment, it should be possible to analyse large molecular weight polymers. However, the analysis of polymers over 100000 Da is rarely reported in the literature [6,7]. The aim of this work was to extend our working mass range up to 50000 Da.

In order to test the capability of our mass spectrometer, which was retro-fitted with a mass gate, polymer calibration standards for GPC columns were analysed. The polymer standards were purchased from Polymer Laboratories Ltd (Church

Stretton, Shropshire, UK) and were well characterised by GPC [8]. The polymers studied were polystyrene (M_p 11000 Da and 20000 Da), poly(ethylene glycol) (M_p 8500 Da and 11000 Da) and poly(methyl methacrylate) (M_p 20000 Da), M_p refers to the most probable mass of a polymer mass distribution.

Various different sample preparation techniques were tried. The most successful procedure for PEG and PMMA was achieved by combining a 10 μL aliquot of $1*10^{-3}$ mol L^{-1} PEG or PMMA solution in 1:1 methanol/water with 90 μL of $50*10^{-3}$ mol L^{-1} 2-(4-hydroxyphenylazo) benzoic acid (HABA) solution in 1,4-dioxane. To this mixture 1 μL of $20*10^{-3}$ mol L^{-1} salt solution was added. A 0.5 μL droplet of the resulting mixture was spotted onto the stainless steel sample holder and was left to crystallise [9].

Polystyrene samples were prepared by combining 10 μL of $1*10^{-3}$ mol L^{-1} polystyrene solution with 90 μL of 0.15 mol L^{-1} *trans*-retinoic acid solution, both in THF. A 1 μL portion of silver nitrate saturated in ethanol was added to the matrix polymer mixture [9].

Dithranol was also used as a matrix for polystyrene and PEG samples. The dithranol sample preparation technique has been used very successfully for oligomers below 5000 Da [10]. Dithranol was made up to $50*10^{-3}$ mol L^{-1} in THF. The polymer samples were made up to $100*10^{-6}$ mol L^{-1} in acetonitrile for PEG and THF for polystyrene. Equal volumes of the polymer and matrix solutions were mixed. A

salt solution droplet (1 g L^{-1}) of between 1 and 3 μL was deposited on the sample holder and a 1-3 μL portion of the polymer matrix mixture was then injected into the salt droplet.

4.4 Results

The results obtained for higher mass polymers are shown in figures 4.2 to 4.8. The results will be discussed in terms of the types of polymer studied and will be compared with mass data obtained using other techniques.

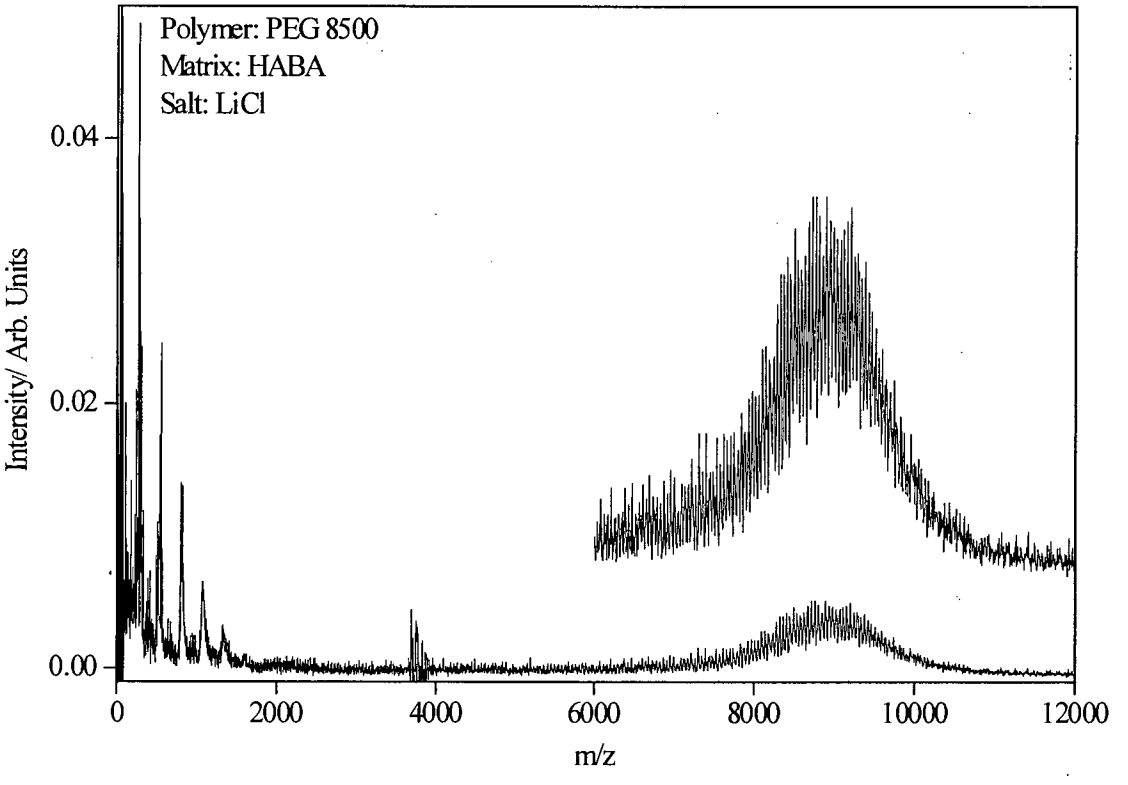

Figure 4.2 MALDI mass spectrum of PEG (av. mol. wt. 8500), HABA was used as the matrix and LiCl as the cation donor

4.4.1 Poly(ethylene glycol)

Figures 4.2 and 4.3 show results obtained for PEG with an average molecular weight of 8500 Da. The matrix used for these experiments was HABA and LiCl was used as the cation source for adduct formation. Figure 4.2 shows the full time-of-flight mass spectrum. The signal below 50 Da is due to switching noise from firing the laser. Similarly, the features observed between 3500 Da and 4000 Da are due to switching noise from the mass gate. The peaks between 200 Da and 2000 Da are due to matrix multimers. The matrix species observed are neutrals formed through post source decay (*c.f.* chapter 5), as all ions are deflected by the deflector plates of the mass gate.

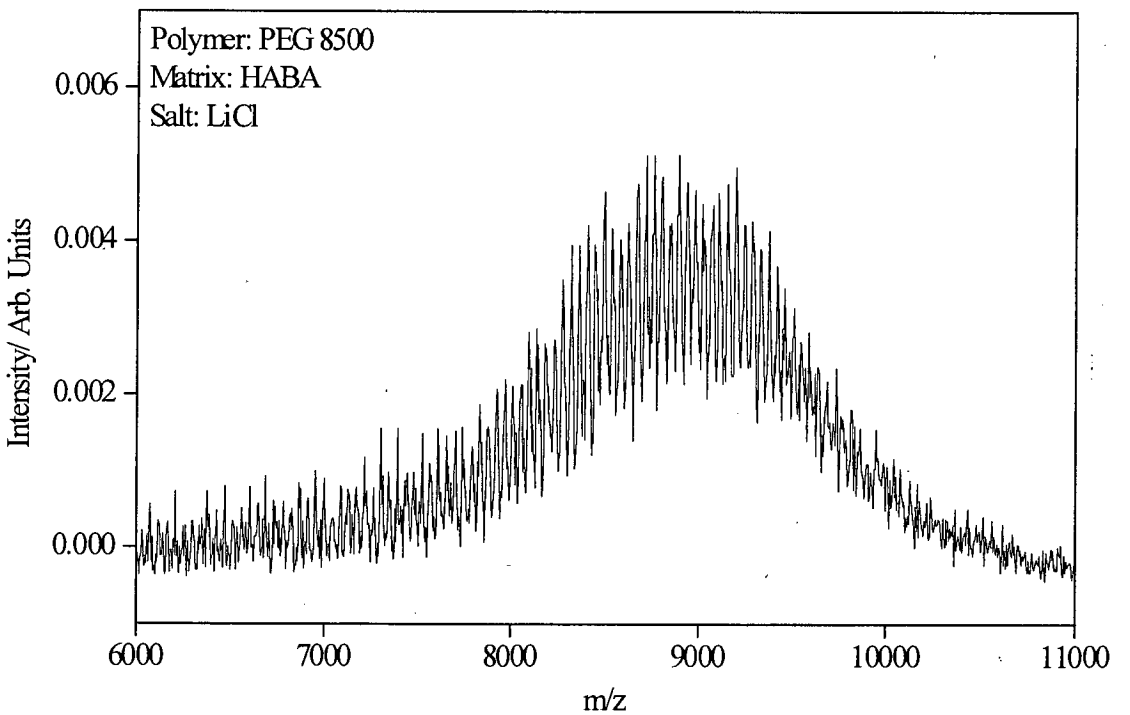

Figure 4.3 Expansion of the polymer distribution shown in figure 4.2

Figure 4.3 is an expansion of the polymer region of figure 4.2. Single oligomer peaks are resolved. The separation between the peaks is 44 Da, the repeat unit mass of PEG. It can be seen from the expanded spectrum that with increasing

mass the oligomer peaks become less well separated. The decreased separation would be expected and is inherent to time-of-flight mass spectrometry

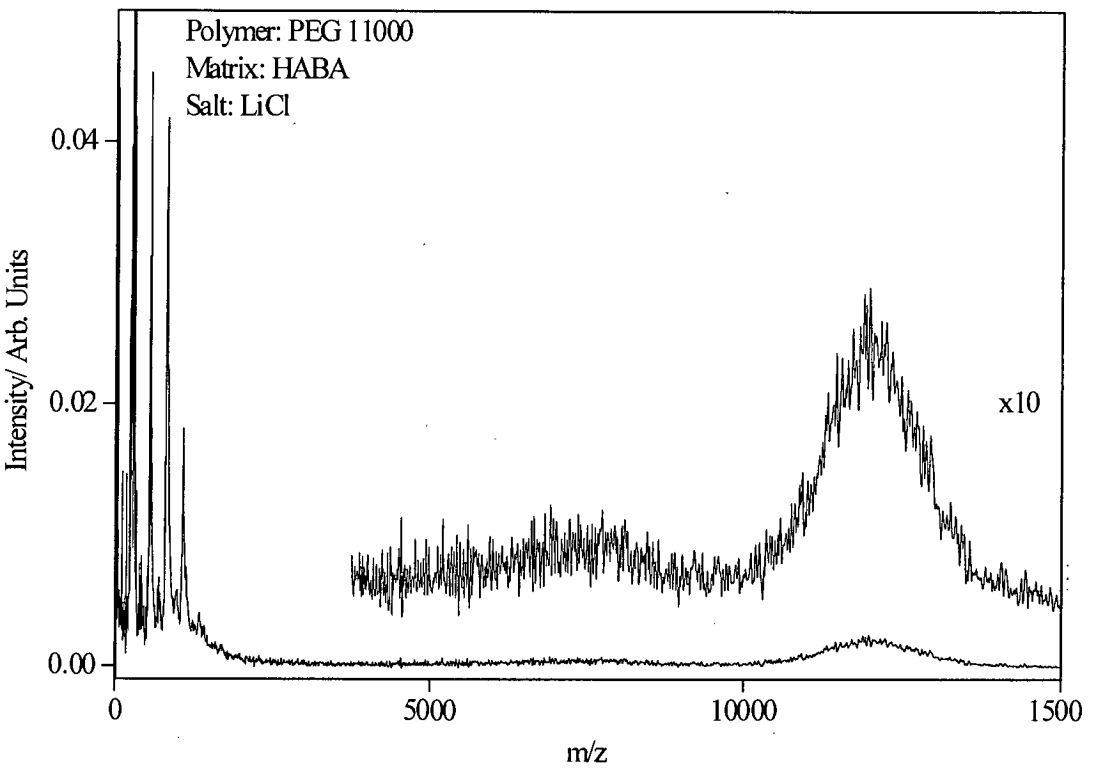

Figure 4.4 Mass spectrum of PEG (av. mol. wt. 11000 Da), the matrix used was HABA and the salt used was LiCl

A second PEG standard with an average molecular weight of 11000 Da was analysed. The mass spectrum obtained for this polymer is shown in figure 4.4. The sample was prepared in the same way as the previous sample. Unlike the PEG with an average molecular weight of 8500 Da discussed previously, no fine structure can be seen in this example. However, the overall mass distribution is clearly discernible. The polymer appears to have a bimodal mass distribution, with maxima at 12000 Da and 7500 Da. The part of the mass distribution centred at 12000 Da appears much stronger than the 7500 Da constituent. The bimodal mass distribution could be due to the method of sample preparation employed by the manufacturer e.g.

mixing of two polymers of different average molecular weights. Contamination of the sample is an unlikely explanation, as these results were readily reproducible on different days with freshly made up samples on each occasion.

4.4.2 Polystyrene

Two polystyrene standards were studied. The first polystyrene that was investigated had a quoted average molecular weight of *ca* 11000 Da. The matrix used in this experiment was *trans*-retinoic acid and $AgNO_3$ was used as the cation donor for adduct formation. The mass spectrum for the polystyrene is shown in figure 4.5. Single oligomers are clearly resolved in the polymer distribution, which ranges from 7500 Da to 14000 Da. The repeat unit observed is 104 Da, as would be expected for polystyrene.

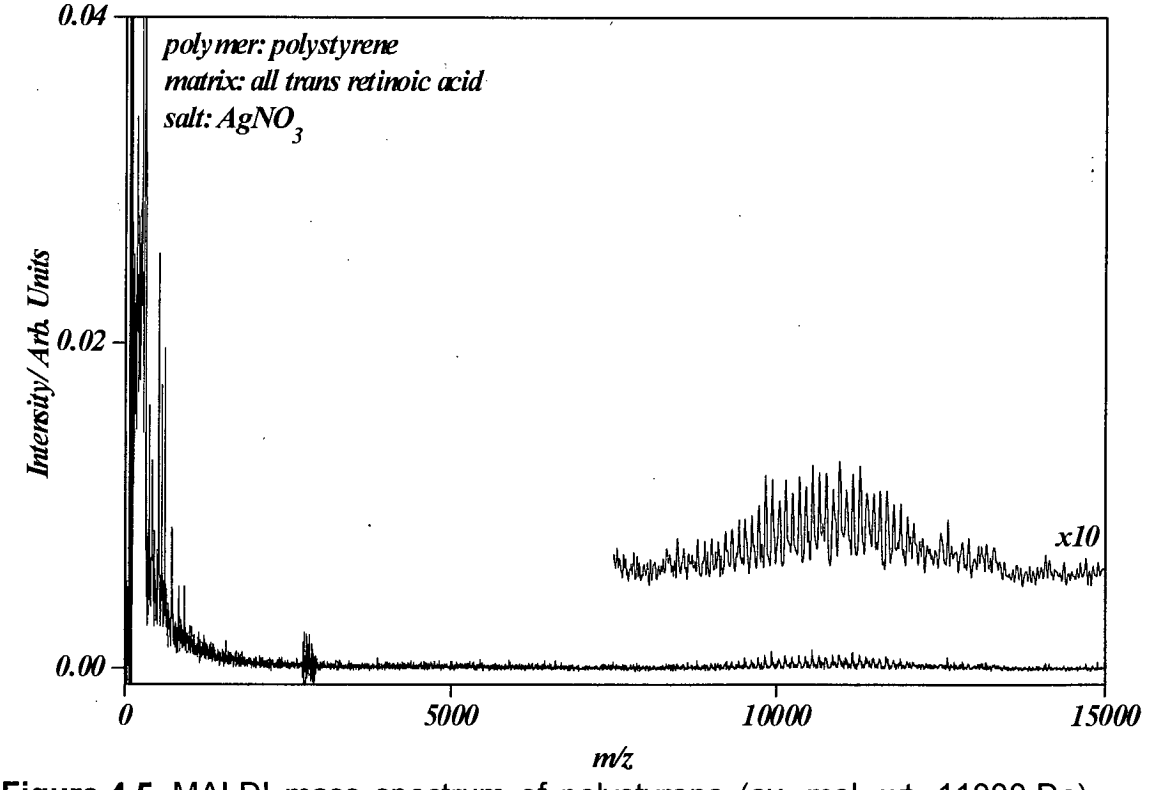

Figure 4.5 MALDI mass spectrum of polystyrene (av. mol. wt. 11000 Da), *trans*-retinoic acid was used as the matrix and $AgNO_3$ as the salt.

Figure 4.6 shows the mass spectrum obtained for a polystyrene sample with an average molecular weight of 20000 Da. A mass distribution centred at 20000 Da can clearly be seen in the spectrum. However, a second mass distribution centred at 40000 Da is also present. The second mass distribution can be attributed to dimerisation of the polymer. The dimerisation of larger synthetic polymers has been seen by other workers in this field. The observation of a polymer mass distribution at 40000 Da, shows that it should be possible to mass analyse polymers of at least 40000 Da, with the instrument in its current configuration. Appropriate polymer standards were not available at the time this work was conducted to test the upper mass detection limit of the instrument.

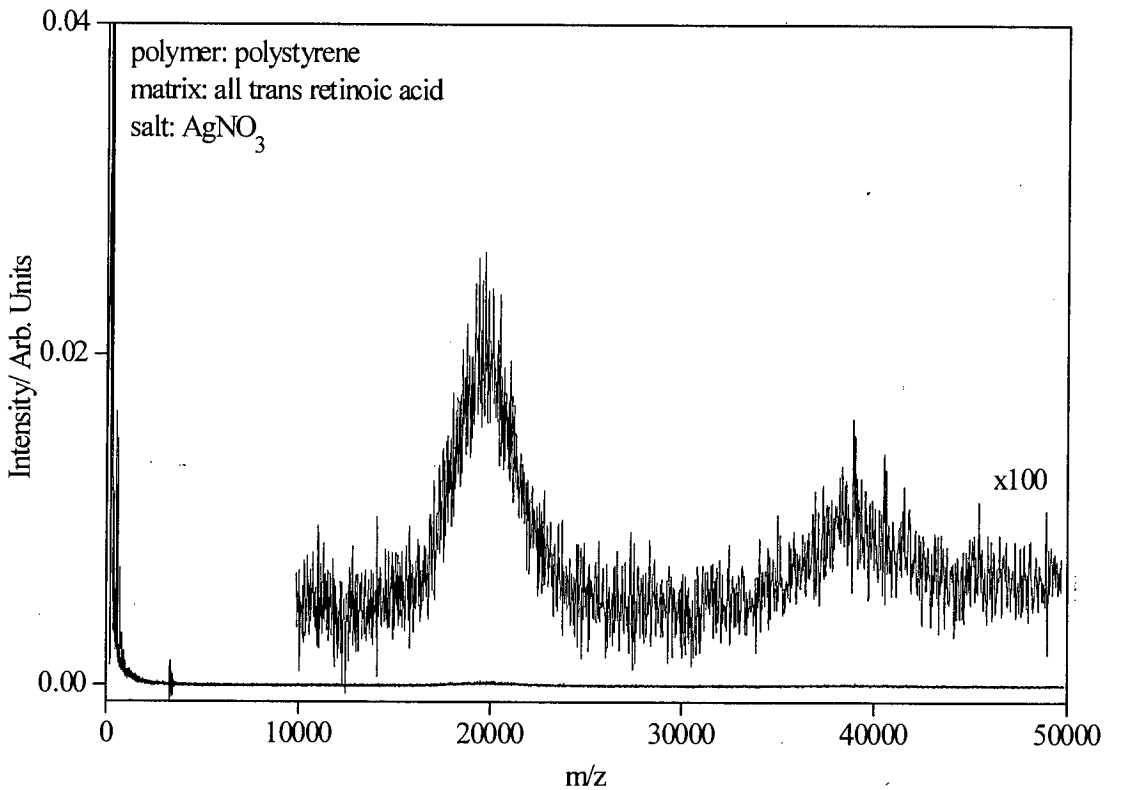

Figure 4.6 MALDI mass spectrum of polystyrene (av. mol. wt. 20000 Da), *trans*-retinoic acid was used as the matrix and $AgNO_3$ as the salt.

4.4.3 Poly(methyl methacrylate)

One PMMA standard was investigated. No detailed information on this sample was available from the manufacturer other than an approximate average molecular weight of 20000 Da. The sample was also assumed to be monodisperse*, as it was intended for use as a GPC standard. The reason for including this comparatively poorly defined sample in this study was to extend the range of polymers studied. The sample preparation employed HABA as the matrix and LiCl as the added salt.

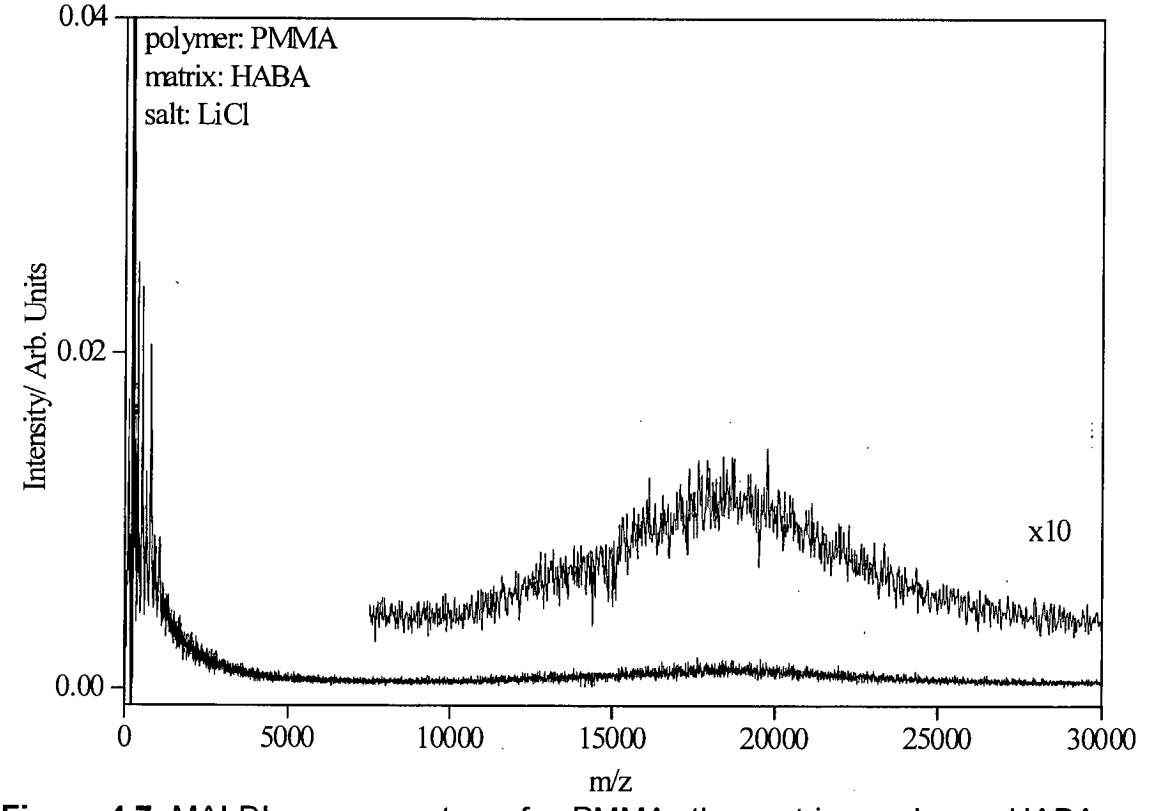

Figure 4.7 MALDI mass spectrum for PMMA, the matrix used was HABA and the added salt was LiCl.

* monodisperse is a general term used to describe narrow polymer distributions. The strict definition of this term is the case where $M_W:M_n=1$, however in practice monodisperse is often taken to mean $M_W:M_n\approx1$

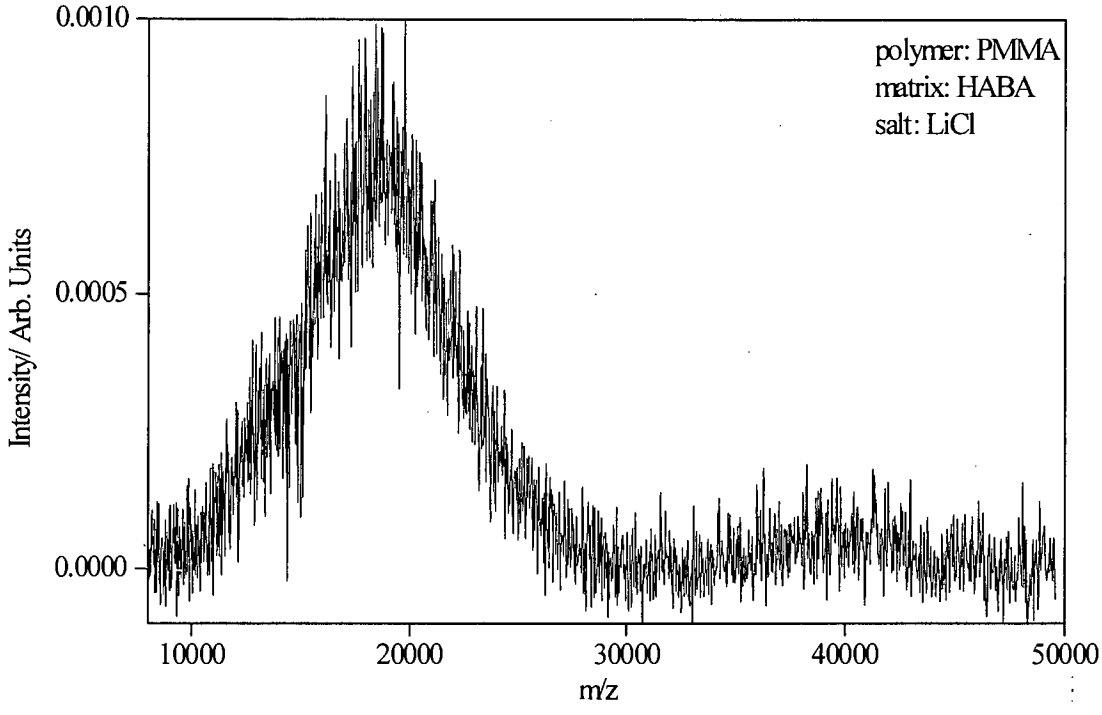

Figure 4.8 Expansion of high-mass region shown in figure 4.7

The mass spectrum recorded for this polymer is shown in figure 4.7. A polymer distribution is seen centred on 18000 Da. Single oligomers would not be expected to be resolved at this mass and no single oligomer peaks are observed. Figure 4.8, is an expansion of the PMMA mass spectrum. The polymer mass distribution is shown in greater detail and the mass range is expanded up to 50000 Da. There appears to be a weak signal for a polymer dimer distribution centred at *ca* 40000 Da.

4.5 Comparison of MALDI results with GPC results

The average molecular weights obtained by MALDI were compared with GPC data obtained from the polymer manufacturers. As all samples studied were monodisperse, good agreement between values obtained using MALDI and GPC was expected.

4.5.1 Number averaged molecular weight

The number averaged molecular weight (M_n) is one of the generally accepted measures of the average molecular weight of synthetic polymers. M_n is calculated using equation 4.1

$$Mn = \frac{\sum NiMi}{\sum Ni} \qquad \textbf{4.1}$$

where M_i is a mass within the polymer distribution and N_i is the signal intensity of mass M_i.

M_n gives greater weighting to the low mass end of the mass distribution. The results for the M_n calculations are presented in Table 4.1. As expected, there is generally good agreement between the values obtained by GPC and MALDI. The difference between the MALDI and GPC values is less than 3% in all but one example. The largest discrepancy between MALDI and GPC values is seen for the lighter PEG sample, which is also the lightest polymer investigated.

Polymer	MALDI	GPC	% difference
	M_n/ Da	M_n/ Da	
Polystyrene	10,684	10,664	0.2
Polystyrene	19,879	19,756	0.6
Poly(ethylene glycol)	8,903	8,338	6.8
Poly(ethylene glycol)	10,660	10,930	2.5
Poly(methyl methacrylate)	18,500	20,000*	-

*No reliable GPC Data available

Table 4.1 Comparison of M_n values obtained by MALDI and GPC

4.5.2 Weight averaged molecular weight

The weight-averaged molecular weight (M_W) is another measure of the average molecular weight of a synthetic polymer. M_W emphasises the higher molecular weight part of the distribution. M_W is given by equation 4.2

$$Mw = \frac{\sum (NiMi)^2}{\sum NiMi} \qquad \textbf{4.2}$$

where M_i is a mass within the polymer distribution and N_i is the signal intensity of mass M_i.

As with M_n there was good agreement between MALDI and GPC values. Again all GPC and MALDI values were within 3% of each other, with the exception of the lighter PEG sample.

Polymer	MALDI	GPC	% difference
	M_W/ Da	M_W/ Da	
Polystyrene	10,874	10,908	0.3
Polystyrene	20,071	20,298	1.1
Poly(ethylene glycol)	9,155	8,454	8.3
Poly(ethylene glycol)	11,020	11,275	2.3
Poly(methyl methacrylate)	19,135	20,000*	-

*No reliable GPC Data available

Table 4.2 Comparison of M_w values obtained by MALDI and GPC

4.5.3 Polydispersity

The polydispersity is a measure of the width of the mass distribution. The polydispersity is determined by dividing M_W by M_n. The agreement between MALDI and GPC is excellent for all polymers studied, with less than 2.5% difference between MALDI and GPC values for all polymers studied.

Polymer	MALDI	GPC	% difference
	M_W/M_n	M_W/M_n	
Polystyrene	1.018	1.02	0.2
Polystyrene	1.01	1.03	2.0
Poly(ethylene glycol)	1.028	1.014	1.4
Poly(ethylene glycol)	1.034	1.032	0.2
Poly(methyl methacrylate)	1.034	-*	-

*No reliable GPC Data available

Table 4.3 Values for polydispersity obtained by MALDI and GPC

4.6 Fragmentation of polymers

Under non-ideal conditions intense low-mass signals were observed when analysing standard polymer samples. Examples of mass spectra showing such low-mass signals are given in figures 4.9 and 4.10, for polystyrene and PEG samples, respectively. The large low mass signal was only observed when dithranol was used as the matrix. One probable reason for this was the higher laser energy required to produce mass spectra with the dithranol samples. Dithranol had previously been used with great success to analyse a large range of smaller polymers.

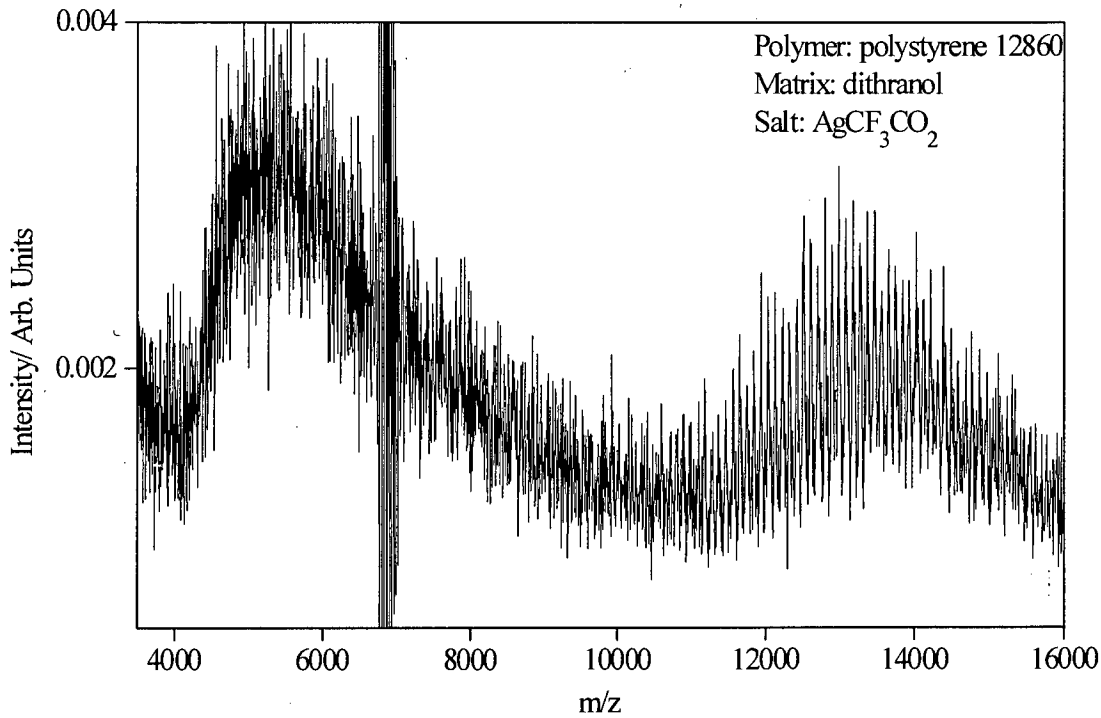

Figure 4.9 Mass spectrum of polystyrene 12860 with an unusual sloping feature (m/z = 4000 - 10000). The matrix used was dithranol and the salt used was $AgCF_3CO_2$

Figure 4.9 shows a mass spectrum of polystyrene. A sloping feature extending from 4000 Da to 10000 Da can be seen as well as the polymer distribution, extending from 10000 Da to 16000 Da. The mass gate deflected all ions of mass lower than 4000 Da, which led to the cut-off at 4000 Da. The sloping feature exhibits no discernible fine structure. The large signal around 7000 Da is due to switching noise from the mass gate.

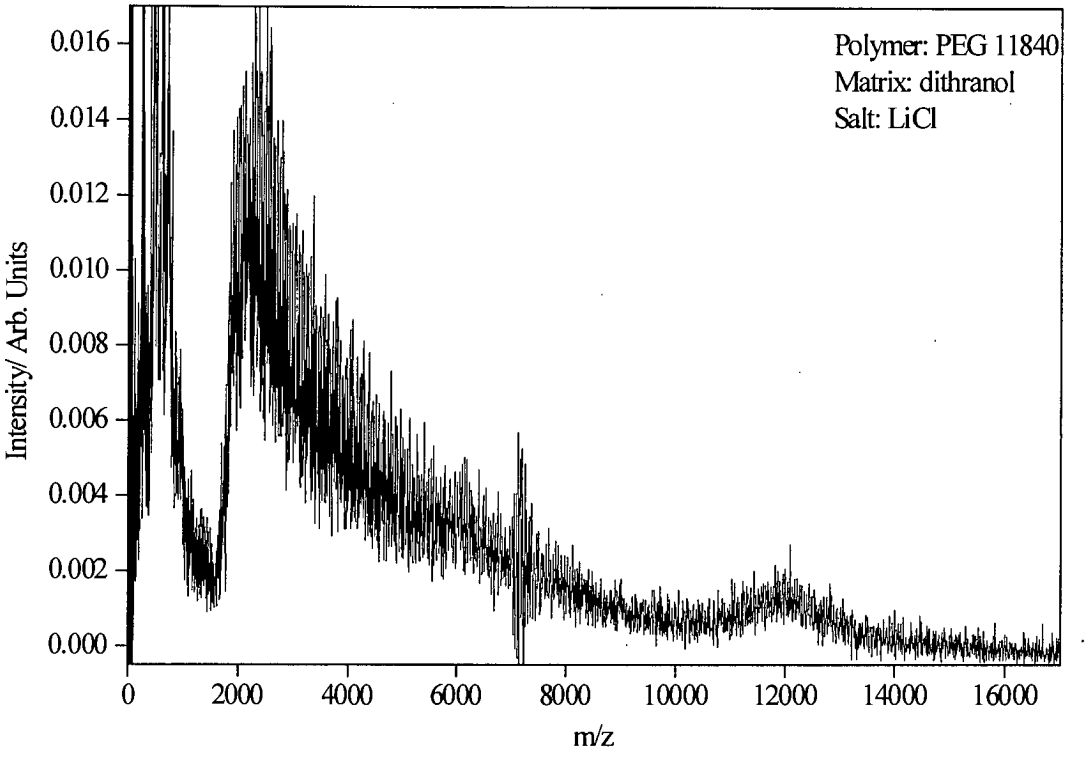

Figure 4.10 Mass spectrum for PEG exhibiting a sloping background

The spectrum in figure 4.10 is dominated by a sloping background extending from 2000 Da upward in mass. The cut-off at 2000 Da is due to the mass gate, which deflected all ions below 2000 Da in mass. Superimposed on the sloping background is the polymer distribution, extending from 10000 Da to 14000 Da. An expansion of the mass region 2400 Da to 3050 Da reveals well resolved peaks within the sloping part of the mass spectrum (see figure 4.11). Three series of peaks, two strong series and one series of peaks of lower intensity are observed. The separation between peaks in each series is 44 Da, the repeat unit of PEG. These peaks were most probably due to fragmentation products of PEG oligomers. The fragmentation behaviour of polyglycols is well documented and it is thus possible to confirm that the peaks are due to fragment ions [11].

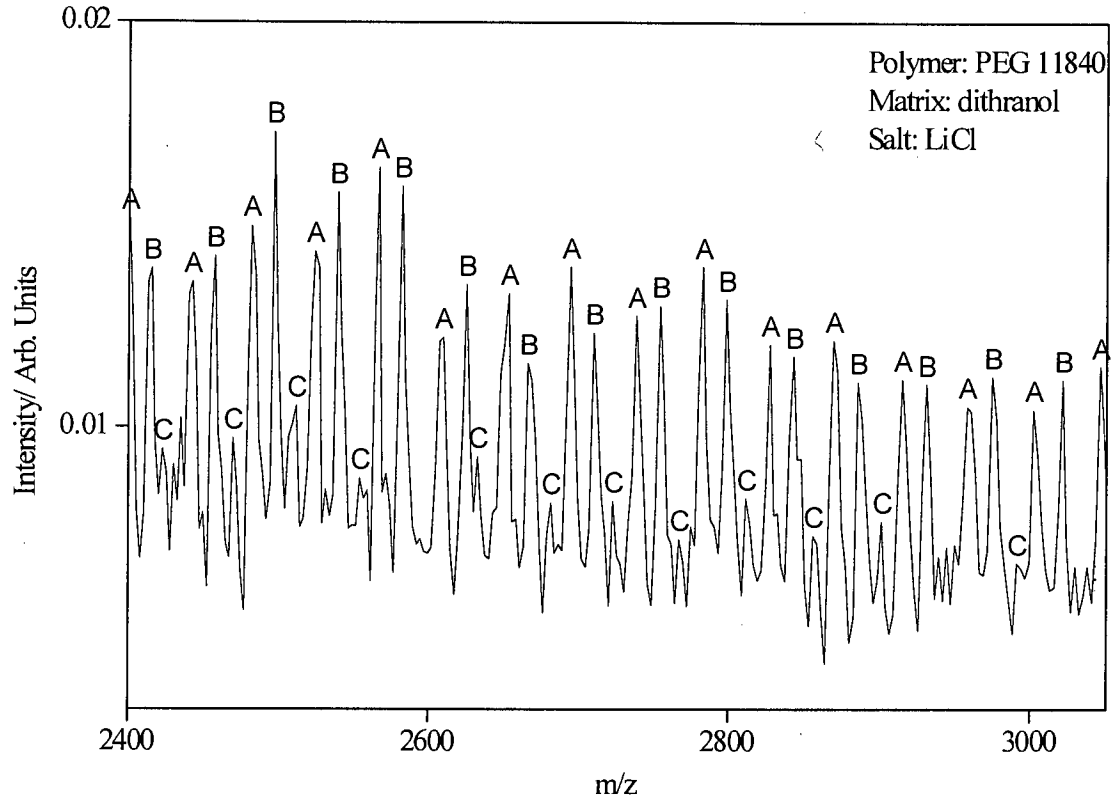

Figure 4.11 Expansion of the sloping part of figure 4.10

Two possible fragmentation pathways are illustrated in figure 4.12. Three possible fragmentation products can be formed through the proposed mechanisms, designated as (A), (B) and (C). Each fragment has its own mass distribution associated with it, with a mass seperation of 44 Da, the repeat unit of PEG. For fragment (A) peaks with masses of (n*44) + 51 are expected for the Li^+ adducts; for Li^+ adducts of (B) expected masses are (n*44) + 67 and for the Li^+ adducts of (C) the expected masses are (n*44) + 39. Therefore, it can easily be shown whether or not the peaks observed in figure 4.11 are caused by fragments formed by the suggested processes, by determining the 'endgroup' masses for the three series of PEG peaks. The expected endgroup masses are 51 Da, 67 Da and 39 Da for (A), (B) and (C), respectively.

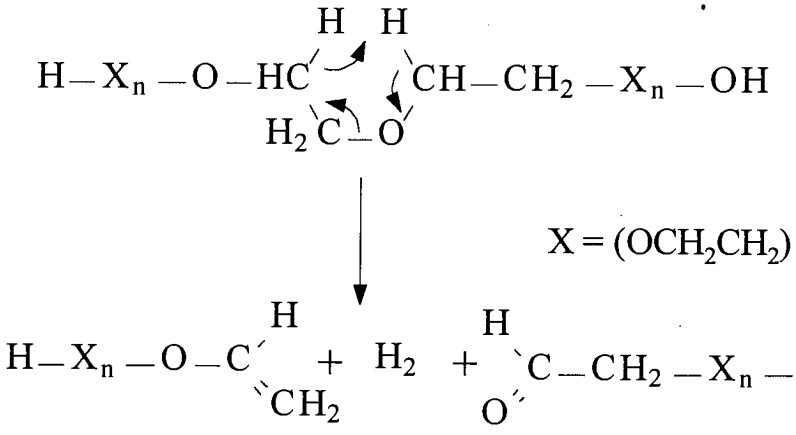

(A)

mass of (A) = (n*44) + 44

mass of Li^+ adduct of (A) = (n*44) + 44 + 7

(B)

mass of (B) = (n*44) + 60

mass of Li^+ adduct of (B) = (n*44) + 60 + 7

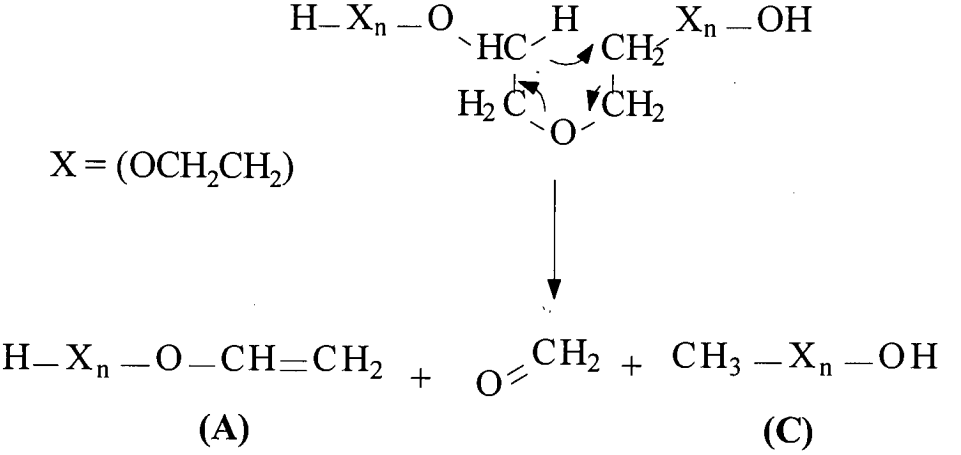

(A)

mass of (A) = (n*44) + 44

mass of Li^+ adduct of (A) = (n*44) + 44 + 7

(C)

mass of (C) = (n*44) + 32

mass of Li^+ adduct of (C) = (n*44) + 32 + 7

Figure 4.12 Suggested fragmentation pathways for poly(ethylene glycol)

The endgroup mass of a polymer with the structure X-$(A)_n$-Y (where A is the repeat unit, X and Y are the endgroups and n is the number of repeat units) can be determined using equation 4.3:

$$X + Y = M - n * A \qquad \textbf{4.3}$$

where M is the mass of the oligomer, A is the mass of the repeat unit, X and Y are the masses of the endgroups and n is the number of repeat units in the oligomer of mass M. This procedure was followed for all well resolved peaks between 2000 Da and 4000 Da in figure 4.10. The endgroup masses determined in this way were plotted against the oligomer mass in figure 4.13.

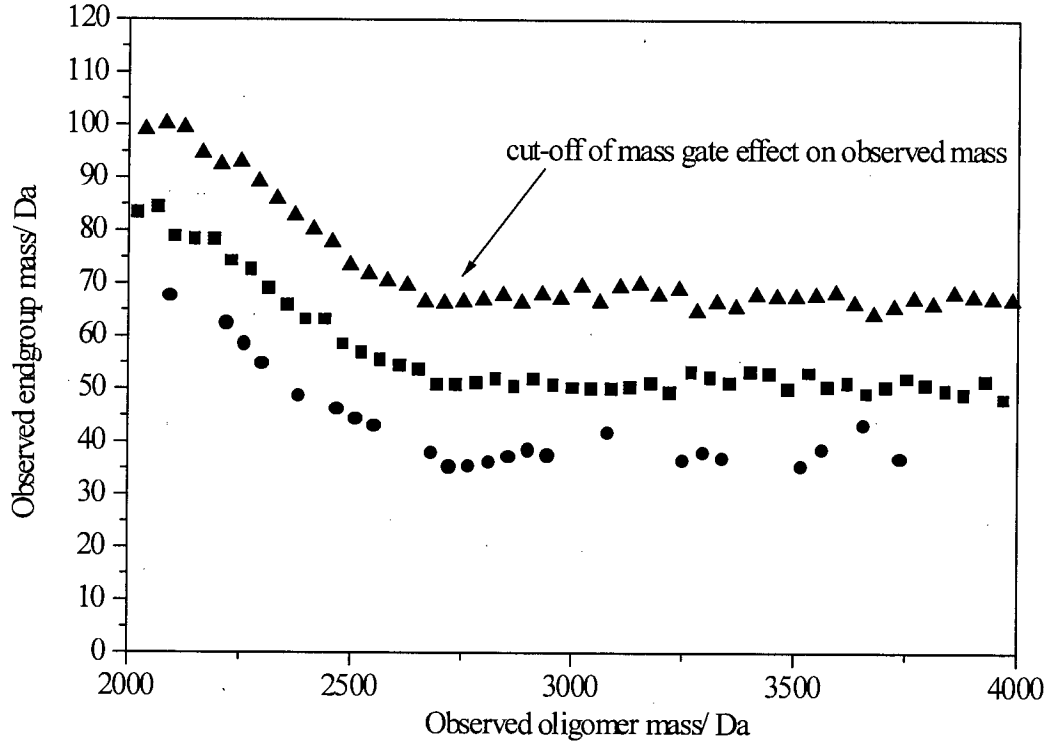

Figure 4.13 Plot of Observed endgroup mass vs observed oligomer mass.

A clear pattern is observed of the calculated endgroup masses decreasing with increasing oligomer mass between oligomer masses of 2000 Da and 2750 Da. For oligomer masses over 2750 Da the endgroup masses stay constant for the three different endgroups observed. The variation in endgroup mass over the lower mass region is an instrumental artefact associated with the type of mass gate employed in obtaining the spectrum. The way in which the mass shift occurs is illustrated in figure 4.14. The ions that appear to have heavier endgroups are in fact retarded by the mass gate, as they had passed through the grounded ion optics before the mass gate was switched off. In order to determine the actual endgroup masses, only endgroup values obtained from peaks in the mass range 2750 to 4000 Da were considered.

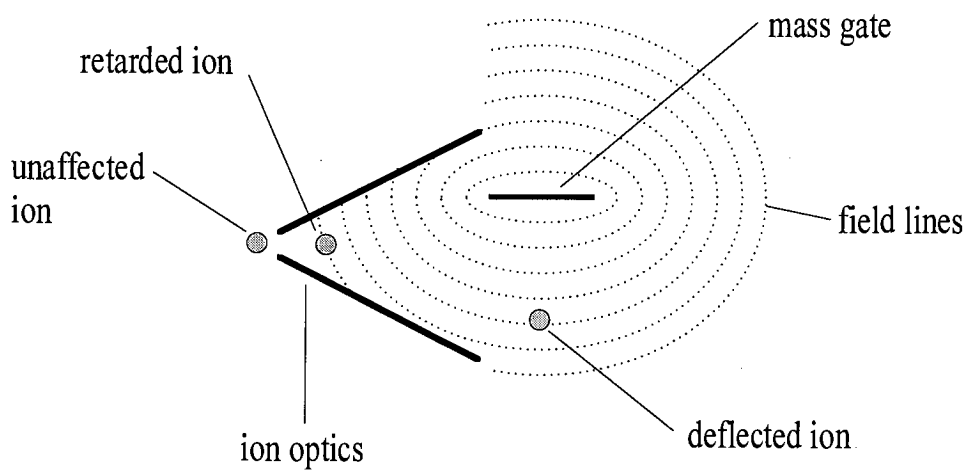

Figure 4.14 Schematic illustration of the effect of the mass gate on ions located in different parts of the mass spectrometer.

Average values were obtained for the three different endgroups; these were 37.3 Da ± 0.5 for the weakest series, and 50.9 Da ± 0.25 and 67.3 Da ± 0.25 for the two stronger series (see figure 4.15). There is good agreement between the expected

and observed endgroup masses for the two most intense series of fragments *i.e.* fragments with an endgroup mass of 51 Da were observed, which matches fragment (A); also fragments with an endgroup mass of 67 Da were seen which is the expected endgroup mass of fragment (B). The weaker series of oligomers in figure 4.11 showed an endgroup mass of 37 Da, which is close to the expected endgroup mass for fragment (C). The discrepancy seen between the expected and observed values for fragment (C) is most likely due to the comparatively weak signal observed for this series in the spectrum, making it difficult to be sure of the exact peak maximum.

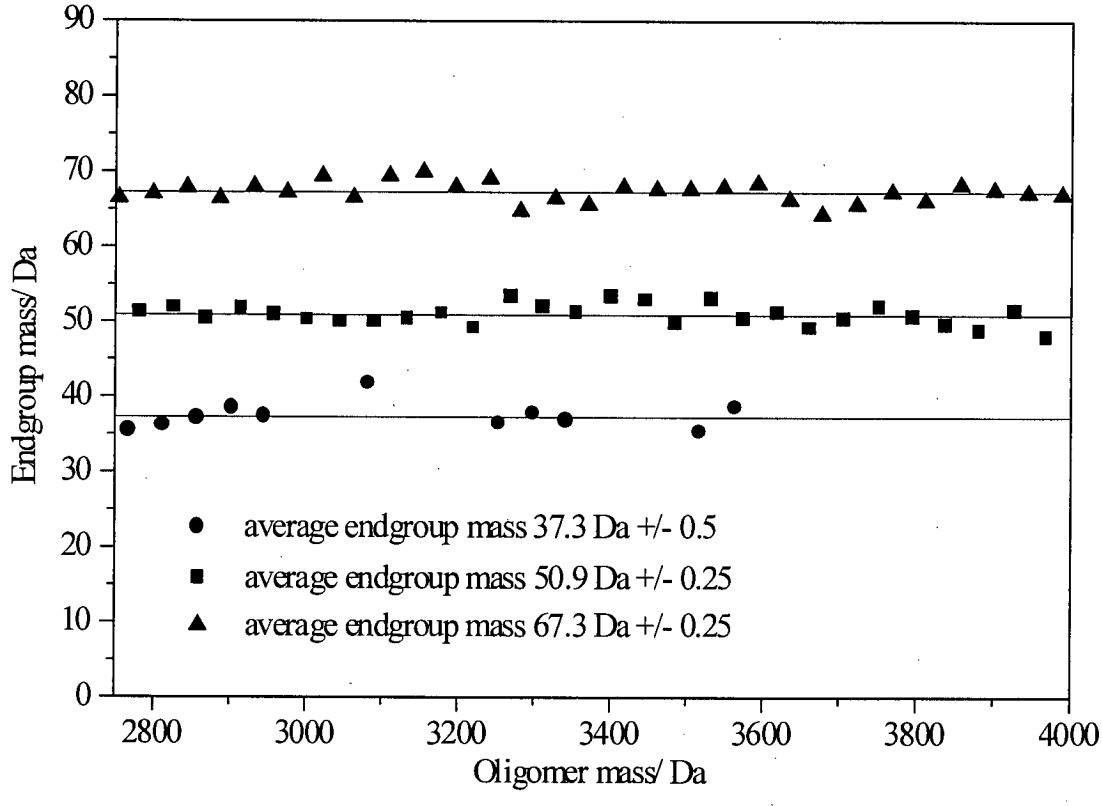

Figure 4.15 Endgroup mass vs oligomer mass used to determine average endgroup masses

No peaks that could be attributed to unfragmented oligomers of lower mass were seen in the region between 2000 Da and 4000 Da. The absence of intact oligomers over this mass range is not unexpected, as the polymer mass distribution

has been shown to be very narrow and confined to a range extending from 10000 Da to 15000 Da (see figure 4.4). Clearly the fragment ions must not be included, when the average molecular weights are calculated. In the example given here, it was easy to distinguish between fragments and molecular ions, as the fragments were well resolved; however, it is obvious that fragmentation could cause a significant distortion of average molecular weights. Inclusion of fragments in the molecular weight distribution is most likely to occur, when fragments and molecular ions are not readily distinguishable, *e.g.* when the resolution does not allow for the identification of single peaks or if there is a strong overlap between fragments and molecular ions. It is therefore very important for accurate average molecular weight determinations that fragmentation be minimised. Fragmentation can be minimised by good sample preparation and judicious use of laser power.

4.7 Conclusions

This chapter shows that with a few instrumental modifications and careful sample preparation, it is possible to characterise polymers with average molecular weights in excess of 5000 Da. The highest mass polymer observed in these experiments had an average molecular weight of around 40000 Da, *i.e.* the dimer ions of polystyrene with an average monomer molecular weight of 20000 Da. The results obtained for a range of polymers by MALDI were compared with the manufacturer's values obtained using GPC. Good agreement was found between the MALDI and the GPC data. Fragmentation was observed when sample preparation was not carried out well. Fragmentation must be carefully controlled and minimised in order to obtain reliable molecular weight data.

4.8 References

[1] D. C. Imrie, J. M. Pentney and J. S. Cottrell, *Rapid Commun. Mass Spectrom.*, **9**, 1293-1296 (1995)

[2] U. Bahr, U. Röhling, C. Lautz, K. Strupat, M. Schürenberg and F. Hillenkamp, *Int. J. Mass Spectrom. Ion Proc.*, **153**, 9-21 (1996)

[3] P. W. Geno and R. D. MacFarlane, *Int. J. Mass Spectrom. Ion Proc.*, **92**, 195-210 (1989)

[4] A. Westman, G. Brinkmalm and D. F. Barofsky, *Int. J. Mass Spectrom. Ion Proc.*, **169/170**, 79-87 (1997)

[5] D. C. Schriemer and L. Li, *Anal. Chem.*, **68**, 2721-2725 (1996)

[6] P. O. Danis and D. E. Karr, *Org. Mass Spectrom.*, **28**, 923-925 (1993)

[7] P. O. Danis, D. E. Karr, F. Mayer, A. Holle and C. H. Watson, *Org. Mass Spectrom.*, **27**, 843-846 (1992)

[8] Calibration notices from Polymer Laboratories Ltd (Church Stretton, Shropshire, UK)

[9] R. M. Whittal, D. C. Schriemer and L. Li, *Anal. Chem.*, **69**, 2734-2741 (1997)

[10] Ian A. Mowat, PhD Thesis, The University of Edinburgh (1995)

[11] L. R. Hittle, D. E. Altland, A. Proctor and D. M. Hercules, *Anal. Chem.*, **66** 2302-2305 (1994)

Chapter 5 – Metal ion detachment studies

5.1 Introduction

The analyte ion species detected in MALDI experiments is usually a neutral-ion complex, commonly referred to as an ion adduct [1]. For peptides and proteins proton adducts are most often seen although alkali metal adducts are also known to form [2]. Synthetic polymers do not readily form adducts with protons but they do form adducts with metal ions [3,4]. The specific metal ion best suited to adduct formation is polymer dependent, although often a range of different metal ions can be used. Several studies have been conducted into metal ion polymer adduct formation [3,5,6]. Metal cations have been shown to attach readily to polystyrene, poly(ethylene glycol) and polybutadiene in IR laser-desorption/time-of-flight experiments [7,8]. Studies of metal ion attachment to polymers under typical MALDI conditions, using salts containing metals of different oxidation states, have shown that only singly charged metal polymer adducts are formed, regardless of the oxidation state of the metal ion in the salt [3,6]. In a recent paper Scrivens *et al.* investigated the collision-induced dissociation (CID) of the alkali metal adducts of poly(methyl methacrylate) (PMMA) oligomers [9]. Different fragmentation patterns were found with different alkali metal ion adducts. The fragmentation was also

shown to vary with oligomer size. As well as fragment ions, a large signal from the bare alkali ions was also observed indicating the loss of the metal ion from the adduct. The alkali metal ion yield was particularly noticeable for Rb^+ and Cs^+ adducts.

The work presented here focuses on the spontaneous post source decay (PSD) of polymer metal ion adducts under standard MALDI conditions. The effect of PSD on the average molecular weight distribution of an oligomeric system was investigated.

5.2 Experimental

For the experiments presented here, the mass spectrometer was operated in two different modes; these were the linear and reflectron modes. In the linear mode, the reflectron was switched off (*i.e.* connected to ground). In this mode of operation, all species that were transmitted into the drift region of the mass spectrometer were detected on the in-line microchannel plate (MCP) detector as illustrated in figure 5.1. The other mode of operation was termed the reflectron mode. In the reflectron mode the reflectron would be switched on. The reflectron is a retarding field produced by a series of lens elements, which are coupled together by a resistor chain, giving rise to a graded field. The front grid of the reflectron is at ground potential and the rear grid is at a high potential, the field strength increasing along the length of the reflectron. The effect that switching on the reflectron has is to retard any charged species that enter it. If the potential on the final element of the reflectron is higher than the

extraction potential applied to the sample holder charged species will not be detected on the in-line MCP detector as they will be turned around by the reflectron and will be accelerated away from the in-line detector (see figure 5.2). This change in direction allows for the ions to be detected using the second MCP (reflectron) detector. If, however, a charged particle *e.g.* a polymer metal ion adduct undergoes decay into a charged and uncharged fragment, in the drift free region of the mass spectrometer, the uncharged fragment is not retarded by the reflectron and is detected on the in-line detector (see figure 5.2). It is therefore possible to determine what species undergo metastable decay in the drift region of the mass spectrometer.

Both the droplet and the aerosol sample preparation methods, described in greater detail in chapter 3, were used.

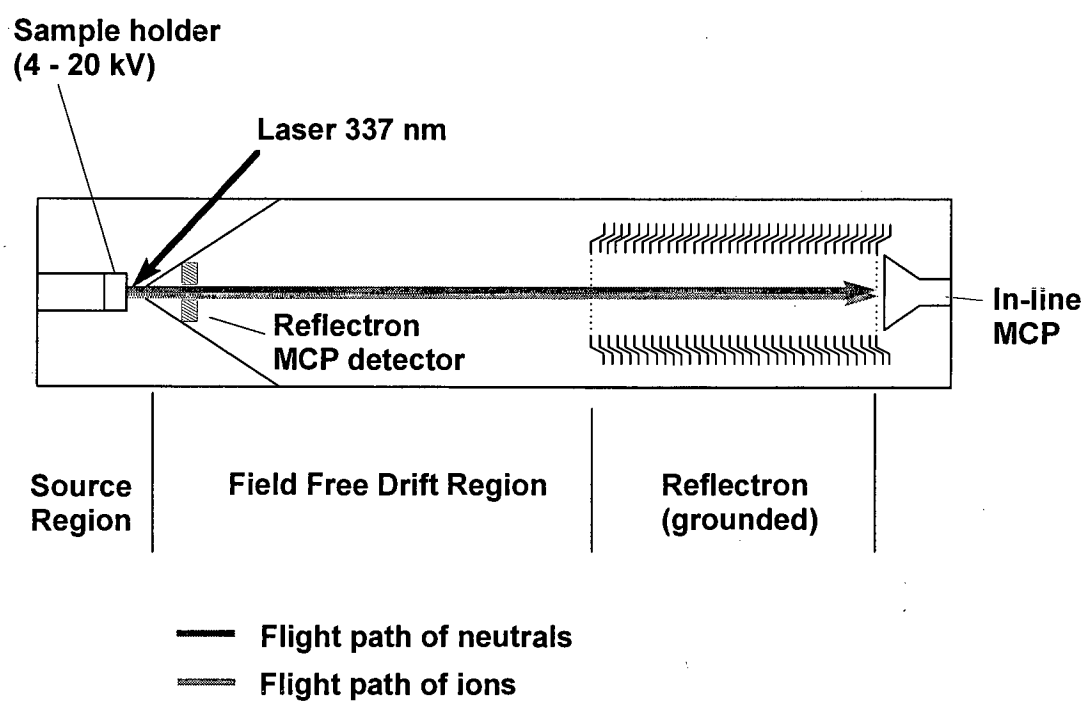

Figure 5.1 Operation of the mass spectrometer in linear mode

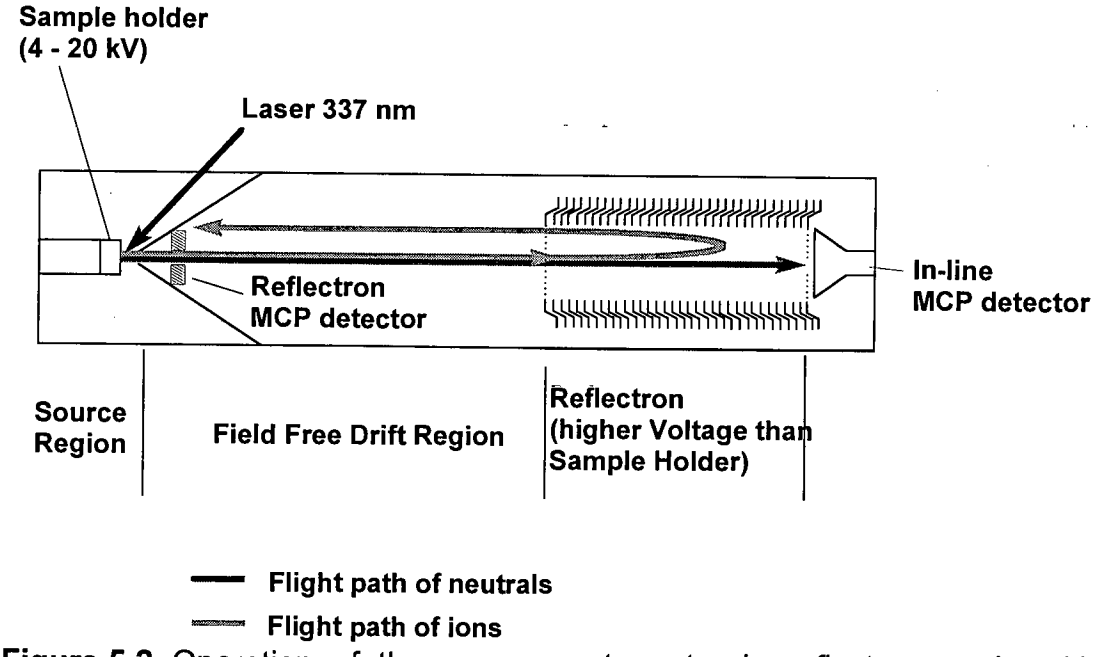

Figure 5.2 Operation of the mass spectrometer in reflectron mode with reflectron voltage above extraction voltage.

5.3 Results and discussion

Various experiments have been carried out to investigate the stability of polymer metal ion adducts. In these experiments use was made of the linear detector in conjunction with the reflectron. With the reflectron switched off ions and neutrals can be detected; however, with the reflectron switched on at a higher voltage than the extraction voltage only neutrals can be detected.

The initial experiment discussed here was a qualitative survey of the post source decay (PSD) behaviour of a range of polymer metal ion systems. A metal ion dependent rate of detachment was found for all polymer systems studied.

A more quantitative study was made using poly(ethylene glycol) adducted to Li^+ and Rb^+, respectively. For these experiments all parameters were fixed apart

from the reflectron voltage which was gradually increased until it was higher than the extraction voltage. The effect of varying the laser energy on the yield of neutrals was also studied.

The effect that fragmentation of polymer/metal ion adducts had on the mass distribution of polydisperse polymers was also investigated.

5.3.1 Qualitative survey of a range of polymer metal ion systems

The aim of these experiments was to find out whether or not polymer metal ion adducts undergo post source decay (PSD), *i.e.* to ascertain whether these systems fragment in the field free drift region of a MALDI mass spectrometer.

A range of different polymer and salt combinations was studied. The polymers used were poly(ethylene glycol) (PEG), poly(methyl methacrylate) (PMMA) and poly(propylene glycol) (PPG) and the salts used were LiCl, NaCl, KCl and RbCl. All samples were prepared using the droplet method described in detail in chapter 3. In these experiment four to five sample spots were prepared on a sample holder. Each sample spot consisted of the same polymer matrix combination; however, a different salt was used for each sample spot. For each polymer salt combination mass spectra were recorded in two different ways. In the first case the reflectron was switched on at a higher potential than the extraction potential so that only neutrals were detected as charged particles were deflected away from the detector. In the other case the reflectron was switched to ground allowing all species that had been transmitted from the source region to the drift region of the mass spectrometer to be detected.

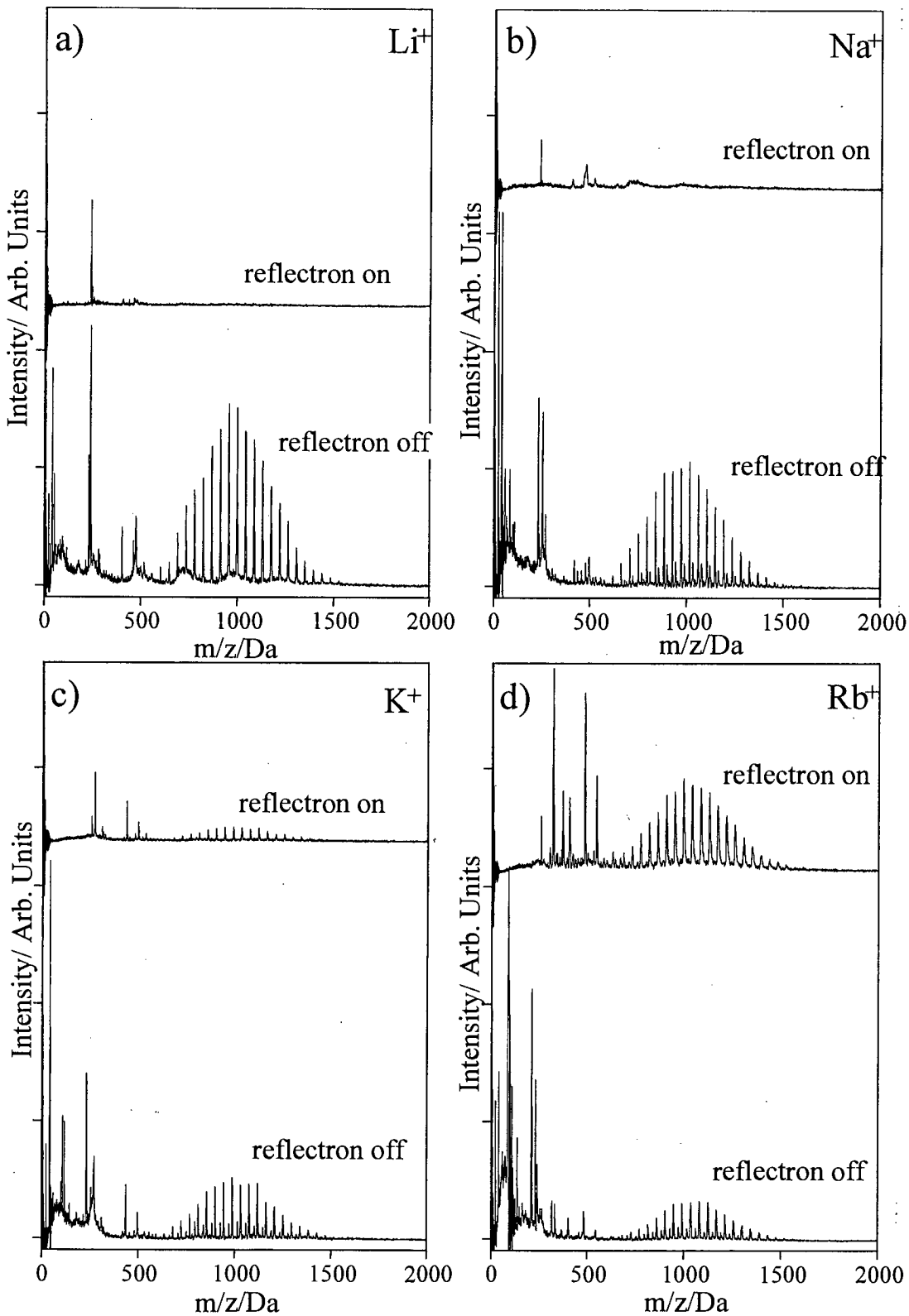

Figure 5.3 MALDI Mass Spectra of PEG with different salts added to provide cations for adduct formation. In the top traces only neutrals are observed while in the bottom traces, neutrals and ions are both observed.

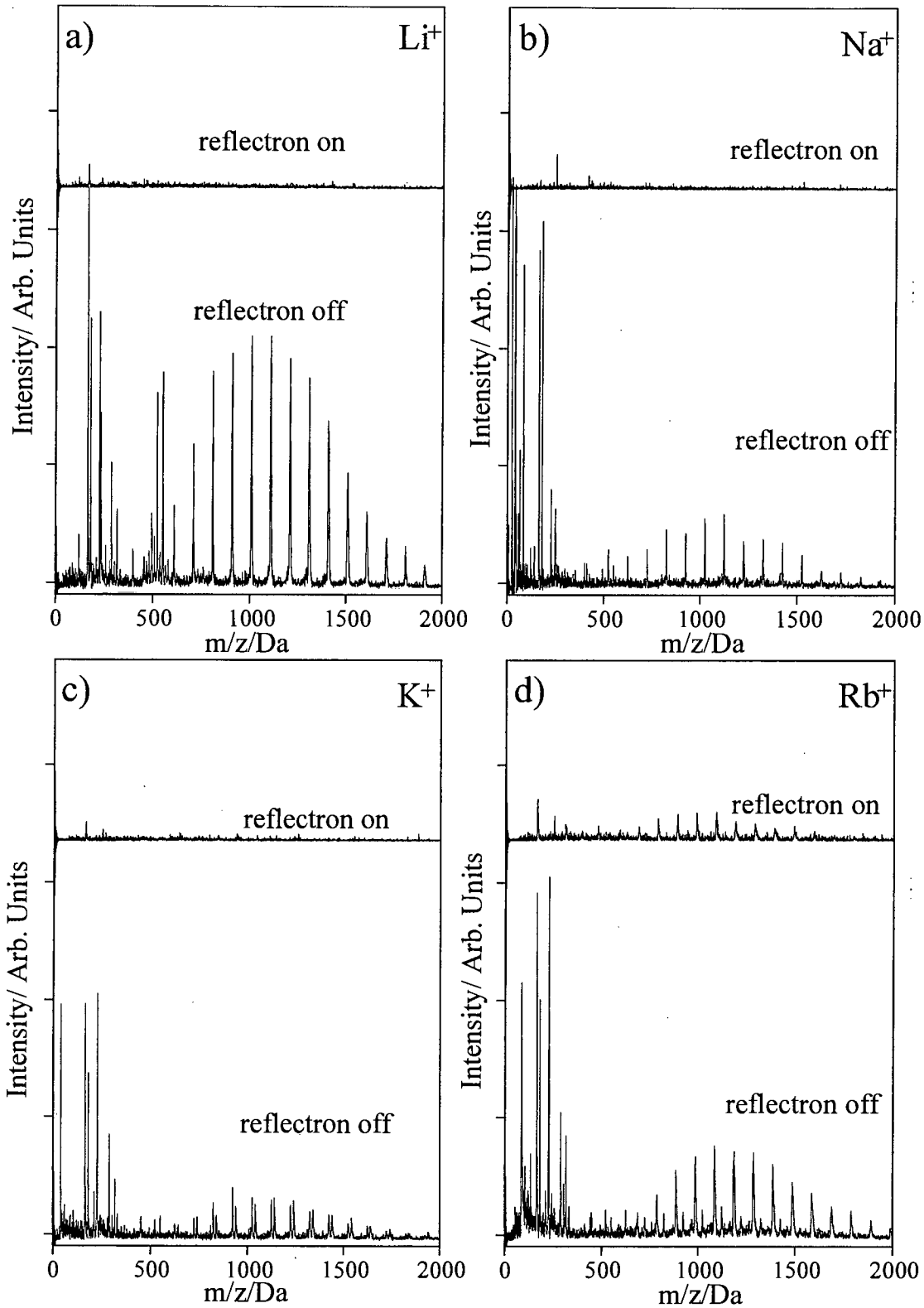

Figure 5.4 MALDI Mass Spectra of PMMA with different salts added to provide cations for adduct formation. In the top traces only neutrals are observed while in the bottom traces, neutrals and ions are both observed.

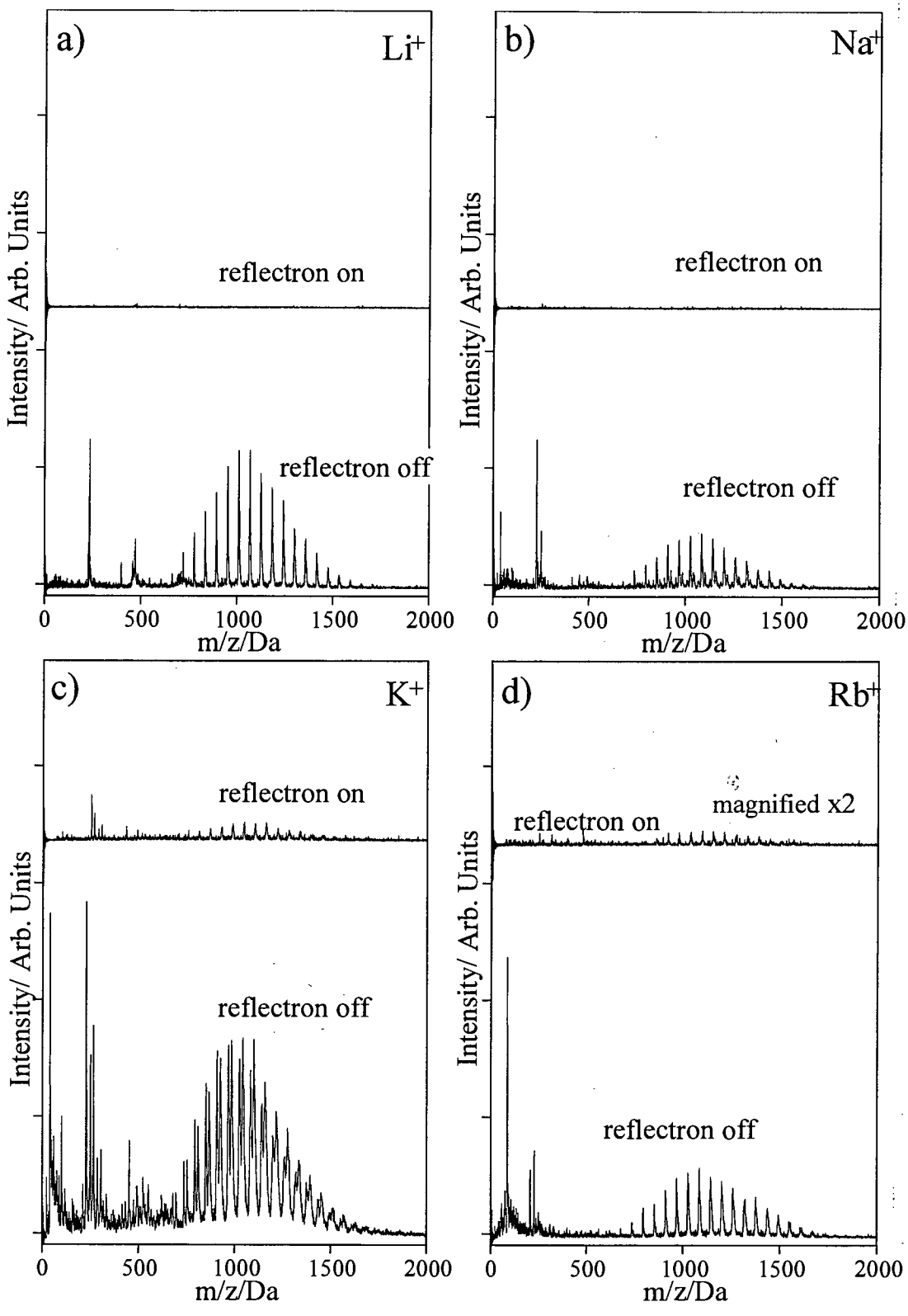

Figure 5.5 MALDI Mass Spectra of PPG with different salts added to provide cations for adduct formation. In the top traces only neutrals are observed while in the bottom traces, neutrals and ions are both observed.

All other experimental parameters, such as the extraction voltage, the gain on the detector and the laser energy, were kept constant.

The results of these experiments showed the same trend for all systems studied. It was found that the larger the metal ion attached to the polymer, the more likely the polymer metal ion adduct was to undergo PSD. These trends will be illustrated here for PEG, PPG and PMMA with Li^+, Na^+, K^+ and Rb^+ attachment; the same phenomena were, however, also observed for higher molecular weight samples. The results obtained for the PEG system are shown in figures 5.3 a-d. The mass spectrum for PEG with LiCl with the reflectron switched to ground is shown in the part spectrum of figure 5.3 a. A polymer distribution can clearly be seen centred on 1000 Da. The separation between oligomer peaks is 44 Da the PEG repeat unit mass. The peaks in the region between 0 and 500 Da are due to metal ions (lithium at 7 Da, sodium at 23 Da and potassium at 39 Da) and to dithranol species *e.g.* the proton adduct of the matrix at 227 Da and at 233 Da, the lithium adduct of the matrix as well as some higher mass peaks caused by protonated and lithiated matrix clusters. It is not clear what the unresolved features underlying the mass spectrum at 500 Da, 750 Da and 1000 Da are; however, they could be due to dithranol clusters. The top mass spectrum in figure 5.3 a was recorded for the lithium PEG system while all ions were deflected away from the detector using the reflectron. As can clearly be seen very few peaks are present in this mass spectrum and notably no peaks are associated with polymer lithium adducts. The most intense peak in this mass spectrum is due to neutrals formed from protonated dithranol. The absence of any polymer-related peaks shows that PEG lithium adducts do not decay under the experimental

conditions. It should also be stressed that no metal ions were detected with the reflectron on, confirming that no charged species were detected with the reflectron at a higher potential than the extraction voltage.

The mass spectra for the NaCl PEG combination (figure 5.3 b) show broadly similar features to the equivalent LiCl PEG mass spectra. The most obvious difference between the mass spectrum for NaCl and PEG with the reflectron off and the corresponding LiCl and PEG mass spectrum is that two overlapping polymer mass distributions are seen in the NaCl case. The major polymer distribution is due to sodiated PEG oligomers whereas the lower intensity polymer distribution, which is offset by 16 Da from the main polymer distribution, can be ascribed to potassiated PEG. Potassium is often found as a contaminant in MALDI mass spectrometry. The top mass spectrum of figure 5.3 b shows no peaks due to polymer related species. The most intense peak is due to neutrals associated with sodiated matrix.

Figure 5.3 c shows the mass spectra for the PEG KCl combination. The lower mass spectrum was recorded with the reflectron off. It shows both sodiated and potassiated PEG oligomers. The less intense polymer distribution being due to sodiated PEG oligomers. The top mass spectrum of figure 5.3 c was recorded with the reflectron on. This mass spectrum is very different from the comparable mass spectra for the lithium and sodium PEG cases as signals corresponding to neutral dissociation products of potassium PEG adducts were observed. It should be noted that only neutrals formed from potassiated PEG oligomers were seen in this mass spectrum. Other neutrals detected were matrix species.

The mass spectra for the RbCl PEG system (figure 5.3 d) show that the Rb^+ adducts of PEG also undergo PSD. Here the signal intensity of the polymer peaks in the upper mass spectrum, *i.e.* the mass spectrum showing only neutral species, is higher than for the lower mass spectrum in which both charged and uncharged particles were detected. As signal intensity can often be used as an approximate measure of the number of particles detected, peaks in mass spectra recorded with the reflectron on would be expected to be less intense than the equivalent peaks in mass spectra recorded with the reflectron off. This is clearly not the case for the polymer peaks in figure 5.3 d. The main reason for this is believed to be detector saturation occurring in the reflectron-off mode due to the large number of low mass ions impacting on the detector which are largely deflected for reflectron-on experiments (see chapter 2 for detailed discussion) [10].

There is a clear trend for the fragmentation of the alkali metal adducts of PEG. The amount of fragmentation observed increases with the size of the alkali metal ion. Whereas lithiated and sodiated PEG does not undergo PSD, both potassiated and rubidiated PEG do.

Similar experiments to those described for PEG were also carried out for PMMA and PPG (figures 5.4 and 5.5). The same trend was observed, *i.e.* the adducts of the heavier alkali metals, rubidium for PMMA and potassium and rubidium for PPG, underwent PSD whereas dissociation products were not detected for the adducts of the lighter alkali metals.

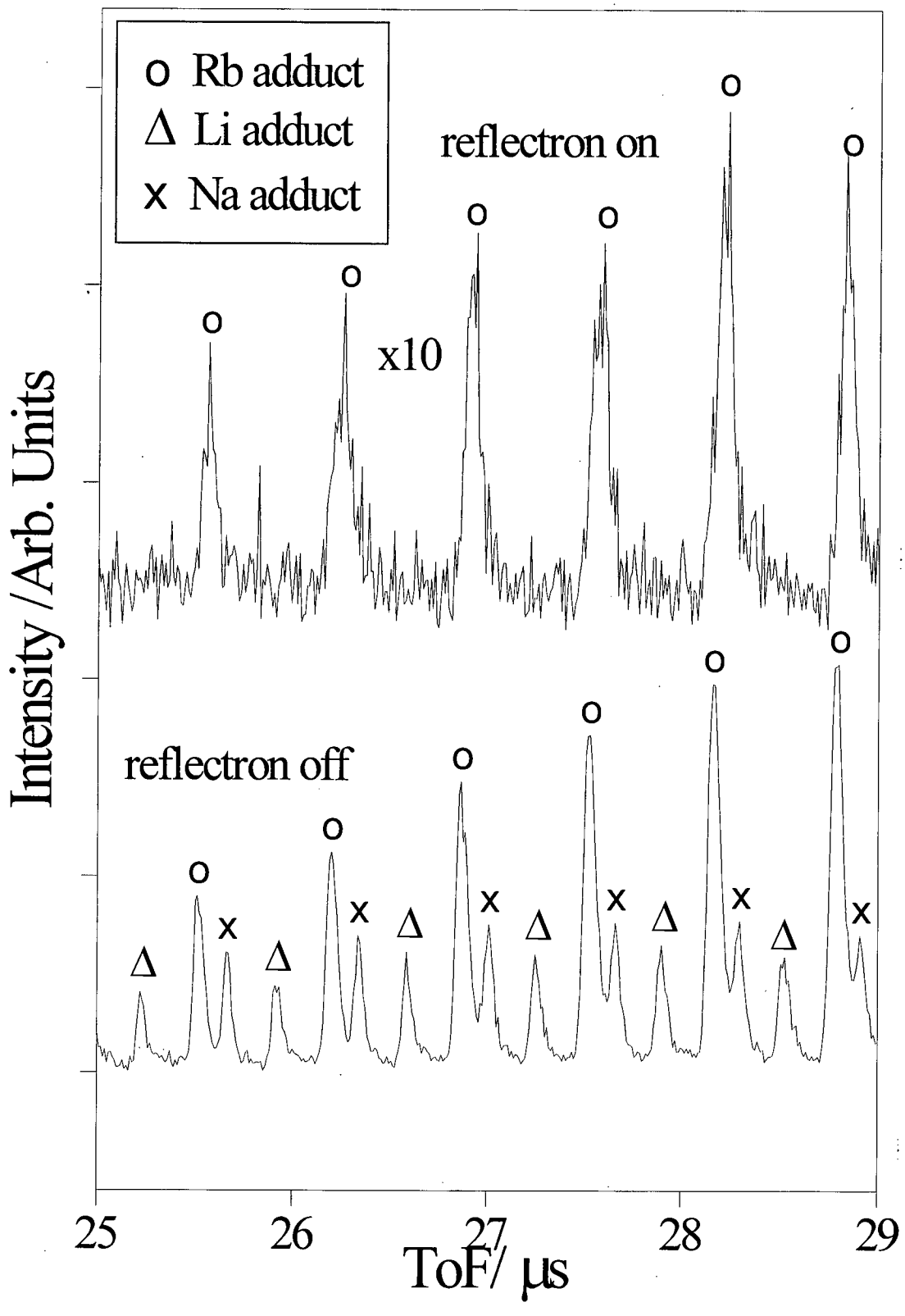

Figure 5.6 MALDI TOF Mass spectra of PEG with a mixture of salts. In the top traces only neutrals are observed while in the bottom traces, neutrals and ions are both observed.

A further experiment was carried out to confirm that the neutral formation observed in the previous experiments was metal ion dependent. A mixture of LiCl and RbCl was used in the sample preparation rather than a single salt to show that under identical conditions Rb^+ adducts dissociate whereas Li^+ adducts do not. The sample prepared for this experiment used PEG and dithranol for the polymer and matrix and a mixture of LiCl and RbCl as the salt. The RbCl concentration (0.0165 M in deionised water) was 30 times larger than the LiCl concentration ($0.5x10^{-3}$ M in deionised water). At a RbCl to LiCl ratio of 30:1 Rb^+ and Li^+ adducts of PEG are both observed, whereas, at a 1:1 ratio, no Rb^+ adduct is observed. The sample was prepared using the aerosol method.

The results for the mixed salts experiment are presented in figure 5.6. When the reflectron is on and only neutrals are detected, only peaks associated with the Rb^+ adduct of PEG was observed. In the reflectron-off mode, Li^+ and Rb^+ adducts were detected, as well as some Na^+ adducts. This experiment shows that, under identical conditions, neutral decay products of the Rb^+ adducts of PEG were detected whereas no such species were detected for Li^+ and Na^+ adducts. These findings indicate that rubidium-containing PEG adducts undergo PSD under typical MALDI conditions and that lithium and sodium adducts of PEG are not subject to PSD.

This initial survey has shown that the tendency for polymer metal adduct ions to dissociate post-source is metal ion dependent. Lithium and sodium-containing polymer adducts do not dissociate post source at a detectable level under typical MALDI conditions. However, a significant fraction of potassium and rubidium

adducts of the polymers studied fragmented in the drift free region of the mass spectrometer.

5.3.2 Post acceleration

It was noted during the initial experiments that neutral fragments had a longer flight time than their charged parent species. The delay seen was *ca* 50 ns over a flight time of 30 μs, the typical flight time of an ion with a mass of 1000 Da at an accelerating voltage of 4 kV (see figure 5.7 a). There are several possible reasons for retardation of neutral fragments. It is conceivable that most of the fragmentation of the adducts occurs in the source region of the mass spectrometer, when the adduct is still being accelerated by the extraction potential. In-source decay would lead to a time delay, as the adduct would not have reached its final velocity at the time of fragmentation and hence the neutral fragment would be moving at a velocity lower than that of the intact adduct. Extensive in-source decay, however, would not just bring about longer average flight times but also considerable peak broadening would be seen for the decay product peaks, as the decay would occur at different stages of the acceleration process. Such peak broadening would be so extensive that detection of neutrals produced in-source would be unlikely. Some peak broadening was seen (see figure 5.7 a) but it is not extensive.

Another possible reason for the delay of the neutrals could be deceleration of ions, by the reflectron prior to decay; however, this process again would have been accompanied by a large amount of peak broadening which was not observed.

The most probable reason for the longer flight times of neutrals compared with those of ions is the post acceleration potential applied to the detector. In order to increase the detection efficiency of the MCP detector, its front face was maintained at a negative potential of -2 kV, which accelerates positive ions into the detector and hence increases their kinetic energy. The post acceleration potential also leads to a decrease of the flight time of positively charged species. Neutral species are not affected by the post acceleration potential and therefore exhibit longer flight times than their parent ions.

A simple experiment was carried out to show whether or not the delay observed was due to the post acceleration or not. For this experiment a sample of RbCl with PEG was made up using the aerosol technique. The detector was set up so that the front face of the detector was at ground potential. Mass spectra were recorded as before, with the reflectron on and with the reflectron off. The same experiment was carried out with the detector set up conventionally, *i.e.* with the -2 kV post acceleration potential. The results are presented in figure 5.7 a for the conventional set-up and figure 5.7 b for the non-post-accelerated set-up. As can be seen from the results, the neutral peaks, *i.e.* the mass spectrum recorded with the reflectron on, in figure 5.7 a are retarded by about 50 ns with respect to the mass spectrum recorded with the reflectron off. The neutral peaks in figure 5.7 b have the same flight time as the peaks in the mass spectrum recorded with the reflectron off. Therefore this experiment shows that the retardation observed was due to the post acceleration potential. All the experiments outlined in this report were carried out with the post acceleration on.

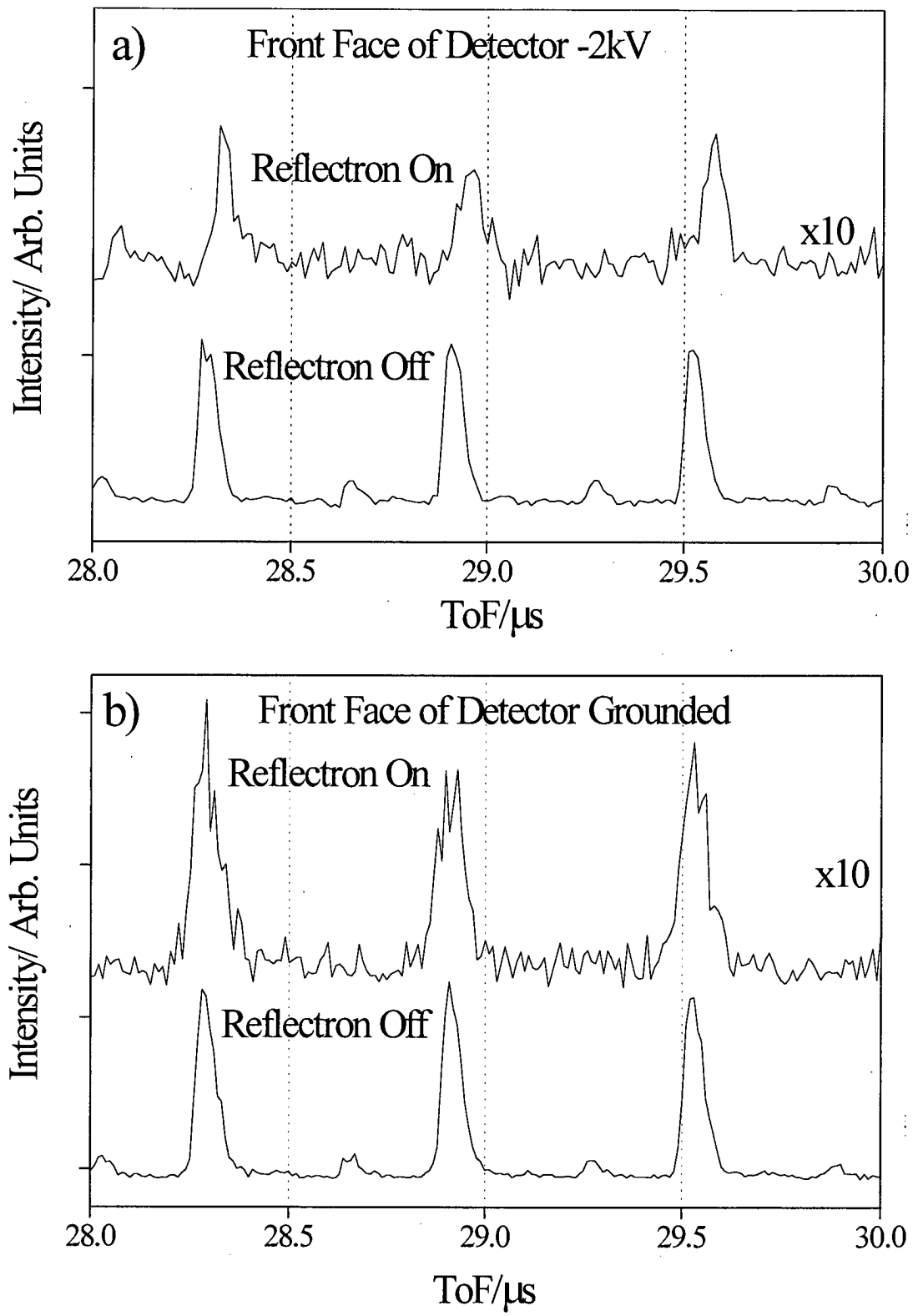

Figure 5.7 Time-of-flight mass spectra of rubidium PEG adducts recorded at 108 μJ laser energy. The traces in a) were recorded with post acceleration whereas the traces in b) were recorded without post acceleration.

The fact that little peak broadening and no retardation are observed for the neutral fragments formed in PSD of polymer metal ion adducts indicates that the neutrals observed were formed in a field free environment *i.e.* in the post-source and pre-reflectron section of the mass spectrometer.

5.3.3 Altering the reflectron voltage

For this experiment the effect of varying the reflectron voltage on the flight times of PEG (average molecular weight 1000 Da) adducts was investigated. The metal ions used to form the adducts were Li^+ and Rb^+ respectively. PEG was chosen, as it is a well defined polymer in terms of average molecular weight and polydispersity and because the various metal ion adduct peaks are well separated. The separation between Li^+ and Rb^+ adducts is 10 Da and the mass separation between Rb^+ and Na^+ adducts is 18 Da. The Rb^+ and Na^+ adduct mass separation is an important consideration in these experiments as there very often is some Na^+ contamination. The mass separation between Rb^+ and Na^+ adducts of PPG for example is only 4 Da, which makes PPG a comparatively poor choice for these experiments, as the Na^+ and Rb^+ adduct peaks can overlap. Rb^+ and Li^+ were chosen for these experiments, as Li^+ adducts do not dissociate under experimental conditions, whereas Rb^+ adducts do (see section 5.3.1).

All the samples used for these experiments were produced using the aerosol method. The extraction voltage applied was always +4 kV. The reflectron voltage was varied between 0 and +5 kV. The mass spectra presented in this section are the average of four separate mass spectra, each of which was the summed average of 50 laser shots. Averaging over four spectra was used to improve reproducibility.

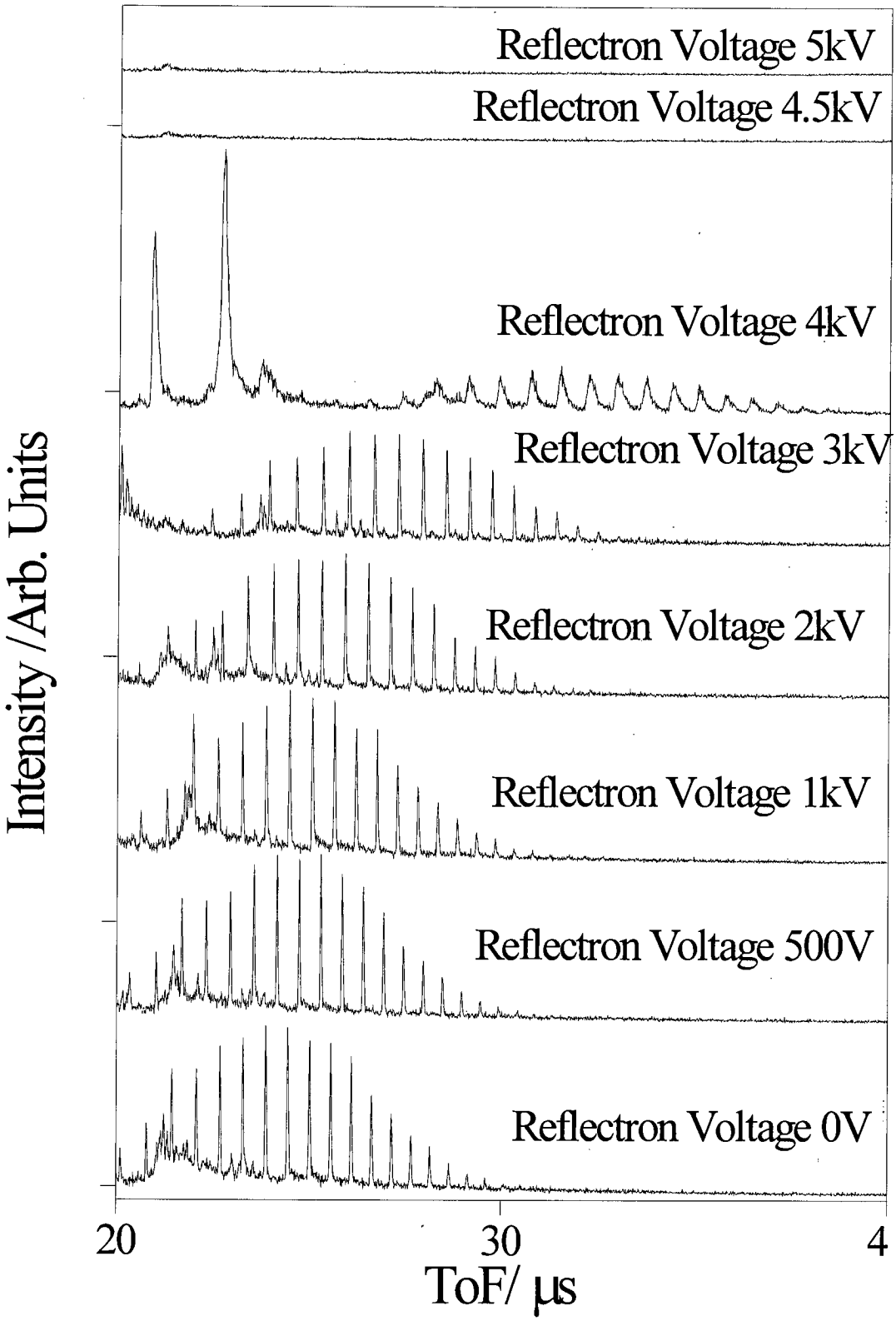

Figure 5.8 Time-of-flight spectra of lithium PEG adducts recorded at varying reflectron voltages.

The results for the LiCl PEG system are shown in figure 5.8. It is clear from these mass spectra that the higher the reflectron voltage is the longer the flight time of the ions becomes. The increase in flight time results in a shift of the polymer distribution to higher flight times. The relationship between ion mass and flight time increase is shown in figure 5.9. The mass of protonated dithranol is 227 Da, the mass of the Li^+ adduct of HO-$(CH_2$-CH_2-$O)_{16}$-H (the 16mer of PEG) is 729 Da and the mass of the Li^+ adduct of HO-$(CH_2$-CH_2-$O)_{20}$-H is 905 Da. It can be seen that the flight time shift increases rapidly with the field strength. Once the reflectron voltage exceeds the extraction voltage (4 kV), no peaks are observed. The disappearance of peaks is in line with the assumption that Li^+ PEG adducts do not fragment during mass analysis in a time-of-flight mass spectrometer.

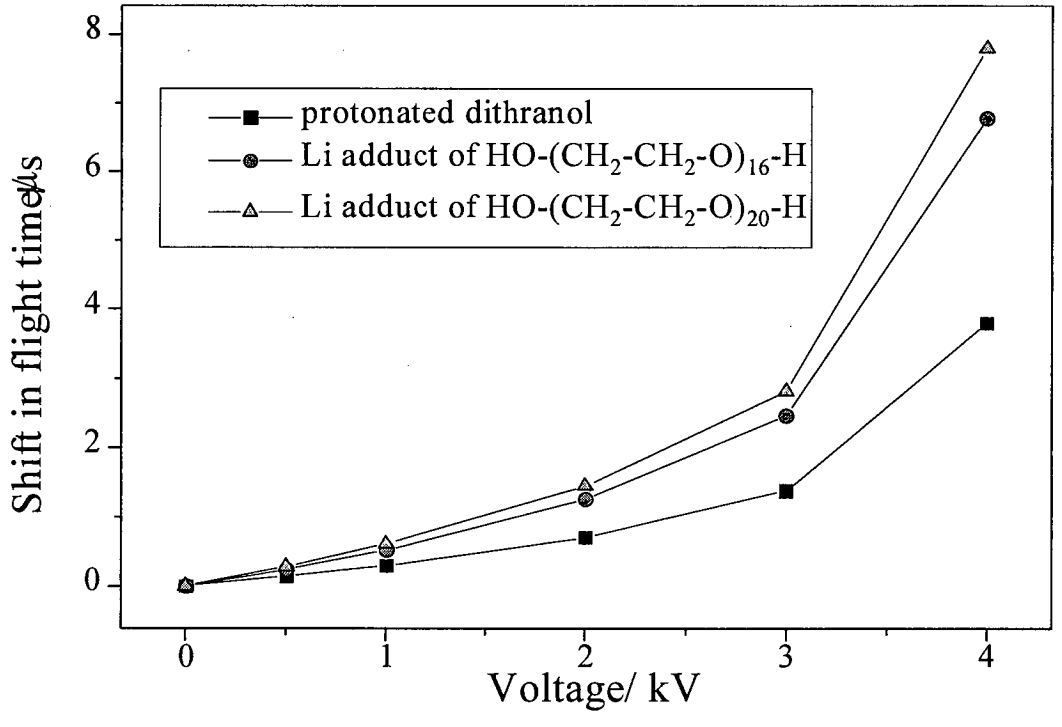

Figure 5.9 The shift in flight time vs voltage applied to the reflectron for selected peaks.

The results of varying the reflectron voltage on the Rb^+ PEG system are shown in figure 5.10. The main polymer distribution at reflectron voltage, 0 V, is

due to the Rb^+ adduct of PEG, the minor distribution being due to the Na^+ adduct. As with the Li^+ PEG adduct ions there is an increase in the flight time of the Rb^+ PEG adduct ions with increasing reflectron voltage. However, the mass spectra recorded for reflectron voltages of 4.5 kV and 5 kV are not featureless unlike in the LiCl PEG case. The peaks observed at 4.5 kV and 5 kV are in the same position as Rb^+ PEG adduct peaks in the 0 V mass spectrum. Furthermore, both 4.5 kV and 5 kV lie above the extraction voltage; therefore, any peaks observed in these two mass spectra must be due to uncharged species. It should also be borne in mind that the neutral peaks should be present in all mass spectra, as they are not affected by the retarding effect of the reflectron. In order to show that neutral peaks are indeed present in all mass spectra, the mass spectra were enlarged (figure 5.11). In the enlarged mass spectra lines were included to match the flight times of neutral peaks. It is apparent that the maximum peak intensities of the neutral peaks in the 4.5 kV and 5 kV mass spectra do not coincide exactly with the Rb^+ PEG oligomer peaks in the 0 V mass spectrum. The Rb^+ PEG peaks in the 0 V mass spectrum were produced by a mixture of ions and neutrals hitting the detector; the ions had a shorter flight time due to post acceleration (*c.f.* section 5.3.2) than the neutral peaks. Because of the width of the peaks neutral and ion signals overlap as ion signals were *ca* ten times more intense than the neutral signal. Thus the overall peaks produced by the overlap of the two signal types appear at shorter flight times than the flight times observed for neutrals alone. Peaks that correspond to neutrals can be seen in all mass spectra although ion peaks sometimes obscure these peaks. It is worth noting that the intensity of the neutral peaks does not appear to change with reflectron voltage indicating that the mechanism for neutral formation is independent of the reflectron voltage.

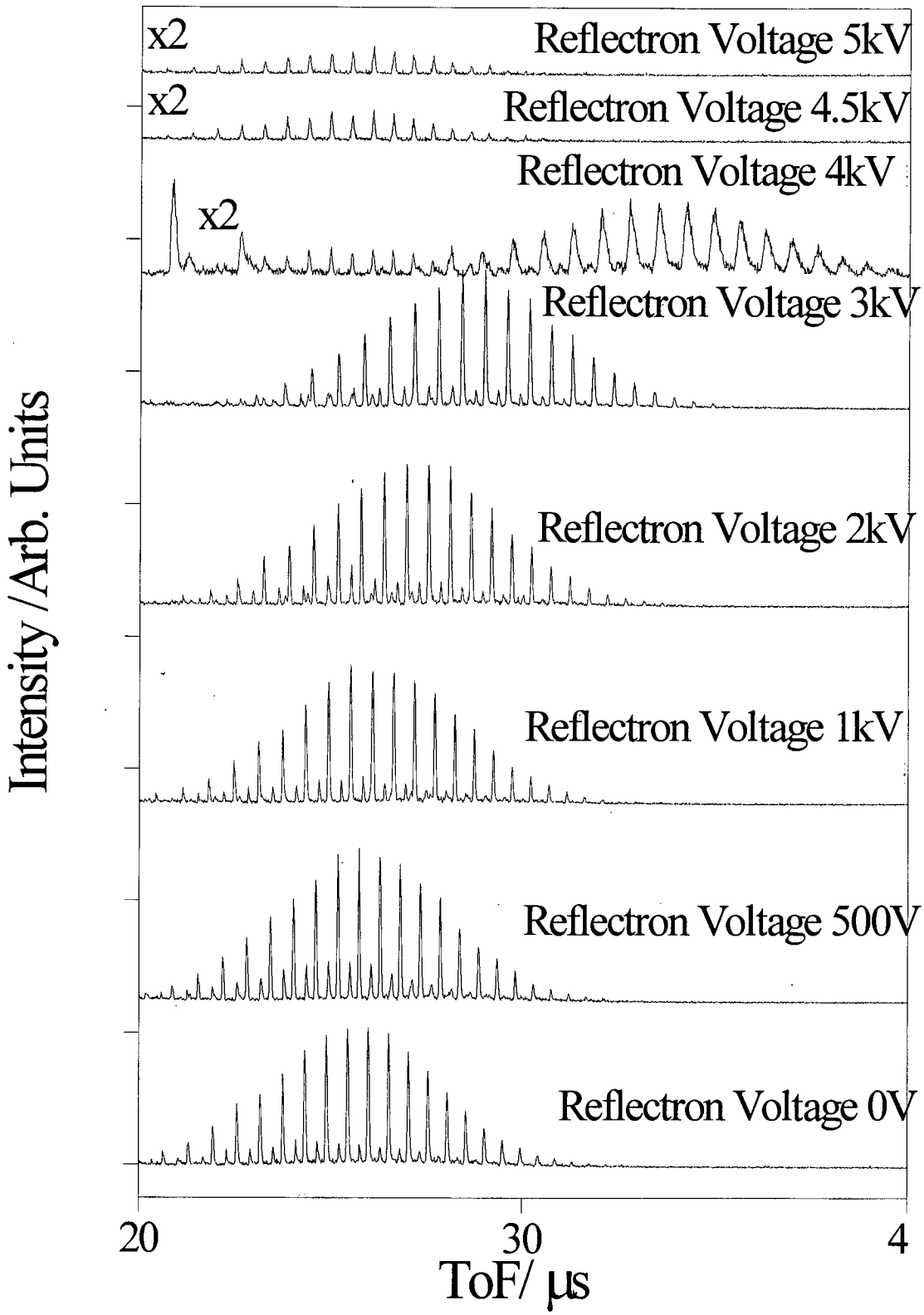

Figure 5.10 Time-of-flight spectra of rubidium PEG adducts recorded at varying reflectron voltages.

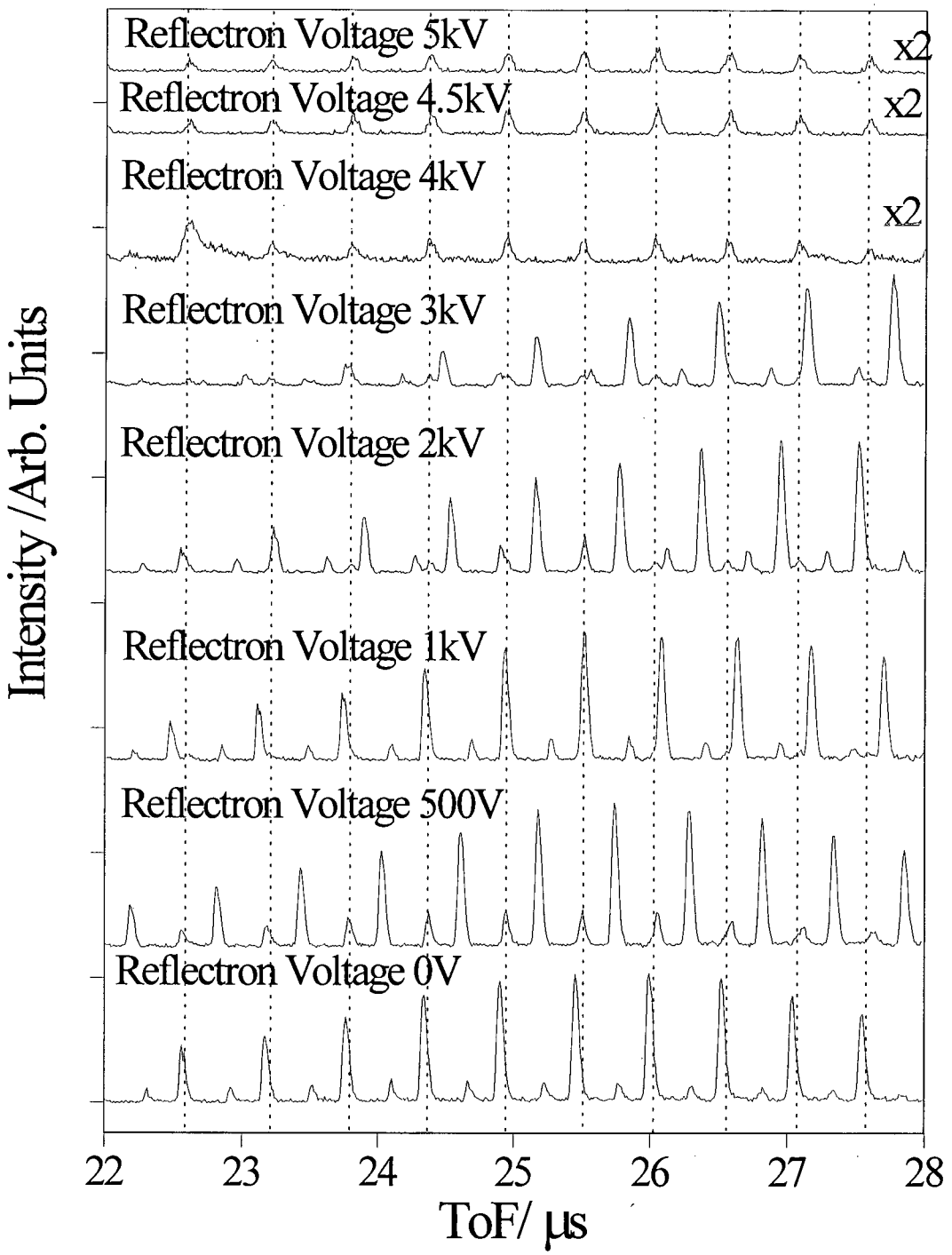

Figure 5.11 Enlargement of figure 5.10 showing the presence of neutral peaks in all traces indicated by the dotted lines.

This experiment has confirmed that PSD is observed for the Rb^+ adducts of PEG whereas it is not observed for the Li^+ adducts. Also the peaks seen at high reflectron voltages for the RbCl PEG sample were confirmed as neutrals. Furthermore, it has also been shown that the reflectron voltage does not affect the dissociation of the Rb^+ adducts of PEG.

5.3.4 Experiments on the variation of the laser energy

The effect of laser energy on the formation of neutrals was investigated. The polymer chosen for these experiments was PEG, for the reasons outlined in section 5.3.3. The four different metal ions used were Li^+, Na^+, K^+ and Rb^+. It was the aim of these experiments to ascertain whether at increased laser energies the amount of fragmentation would increase. If an increase in fragmentation was observed it would suggest that the internal energy of the polymer metal ion complex was raised. If no increase in the amount of fragmentation was seen internal energies would appear not to be sufficiently increased to raise the fragmentation probability.

The samples were prepared using the aerosol method. The laser energy was varied by means of a neutral density filter. The range of laser energies studied was from 69 μJ to 108 μJ for PEG with LiCl, NaCl, KCl and RbCl and a wider range of energies for PEG with Li^+ and Rb^+ (76 μJ to 158 μJ). For the lower energy range experiments (69 μJ to 108 μJ) the detector was set to a lower voltage (3.5 kV),

whereas for the higher energies (76 μJ to 158 μJ) the detector voltage was increased (3.9 kV). Higher detector voltage meant that the sensitivity of the detector was increased. However, there is a trade off between increased sensitivity and detector saturation.

5.3.5 Lower laser energy experiments

The results for the 69 μJ to 108 μJ experiments are shown in figures 5.12 to 5.19. The mass spectra are shown as waterfall plots to make comparisons easier and to show up trends. The x and y axes show time-of-flight and signal intensity, respectively. The laser energy is displayed on the z-axis (*N.B.* The z-axis is not linear). The range of laser energies and the detector voltage (sensitivity) were chosen, so that at the lowest laser energy a signal was obtained. The highest laser energy that could be used was limited by detector saturation.

For the lower laser energy experiment a comparison was made between mass spectra recorded with the reflectron switched off (ions and neutrals are both detected) and mass spectra recorded with the reflectron switched on (only neutrals can be detected) for a range of polymer salt combinations.

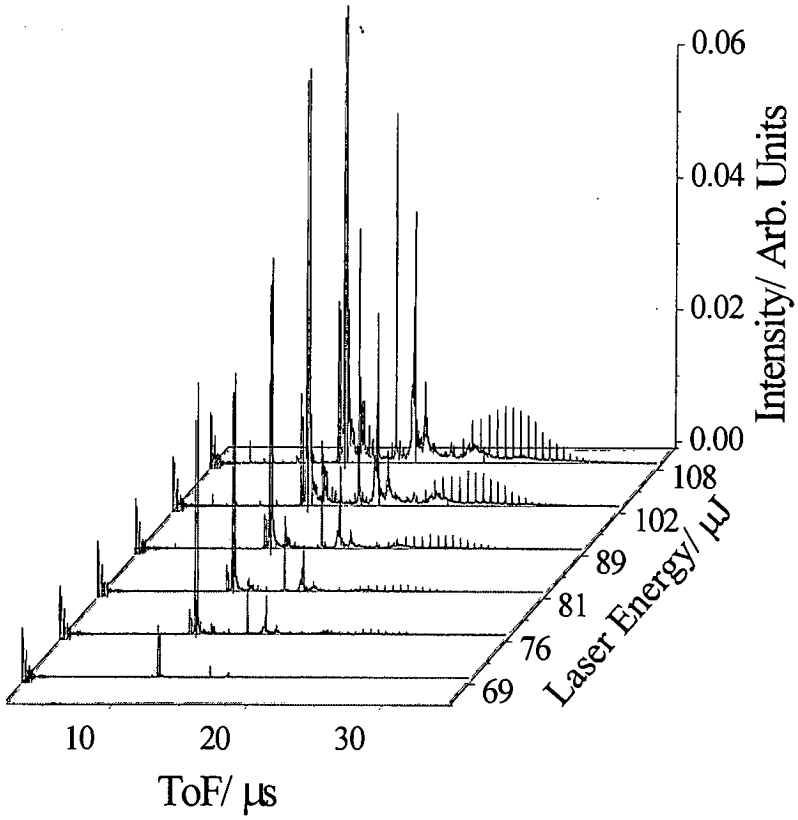

Figure 5.12 Time-of-flight Spectra of PEG with LiCl with the Reflectron off, recorded at laser energy varying between 69 μJ and 108 μJ.

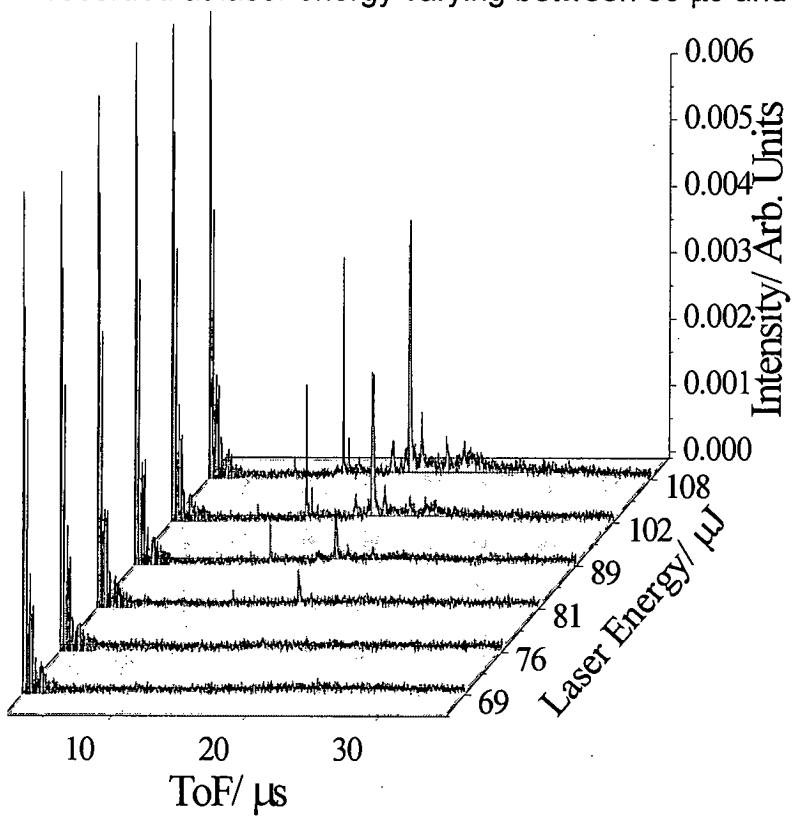

Figure 5.13 Time-of-flight Spectra of PEG with LiCl with the Reflectron on, recorded at laser energy varying between 69 μJ and 108 μJ.

5.3.5.1 Results for PEG and LiCl

The results for LiCl and PEG are shown in figures 5.12 and 5.13. From figure 5.12 a clear correlation between laser energy and signal intensity can be seen for the neutral/ion mass spectra. At 69 μJ no signal is obtained for the polymer and only small peaks due to matrix species are observed. The matrix species observed are protonated and lithiated matrix and matrix dimer. A polymer distribution is first observed at 81 μJ. The polymer distribution extends from *ca* 20 μs to 30 μs. As the laser energy increases the signal intensity of the polymer and matrix species increases. At laser energies above 89 μJ broad peaks underlying the polymer mass spectrum are seen. Similar broad peaks were observed earlier in figure 5.3. They are most likely due to trimer and tetramer species of the matrix. The peaks at lower flight times in the higher laser energy mass spectra are due to matrix species. These matrix species include sodiated matrix and matrix that has lost one or more hydroxyl groups.

The neutral mass spectra (figure 5.13) are very different from the neutral/ion mass spectra. The first neutral species to be detected is a peak at 17 μs in the 81 μJ mass spectrum. This peak corresponds to a neutral decay product of the dimer of the matrix. The matrix dimer is also observed in figure 5.12, but it is not the strongest peak. It may be assumed that the difference in relative intensity between the peaks in the neutral mass spectrum and those seen in the ion/neutral mass spectrum is an indication of how easily the relevant species undergo decay. The next peak that

appears in the neutral mass spectrum is the lithiated matrix peak at a time-of-flight of 11.98 μs first seen at a laser energy of 89 μJ. This peak is the strongest peak in figure 5.12, the next strongest being the protonated matrix peak, which is only marginally weaker. The protonated matrix peak is not seen in the neutral mass spectra, even at the highest laser energies. The absence of a protonated matrix signal in the neutral mass spectrum indicates that the protonated species is less likely to decay. Also present in the 102 μJ and 108 μJ neutral mass spectra is a signal at a flight time of 12.57 μs corresponding to sodiated matrix which is not seen in the ion/neutral mass spectra (figure 5.12) as its intensity is too low. It is, however, observed in figure 5.13 as these mass spectra were magnified by a factor of ten. The signal intensity of the neutral signal from sodiated matrix decay products is large relative to the signal intensity of sodiated matrix species in the ion/neutral mass spectrum. If the ratio between the sodiated and lithiated matrix peaks was the same in the figure 5.12 as in figure 5.13, a sizeable peak would have been seen in figure 5.12 for the sodiated matrix. This indicates that sodiated matrix is more likely to undergo PSD than is the lithiated matrix. The highest laser energy mass spectrum of figure 5.13 shows a broad feature at a flight time of 24 μs. This is believed to be due to the decay products of matrix trimer species. No peaks associated with the polymer were observed in figure 5.13 which indicates that lithiated PEG does not undergo extensive PSD under the experimental conditions used.

In summary, the LiCl PEG mass spectra showed that under standard MALDI conditions, lithiated PEG does not undergo PSD. The signal intensity of peaks

increases with laser energy over the chosen range of laser energies for all peaks. For the dithranol matrix, there is a relationship between the intensity of the neutral signal obtained and the cation attached. The cation to intensity relationship showed that protonated dithranol was least susceptible to decay, followed by lithiated dithranol and that sodiated dithranol was the most likely to undergo PSD. It seems reasonable to suggest that the conversion from adduct to neutral is via the loss of the attached cation and that the percentage of adducts that decay to neutrals and cations is a function of the bond strength between the cationic and the neutral part of the adduct.

5.3.5.2 Results for PEG and NaCl

The mass spectra for NaCl and PEG are presented in figures 5.14 and 5.15. Figure 5.14 shows the mass spectra recorded with the reflectron off, *i.e.* showing both ions and neutrals. The trends observed for the LiCl and PEG system with the reflectron off (figure 5.12) are seen again. The signal intensity of all peaks increases as the laser energy is increased. The first peaks to appear at 69 μJ are due to protonated matrix and sodiated matrix. The signal for the protonated matrix is considerably greater than that of its sodiated equivalent. At 76 μJ the first sodiated polymer peaks are observed. At 81 μJ two peaks appear with flight times of 16.15 μs and 16.85 μs, respectively. These peaks were assigned as the protonated and sodiated dithranol dimer. A notable difference between the LiCl PEG spectra (figure 5.12) and the NaCl PEG mass spectra

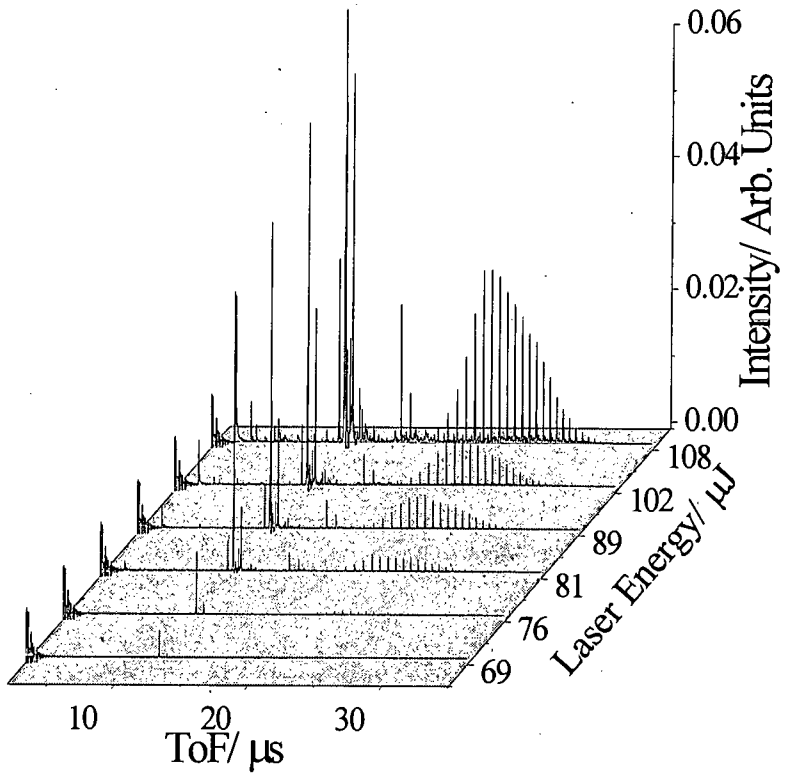

Figure 5.14 Time-of-flight Spectra of PEG with NaCl with the Reflectron off, recorded at laser energy varying between 69 μJ and 108 μJ.

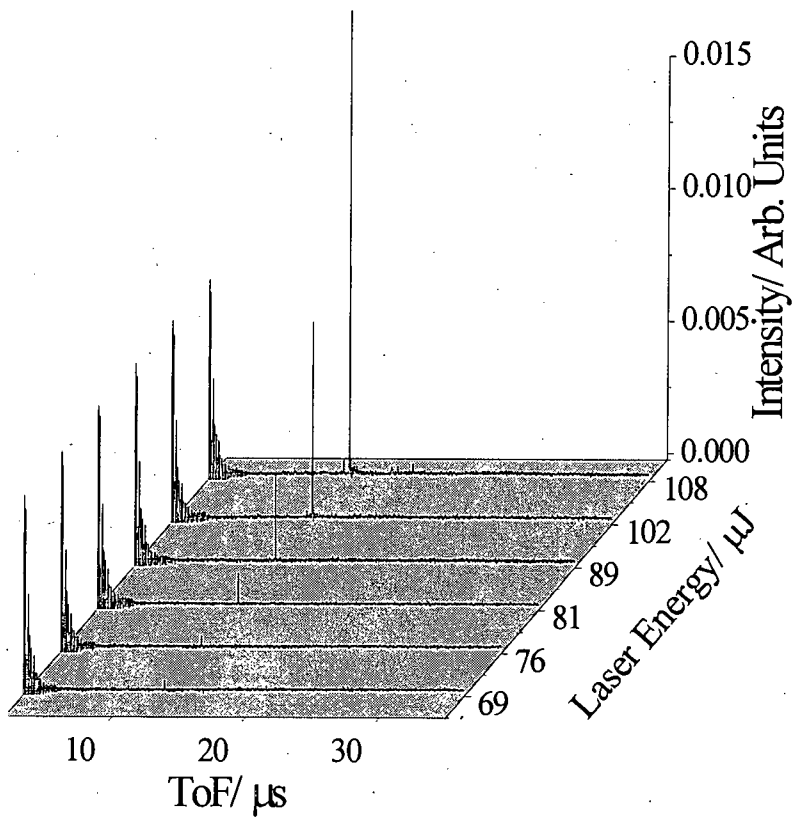

Figure 5.15 Time-of-flight Spectra of PEG with NaCl with the Reflectron on, recorded at laser energy varying between 69 μJ and 108 μJ.

(figure 5.14) is the absence of trimer and tetramer peaks underlying the polymer peaks for the NaCl case.

The NaCl PEG mass spectra recorded with the reflectron on (figure 5.15), in other words the mass spectra showing only neutrals, are very straightforward. Only one strong peak is observed in these mass spectra, due to the decay products of the sodiated matrix. As expected the signal intensity of this peak increases with increasing laser energy. For the two highest laser energies a small signal appears, which is due to the neutral decay products of protonated dithranol. It is noteworthy that the signal associated with sodiated dithranol is much larger than the signal due to protonated dithranol decay products in the neutral mass spectra (figure 5.15), whereas in the neutrals/ions mass spectra the protonated dithranol peak was larger than the sodiated peak. This confirms that the protonated matrix is far less likely to undergo PSD than the sodiated equivalent. As with lithiated PEG, sodiated PEG does not dissociate to produce neutral peaks.

The NaCl PEG experiment reaffirmed the results from the LiCl PEG experiment. Most notably it showed again that the susceptibility of dithranol adducts to dissociate is linked to the cation used in adduct formation.

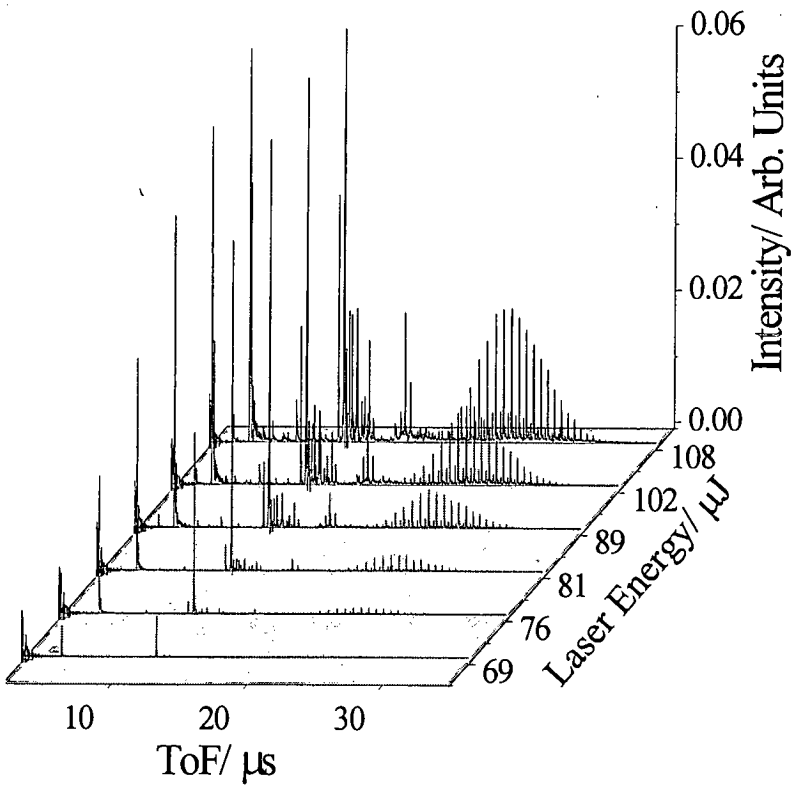

Figure 5.16 Time-of-flight Spectra of PEG with KCl with the Reflectron off, recorded at laser energies varying between 69 μJ and 108 μJ.

5.3.5.3 Results for PEG and KCl

The mass spectra recorded for a sample consisting of a combination of KCl with PEG are shown in figures 5.16 and 5.17. The trends for the mass spectra recorded with the reflectron switched off are the same as those seen for the LiCl and the NaCl PEG systems. In the mass spectra shown in figure 5.16, two types of PEG peaks are observed. The larger PEG distribution is due to the potassiated polymer whereas the smaller PEG distribution is due to the sodiated polymer.

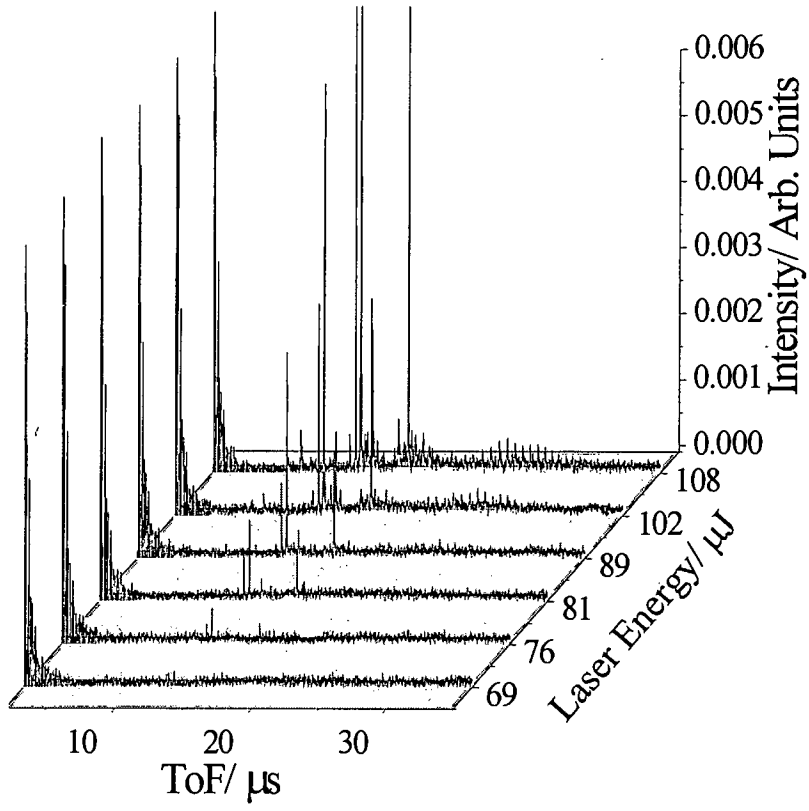

Figure 5.17 Time-of-flight Spectra of PEG with KCl with the Reflectron on, recorded at laser energy varying between 69 μJ and 108 μJ.

The mass spectra recorded for the potassium PEG system, with the reflectron on (figure 5.17), differ significantly from the equivalent series of mass spectra for the lithium and the sodium cases. At the higher laser energies (102 μJ and 108 μJ), distinct polymer signals are seen between 20 μs and 30 μs. This means that PEG potassium adducts undergo PSD. The fact that the potassium adduct dissociates more easily than the lithium or sodium adducts is not unexpected, bearing in mind the cation dependent behaviour of matrix adducts discussed earlier. In order to study the relationship between neutral yield and laser energy more closely, a comparison was made between neutral peak areas and the ion/neutral peak areas of three oligomers of PEG. The oligomers chosen were the 18, 19 and 20-mers of PEG, as

these were the most intense oligomer peaks for this polymer. The results of this comparison are shown in figure 5.18. As can clearly be seen, the trends for the neutrals and the total signal are very similar in all cases. As the laser energy is increased, the signal intensity increases. Over the range studied, it would appear that the relationship between laser energy and signal intensity is near linear. The ratio between the total signal intensity and the neutral signal intensity is *ca* 30:1. This would suggest that in the region of 3.5% of the polymer adducts produced dissociate in the drift free region of the mass spectrometer. This value for the amount of post-source dissociation is an underestimate of the total extent of dissociation. The ions, unlike the neutrals, experience post acceleration, which leads to an enhancement of the ion signal, as discussed in detail in section 5.3.2. Also only post-source decay could be measured in this experiment. Another possible loss process, which could not be measured in the experiments described here, is in-source decay which is known to occur in MALDI experiments [11].

The PEG KCl system is very different from the LiCl and the NaCl systems in that the polymer adducts dissociate in the time-of-flight mass analyser. It has been shown, that the yield of neutral species from PEG adducts is independent of laser energy over the energy range studied.

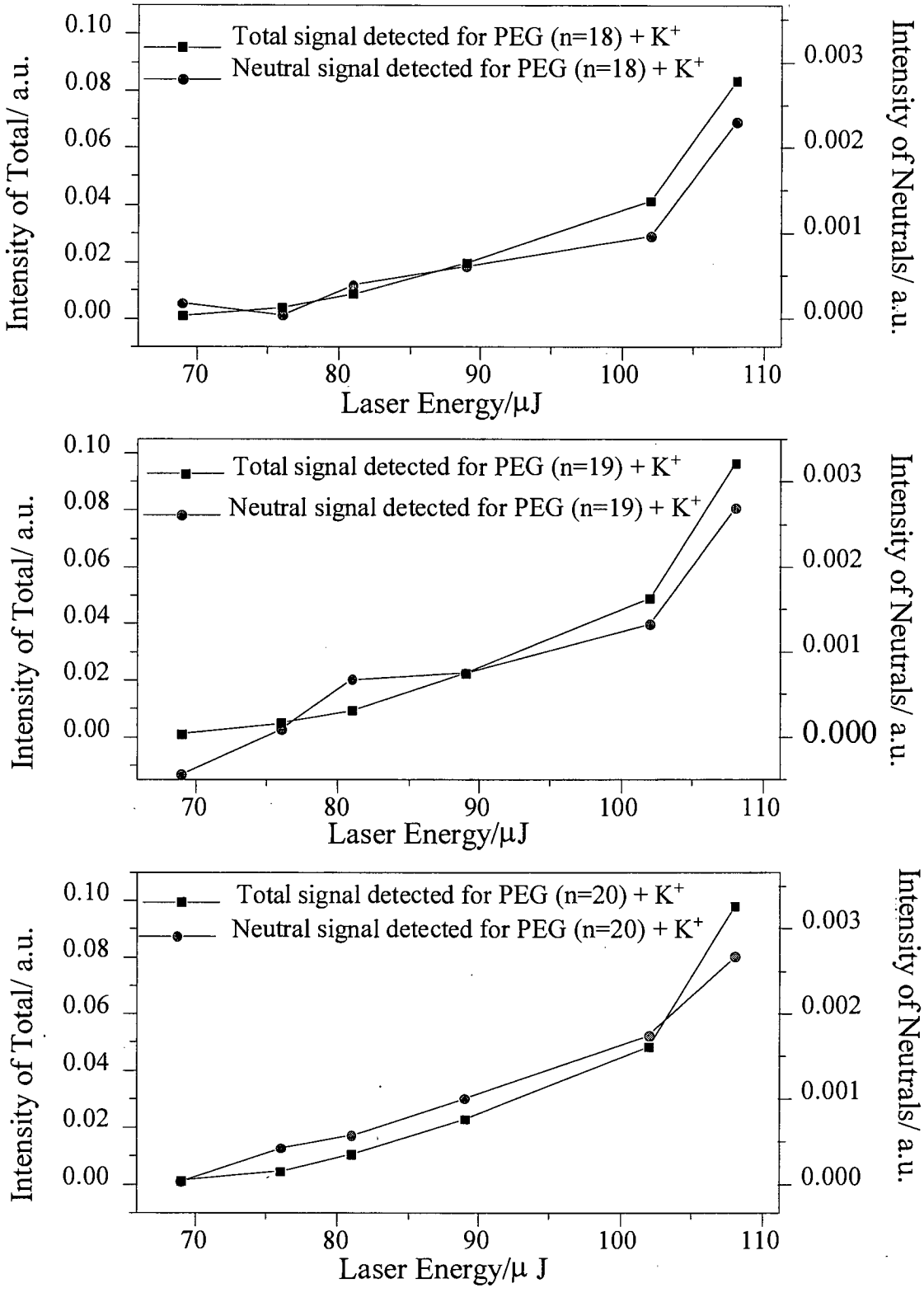

Figure 5.18 A comparison between the Signal intensity of neutrals vs laser energy and the signal intensity of the combined neutrals and ions vs laser energy for three PEG oligomer potassium adducts.

5.3.5.4 Results for PEG and RbCl

The RbCl PEG system behaves in a similar way to the KCl system. As in the case of potassiated PEG, rubidiated PEG also dissociates. This can clearly be seen in figure 5.20. The mass spectra showing both ions and neutrals behave similarly to the other three salt polymer combinations (figure 5.19). The neutral mass spectra (figure 5.20) are similar to the neutral mass spectra for KCl and PEG (figure 5.16). The non-polymer peaks that are seen in the RbCl neutral mass spectra have the masses 249 Da, 311 Da, 395 Da and 475 Da. The 249 Da peak is due to sodiated dithranol and the 311 Da peak is due to rubidiated dithranol. The 395 Da and 475 Da peaks could not be easily identified. However, it is likely that the 395 Da peak is a Rb^+ adduct as the corresponding signal in the ion and neutral mass spectrum consists of two peaks separated by 2 Da. This would be expected for a rubidium adduct as rubidium has two isotopes separated by 2 Da (^{85}Rb (abundance 72%) and ^{87}Rb (abundance 28%)).

A comparison was made between neutral peak areas and the ion/neutral peak areas of three oligomers of PEG. The oligomers chosen were the 18, 19 and 20-mers of PEG, as these were the most intense oligomer peaks for this polymer. The results are shown in figure 5.21. A rise in signal intensity with increasing laser energy is seen for both the neutral signal and the total signal. The ratio between the total signal and the neutral signal stays constant, within the experimental uncertainty, over the range of laser energies studied. The neutral signal is *ca* 5% of the total signal. This value is a slight underestimate for the reasons outlined in section 5.3.5.3.

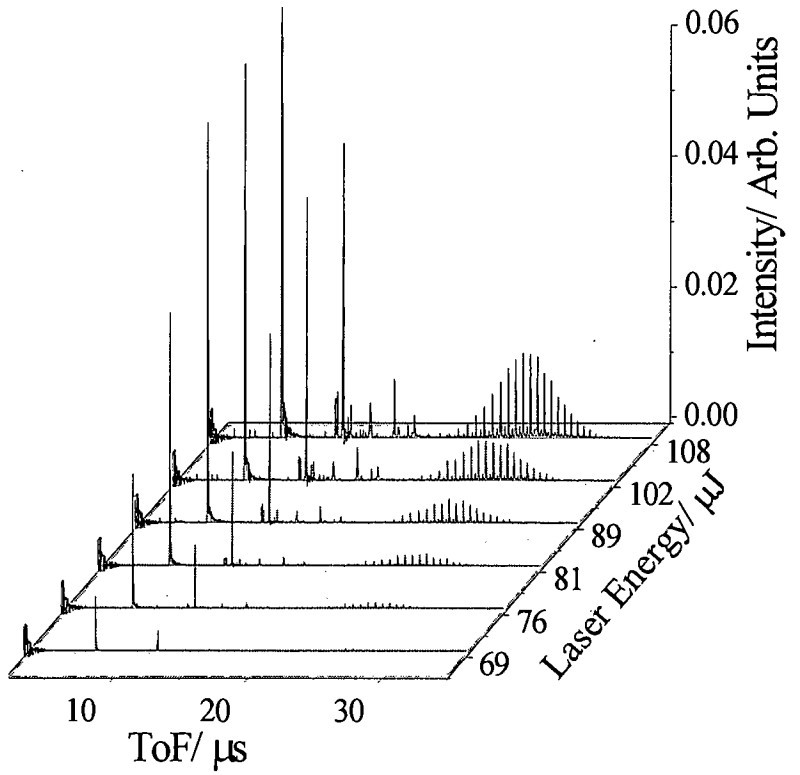

Figure 5.19 Time-of-flight Spectra of PEG with RbCl with the Reflectron off, recorded at laser energy varying between 69 μJ and 108 μJ.

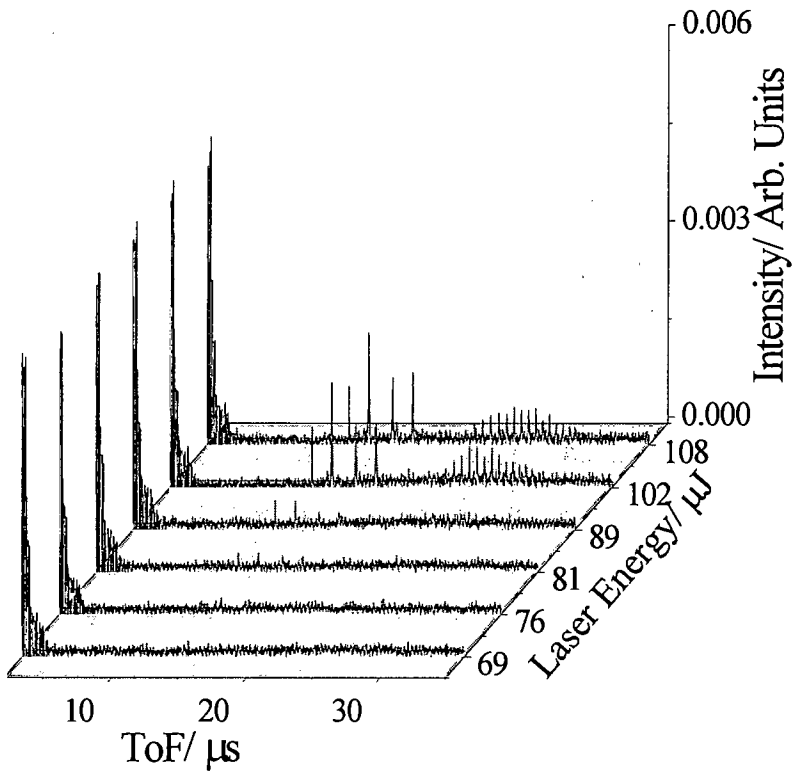

Figure 5.20 Time-of-flight Spectra of PEG with RbCl with the Reflectron on, recorded at laser energy varying between 69 μJ and 108 μJ.

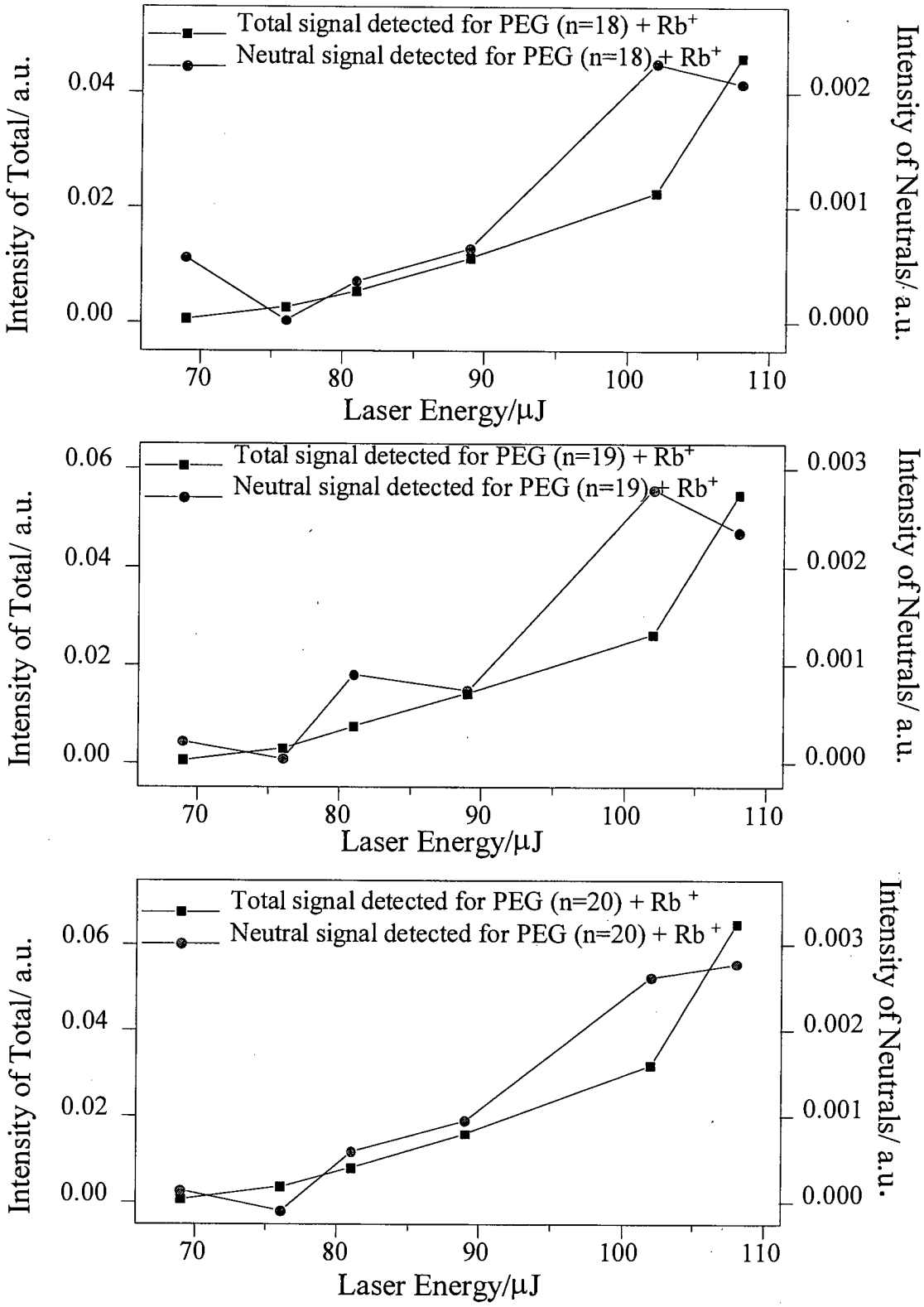

Figure 5.21 A comparison between the Signal intensity of neutrals vs laser energy and the signal intensity of the combined neutrals and ions vs laser energy for three PEG oligomer rubidium adducts.

5.3.5.5 Conclusions of the lower laser energy experiments

Some very clear trends were observed in these experiments. The signal intensity for all species observed increased with increasing laser energy. The generation of neutrals was found to be dependent on the type of cation used in adduct formation. For dithranol, it was found that protonated dithranol did not dissociate under experimental conditions. All the metal ion adducts of dithranol did dissociate to varying extents. The lithium adduct dissociated least readily, followed by the sodium adduct, then the potassium adduct and finally the rubidium adduct dissociated most readily. The degree of dissociation is linked directly to the size of the attached cation. The smaller the cation, the more stable the adduct. The same trend was observed for the metal ion adducts of PEG. The Li^+ and Na^+ adducts of PEG did not dissociate under experimental conditions. Potassiated and sodiated PEG did both dissociate. The fraction of the adducts that dissociated did not vary with applied laser energy. A larger percentage of the rubidium adduct of PEG dissociated than of the potassium adduct of PEG (5% and 3.5%, respectively). The extent to which the K^+ and Rb^+ adducts of PEG dissociate appears to be independent of the laser energy. This would suggest that the internal energy of these adducts is not greatly increased by the increase in laser energy. An increase in internal energy would be expected to increase the proportion of adducts that undergo decay.

5.5.6 Higher laser energy experiments

For these experiments the range of laser energies was extended, going from 76 μJ to 158 μJ. Also the detector gain was increased, giving a more sensitive detector response. Two samples were studied, namely PEG (average molecular weight 1000 Da) with a dithranol matrix and LiCl as the salt and the same polymer and matrix with RbCl as the salt. The samples were prepared using the aerosol method. The aim of these experiments was to determine whether or not the strongly bound lithium adduct of PEG would dissociate at these higher laser energies. As a comparison the effects on the Rb^+ PEG system were also studied under these conditions. These experiments also give an illustration of the response of the microchannel plate detector under these conditions.

The results for the LiCl PEG combination are shown in figures 5.22 and 5.23. The mass spectra presented in figure 5.22 were recorded with the reflectron switched off, allowing charged and uncharged species to be detected. The peaks at 20 μs and above are due to lithiated PEG. Between laser energies of 76 μJ and 108 μJ, the trend observed is the same as for the lower energy experiments described earlier. At 132 μJ the polymer peak intensity drops sharply and the peaks broaden. At 158 μJ the polymer signal disappears almost completely. The lower mass peaks below 15 μs increase in intensity with increasing laser energy. Figure 5.23 shows the neutral mass spectrum for the LiCl PEG system. It is clear that in the neutral mass

spectra, all peaks increase in intensity with increasing laser energy. However, even at 158 μJ no neutral peaks associated with the lithium PEG adduct were observed.

Figure 5.24 shows the ion/neutral mass spectra for PEG and RbCl. The peaks at flight times of 20 μs and above are due to polymer adducts. Rubidium and sodium adducts are seen, the rubidium PEG adducts being the strongest polymer distribution. The intensity of the polymer peaks increases with laser energy up to an energy of 89 μJ. At laser energies of 108 μJ and higher the polymer peak intensity decreases and the peak width increases. The polymer peaks in the mass spectrum recorded at 158 μJ have been reduced to a low intensity continuum. The lower mass peaks observed in figure 5.24 (below 15 μs) increase with laser energy over the whole energy range. In the mass spectrum recorded at 158 μJ there is a group of peaks centred at 5 μs which overlap and are so intense that they go off scale. Figure 5.25 shows the neutral mass spectra for the RbCl PEG system. Polymer peaks are seen in all mass spectra. The polymer peak height increases with increasing laser energy up to a laser energy of 132 μJ. The polymer peak heights of the 158 μJ mass spectrum are comparable to the equivalent peaks in the 132 μJ mass spectrum. The lower mass peaks, below 20 μs, increase in signal intensity with laser energy up to 132 μJ, and the peak height decreases in the 158 μJ mass spectrum. The peak widths always increase with increasing laser energy.

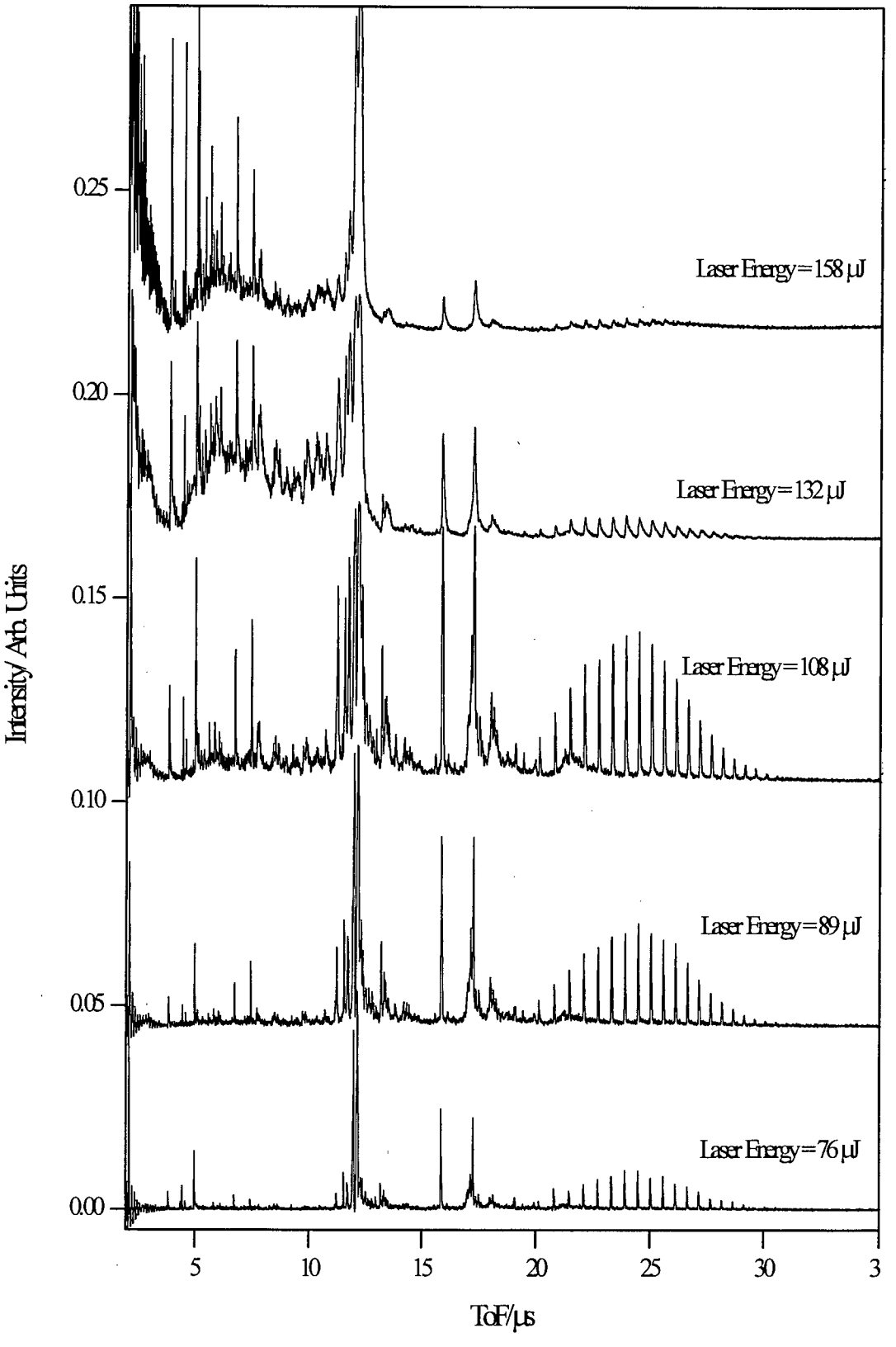

Figure 5.22 Time-of-flight spectra of PEG with LiCl with the reflectron off recorded at laser energies between 76 μJ and 158 μJ.

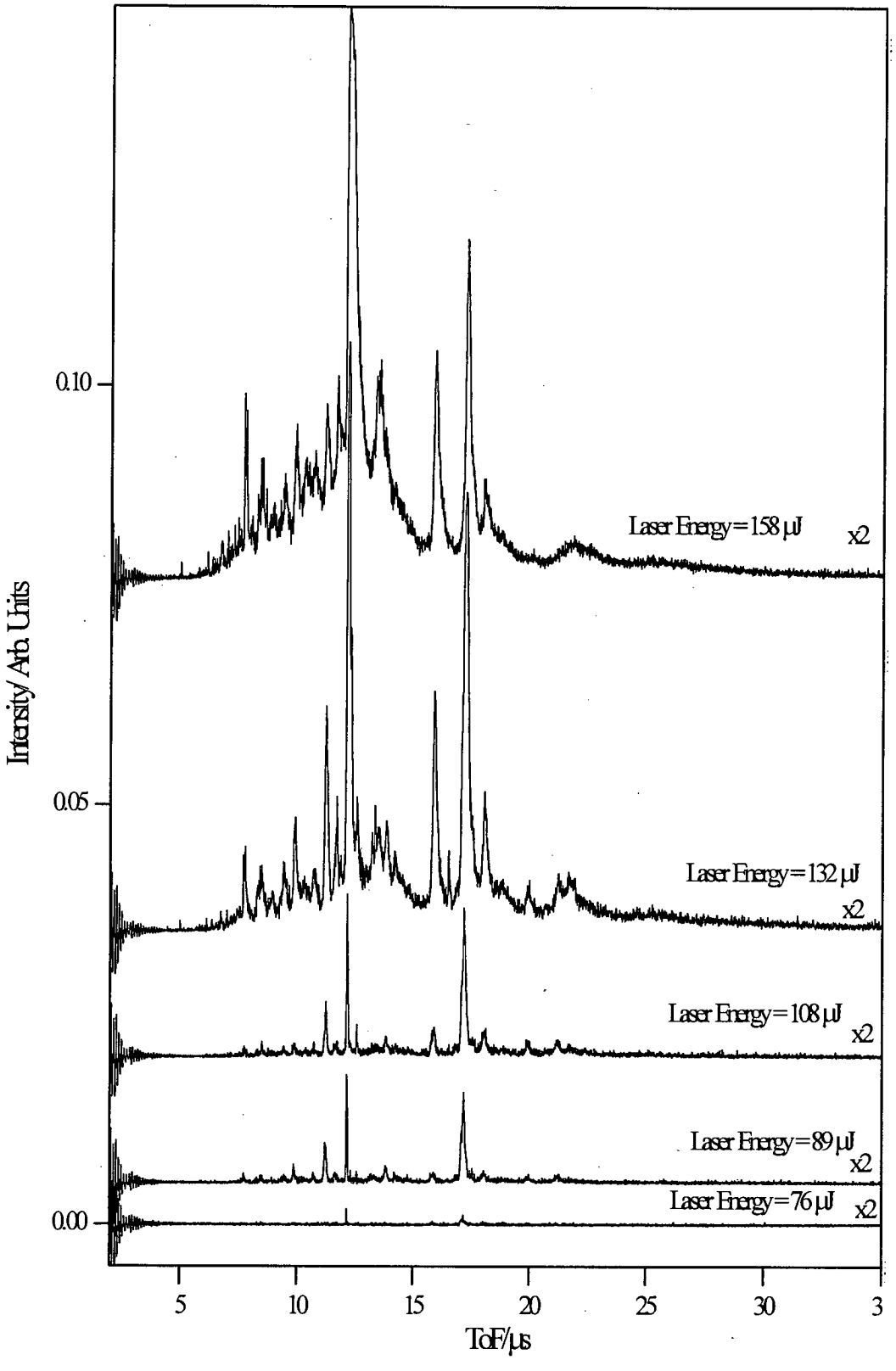

Figure 5.23 Time-of-flight spectra of PEG with LiCl with the reflectron on recorded at laser energies between 76 μJ and 158 μJ.

When comparing figure 5.24 with figure 5.25, an unexpected trend can be seen. At the two highest laser energies, the polymer peaks in the neutral mass spectrum of the RbCl PEG system (figure 5.25) are more intense than the polymer peaks in the mass spectra showing the combined neutral and ion signals (figure 5.24). The number of neutrals produced can never be larger than the sum of the neutrals produced and the unfragmented adducts. The neutral signal must always be less than or equal to the total number of adducts produced and extracted into the time-of-flight tube. The appearance of signals for the neutral polymer peaks that are stronger than the equivalent total ion and neutral signals must therefore be an experimental artefact. The probable reason for the low intensity of the polymer signal at higher laser energies in the RbCl and LiCl mass spectra recorded with the reflectron switched off (figures 5.22 and 5.23) is overloading of the detector with low mass ions, *i.e.* matrix species and metal ions. This probable overloading of the detector means that no direct comparison can be made between mass spectra recorded with the reflectron on and mass spectra recorded with the reflectron switched off.

These experiments showed that dissociation of lithium PEG adducts was not detected under MALDI conditions, not even at high laser energies and very sensitive detector settings. It was shown that the high-mass performance of the microchannel plate detector was seriously affected by the impact of large numbers of low-mass ions (*c.f.* chapter 2).

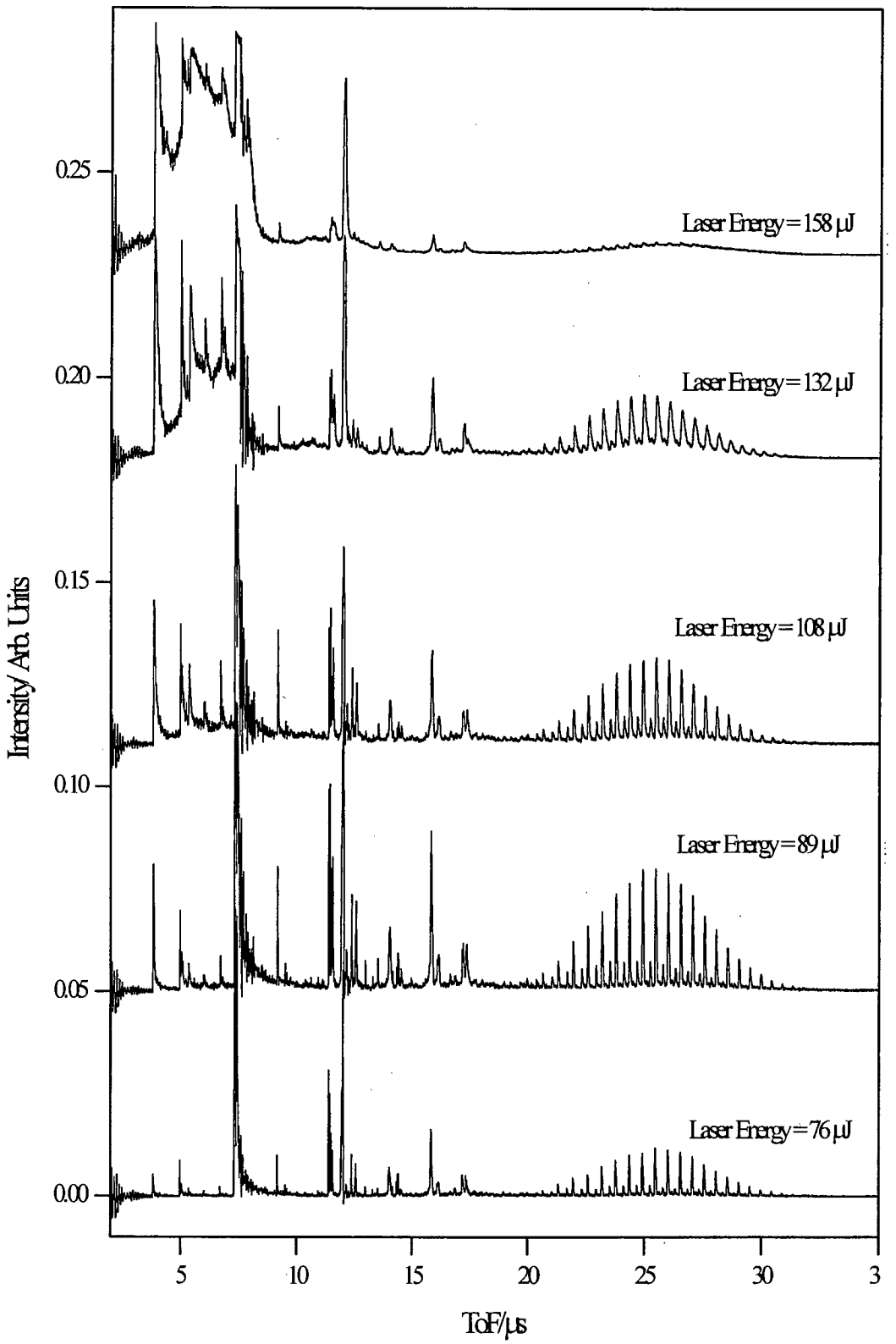

Figure 5.24 Time-of-flight spectra of PEG with RbCl with the reflectron off recorded at laser energies between 76 μJ and 158 μJ.

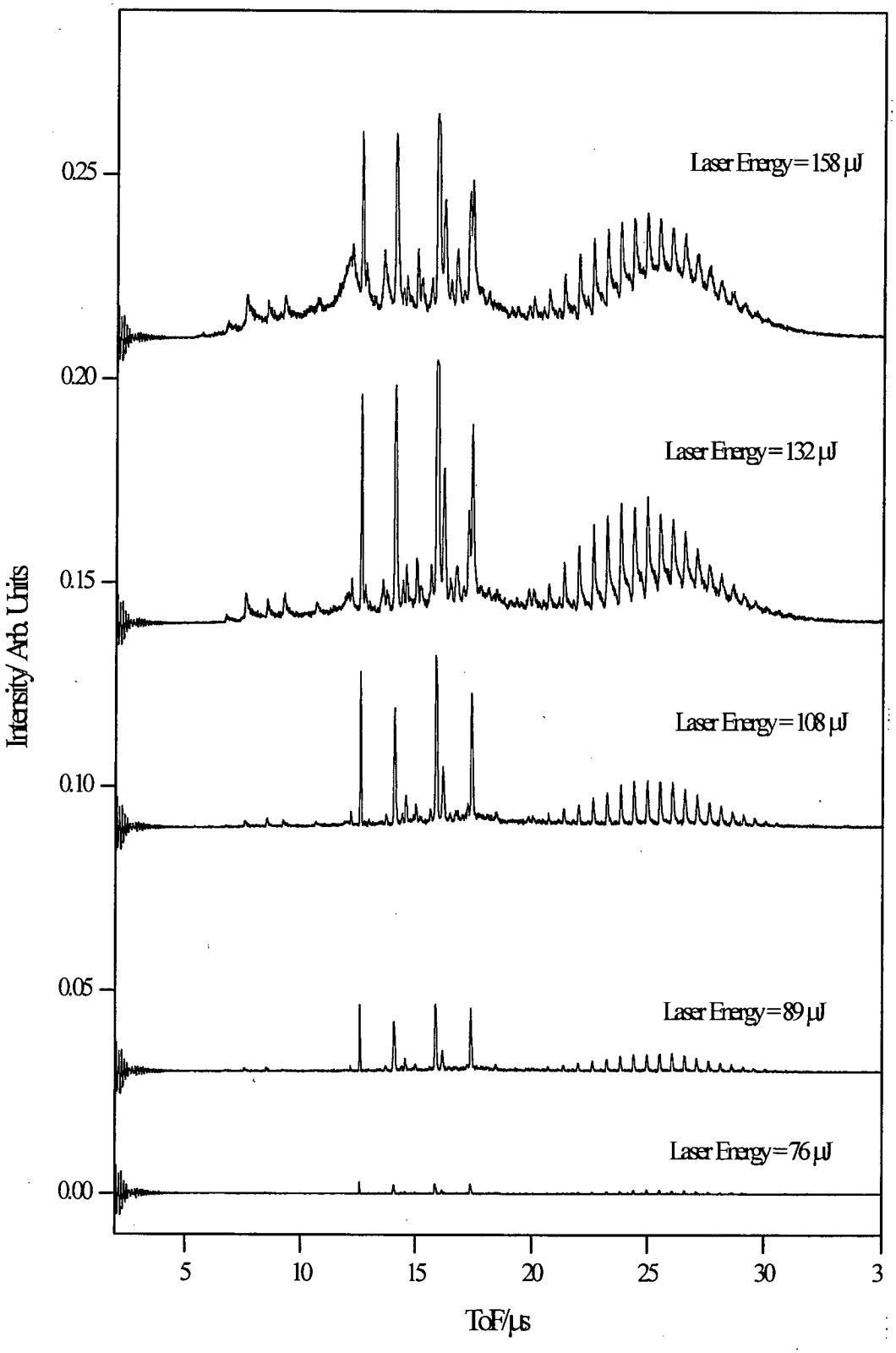

Figure 5.25 Time-of-flight spectra of PEG with RbCl with the reflectron on recorded at laser energies between 76 μJ and 158 μJ.

5.5.7 Effect of fragmentation on the mass distribution of polydisperse polymers

One of the greatest problems in the mass determination of synthetic polymers using MALDI is the poor agreement sometimes observed between average masses of polydisperse polymers determined using traditional techniques and the average molecular mass arrived at using MALDI [12,13]. Various reasons for the average molecular weight discrepancies have been put forward [14,15]. The possibility of different adduct dissociation rates has, however, not yet been addressed. An apparent shift in molecular weight would be observed if high-mass oligomer adducts were more prone to dissociation than low-mass oligomers or vice versa. The experiment outlined below aims to show whether the dissociation rate of oligomer adducts is mass dependent and whether this could be a factor affecting the accurate determination of average molecular weights of polymers by MALDI mass spectrometry.

In the following experiments three positive ion detection modes were used. The linear detector, with the reflectron switched off, was used to examine the molecular weight distribution of a polymer obtained, when intact adducts and those that have fragmented in the field free drift region of the mass spectrometer, are both detected. In this reflectron-off mode, every oligomer adduct that has entered the time-of-flight detector is detected regardless of whether it has dissociated or not (see figure 5.1).

The linear detector with the reflectron switched on was used to examine the molecular weight distribution of the neutral dissociation products of polymer adducts (see figure 5.2).

The reflectron detector was used to determine the fraction of oligomer adducts that did not dissociated by the time they had reached the linear detector. This was possible as only ionised species could be reflected by the reflectron and hence be detected using the reflectron detector (see figure 5.2).

The samples studied consisted of dithranol as the matrix, KCl as the salt and PEG, as the polymer. Different molecular weight PEG samples were used. The PEG samples used were PEG 1000 (average molecular weight 1000 Da) and PEG 2000 (average molecular weight 2000 Da). Both of these PEG samples were monodisperse. Another sample was prepared in which two monodisperse PEG samples were combined to make up a more polydisperse sample. The PEG samples in the mixture were PEG 1000 and PEG 3400, with average molecular weights of 1000 Da and 3400 Da, respectively. These polymer samples were mixed in a 1:9 ratio, PEG 1000 to PEG 3400. This mixing ratio was chosen to give a bimodal mass distribution, with two maxima of roughly similar intensities. All samples were prepared using the aerosol method. The gain on the detectors was varied for all

modes to give comparable signal intensities in order to facilitate comparison of mass spectra and to produce a similar detector response.

No significant differences were found in the polymer mass distributions between the three different types of mass spectra recorded for PEG 1000 and PEG 2000. As both PEG 1000 and PEG 2000 polymer distributions cover a comparatively small mass range only a small difference in dissociation behaviour of the high-mass adducts and the low-mass adducts of this oligomer range would be expected.

The results for the experiment for which a more polydisperse polymer sample was produced by mixing PEG 1000 and PEG 3400 are shown in figure 5.26. All three mass spectra exhibit a bimodal polymer distribution, the maxima of which are centred on 1000 Da and 3400 Da, respectively. The polymer distribution in figure 5.26 a contains some intense peaks due to matrix trimer and tetramer species between 750 Da and 1250 Da. These matrix peaks are more intense than the polymer peaks in this part of the mass spectrum. There is no apparent obvious difference between the polymer distributions in the three mass spectra shown in figure 5.26. This indicates that, for the system investigated, there is no significant difference in the extent of dissociation between high-mass and low-mass oligomers. Polymer adduct dissociation would appear not to be a major factor to the skewing of polymer mass distributions of polydisperse polymers often seen in MALDI mass spectrometry.

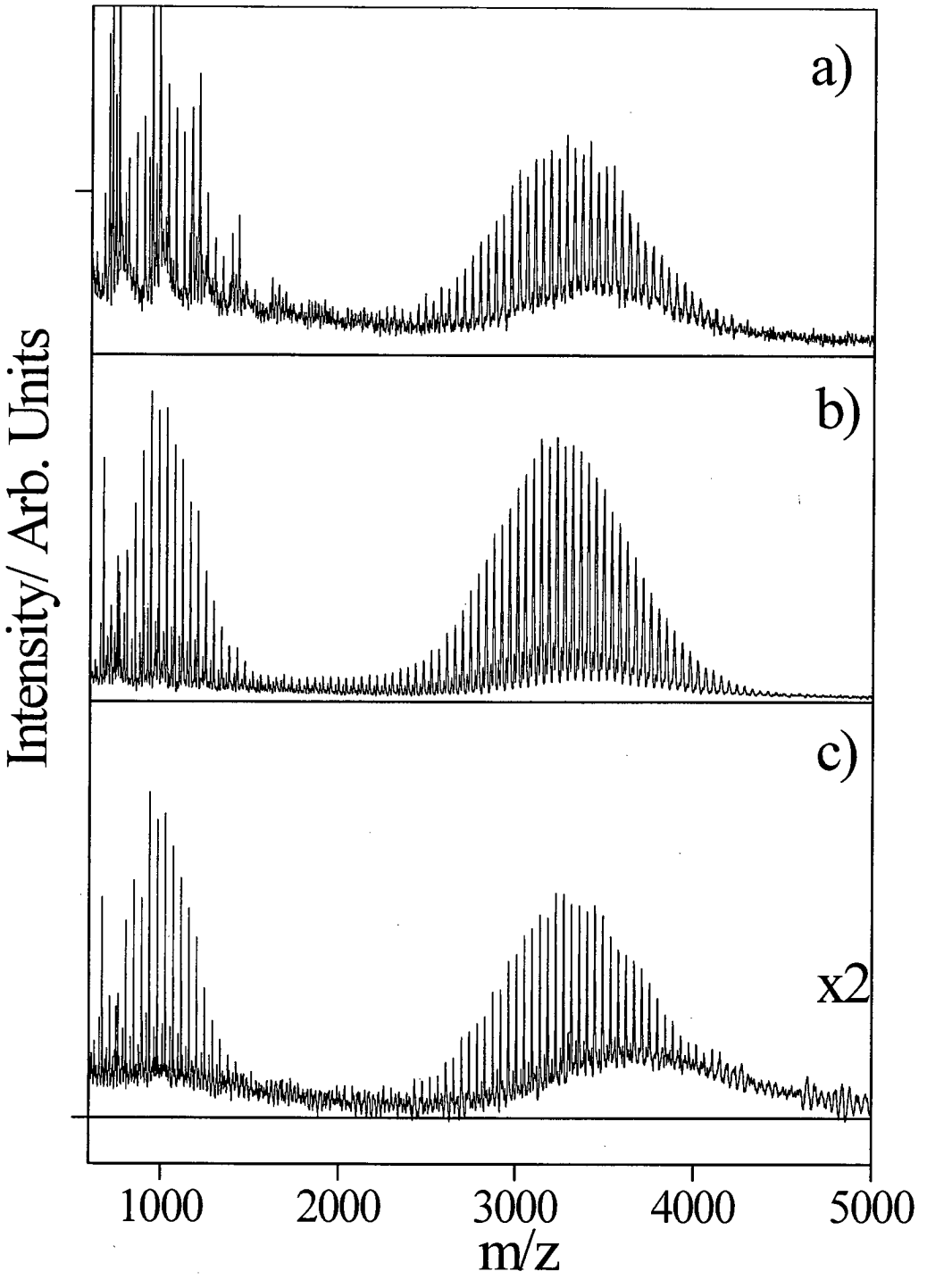

Figure 5.26 Mass spectra of a mixture of potassiated PEG 1000 and PEG 3400 recorded using three different detection systems. a) The mass spectrum was recorded on the linear detector with the reflectron switched on; only neutrals are observed. b) The mass spectrum was recorded on the linear detector with the reflectron switched off; both ions and neutrals are observed. c) The mass spectrum was recorded on the reflectron detector with the reflectron switched on; only reflected ions are observed.

5.4 Conclusions

The work outlined in this chapter investigates the production of neutral species through the dissociation of adducts in the field free drift region of a time-of-flight mass spectrometer in polymer MALDI experiments. It was shown that certain polymer metal ion adducts dissociate post-source. The proportion of the polymer metal ion adducts which dissociated was dependent on the metal ion. It was found that for alkali metal adducts of polymers, the lithium and sodium adducts did not dissociate, whereas the potassium and rubidium adducts did dissociate. Potassium adducts dissociated to a lesser extent than rubidium adducts, suggesting that the higher the charge density of the cation, the more stable the adduct. This dissociation behaviour was found to be similar for a range of different polymers, namely poly(ethylene glycol), poly(propylene glycol) and poly(methyl methacrylate). A more detailed study of poly(ethylene glycol) revealed that the dissociation rate of the potassium and rubidium adducts was independent of laser energy over an energy range of 69 μJ to 108 μJ. This suggests that the increase in laser energy did not greatly increase the average internal energy of the polymer adduct. It was found that over this laser energy range *ca* 3.5% of potassium adducts and 5% of rubidium adducts underwent PSD. The extent of dissociation of potassium adducts of poly(ethylene glycol) does not significantly change over the mass range of 673 Da to 4545 Da. The trend in alkali metal ion size compared with the extent of fragmentation would suggest that the post-source decay seen is dependent on the metal ion oligomer bond. The neutrals observed were most probably formed through the loss of the metal ion from the polymer metal adduct ion.

5.5 References

[1] B. Stahl, M. Steup, M. Karas and F. Hillenkamp, *Anal. Chem.*, **63**, 1463-1468 (1991)

[2] K. O. Bornsen, M. Scharr, E. Gassmann and V. Steiner, *Biol. Mass Spectrom.*, **20**, 471-475 (1991)

[3] I. A. Mowat and R. J. Donovan, *Rapid Commun. Mass Spectrom.*, **9**, 82-90 (1995)

[4] H. Rashidezadeh and B. C. Guo, *J. Am. Soc. Mass Spectrom.*, 9, 724-730 (1998)

[5] M. J. Deery, K. R. Jennings, C. B. Jasieczek, D. M. Haddleton, A.T. Jackson, H. T. Yates and J. H. Scrivens, *Rapid Commun. Mass Spectrom.*, **11**, 57-62 (1997)

[6] C. K. L. Wong and T. W. D. Chan, *Rapid Commun. Mass Spectrom.*, **11**, 513-519 (1997)

[7] C. F. Llens and R. M. O'Malley, *Rapid Commun. Mass Spectrom.*, **6**, 564-570 (1992)

[8] P. A. Dean and R. M. O'Malley, *Rapid Commun. Mass Spectrom.*, **7**, 53-57 (1993)

[9] J. H. Scrivens, A. T. Jackson, H. T. Yates, M. R. Green, G. Critchley, J. Brown, R. H. Bateman, M. T. Bowers and J. Gidden, *Int. J. Mass Spectrom. Ion Proc.*, **165**, 363-375 (1997)

[10] A. Westman, G. Brinkmalm and D. F. Barofsky, *Int. J. Mass Spectrom. Ion Proc.*, **169/170**, 79-87 (1997)

[11] D. C. Reiber, T. A. Grover and R. S. Brown, *Anal. Chem.*, **70**, 673-683 (1998)

[12] R. S. Lehrle and D. S. Sarson, *Rapid Commun. Mass Spectrom.*, **9**, 91-92 (1995)

[13] K. Martin, J. Spickermann, H. J. Rader and K. Mullen, *Rapid Commun. Mass Spectrom.*, **10**, 1471-1474 (1996)

[14] D. C. Schriemer and L. Li, *Anal. Chem.*, **69**, 4169-4175 (1997)

[15] D. C. Schriemer and L. Li, *Anal. Chem.*, **69**, 4176-4183 (1997)

Chapter 6 – Delayed extraction experiments

6.1 Introduction

Delayed extraction techniques have come into wide use over recent years [1,2,3]. Delayed extraction is often employed to improve the resolution of time-of-flight mass spectrometers. In the work described in this chapter, delayed extraction was not used for this purpose but it was used to investigate cation attachment reactions and initial velocity distributions in the MALDI source. Mowat *et al.* [4] and Wang and co-workers [5] have previously described similar experiments into cation attachment. In both these experiments an increase in signal intensity was seen with increasing delay time for adduct ion formation up to a maximum intensity, after which the signal intensity dropped off again.

An increase in signal intensity was observed for peptides [5] and polymers [4]. The maximum intensities were recorded at the following delay times, 500 ns for polystyrene with Ag^+ [4], 700 ns for poly(propylene glycol) with Na^+ [4] and between 340 ns and 550 ns for gramicidin S with K^+ [5]. These results were interpreted as evidence for gas-phase adduct formation, with the increase in signal intensity with delay time, being due to continued adduct formation in the source region during the time delay. In a more recent paper Schanen *et al.* demonstrated

efficient gas-phase adduct formation in supersonic beam experiments [6]. Hoberg and co-workers, through use of a layered sample deposition technique provided further evidence for gas-phase cationisation [7]. In this experiment, the matrix and analyte were sandwiched between two salt layers, each salt layer consisting of a different salt. Only cations from the bottom salt layer attached to the analyte. This selective attachment was seen as evidence for gas-phase reactions as, after laser ablation, the metal ions from the bottom layer would pass through the matrix analyte layer, whereas the top layer metal ions would not have an opportunity to interact in such a way. There are indications from work on whether photochemical or thermal processes occur during MALDI that different mechanisms operate for proton and metal-ion attachment [8]. Proton adducts were only observed if photochemical processes occurred, whereas metal ion adducts were observed even if only thermal processes were possible [8]. These observations would suggest that photoexcited matrix species are not necessary for metal ion adduct formation. The possibility of thermal desorption was interpreted as evidence for preformation of metal ion adducts in the solid phase [8]. Recent work by Knochenmuss *et al.* suggests that adduct formation occurs 'promptly' after the laser shot and that two photoexcited matrix molecules are required to bring about adduct formation [10,11]. It seems probable that more than one channel exists for adduct formation and that some, if not all, the mechanisms proposed play a part.

The aim of the work described in this chapter was to investigate the adduct formation for the polystyrene silver system using delayed ion extraction. A similar approach was taken to that of Mowat [4,9] but there were several important

differences; first a novel sample preparation method was employed, giving improved reproducibility and secondly the work was carried out using a linear TOF mass spectrometer. The effect that salt concentration had on the ionisation behaviour was investigated. The aim was to test the hypothesis of Knochenmuss and co-workers that a minimum of two photoexcited matrix molecules were required to bring about ionisation [10,11]. At low salt concentrations, the probability of two photoexcited matrix molecules being nearest neighbours in the solid is high and therefore the proposed prompt ionisation mechanism can occur. However, at very high salt concentrations, it is far less likely that two photoexcited matrix molecules are next to each other, as salt molecules make up a large number of a given matrix molecule's nearest neighbours. Consequently, it is reasonable to expect fewer gas-phase cation adductions at low salt concentrations than in the high salt concentration scenario, as the probability of prompt reactions occurring is greatly increased at low salt concentrations.

6.2 Experimental

The power supply to the sample holder in the source had to be modified to carry out delayed extraction experiments. A schematic illustration of the delayed extraction configuration of the instrument is shown in figure 6.1. A potential of up to 5 kV was delivered by a high voltage power supply (model PS350, Stanford Research Systems, Inc.), driving a fast high voltage push-pull switch (Behlke, Germany). The switch was triggered by a pulse generator (Lyons Instruments), which produced a square wave. The trigger for the pulse generator was provided by the synchronous output of the laser. A time delay of from 0 to 2 μs between the

trigger from the synchronous output of the laser and the pulsed output from the pulse generator was used. The high voltage pulse produced had a rise time of less than 50 ns from 0 to 4 kV. The pulse width of the extraction pulse was 2.5 μs, which was long enough to ensure that all ions of interest were extracted from the source region. An example of the sequence between the laser pulse and the extraction pulse is shown in figure 6.2.

All samples were prepared using the aerosol sample deposition technique described in detail in chapter 3. This meant that an even homogenous sample surface was produced, from which a large number of spectra could be obtained, each laser shot using a fresh sample surface. Every spectrum shown in this chapter is the average of three to five spectra, each of which was summed over 50 shots. In this way very good reproducibility was achieved.

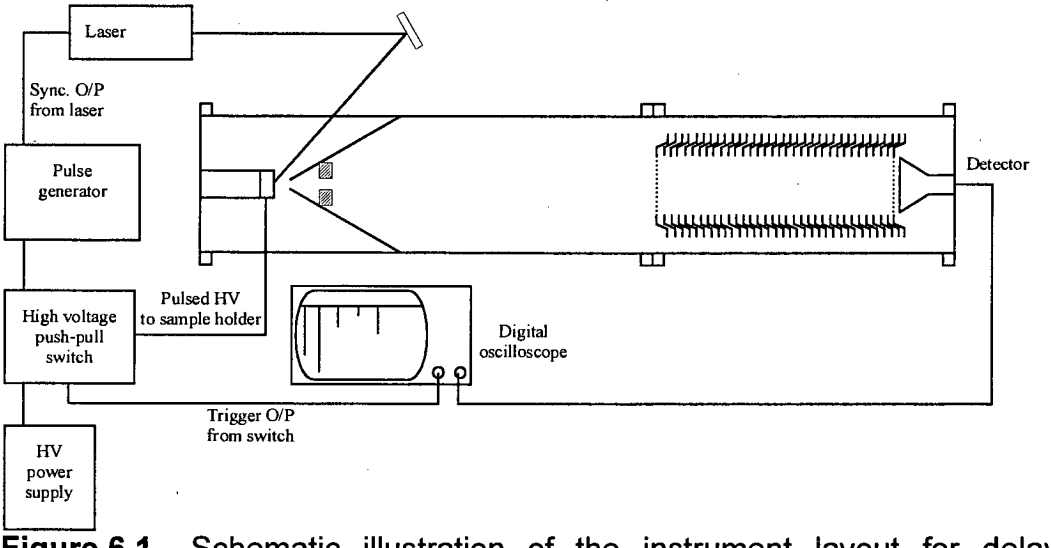

Figure 6.1 Schematic illustration of the instrument layout for delayed extraction operation

One-stage sample deposition was employed for the experiments using polystyrene as the polymer, *i.e.* the polymer, salt and matrix were dissolved in a

common solvent and this mixture was sprayed onto the sample holder. Two-stage sample deposition was used in the experiments using poly(ethylene glycol) (PEG) and poly(methyl methacrylate) (PMMA). In this case the salt solution was sprayed onto the sample holder first, then a mixture of polymer and matrix solution was sprayed onto the salt layer.

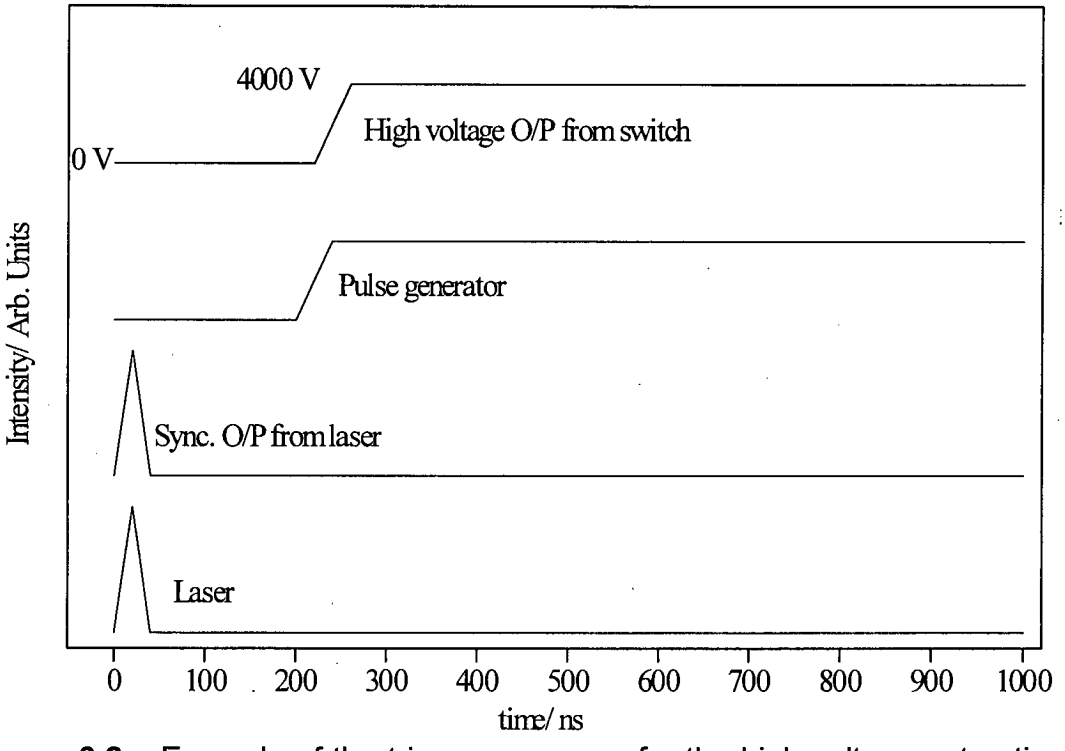

Figure 6.2 Example of the trigger sequence for the high voltage extraction pulse. The synchronous output from the N_2 laser triggers the pulse generator, which in turn triggers the high voltage switch.

6.2.1 Treatment of results

All data manipulation was done using Microcal Origin software. Traces recorded at a given delay time were averaged. The peak areas of single peaks were obtained from the time-of-flight spectra by using the 'integrate function' provided by the Origin software. In order to be able to compare peak areas obtained at different

delay times, it was necessary to integrate over a wide time-of-flight interval. For example, to determine the peak area of the 10-mer of polystyrene, the trace obtained for each delay time was integrated between 26 μs and 27.2 μs, as the 10-mer would always arrive at the detector in this time interval (see figure 6.14).

6.3 Results

6.3.1 Results obtained for delayed extraction experiments with varying salt concentrations

In this series of experiments, the proportion of salt added to a polymer sample was varied. The polymer studied was polystyrene (average molecular weight 1340 g mol^{-1}), the matrix used was dithranol and the salt used was silver trifluoroacetate. The molar matrix to analyte ratio was kept constant at 60:1 (using the average molar mass of the polymer as a point of reference). The molar ratio of matrix to salt was varied from 10:1 to 1:5. The delay times chosen were 0 ns, 100 ns, 200 ns, 300 ns, 400 ns and 600 ns. These delay times were selected as in previous work the most intense signal was observed between 0 ns and 700 ns [4,5].

A typical example of the results obtained is shown in figure 6.3. All traces shown are the average of four separate data sets collected over 50 laser shots each. Although differing in intensity and resolution, all traces shown were fundamentally very similar.

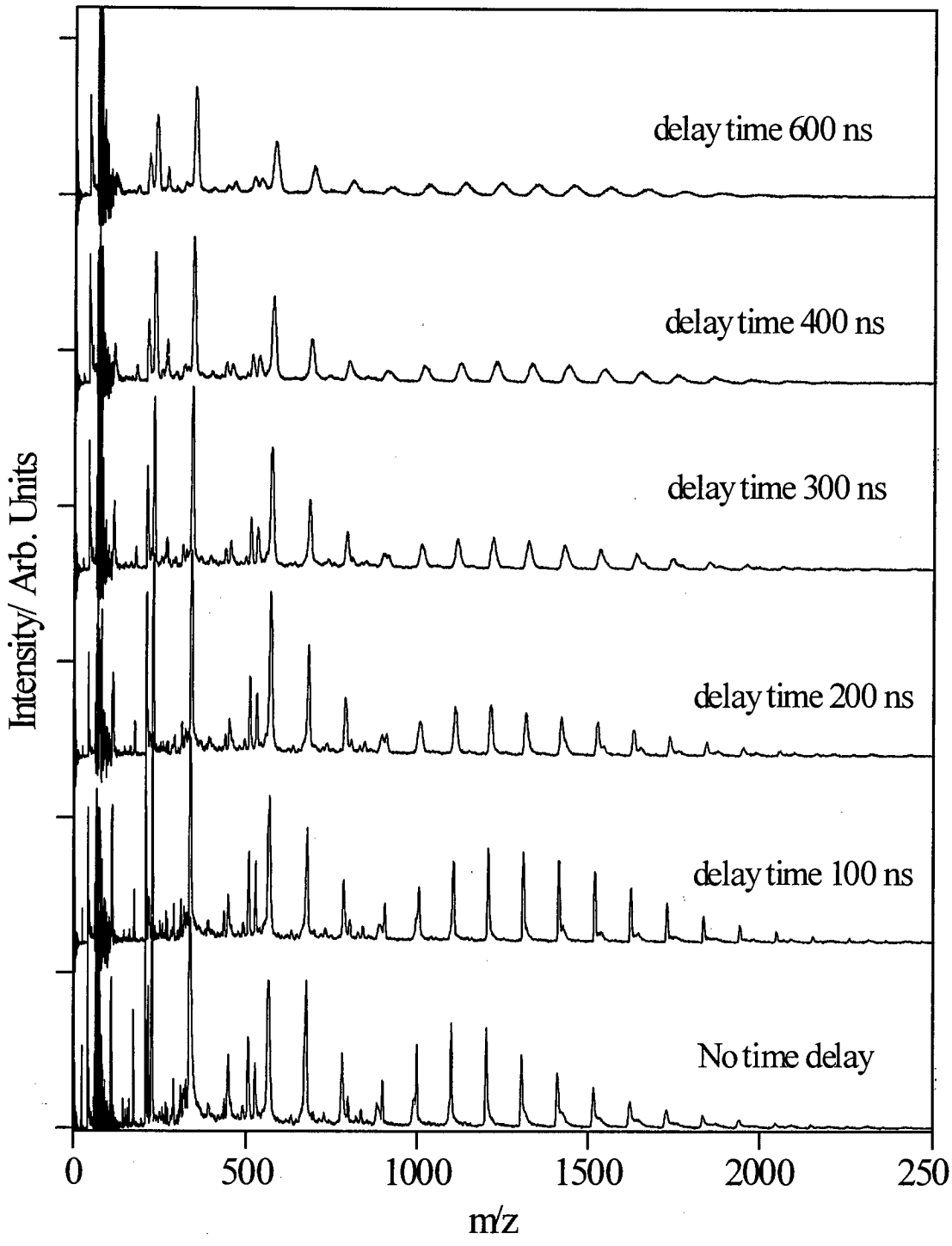

Figure 6.3 Effect of delayed ion extraction on the MALDI mass spectra of polystyrene. In the bottom trace no delay between the laser shot and ion extraction was used. For the other traces, a delay of between 100 ns and 600 ns was used, as shown. The matrix used was dithranol and the salt used was $AgCF_3CO_2$. The matrix to salt ratio was 1 to 5.

The peaks above 900 Da, which are all separated from each other by 104 Da, are due to the silver ion adducts of polystyrene. The polystyrene sample investigated here has the following structure, Bu^t-$(CH_2$-$CH(C_6H_5))_n$-H. The masses observed for polystyrene are therefore given by:

$$58\ Da + 108\ Da + n*104\ Da \qquad \textbf{6.1}$$

where 58 Da is the combined mass of the endgroups, 108 Da is the average mass of the silver ion attached to the polystyrene oligomer (*N.B.* the 107 and 109 isotopes of silver are not resolvable at this mass) and 104 Da is the repeat unit mass.

Peaks at masses less than 700 Da are due to a number of different species which include protonated and cationised matrix molecules, metal ions and also switching noise from the high voltage switch.

The peak areas for a range of different polystyrene oligomers were calculated in order to investigate the effect time delay had on the signal intensity. Peak area rather than peak height was chosen as a measure of signal intensity, as the peak width varied considerably with delay time, owing to the initial velocity distribution of ions generated by MALDI. The actual peak areas measured are listed in Appendix I. The results of the signal intensity study are shown in figures 6.4 to 6.8.

The signal intensities of all oligomer ions investigated would have been expected to exhibit similar behaviour, as only a mass range of 600 Da was covered by the oligomers considered. No significant difference in the signal intensity versus

delay time behaviour can be seen for different oligomers at any of the salt concentrations studied (see figures 6.4 to 6.8).

In order to examine the overall trends in signal intensity, the average value for all oligomers was determined for each different salt concentration. These averaged results are shown in figure 6.9. The signal intensity response to delay time is very similar at all matrix to salt ratios, with the possible exception of the 1:2 salt to matrix case. The general trend is for signal intensity to decrease with increasing delay time. This finding is in direct contrast to previous observations [4,5] where significant increases in signal intensity were observed at early delay times.

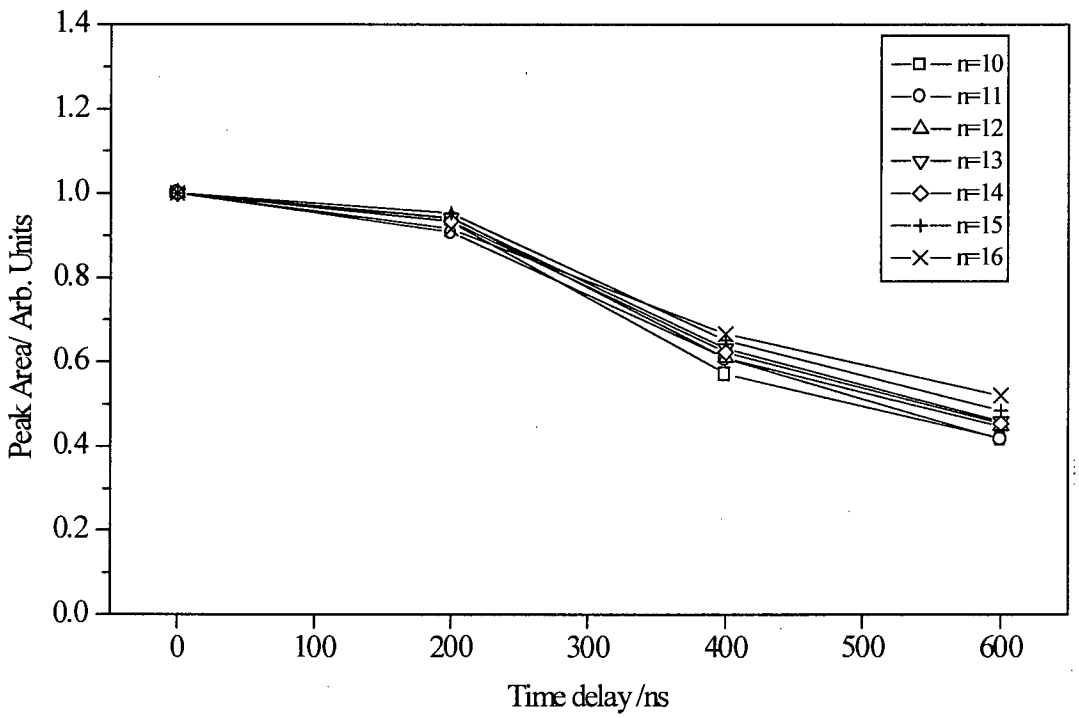

Figure 6.4 The variation in normalised peak areas for a range of different polystyrene oligomer silver adducts with delay time (n = the number of styrene repeat units). The matrix used was dithranol and the salt used was $AgCF_3CO_2$. The mole ratio of dithranol to $AgCF_3CO_2$ used was 10:1.

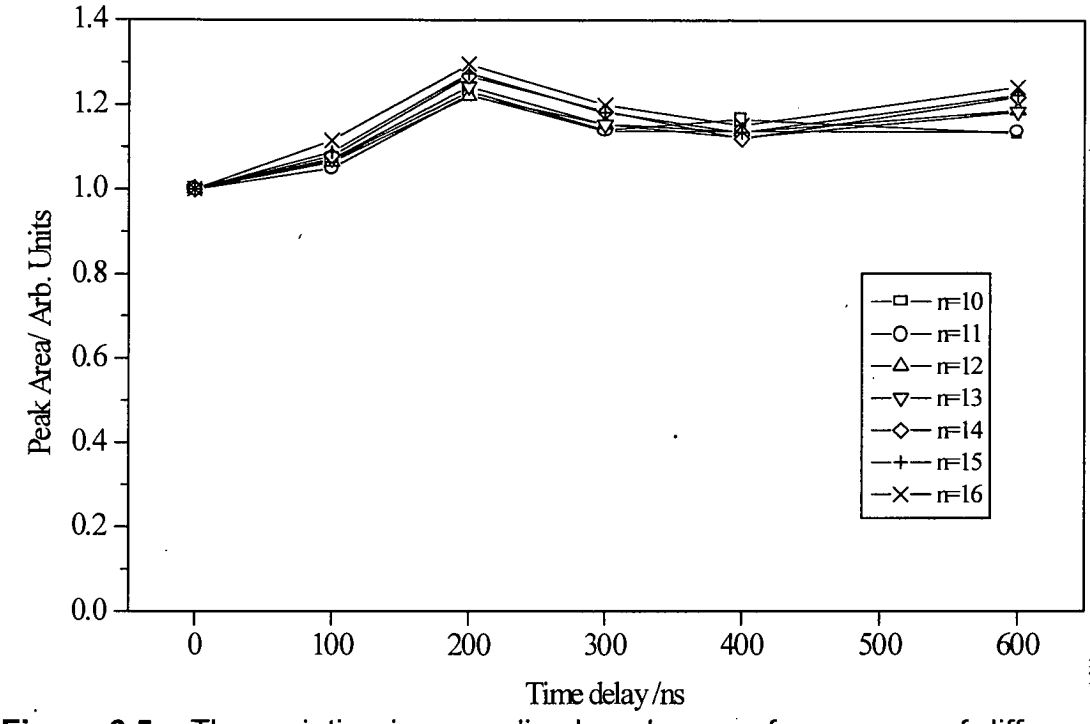

Figure 6.5 The variation in normalised peak areas for a range of different polystyrene oligomer silver adducts with delay time (n = the number of styrene repeat units). The matrix used was dithranol and the salt used was $AgCF_3CO_2$. The mole ratio of dithranol to $AgCF_3CO_2$ used was 2:1.

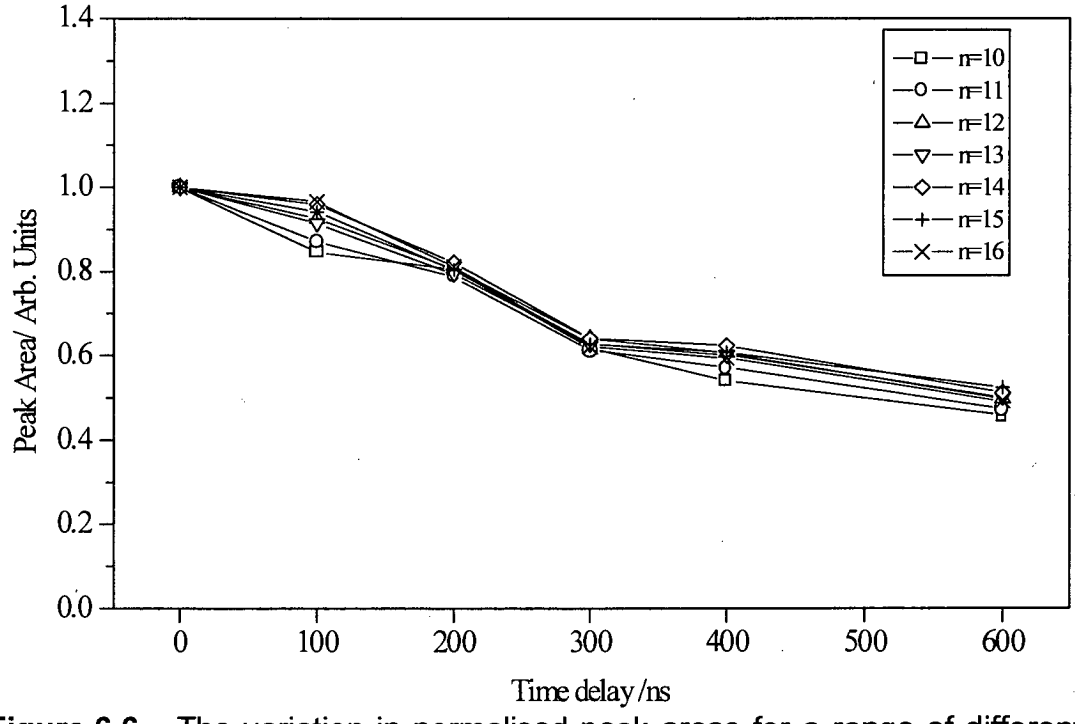

Figure 6.6 The variation in normalised peak areas for a range of different polystyrene oligomer silver adducts with delay time (n = the number of styrene repeat units). The matrix used was dithranol and the salt used was $AgCF_3CO_2$. The mole ratio of dithranol to $AgCF_3CO_2$ used was 1:1.

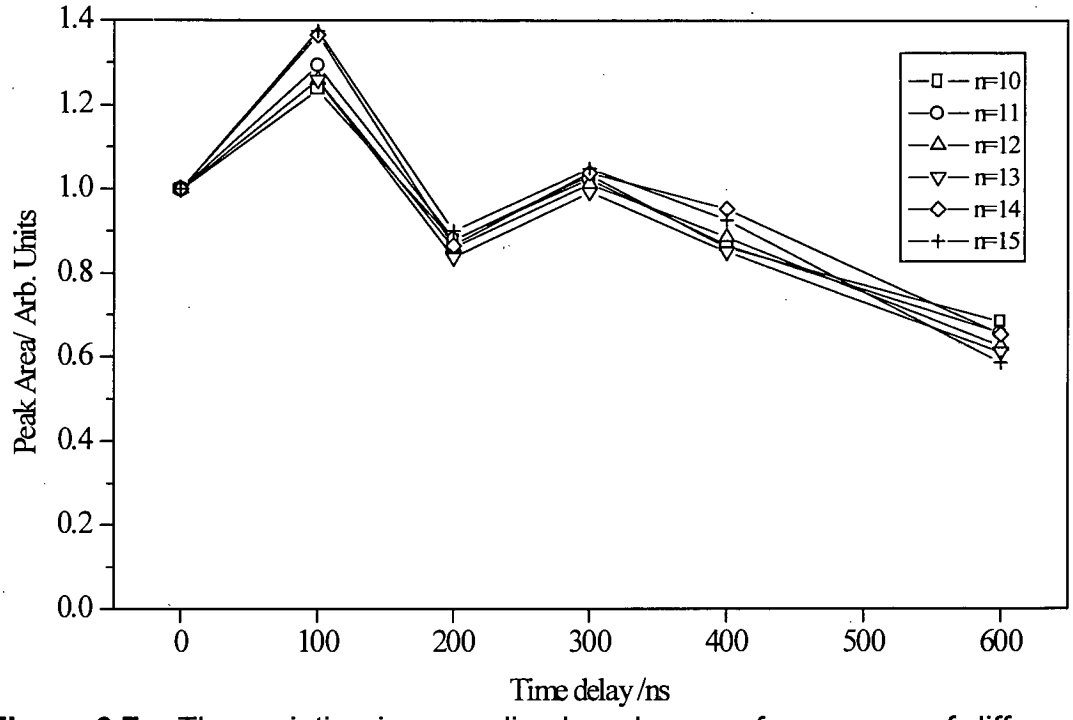

Figure 6.7 The variation in normalised peak areas for a range of different polystyrene oligomer silver adducts with delay time (n = the number of styrene repeat units). The matrix used was dithranol and the salt used was $AgCF_3CO_2$. The mole ratio of dithranol to $AgCF_3CO_2$ used was 1:2.5.

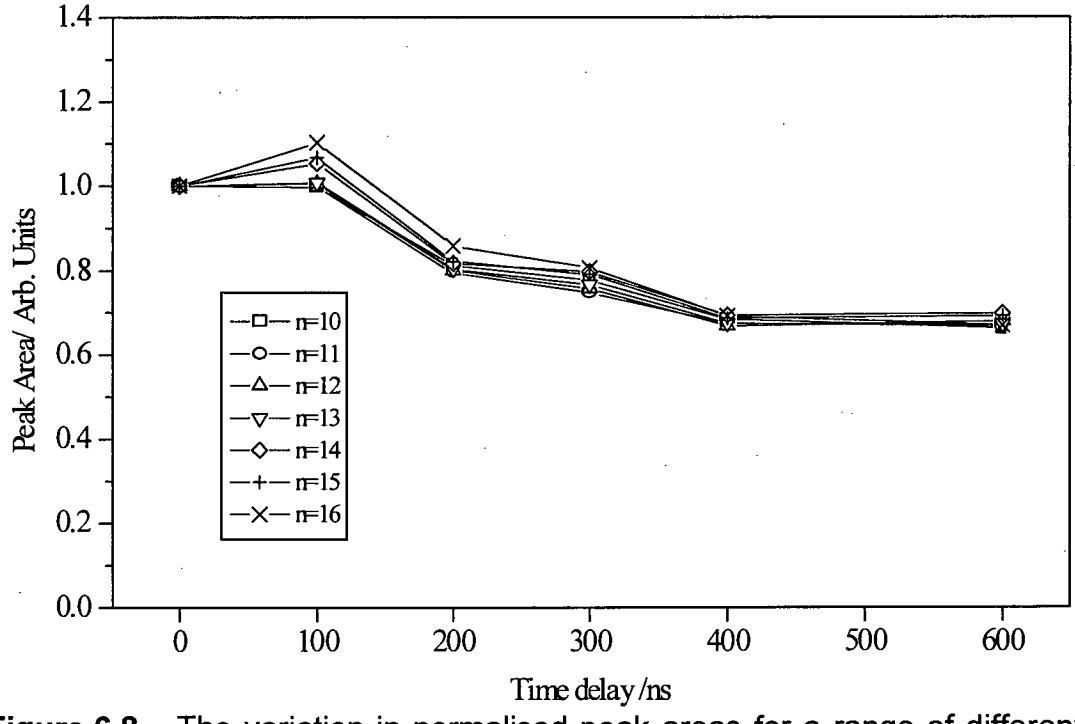

Figure 6.8 The variation in normalised peak areas for a range of different polystyrene oligomer silver adducts with delay time (n = the number of styrene repeat units). The matrix used was dithranol and the salt used was $AgCF_3CO_2$. The mole ratio of dithranol to $AgCF_3CO_2$ used was 1:5.

An increase in signal intensity has usually been interpreted as being due to an actual increase in the number of ions and hence evidence for a mechanism producing these ions [4,5]. It is, however, conceivable that an increase in signal intensity could be the result of an instrumental factor, such as improved detection efficiency at longer delay times. The detection efficiency of high-mass ions by microchannel plate detectors has been shown to be adversely affected by large numbers of lighter ions hitting the detector prior to the arrival of the high-mass ions [12]. These effects are usually termed saturation effects. One way of combating saturation problems is the use of deflector plates to stop low-mass ions from reaching the detector. Time delays between the laser shot and extraction lead to depletion in the number of low-mass ions reaching the detector as low-mass ions have a greater velocity distribution than high-mass ions [13], as discussed later. This reduction could conceivably lead to increased detection efficiency of high-mass ions and, therefore, an increase in high-mass signal intensity with delay time would be expected. It is worth noting that in the previous delayed extraction experiments in which signal enhancement was seen [4,5], low-mass ions were not deflected and hence the type of signal enhancement discussed proposed here is feasible. It should be mentioned that in the experiments described here low-mass deflection was not used either as the mass gate was only installed later. However, the effect of low-mass ions was minimised by using the lowest laser powers possible. A future study making use of the mass gate recently fitted to the mass spectrometer used in this research should be carried out to test this hypothesis.

The study presented here shows an overall decrease in signal intensity with increasing delay time. This decrease can be accounted for by two main loss pathways. First, as ions formed by MALDI can have considerable initial velocities, ions can be lost by moving away from the extraction region of the source. Typical average initial ion velocities reported for analyte ions (i.e. ions with mass >1000 Da) are in the range of 500 to 1000 m s^{-1} [13,14,15,16 and 17]. The diameter of the extraction optics used for this experiment used was 2 mm. An ion with a velocity of 1000 m s^{-1} (typical velocity reported for analyte ions) covers a distance of 1 mm in 1 μs. Therefore, it can be assumed that drift of ions out of the extraction region is one of the factors leading to a decrease in signal intensity with increasing delay time. Another possible loss mechanism is the collision induced and/or spontaneous decay of polymer ions, for instance through the loss of the metal cation. In-source decay has been reported [18]. Collisions between ions and neutrals are probable in the source region; also ions can have large internal energies which can lead to dissociation.

The results presented here do not point clearly to any specific ionisation mechanism. However, they show that for the system studied, delayed extraction did not lead to an increase in signal intensity, which would suggest that gas-phase reactions taking place after the laser shot do not play an important part in the adduct ion formation mechanism. Of course gas-phase reaction may still be taking place; however, the number of ions produced in this way must be smaller than the number of ions lost through decay/non-detection.

The signal intensity versus delay time relationship does not appear to be affected by the salt concentration used. This would suggest that the cation-adduction mechanism does not require two photoexcited matrix molecules, as was recently suggested by Knochenmuss *et al.* [10].

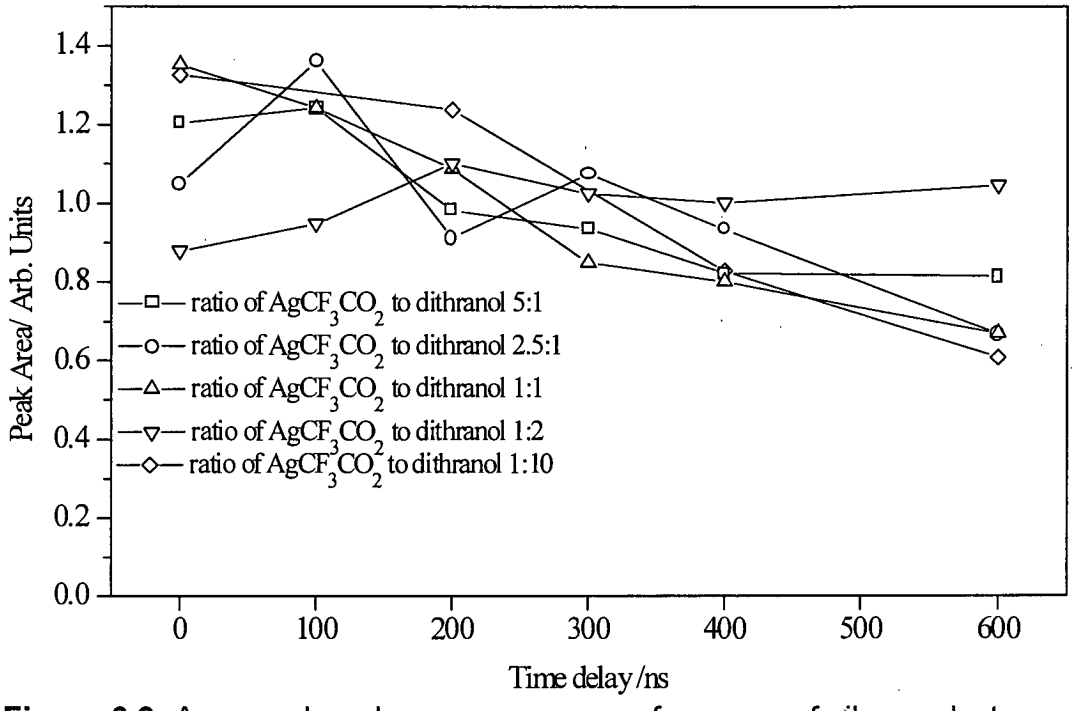

Figure 6.9 Averaged peak area responses of a range of silver polystyrene oligomer adducts to delay time for a range of different $AgCF_3CO_2$ to dithranol ratios

The experiments described here show that a time delay between the laser shot and ion extraction does not lead to an increase in the number of adduct ions formed. This suggests that gas-phase ion attachment reactions are comparatively rare after the laser shot. It has been shown in previous experiments, where gas-phase neutrals were combined with metal ions, that gas-phase ion attachments are possible [5,6]. The reason that adducts are not formed efficiently in this way in MALDI may be due to the high kinetic and internal energies of ions and neutrals formed by MALDI [19].

This high internal energy may lead to a lack of stability of adducts formed by gas-phase reactions.

6.3.2 Results obtained for other polymer salt systems

Delayed extraction experiments were also carried out using other polymer/salt systems. These were PMMA/LiCl and PEG/NaCl. Two sets of results, recorded over different delay time ranges, are presented for each polymer/salt combination. The results from these experiments were treated in the same way as the results from the polystyrene experiments. For these systems, only one polymer to salt concentration ratio was studied. The results for the two PMMA/LiCl experiments are shown in figures 6.10 and 6.11 and the results for the two PEG/NaCl experiments are shown in figures 6.12 and 6.13. The actual peak areas as measured are listed in Appendix I.

For these experiments only one salt to polymer to matrix ratio was employed. The aim of these experiments was to determine whether different polymers demonstrated different ionisation behaviour. The results obtained showed clearly that - as with the polystyrene samples - a decrease in signal intensity was observed with increasing delay time. This indicates that similar processes are involved in the ionisation for these three different polymer/cation systems. It also suggests that gas-phase reactions after the laser shot play a minor role in the cationisation process.

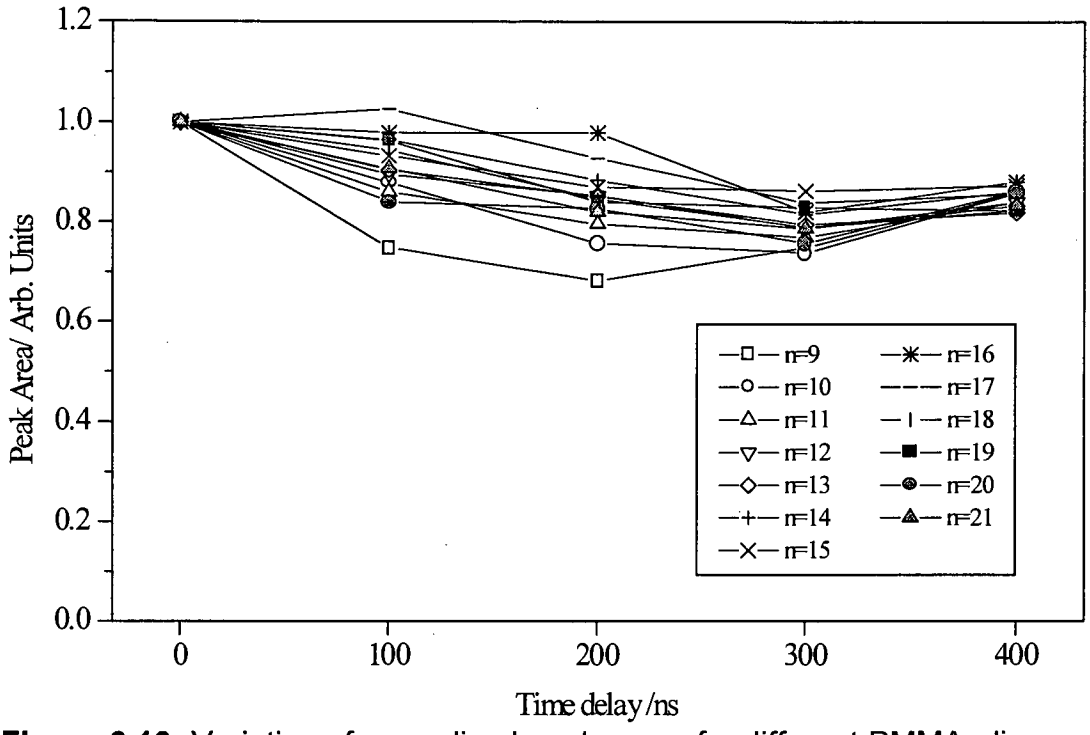

Figure 6.10 Variation of normalised peak areas for different PMMA oligomer lithium adducts with delay time (n = tho the number of MMA subunits). The matrix used was dithranol with LiCl at a mole ratio of 1:1. Delay time range for this experiment was 0 ns to 400 ns.

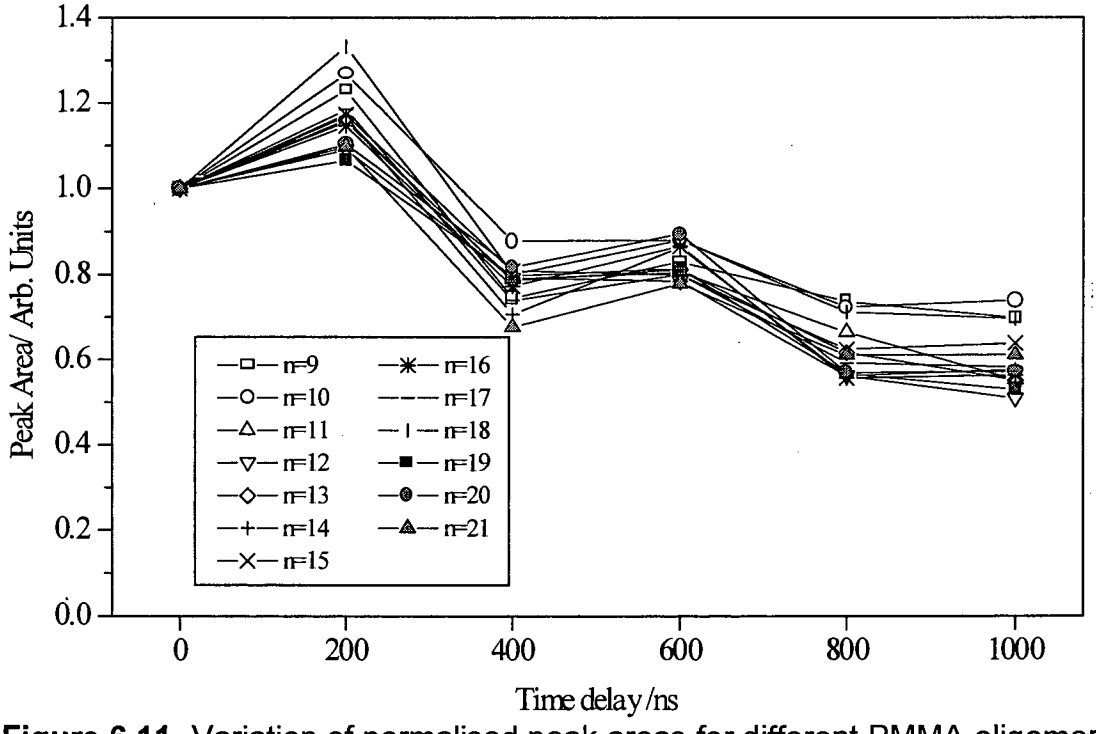

Figure 6.11 Variation of normalised peak areas for different PMMA oligomer lithium adducts with delay time (n = tho the number of MMA subunits). The matrix used was dithranol with LiCl at a mole ratio of 1:1. Delay time range for this experiment was 0 ns to 1000 ns.

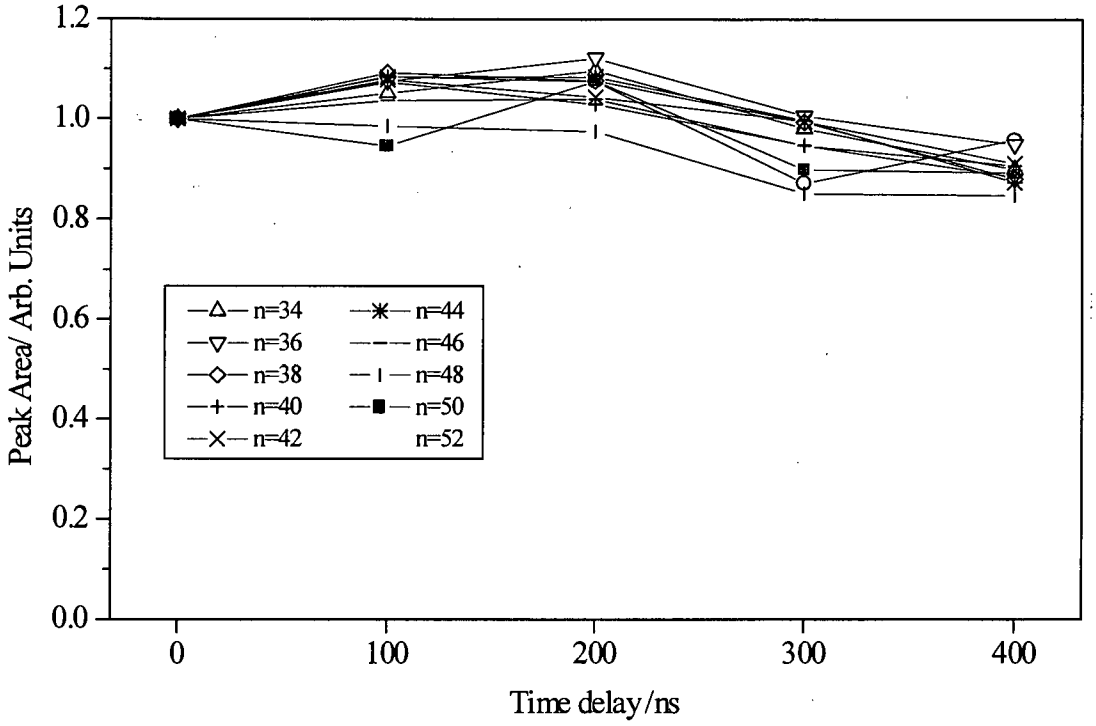

Figure 6.12 Variation of normalised peak areas for different PEG oligomer sodium adducts with delay time (n = tho the number of subunits). The matrix used was dithranol and the salt used was NaCl at a mole ratio of 1:1. Delay time range for this experiment was 0 ns to 400 ns.

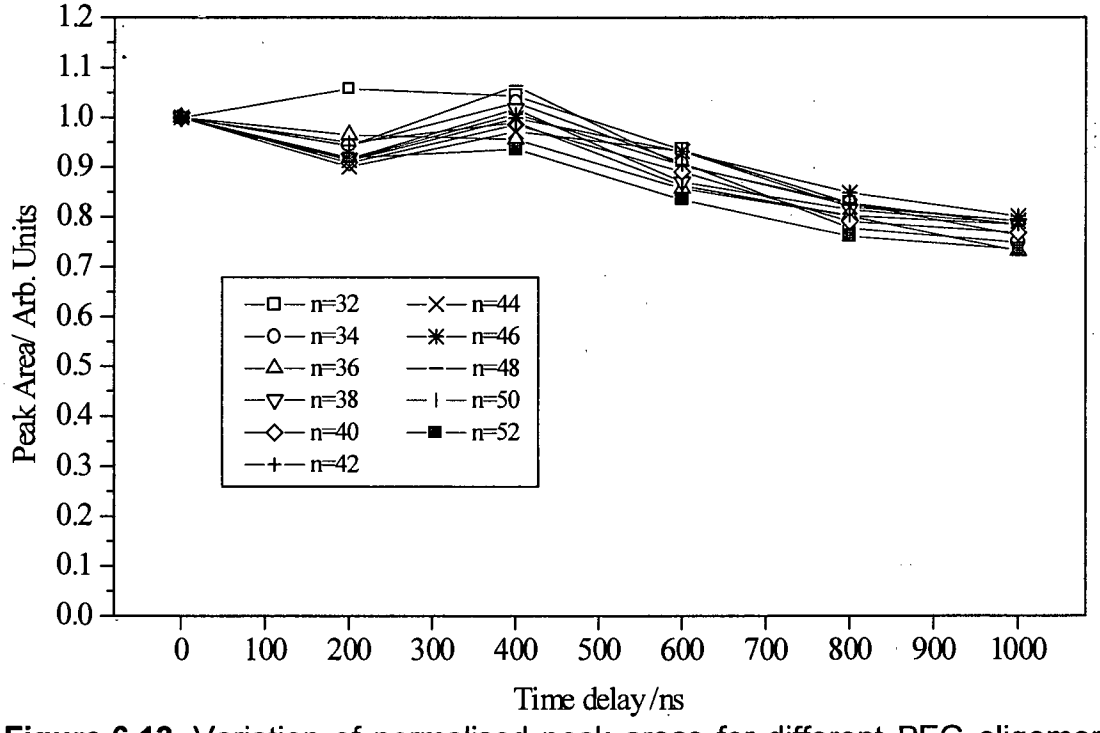

Figure 6.13 Variation of normalised peak areas for different PEG oligomer sodium adducts with delay time (n = the the number of subunits). The matrix used was dithranol with NaCl at a mole ratio of 1:1. Delay time range for this experiment was 0 ns to 1000 ns.

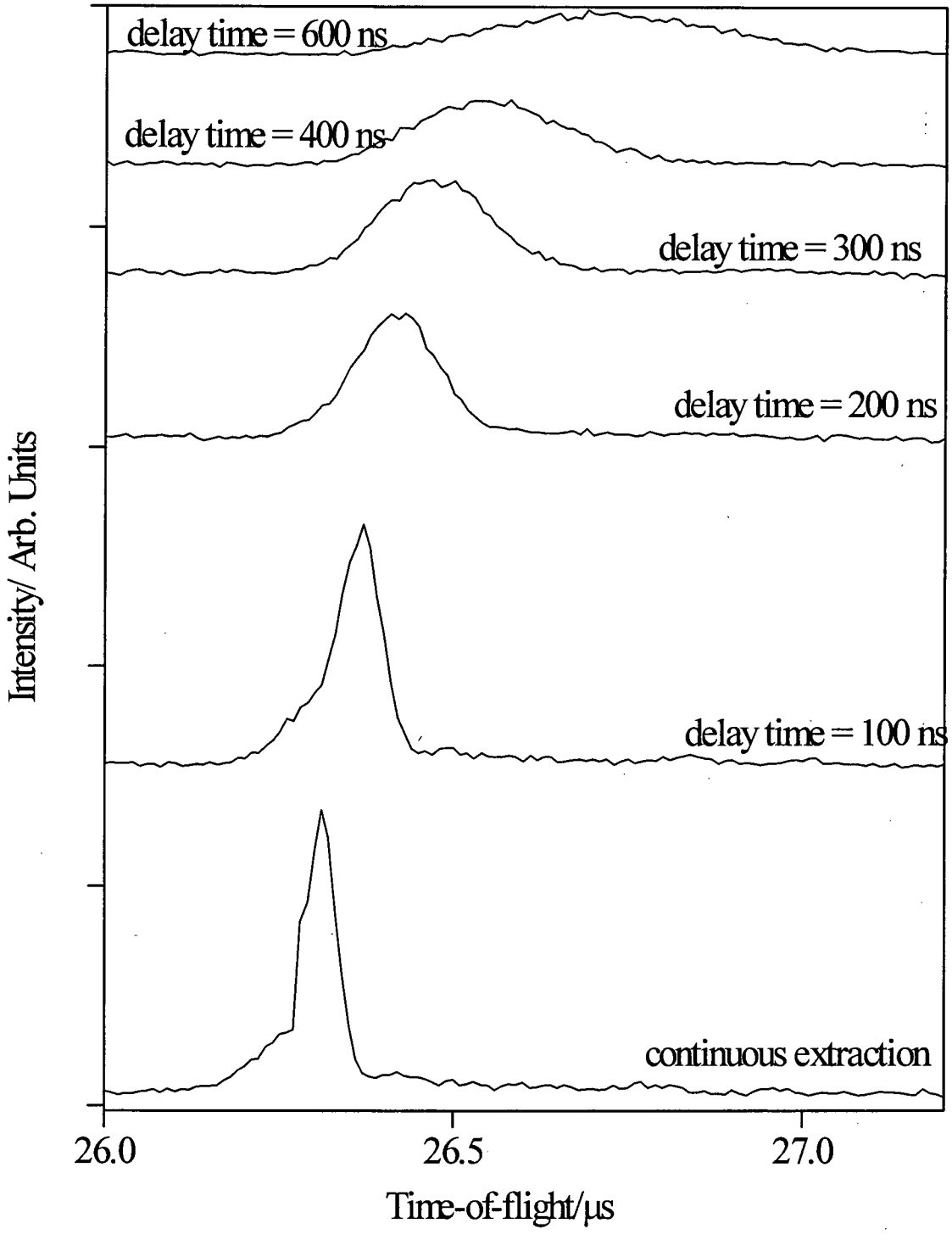

Figure 6.14 Illustration of the shift in time-of-flight seen under delayed extraction conditions owing to the initial velocity of ions. The peaks shown are silver adducts of the 10-mer of polystyrene.

6.3.3 Initial ion velocities

It was observed in the delayed extraction experiments outlined above that the peak positions of polymer adducts changed with delay time. The peak-position shift is illustrated in figure 6.14. As can clearly be seen the peak maxima shift to higher flight times with time delay. It is also noticeable that the peak width increases noticeably with delay time. Both these phenomena are direct consequences of the kinetic energy imparted to the ions during the MALDI process. The increase in flight time when a time delay is used is due to the ions moving away from the repeller owing to their initial velocity. The movement of ions away from the sample holder during the time delay means that they do not experience the full accelerating potential. As would be expected, the ions do not move at a uniform velocity. This leads to the peak broadening observed, *i.e.* some ions travel further from the repeller than others and therefore their flight time is increased more. A simple computer model (not shown here) indicated that the initial ion velocities were in the range of 500 m s^{-1} to 1500 m s^{-1}, which is in good agreement with published data [13,14].

6.4 Conclusions

The experiments described in this chapter show that the number of polymer adduct ions detected decrease when a time delay between the laser shot and ion extraction is used. This decrease in signal intensity is more marked at longer delay times. No evidence for increased adduct yield with time delay was found, contrary to previously published work. Possible reasons for this discrepancy were discussed.

The signal intensity to delay time response was unaffected by salt concentration even at very high salt concentrations suggesting that the ionisation process can operate when the probability of two photoexcited matrix molecules being nearest neighbours is small.

The initial velocity of ions generated using MALDI was clearly noticeable by an increase in time-of-flight of ions when a time delay was used between ion extraction and the laser shot.

6.5 References

[1] M. L. Vestal, P. Juhasz and S. A. Martin, *Rapid Commun. Mass Spectrom.*, **9**, 1044-1050 (1995)

[2] R. M. Whittal and L. Li, *Anal. Chem.*, **67**, 1950-1954 (1995)

[3] U. Bahr, J. Stahl-Zeng, E. Gleitsmann and M. Karas, *J. Mass Spectrom.*, **32**, 1111-1116 (1997)

[4] I. A. Mowat, R. J. Donovan and R. J. Maier, *Rapid Commun. Mass Spectrom.*, **11**, 89-98 (1997)

[5] B. H. Wang, K. Dreisewerd, U. Bahr, M. Karas and F. Hillenkamp, *J. Am. Soc. Mass Spectrom.*, **4**, 393-398 (1993)

[6] P. Schanen, D. Yang, R. Weinkauf and E. W. Schlag, *Int. J. Mass Spectrom. Ion Proc.*, **167/168**, 447-470 (1997)

[7] A. –M. Hoberg, D. M. Haddleton and P. J. Derrick, *Eur. Mass Spectrom.*, **3**, 471-473 (1997)

[8] H. Ehring, C. Costa, P. A. Demirev and B. U. R. Sundqvist, *Rapid Commun. Mass Spectrom.*, **10**, 821-824 (1996)

[9] "Synthetic polymer analysis using matrix assisted laser desorption/ ionisation time-of-flight mass spectrometry", I. A. Mowat, PhD thesis, The University of Edinburgh (1995).

[10] R. Knochenmuss, F. Dubois, M. J. Dale and R. Zenobi, *Rapid Commun. Mass Spectrom.*, **10**, 871-877 (1996)

[11] R. Knochenmuss, V. Karbach, U. Wiesli, K. Breuker and R. Zenobi, *Rapid Commun. Mass Spectrom.*, **12**, 529-534 (1998)

[12] A. Westman, G. Brinkmalm and D. F. Barofsky, *Int. J. Mass Spectrom. Ion Proc.*, **169/170**, 79-87 (1997)

[13] V. Bokelmann, B. Spengler and R. Kaufmann, *Eur. Mass Spectrom.*, **1**, 81-93 (1995)

[14] T. –W. D. Chan, I. Thomas, A. W. Colburn and P. J. Derrick, *Chem. Phys. Lett.*, **222**, 579-585 (1994)

[15] T. Huth-Fehre and C. H. Becker, *Rapid Commun. Mass Spectrom.*, **5**, 378-382 (1991)

[16] R. C. Beavis and B. T. Chait, *Chem. Phys. Lett.*, **181**, 479-484 (1991)

[17] Y. Pan and R. J. Cotter, *Org. Mass Spectrom.*, **27**, 3-8 (1992)

[18] D. C. Reiber, T. A. Grover and R. S. Brown, *Anal. Chem.*, **70**, 673-683 (1998)

[19] A. Bencsura, V. Navale, M. Sadeghi and A. Vertes, *Rapid Commun. Mass Spectrom.*, **11**, 679-682 (1997)

Chapter 7 – Copolymer analysis

7.1 Introduction to copolymer analysis

MALDI is uniquely well suited to the analysis of copolymers, as was demonstrated recently by several groups [1,2]. Unlike other techniques used for polymer mass analysis, MALDI can yield detailed information on the fine structure of polymers, such as endgroup and repeat unit masses. A major chemical company supplied the copolymers studied in this work. No analytical data were available for these compounds. The work discussed in this chapter illustrates how MALDI can be used to solve 'real industrial' problems.

7.2 Synthesis of the copolymer samples

Six copolymer samples were studied. These were oligomeric diisocyanate prepolymers. The following information was available about the manufacturing process [3]. An overview of the compounds used in copolymer synthesis is shown in table 7.1

The prepolymer samples were produced by reacting isophorone diisocyanate (IPDI) in N-methylpyrrolidone with a mixture of dimethylolpropionic acid (DMPA) and polypropylene glycols (PPG). The PPG used was prepared by mixing two monodisperse PPG samples to produce a wider polydispersity PPG sample. The M_p values of the two PPG constituents were 425 Da and 1000 Da, respectively. For ease

of reference the different samples will be referred to as Sample 1 to Sample 6. Sample 1 and Sample 2 were quenched with excess N-methylaniline (NMA). Sample 3 and Sample 4 were quenched with a minimum of N-methylaniline. Samples 5 and 6 were prepared by neutralising the prepolymers with Et_3N followed by dispersion into water containing hydrazine monohydrate. In preparing Samples 2, 4 and 6, the DMPA containing copolymer was reacted with triethylamine.

Name	Abbreviation	Formula
isophorone diisocyanate	IPDI	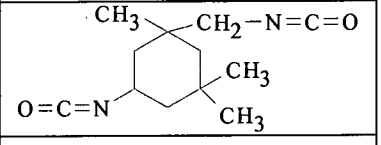
N-methylpyrrolidone	-	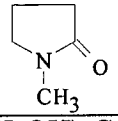
dimethylolpropionic acid	DMPA	$CH_3C(CH_2OH)_2CO_2H$
poly(propylene glycol)	PPG	$-(CH(CH_3)CH_2O)_n-$
N-methylaniline	NMA	$C_6H_5NHCH_3$

Table 7.1 Overview of the compounds used in copolymer synthesis

7.3 MALDI sample preparation and mass analysis

The two-stage droplet method of MALDI sample preparation described in detail in chapter 3 was employed. The prepolymer samples were dissolved in THF to a concentration of 1 g L^{-1}. The matrix used was dithranol (10 g L^{-1} in THF). Equal volumes of the matrix and the polymer solutions were combined. Droplets of 1 to 3 μL of salt solution were deposited on the sample holder. An aliquot of between 1 and 3 μL of the polymer matrix mixture was then injected using a micropipette into the salt droplet on the sample holder.

The instrument configuration used was the MALDI instrument prior to the flight-tube extension and the addition of the mass gate described in chapter 2. All

spectra were recorded in the reflectron mode. PEG standards were used for external calibration.

7.4 Results

7.4.1 Predicted products

The aim of the polymer preparation employed in the manufacture of Samples 1 to 4 was the production of polymers with the structures shown in table 7.2. MALDI was used to determine whether the anticipated copolymers had been synthesised. The results of the MALDI analysis will be discussed in three groups. Samples produced under similar conditions will be grouped together. The first group consists of Samples 1 and 2, the second group is made up of Samples 3 and 4 and the final group discussed contains Samples 5 and 6.

The evaluation of the results will be qualitative *i.e.* attention will be confined to the determination of the structure of the polymers present. Quantitative analysis, *e.g.* average molecular weight determination and relative abundance of the various polymer species present in each sample, was not attempted. The main reason for not carrying out quantitative analysis was due to uncertainty over the ionisation efficiency of the various polymer species present, as differences in ionisation efficiency could lead to inaccurate relative abundance as well as inaccurate average molecular weights. Another reason for not carrying out quantitative analysis is the comparatively wide mass ranges of the polymers under investigation. MALDI has been shown to give poor agreement with other techniques for average mass determination of polydisperse polymer samples [4,5].

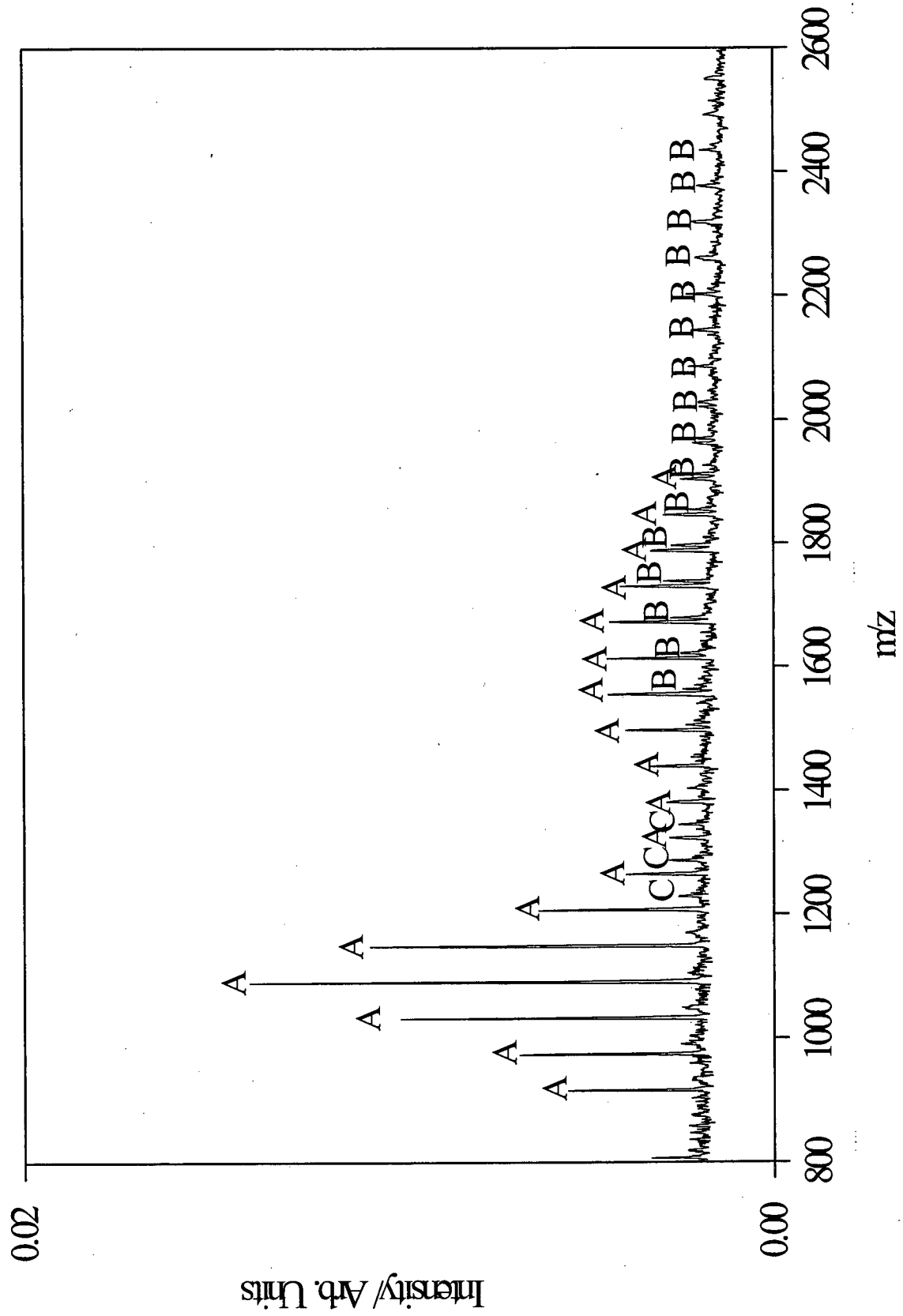

Figure 7.1 MALDI mass spectrum of Sample 1 produced using dithranol as the matrix and LiCl as the salt

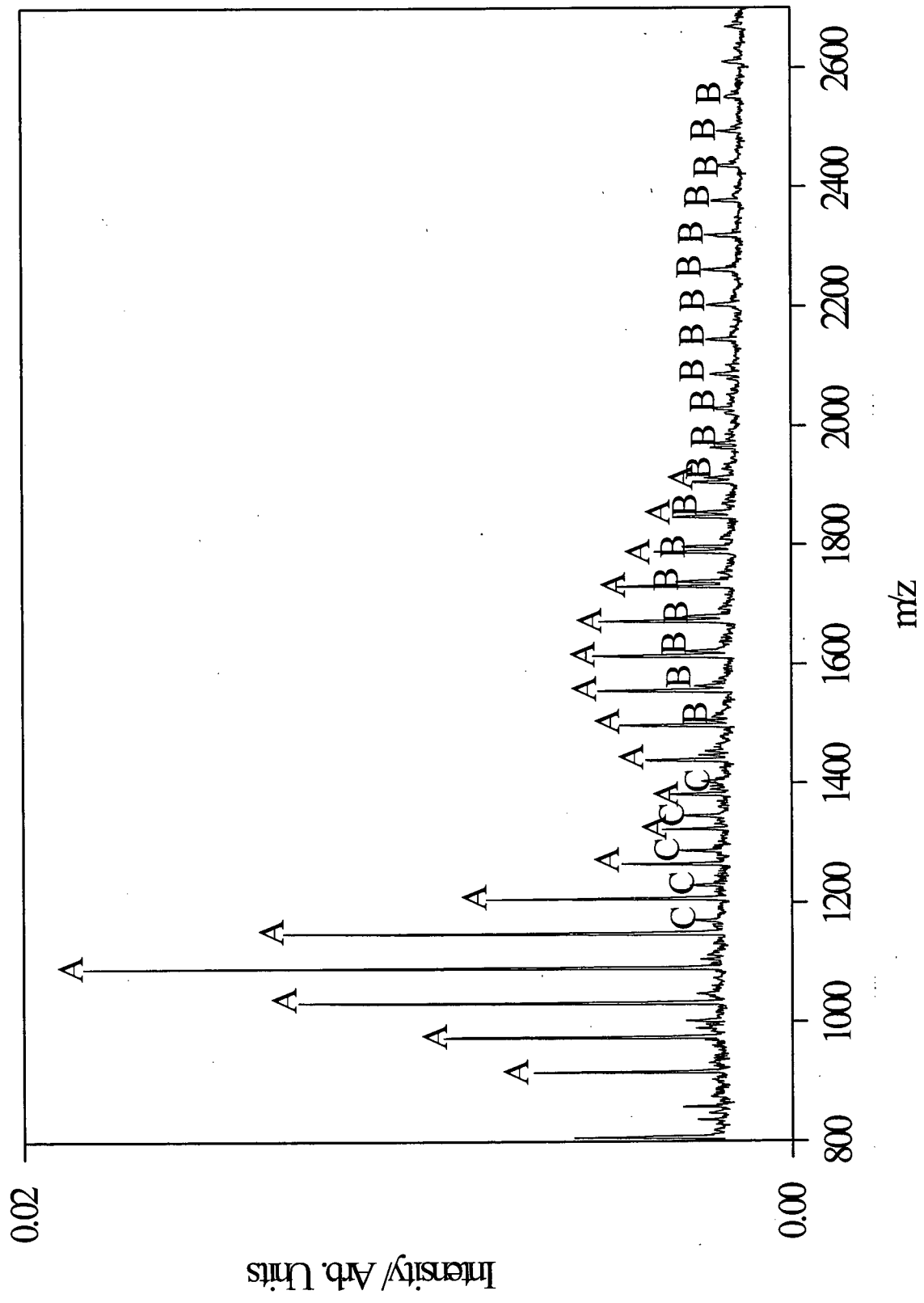

Figure 7.2 MALDI mass spectrum of Sample 2 produced using dithranol as the matrix and LiCl as the salt

7.4.2 Results for Sample1 and Sample 2

The MALDI mass spectra of Samples 1 and 2 are shown in figure 7.1 and figure 7.2. The two mass spectra are very similar and three distinct groups of peaks were identified. The groups were labelled as A, B and C. The masses associated with the peaks are tabulated in Appendix II. The structures assigned to A, B and C are shown in table 7.2.

The assignment of the polymer labelled A (polymer A) which appears in both figures 7.1 and 7.2 is described in this paragraph. The repeat unit mass of polymer A is 58 Da and the overall shape of the polymer distribution is bimodal. The 58 Da repeat unit is the repeat unit of PPG. The PPG used in the sample preparation had a bimodal mass distribution, as it consisted of a mixture of two monodisperse molecular weight fractions of PPG [3]. The most abundant oligomer of the PPG distribution, and hence the most intense peak in the mass spectrum, corresponded to n=7 (-(O-CH_2-$C(CH_3)_7$-); 422 Da) [3]. The most intense peak of polymer A is at 1082 Da. As polymer A is present in both Samples 1 and 2 it cannot contain DMPA, as Sample 1 was prepared using DMPA and Sample 2 was produced using DMPA that had been reacted with triethylamine. The remaining 660 Da of polymer A's mass not accounted for by the PPG constituent must therefore be made up of IPDI and/or NMA. 660 Da is equivalent to two units of IPDI and two units of NMA. The proposed structure of polymer A is shown in table 7.2. Polymer A is one of the predicted polymers, namely the p=0, q=1 case.

Polymer B is present in both Samples 1 and 2. The repeat unit is 58 Da and the shape of the mass distribution appears to be bimodal; however, the mass distribution is considerably wider than the mass distribution observed for polymer A.

The 58 Da repeat unit is PPG. The greater width of the mass distribution suggests that this polymer contains two PPG units. The shape of the mass distribution should then be trimodal. However, as the signal intensity decreases at higher masses this is not actually observed. The most intense peak in the polymer B distribution is seen where the sum of the number of PPG subunits is 14 *i.e.* both PPG subunits are the 7mer or a combination of the 6mer and the 8mer *etc.* The mass of the most intense polymer B peak is 1728 Da. The PPG constituents account for 844 Da of this mass. As with polymer A, the rest of the polymer is made up of IPDI and NMA, in this case three IPDI units and 2 NMP units. Polymer B corresponds to the predicted polymer (table 7.2) with p=0 and q=2. Polymer B is shown in table 7.2.

Polymer C is only gives rise to a weak signal, with only five peaks of the mass distribution having a sufficiently good signal to noise ratio to be unambiguously recognisable (see figures 7.1 and 7.2). The most intense peak of the polymer C distribution has a mass of 1278 Da. Polymer C is 196 Da heavier than Polymer A. Isocyanates are known to form dimers in the presence of water with the loss of CO (see figure 7.3) [6]. The mass of IPDI that has lost CO is 196 Da. The most probable structure for polymer C, therefore, is analogous to polymer A, with one of the diisocyanates replaced by the diisocyanate dimer. The proposed structure of polymer C is given in table 7.2.

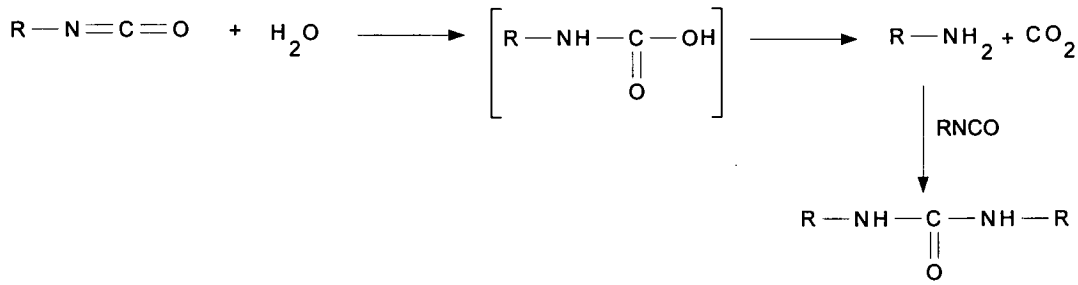

Figure 7.3 Dimer formation in isocyanates

The analysis of Samples 1 and 2 by MALDI MS confirms that two of the copolymers predicted from the synthesis are produced, namely the p=0, q=1 and the p=0, q=2 possibilities. The presence of a by-product due to dimerisation of the diisocyanate was also observed. DMPA is not incorporated into any of the copolymers detected.

7.4.3 Results for Sample 3 and Sample 4

Samples 3 and 4 gave very similar mass spectra (figures 7.4 and 7.5). In the mass spectra for both samples three polymer distributions could be distinguished, labelled as A, D and E. The fact that the same species were found in Samples 3 and 4 indicates that as with Samples 1 and 2, DMPA-containing polymers were not detected.

All the three polymer distributions have a very similar overall shape. Polymer A is the same as polymer A in figures 7.1 and 7.2. The differences in mass

Structure	Comments
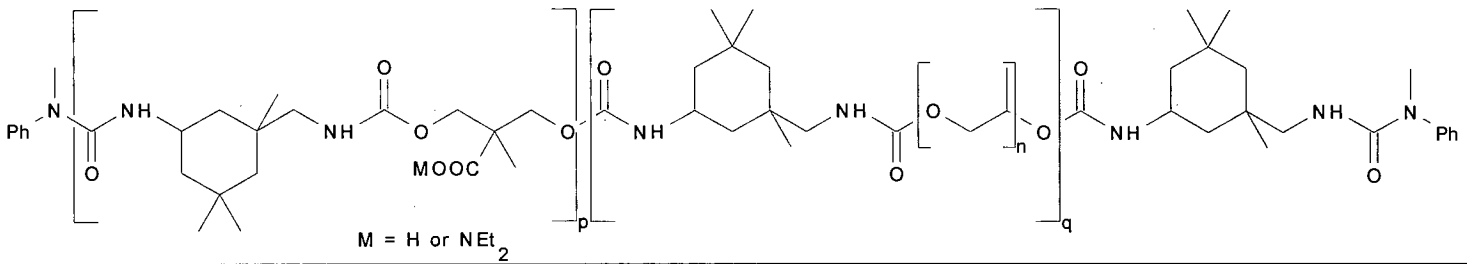	general structure
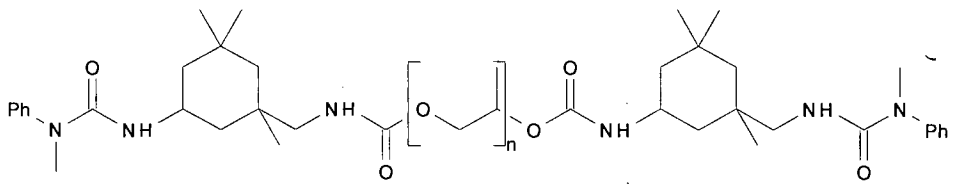	Polymer A
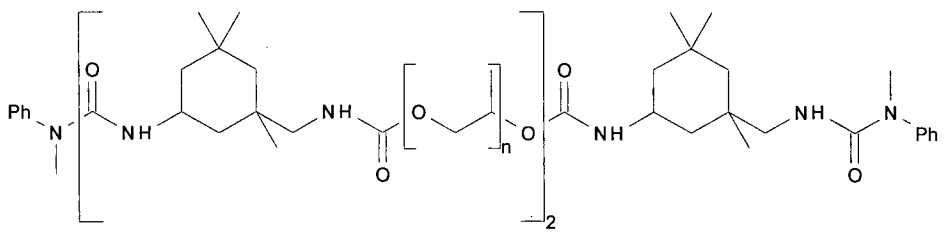	Polymer B
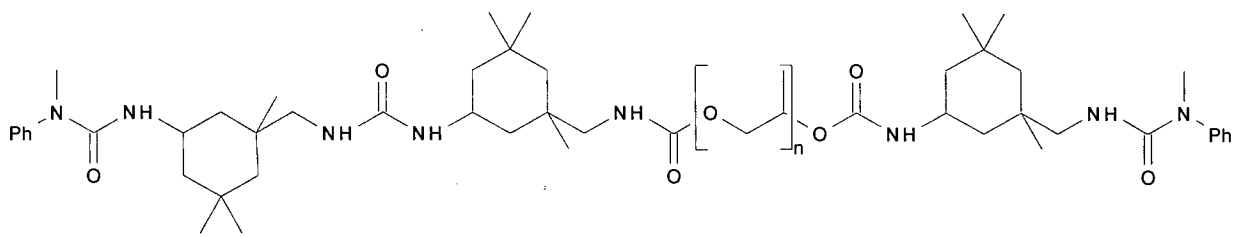	Polymer C

Table 7.2 Summary of the structures of the polymers found in Sample 1 and Sample 2

of the most intense peak of polymer A (1082 Da) compared with the masses of the most intense peaks of polymer D (975 Da) and polymer E (868 Da) are 107 Da and 214 Da, respectively. 107 Da corresponds to the mass of NMA, the endgroup of polymer A, and 214 Da corresponds to twice the mass of NMA. Therefore polymer D is equivalent to polymer A with only one NMA endgroup and polymer E is the same as polymer A with no NMA endgroups (see table 7.3). The presence of polymers with only one or no NMA endgroups would be expected, as a minimal amount of NMA was used in the synthesis of Samples 3 and 4 [3].

It is worth noting that peaks are observed with masses greater than 2000 Da. These peaks do not form part of the mass distributions of polymers A, D and E. These peaks were not assigned, as it was not possible to determine which peak was the most intense and it was therefore not possible to know the number of PPG subunits present in each polymer. However, it would seem reasonable to assume that the peaks with masses greater than 2000 Da are due to polymer B (compare with Samples 1 and 2) and polymers similar to polymer B with only one or no NMA endgroups.

The analysis of Samples 3 and 4 shows that MALDI can be used successfully to detect changes in the product caused by a small change in the sample preparation procedure. In this case the amount of NMA added at the end of the reaction was considerably lower than the amount used in producing Samples 1 and 2. The result of this change in sample preparation was the production of polymers with only one or no NMA endgroups for samples 3 and 4, as well as the polymer with two NMA endgroups. In the case of Samples 1 and 2, where an excess of NMA was used, only polymers with two NMA endgroups were produced.

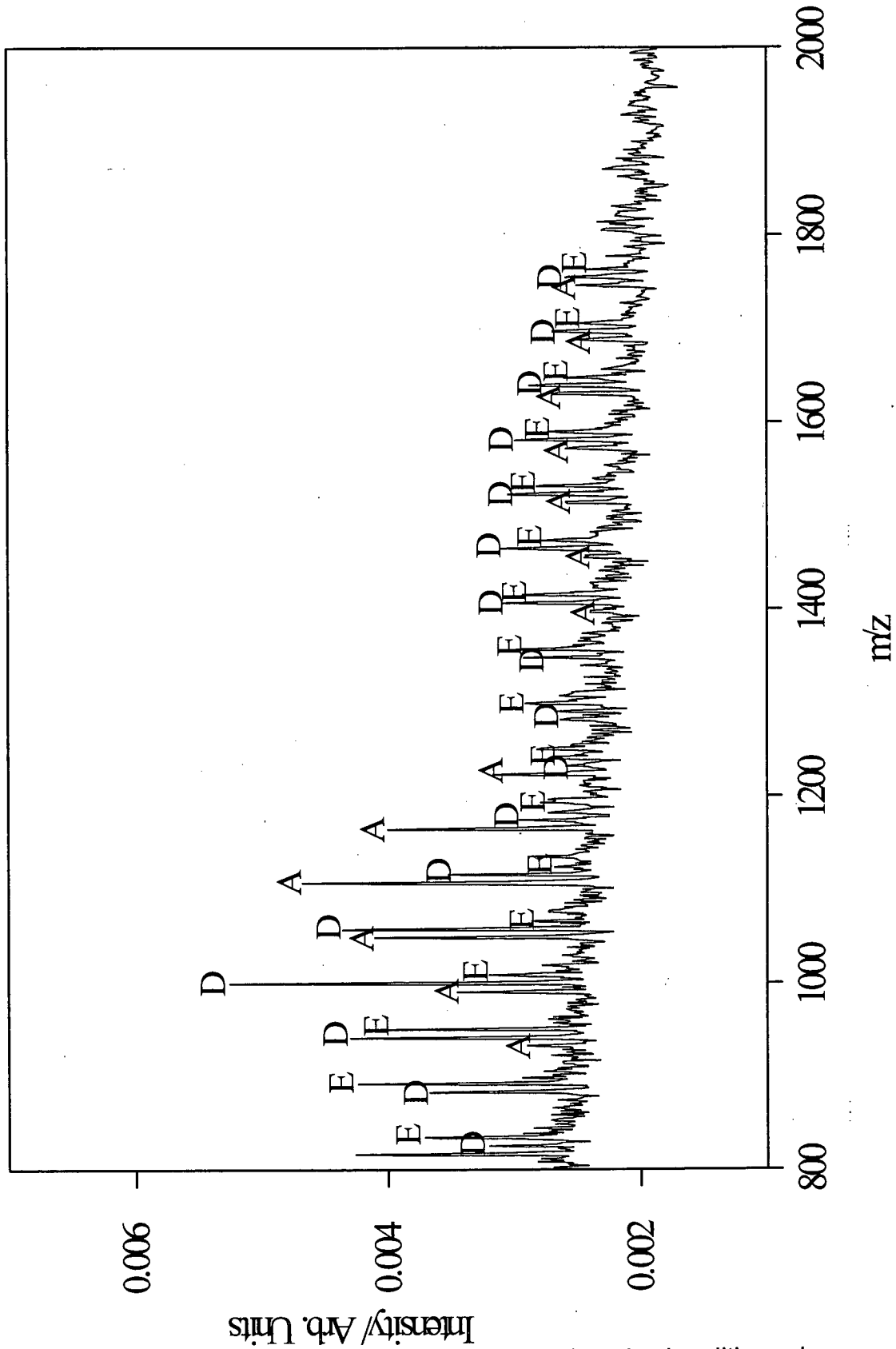

Figure 7.4 MALDI mass spectrum of Sample 3 produced using dithranol as the matrix and NaCl as the salt

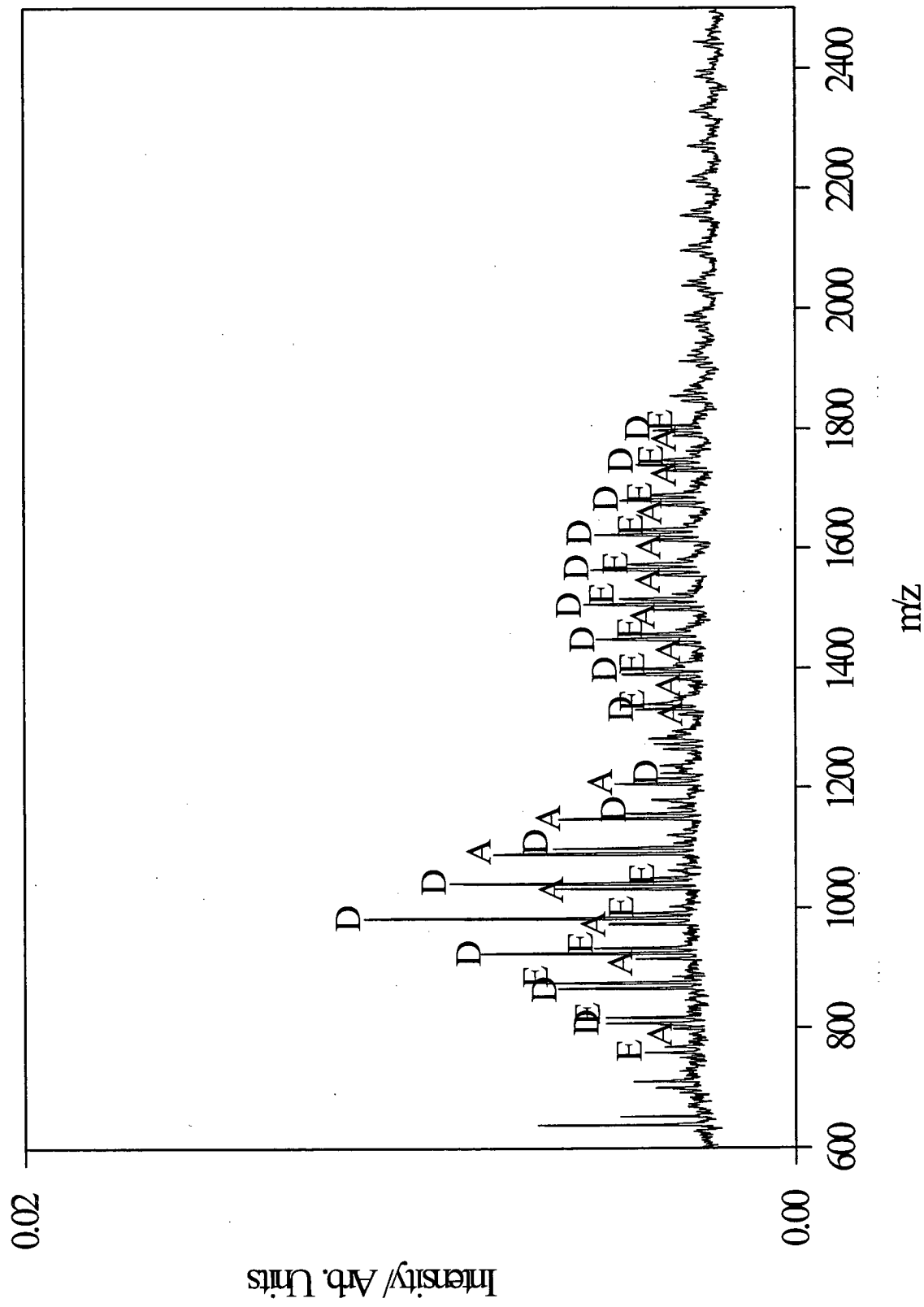

Figure 7.5 MALDI mass spectrum of Sample 4 produced using dithranol as the matrix and LiCl as the salt

Structure	Comments
	Polymer A
	Polymer D
	Polymer E

Table 7.3 Summary of the structures of the polymers found in Sample 3 and Sample 4

7.4.4 Results for Sample 5 and Sample 6

As with the other samples, both the sample produced with DMPA that had not been reacted with triethylamine, Sample 5, and the sample produced using DMPA that had been reacted with triethylamine, showed the same masses in their respective mass spectra (figures 7.6 and 7.7). Only two different polymer distributions were, observed labelled F and G. The relative amounts of polymer F and polymer G present in Samples 5 and 6 are different, with Sample 5 containing relatively more polymer G than Sample 6. As with Samples 1 to 4, the repeat units of the polymers are 58 Da, *i.e.* PPG.

The mass of the most intense peak in the polymer F distribution is 646 Da. Polymer F consists of a PPG constituent and an IPDI constituent. The proposed structure of polymer F is detailed in table 7.4.

The mass of the most intense peak of polymer G is 900 Da. 422 Da of this mass are due to PPG. The remaining 478 Da was known from the synthesis to be made up of IPDI, hydrazine and/ or triethylamine. 478 Da corresponds to two IPDIs and one hydrazine. The most probable structure for polymer G was assumed to be polymer F with IPDI linked to the IPDI end of polymer F through a hydrazine (see table 7.4). This particular configuration was chosen as the most probable, as hydrazines are known to react with amines [6].

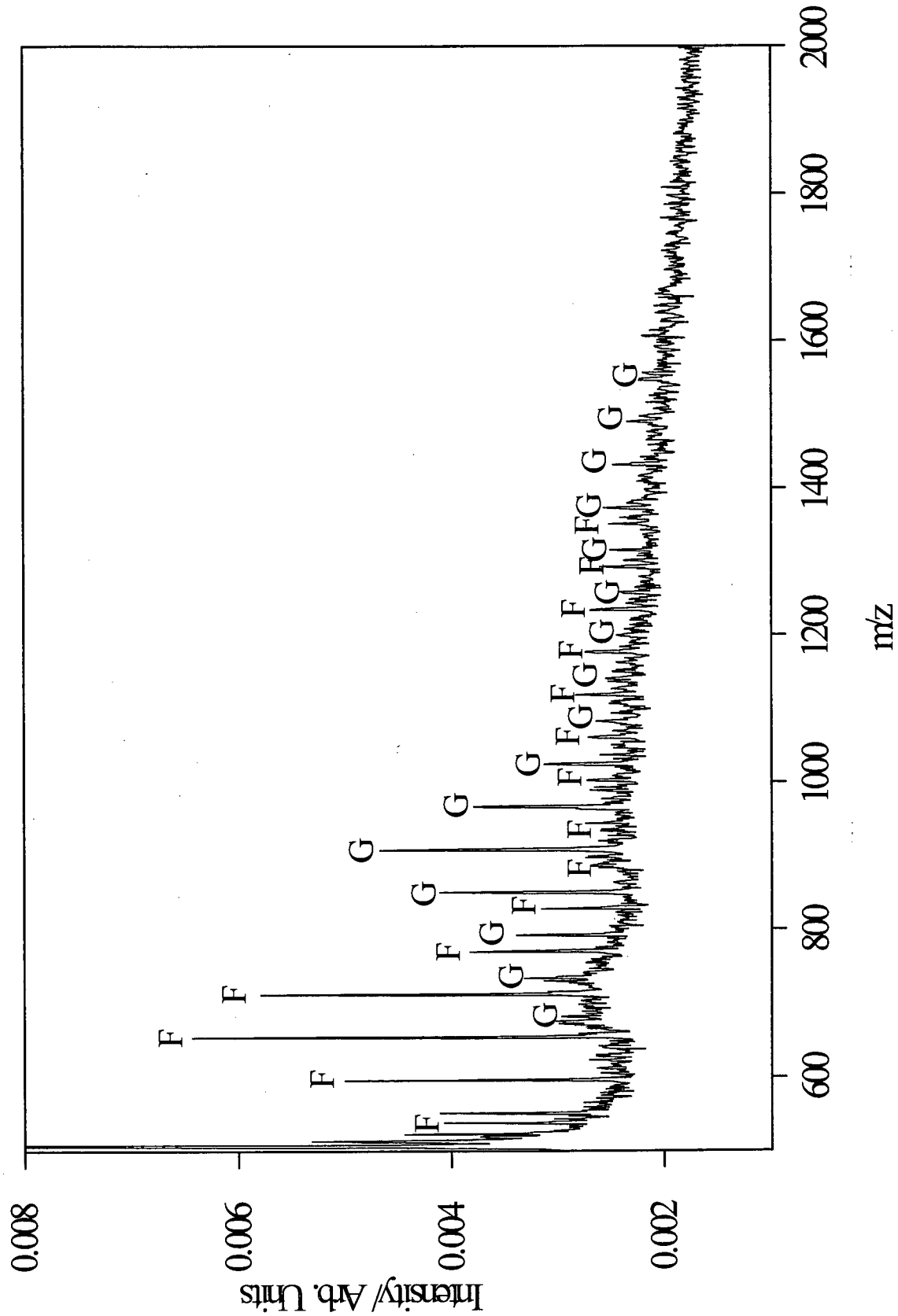

Figure 7.6 MALDI mass spectrum of Sample 5 produced using dithranol as the matrix and LiCl as the salt

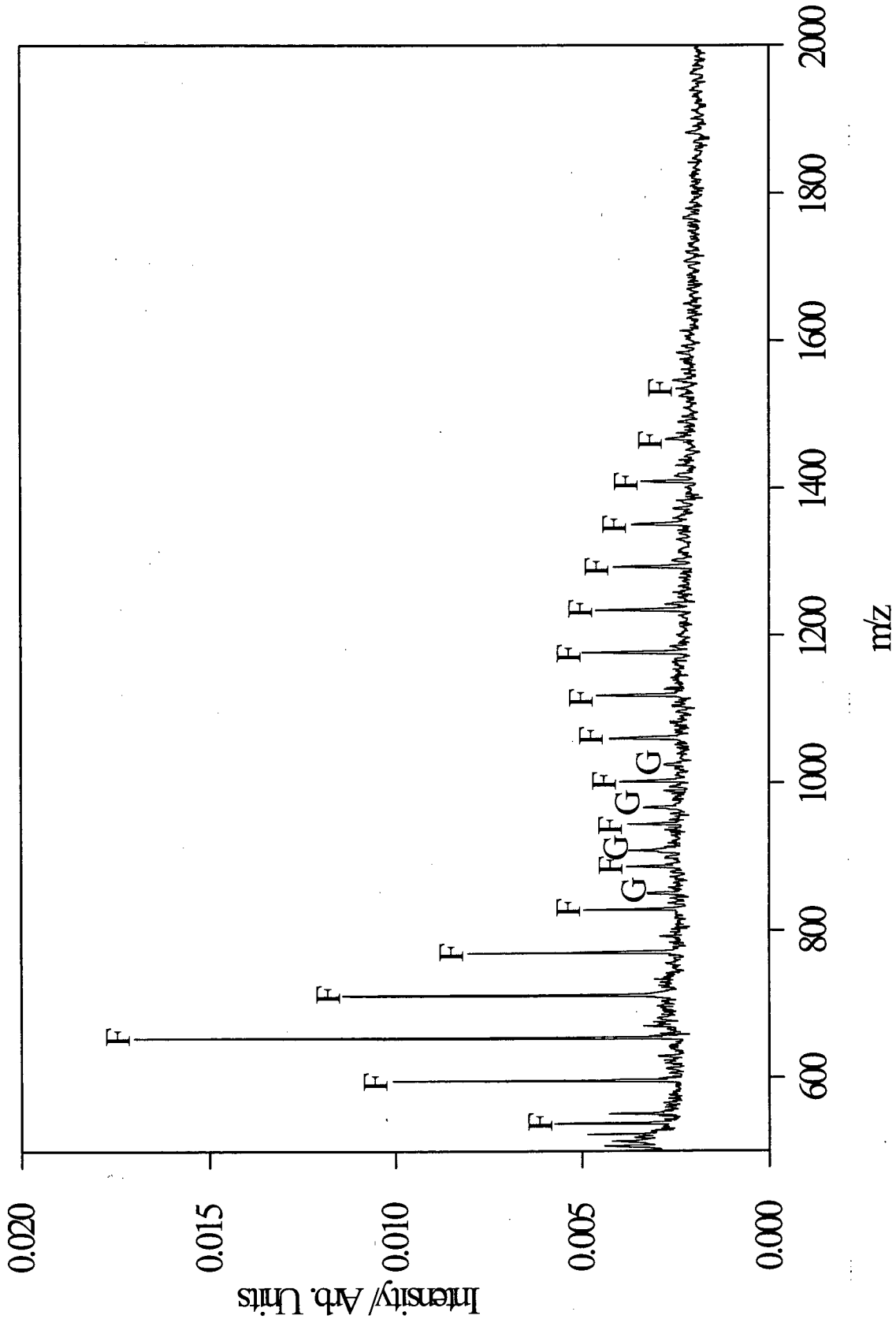

Figure 7.7 MALDI mass spectrum of Sample 6 produced using dithranol as the matrix and LiCl as the salt

Structure	Comments
	Polymer F
	Polymer G

Table 7.4 Summary of the structures of the polymers found in Sample 5 and Sample 6

7.5 Conclusions

The results described in this chapter show that MALDI can be a very powerful tool for copolymer analysis. It was possible to determine a large amount of information on the structure of the polymers under investigation using only the MALDI mass spectra obtained and information on the sample preparation. The structural information obtained included repeat unit masses and endgroup information, from samples consisting of more than one polymer. The analysis was limited to qualitative evaluation, as the relative ionisation efficiencies of the different polymers are not known.

The appearance of new polymer species due to changes in the reaction conditions during polymer synthesis was readily detected. This was best illustrated by comparing two polymer samples, one of which had been produced using an excess of N-methylaniline (NMA), and the other with a minimal amount of NMA. All polymers produced in the presence of excess NMA had two NMA endgroups, whereas the polymers produced using minimal NMA had a range of different numbers of NMA endgroups.

7.6 References

[1] S. Yoshida, S. Yamoto and T. Takamatsu, *Rapid Commun. Mass Spectrom.*, **9**, 535-544 (1998)

[2] V. Schädler, J. Spickermann, H. J. Räder and U. Wiesner, *Macromolecules*, **29**, 4865-4870 (1996)

[3] Private correspondence with manufacturer (1995)

[4] J. Axelsson, E. Scrivener, D. M. Haddleton and P. J. Derrick, *Macromolecules*, **29**, 8875-8882 (1996)

[5] K. Martin, J. Spickermann, H. J. Rader and K. Mullen, *Rapid Commun. Mass Spectrom.*, **10**, 1471-1474 (1996)

[6] R. T. Morrison and R. N. Boyd, 'Organic Chemistry', Fifth Edition, Allyn and Bacon, Inc., Newton, Massachusetts 02159, USA

Chapter 8 – Conclusions and further work

8.1 Introduction

Matrix Assisted Laser Desorption/Ionisation (MALDI) time-of-flight mass spectrometry has been shown to have great potential as a technique for synthetic polymer mass analysis. It was the aim of this research to build on and extend previous work on the mass spectrometric analysis of synthetic polymers carried out at the University of Edinburgh.

The studies carried out can be divided into two broad categories. The first category concerns the practical aspects of polymer analysis by MALDI; here the issues of improving sample preparation, extending the high-mass capability of the mass spectrometer and the study of novel synthetic polymers were addressed. The second group of studies dealt with more fundamental issues affecting polymer mass analysis by MALDI. For this work a study of post source decay of synthetic polymers was made and delayed extraction experiments were carried out.

8.2 Practical development of MALDI mass spectrometry for synthetic polymers

Sample preparation improvements were made in two ways. First, a more reproducible sample preparation method was developed in order to be able to carry out high quality quantitative studies. The technique developed to this end was an aerosol sample deposition technique. Secondly, the range of matrices and matrix to analyte ratios used in sample preparation was reviewed and extended which led to great improvements in high-mass detection.

In order to detect high-mass polymers effectively the mass spectrometer was upgraded by the addition of a mass gate. This is a gated deflection plate, which was used to deflect low-mass ions that would otherwise have lead to detector saturation. Through instrument modification and improved sample preparation, it was possible to detect polymers with average molecular weights of 20000 Da. Dimers of these polymers were also detected with masses in excess of 40000 Da. The previous upper detection limit for the Edinburgh instrument was *ca* 10000 Da.

During the course of this work numerous novel polymers were analysed using MALDI. These studies illustrated the capacity of MALDI mass spectrometry to yield detailed information on end-group and repeat unit masses of copolymers.

8.3 Studies of the MALDI process

Two studies were conducted to investigate the ionisation process and post source decay respectively.

In the ionisation study use was made of delayed extraction. In these experiments the improvements in quantification afforded by the aerosol sample preparation technique, which had been developed previously, were exploited. The most notable result obtained from this work was the observation that metal ion adduct yields *did not* increase by allowing a time delay between the laser shot and ion extraction. Previously reported work suggested otherwise. The present work is interpreted as evidence against the often-suggested gas-phase ion attachment process and lends weight to a 'prompt' ionisation process.

Post source decay experiments were carried out. These experiments showed a clear correlation between the size of alkali metal ions attached to polymers and the extent to which these polymer metal ion adducts dissociated. Rb^+ and, to a lesser extent, K^+ adducts of a range of polymers underwent post source decay, but Li^+ and Na^+ adducts of the same polymers did not decay.

8.4 Results not included

Several pieces of work were carried out that have not been included. One such project was the mass analysis of industrial copolymer samples, which could not be reported on for confidentiality reasons. A series of experiments was carried out

on the 'matrix-suppression' effect. The results of these experiments were not deemed to be of high enough quality to be included in this thesis. Also several peptides were mass analysed. The biomolecule work was primarily done to test the high-mass capability of the instrument, work that was repeated using synthetic polymers.

8.5 Future work

In the light of research completed to date several further experiments can be suggested.

The aerosol sample preparation technique would lend itself to coupling with liquid chromatography separation. It may be possible to couple this sample deposition method directly to the source of a mass spectrometer, leading to an automated interface.

The dynamics of post source decay could be further investigated by means of a movable deflection plate within the flight tube of the mass spectrometer.

Improvements in high-mass detection could be brought about by redesigning the source region of the mass spectrometer to make high-voltage delayed extraction possible. It would also be desirable to move to a detection system that is more sensitive to slow heavy ions than the traditional microchannel plate detector.

Finally, it would be interesting to investigate the use of different laser systems such as femtosecond lasers for MALDI.

Appendix I

This appendix contains tables of peak areas, peak widths and peak positions observed in the mass spectra used to generate the graphs in Chapter 6.

Table 1 Polymer studied polystyrene. Dithranol to $AgCF_3CO_2$ ratio 10:1 (*c.f.* figure 6.4)

delay time/ ns	number of PS units in polymer (n)	peak area	peak width/ μs	peak position/ μs
0	10	0.00105	0.06	26.32
200	10	$9.77752*10^{-4}$	0.07	26.30
400	10	$6.02265*10^{-4}$	0.07	26.28
600	10	$4.36033*10^{-4}$	0.07	26.27
0	11	0.00110	0.06	27.52
200	11	0.00100	0.06	27.50
400	11	$6.67466*10^{-4}$	0.07	27.48
600	11	$4.57166*10^{-4}$	0.07	27.47
0	12	0.00105	0.06	28.68
200	12	$9.93638*10^{-4}$	0.07	28.65
400	12	$6.35895*10^{-4}$	0.07	28.63
600	12	$4.67385*10^{-4}$	0.07	28.63
0	13	$8.72601*10^{-4}$	0.06	29.79
200	13	$8.20662*10^{-4}$	0.06	29.77
400	13	$5.48303*10^{-4}$	0.07	29.75
600	13	$3.98620*10^{-4}$	0.07	29.74
0	14	$7.73417*10^{-4}$	0.07	30.87
200	14	$7.20767*10^{-4}$	0.07	30.85
400	14	$4.78089*10^{-4}$	0.07	30.82
600	14	$3.46757*10^{-4}$	0.07	30.81
0	15	$6.60998*10^{-4}$	0.07	31.91
200	15	$6.31276*10^{-4}$	0.07	31.88
400	15	$4.27153*10^{-4}$	0.08	31.87
600	15	$3.18898*10^{-4}$	0.08	31.85
0	16	$4.81759*10^{-4}$	0.07	32.92
200	16	$4.43732*10^{-4}$	0.07	32.90
400	16	$3.19148*10^{-4}$	0.08	32.89
600	16	$2.51303*10^{-4}$	0.10	32.87

Table 2 Polymer studied polystyrene. Dithranol to $AgCF_3CO_2$ ratio 2:1 (*c.f.* figure 6.5)

delay time/ ns	number of PS units in polymer (n)	peak area	peak width/ μs	peak position/ μs
0	10	0.00346	0.06	26.29
100	10	0.00370	0.07	26.35
200	10	0.00426	0.13	26.40
300	10	0.00395	0.19	26.47
400	10	0.00403	0.30	26.56
600	10	0.00392	0.43	26.70
0	11	0.00354	0.07	27.50
100	11	0.00372	0.06	27.54
200	11	0.00433	0.12	27.61
300	11	0.00403	0.17	27.68
400	11	0.00403	0.30	27.78
600	11	0.00403	0.40	27.93
0	12	0.00337	0.08	28.67
100	12	0.00359	0.06	28.70
200	12	0.00411	0.11	28.76
300	12	0.00389	0.17	28.84
400	12	0.00383	0.29	28.92
600	12	0.00400	0.42	29.12
0	13	0.00308	0.08	29.80
100	13	0.00330	0.06	29.82
200	13	0.00383	0.09	29.88
300	13	0.00355	0.15	29.95
400	13	0.00346	0.30	30.05
600	13	0.00365	0.42	30.23
0	14	0.00265	0.11	30.90
100	14	0.00286	0.06	30.91
200	14	0.00336	0.10	30.98
300	14	0.00314	0.15	31.05
400	14	0.00297	0.29	31.16
600	14	0.00323	0.39	31.31
0	15	0.00215	0.12	31.97
100	15	0.00234	0.06	31.98
200	15	0.00274	0.09	32.05
300	15	0.00254	0.15	32.11
400	15	0.00244	0.28	32.23
600	15	0.00263	0.42	32.39
0	16	0.00165	0.11	33.00
100	16	0.00184	0.06	33.01
200	16	0.00214	0.08	33.08
300	16	0.00198	0.16	33.15
400	16	0.00190	0.30	33.25
600	16	0.00205	0.43	33.45

Table 3 Polymer studied polystyrene. Dithranol to $AgCF_3CO_2$ ratio 1:1 (*c.f.* figure 6.6)

delay time/ ns	number of PS units in polymer (n)	peak area	peak width/ μs	peak position/ μs
0	10	0.00433	0.05	26.29
100	10	0.00366	0.08	26.35
200	10	0.00349	0.14	26.40
300	10	0.00268	0.19	26.46
400	10	0.00234	0.29	26.56
600	10	0.00199	0.39	26.68
0	11	0.00406	0.06	27.49
100	11	0.00354	0.07	27.54
200	11	0.00320	0.13	27.62
300	11	0.00249	0.19	27.67
400	11	0.00232	0.29	27.81
600	11	0.00193	0.40	27.93
0	12	0.00348	0.07	28.65
100	12	0.00322	0.06	28.69
200	12	0.00281	0.13	28.76
300	12	0.00223	0.20	28.83
400	12	0.00211	0.30	28.92
600	12	0.00173	0.41	29.08
0	13	0.00317	0.08	29.77
100	13	0.00290	0.06	29.80
200	13	0.00252	0.13	29.87
300	13	0.00199	0.21	29.96
400	13	0.00191	0.33	30.06
600	13	0.00159	0.42	30.21
0	14	0.00248	0.08	30.85
100	14	0.00238	0.06	30.89
200	14	0.00204	0.10	30.97
300	14	0.00159	0.20	31.04
400	14	0.00155	0.31	31.17
600	14	0.00127	0.37	31.28
0	15	0.00204	0.11	31.94
100	15	0.00192	0.06	31.95
200	15	0.00164	0.11	32.02
300	15	0.00128	0.19	32.08
400	15	0.00124	0.35	32.23
600	15	0.00107	0.40	32.36
0	16	0.00148	0.10	32.97
100	16	0.00143	0.05	32.98
200	16	0.00120	0.09	33.05
300	16	$9.18276*10^{-4}$	0.18	33.13
400	16	$8.84717*10^{-4}$	0.27	33.20
600	16	$7.28138*10^{-4}$	0.42	33.33

Table 4 Polymer studied polystyrene. Dithranol to $AgCF_3CO_2$ ratio 1:2.5 (*c.f.* figure 6.7)

delay time/ ns	number of PS units in polymer (n)	peak area	peak width/ μs	peak position/ μs
0	10	0.00238	0.07	26.3
100	10	0.00294	0.10	26.36
200	10	0.00209	0.16	26.41
300	10	0.00246	0.20	26.47
400	10	0.00205	0.32	26.63
600	10	0.00163	0.41	26.69
0	11	0.00201	0.10	27.52
100	11	0.00260	0.09	27.56
200	11	0.00177	0.15	27.62
300	11	0.00206	0.19	27.70
400	11	0.00174	0.31	27.80
600	11	0.00132	0.36	27.99
0	12	0.00166	0.09	28.69
100	12	0.00209	0.08	28.70
200	12	0.00143	0.17	28.80
300	12	0.00168	0.23	28.88
400	12	0.00147	0.30	28.93
600	12	0.00104	0.43	29.06
0	13	0.00147	0.09	29.82
100	13	0.00185	0.06	29.82
200	13	0.00123	0.20	29.90
300	13	0.00146	0.25	30.02
400	13	0.00125	0.39	30.18
600	13	$9.03796*10^{-4}$	0.37	30.40
0	14	0.00104	0.14	30.93
100	14	0.00142	0.07	30.91
200	14	$9.00774*10^{-4}$	0.14	30.98
300	14	0.00108	0.31	31.08
400	14	$9.92947*10^{-4}$	0.31	31.24
600	14	$6.75848*10^{-4}$	0.26	31.35
0	15	$8.00941*10^{-4}$	0.13	31.99
100	15	0.0011	0.06	31.96
200	15	$7.24616*10^{-4}$	0.09	32.05
300	15	$8.39225*10^{-4}$	0.21	32.11
400	15	$7.37971*10^{-4}$	0.45	32.19
600	15	$4.66581*10^{-4}$	0.25	32.52

Table 5 Polymer studied polystyrene. Dithranol to $AgCF_3CO_2$ ratio 1:5 (*c.f.* figure 6.8)

delay time/ ns	number of PS units in polymer (n)	peak area	peak width/ μs	peak position/ μs
0	10	0.00359	0.06	26.31
100	10	0.00358	0.08	26.37
200	10	0.00292	0.15	26.43
300	10	0.00279	0.21	26.47
400	10	0.00246	0.28	26.58
600	10	0.00238	0.44	26.69
0	11	0.00342	0.06	27.49
100	11	0.00341	0.07	27.55
200	11	0.00272	0.13	27.62
300	11	0.00256	0.17	27.69
400	11	0.00231	0.26	27.71
600	11	0.00229	0.38	27.92
0	12	0.00297	0.05	28.64
100	12	0.00299	0.06	28.69
200	12	0.00238	0.12	28.77
300	12	0.00225	0.19	28.84
400	12	0.00199	0.28	28.90
600	12	0.00202	0.41	29.08
0	13	0.00265	0.05	29.75
100	13	0.00267	0.06	29.80
200	13	0.00213	0.13	29.86
300	13	0.00203	0.20	29.94
400	13	0.00179	0.28	30.05
600	13	0.00178	0.40	30.26
0	14	0.00203	0.06	30.83
100	14	0.00214	0.05	30.88
200	14	0.00166	0.10	30.93
300	14	0.00162	0.17	31.01
400	14	0.00141	0.30	31.10
600	14	0.00142	0.46	31.33
0	15	0.00163	0.06	31.88
100	15	0.00174	0.06	31.93
200	15	0.00134	0.10	31.99
300	15	0.00129	0.17	32.06
400	15	0.00112	0.30	32.14
600	15	0.00113	0.41	32.33
0	16	0.00116	0.07	32.91
100	16	0.00128	0.05	32.95
200	16	$9.97093*10^{-4}$	0.09	33.02
300	16	$9.36166*10^{-4}$	0.15	33.08
400	16	$8.03506*10^{-4}$	0.30	33.16
600	16	$7.77543*10^{-4}$	0.43	33.46

Table 6 Polymer studied PMMA. Dithranol to LiCl ratio 1:1 (*c.f.* figure 6.10)

delay time/ ns	number of PMMA units in polymer (n)	peak area	peak width/ μs	peak position/ μs
0	9	$4.739*10^{-4}$	0.07	30.35
100	9	$3.587*10^{-4}$	0.05	30.32
200	9	$3.273*10^{-4}$	0.06	30.31
300	9	$3.584*10^{-4}$	0.06	30.30
400	9	$4.115*10^{-4}$	0.07	30.29
0	10	$4.982*10^{-4}$	0.07	31.97
100	10	$4.379*10^{-4}$	0.05	31.94
200	10	$3.772*10^{-4}$	0.06	31.93
300	10	$3.675*10^{-4}$	0.05	31.92
400	10	$4.270*10^{-4}$	0.06	31.92
0	11	$5.488*10^{-4}$	0.06	33.52
100	11	$4.716*10^{-4}$	0.05	33.49
200	11	$4.368*10^{-4}$	0.06	33.48
300	11	$4.221*10^{-4}$	0.06	33.47
400	11	$4.605*10^{-4}$	0.06	33.46
0	12	$5.599*10^{-4}$	0.06	35.00
100	12	$5.015*10^{-4}$	0.05	34.97
200	12	$4.769*10^{-4}$	0.05	34.96
300	12	$4.410*10^{-4}$	0.05	34.95
400	12	$4.702*10^{-4}$	0.06	34.94
0	13	$6.123*10^{-4}$	0.06	36.41
100	13	$5.539*10^{-4}$	0.05	36.38
200	13	$5.209*10^{-4}$	0.06	36.37
300	13	$4.862*10^{-4}$	0.06	36.37
400	13	$5.015*10^{-4}$	0.06	36.36
0	14	$6.271*10^{-4}$	0.06	37.78
100	14	$6.052*10^{-4}$	0.05	37.75
200	14	$5.542*10^{-4}$	0.06	37.74
300	14	$5.114*10^{-4}$	0.05	37.73
400	14	$5.403*10^{-4}$	0.07	37.72
0	15	$6.197*10^{-4}$	0.06	39.09
100	15	$5.783*10^{-4}$	0.05	39.06
200	15	$5.391*10^{-4}$	0.05	39.05
300	15	$5.342*10^{-4}$	0.06	39.04
400	15	$5.408*10^{-4}$	0.06	39.03
0	16	$5.561*10^{-4}$	0.06	40.36
100	16	$5.446*10^{-4}$	0.05	40.33
200	16	$5.443*10^{-4}$	0.06	40.32
300	16	$4.560*10^{-4}$	0.06	40.31
400	16	$4.897*10^{-4}$	0.07	40.30
0	17	$4.934*10^{-4}$	0.06	41.59
100	17	$5.064*10^{-4}$	0.06	41.56
200	17	$4.579*10^{-4}$	0.06	41.55
300	17	$4.136*10^{-4}$	0.06	41.54
400	17	$4.226*10^{-4}$	0.07	41.53
0	18	$4.765*10^{-4}$	0.07	42.79
100	18	$4.501*10^{-4}$	0.05	42.76
200	18	$4.028*10^{-4}$	0.06	42.75
300	18	$3.759*10^{-4}$	0.07	42.74
400	18	$3.917*10^{-4}$	0.07	42.73
0	19	$4.401*10^{-4}$	0.07	43.95
100	19	$4.240*10^{-4}$	0.06	43.92
200	19	$3.696*10^{-4}$	0.06	43.91
300	19	$3.647*10^{-4}$	0.07	43.90
400	19	$3.620*10^{-4}$	0.07	43.90
0	20	$3.922*10^{-4}$	0.08	45.08
100	20	$3.298*10^{-4}$	0.06	45.06
200	20	$3.240*10^{-4}$	0.07	45.05

300	20	$2.970*10^{-4}$	0.07	45.04
400	20	$3.376*10^{-4}$	0.08	45.03
0	21	$3.424*10^{-4}$	0.08	46.20
100	21	$3.109*10^{-4}$	0.07	46.16
200	21	$2.810*10^{-4}$	0.07	46.15
300	21	$2.694*10^{-4}$	0.07	46.15
400	21	$2.850*10^{-4}$	0.08	46.13

Table 7 Polymer studied PMMA. Dithranol to LiCl ratio 1:1 (*c.f.* figure 6.11)

delay time/ ns	number of PMMA units in polymer (n)	peak area	peak width/ μs	peak position/ μs
0	9	$3.027*10^{-4}$	0.06	30.33
200	9	$3.719*10^{-4}$	0.06	30.29
400	9	$2.255*10^{-4}$	0.06	30.28
600	9	$2.512*10^{-4}$	0.06	30.26
800	9	$2.231*10^{-4}$	0.04	30.25
1000	9	$2.118*10^{-4}$	0.04	30.25
0	10	$3.169*10^{-4}$	0.05	31.96
200	10	$4.020*10^{-4}$	0.05	31.92
400	10	$2.784*10^{-4}$	0.06	31.90
600	10	$2.792*10^{-4}$	0.06	31.88
800	10	$2.293*10^{-4}$	0.05	31.87
1000	10	$2.345*10^{-4}$	0.03	31.87
0	11	$3.929*10^{-4}$	0.05	33.50
200	11	$4.542*10^{-4}$	0.06	33.46
400	11	$3.102*10^{-4}$	0.06	33.44
600	11	$3.164*10^{-4}$	0.06	33.43
800	11	$2.611*10^{-4}$	0.05	33.41
1000	11	$2.172*10^{-4}$	0.04	33.41
0	12	$4.539*10^{-4}$	0.06	34.98
200	12	$4.953*10^{-4}$	0.05	34.94
400	12	$3.597*10^{-4}$	0.06	34.92
600	12	$3.559*10^{-4}$	0.06	34.90
800	12	$2.552*10^{-4}$	0.06	34.89
1000	12	$2.314*10^{-4}$	0.04	34.88
0	13	$4.791*10^{-4}$	0.05	36.40
200	13	$5.558*10^{-4}$	0.06	36.36
400	13	$3.765*10^{-4}$	0.07	36.34
600	13	$3.886*10^{-4}$	0.06	36.31
800	13	$2.954*10^{-4}$	0.07	36.29
1000	13	$2.640*10^{-4}$	0.05	36.29
0	14	$5.145*10^{-4}$	0.05	37.76
200	14	$6.010*10^{-4}$	0.05	37.72
400	14	$3.633*10^{-4}$	0.06	37.70
600	14	$4.443*10^{-4}$	0.07	37.68
800	14	$2.892*10^{-4}$	0.06	37.66
1000	14	$2.966*10^{-4}$	0.05	37.66
0	15	$5.019*10^{-4}$	0.06	39.07
200	15	$5.882*10^{-4}$	0.05	39.03
400	15	$4.058*10^{-4}$	0.07	39.01
600	15	$4.013*10^{-4}$	0.07	38.99
800	15	$3.132*10^{-4}$	0.07	38.98
1000	15	$3.209*10^{-4}$	0.06	38.97
0	16	$4.720*10^{-4}$	0.06	40.34
200	16	$5.414*10^{-4}$	0.06	40.30
400	16	$3.650*10^{-4}$	0.07	40.28
600	16	$4.092*10^{-4}$	0.07	40.26
800	16	$2.631*10^{-4}$	0.07	40.24
1000	16	$2.654*10^{-4}$	0.06	40.24
0	17	$4.147*10^{-4}$	0.06	41.57
200	17	$4.912*10^{-4}$	0.06	41.53
400	17	$3.069*10^{-4}$	0.06	41.51
600	17	$3.318*10^{-4}$	0.07	41.49
800	17	$2.452*10^{-4}$	0.07	41.47
1000	17	$2.413*10^{-4}$	0.06	41.47
0	18	$3.674*10^{-4}$	0.06	42.77
200	18	$4.894*10^{-4}$	0.07	42.73
400	18	$2.945*10^{-4}$	0.07	42.71
600	18	$3.232*10^{-4}$	0.07	42.69

800	18	$2.620*10^{-4}$	0.07	42.67
1000	18	$2.560*10^{-4}$	0.06	42.67
0	19	$3.916*10^{-4}$	0.06	43.93
200	19	$4.173*10^{-4}$	0.06	43.89
400	19	$3.122*10^{-4}$	0.08	43.87
600	19	$3.187*10^{-4}$	0.08	43.85
800	19	$2.224*10^{-4}$	0.08	43.84
1000	19	$2.074*10^{-4}$	0.06	43.83
0	20	$3.068*10^{-4}$	0.06	45.06
200	20	$3.386*10^{-4}$	0.06	45.02
400	20	$2.507*10^{-4}$	0.08	45.00
600	20	$2.749*10^{-4}$	0.08	44.98
800	20	$1.745*10^{-4}$	0.07	44.97
1000	20	$1.754*10^{-4}$	0.07	44.97
0	21	$2.733*10^{-4}$	0.07	46.17
200	21	$2.998*10^{-4}$	0.07	46.13
400	21	$1.851*10^{-4}$	0.08	46.11
600	21	$2.126*10^{-4}$	0.08	46.10
800	21	$1.671*10^{-4}$	0.08	46.07
1000	21	$1.671*10^{-4}$	0.06	46.07

Table 8 Polymer studied PEG. Dithranol to NaCl ratio 1:1 (*c.f.* figure 6.12)

delay time/ ns	number of PEG units in polymer (n)	peak area	peak width/ μs	peak position/ μs
0	32	$1.42337*10^{-4}$	0.06	38.31
100	32	$1.65039*10^{-4}$	0.06	38.29
200	32	$1.51174*10^{-4}$	0.06	38.26
300	32	$1.66117*10^{-4}$	0.07	38.26
400	32	$1.49362*10^{-4}$	0.08	38.25
0	34	$2.09827*10^{-4}$	0.05	39.45
100	34	$2.27745*10^{-4}$	0.05	39.43
200	34	$2.25684*10^{-4}$	0.07	39.41
300	34	$1.83101*10^{-4}$	0.07	39.40
400	34	$2.01258*10^{-4}$	0.07	39.39
0	36	$3.17611*10^{-4}$	0.06	40.56
100	36	$3.34026*10^{-4}$	0.05	40.54
200	36	$3.48645*10^{-4}$	0.07	40.52
300	36	$3.11534*10^{-4}$	0.06	40.51
400	36	$2.85967*10^{-4}$	0.07	40.50
0	38	$4.08681*10^{-4}$	0.06	41.64
100	38	$4.39870*10^{-4}$	0.05	41.62
200	38	$4.58787*10^{-4}$	0.05	41.60
300	38	$4.11218*10^{-4}$	0.06	41.60
400	38	$3.87986*10^{-4}$	0.07	41.58
0	40	$5.14006*10^{-4}$	0.06	42.70
100	40	$5.61738*10^{-4}$	0.05	42.67
200	40	$5.53812*10^{-4}$	0.06	42.65
300	40	$5.10998*10^{-4}$	0.07	42.65
400	40	$4.52991*10^{-4}$	0.07	42.64
0	42	$5.63116*10^{-4}$	0.06	43.72
100	42	$6.04627*10^{-4}$	0.06	43.70
200	42	$5.80073*10^{-4}$	0.07	43.68
300	42	$5.33777*10^{-4}$	0.06	43.67
400	42	$4.98389*10^{-4}$	0.08	43.66
0	44	$5.32025*10^{-4}$	0.06	44.72
100	44	$5.74025*10^{-4}$	0.05	44.70
200	44	$5.55283*10^{-4}$	0.07	44.68
300	44	$5.29336*10^{-4}$	0.07	44.68
400	44	$4.85034*10^{-4}$	0.07	44.67
0	46	$4.98155*10^{-4}$	0.07	45.70
100	46	$5.39914*10^{-4}$	0.06	45.68
200	46	$5.40656*10^{-4}$	0.07	45.66
300	46	$4.96495*10^{-4}$	0.07	45.66
400	46	$4.35700*10^{-4}$	0.07	45.65
0	48	$4.31516*10^{-4}$	0.07	46.66
100	48	$4.47498*10^{-4}$	0.07	46.64
200	48	$4.48801*10^{-4}$	0.07	46.62
300	48	$4.08707*10^{-4}$	0.07	46.61
400	48	$3.91414*10^{-4}$	0.08	46.61
0	50	$3.84292*10^{-4}$	0.09	47.61
100	50	$3.78803*10^{-4}$	0.07	47.58
200	50	$3.74816*10^{-4}$	0.09	47.55
300	50	$3.27501*10^{-4}$	0.09	47.56
400	50	$3.25947*10^{-4}$	0.09	47.55
0	52	$3.28731*10^{-4}$	0.11	48.53
100	52	$3.10892*10^{-4}$	0.08	48.51
200	52	$3.53935*10^{-4}$	0.12	48.49
300	52	$2.95685*10^{-4}$	0.10	48.47
400	52	$2.93747*10^{-4}$	0.11	48.47

Table 9 Polymer studied PEG. Dithranol to NaCl ratio 1:1 (*c.f.* figure 6.13)

delay time/ ns	number of PEG units in polymer (n)	peak area	peak width/ μs	peak position/ μs
0	32	$1.77665*10^{-4}$	0.07	38.29
200	32	$1.87889*10^{-4}$	0.08	38.26
400	32	$1.85335*10^{-4}$	0.07	38.23
600	32	$1.66130*10^{-4}$	0.09	38.21
800	32	$1.46886*10^{-4}$	0.09	38.20
1000	32	$1.35622*10^{-4}$	0.06	38.19
0	34	$2.92460*10^{-4}$	0.07	39.43
200	34	$2.76033*10^{-4}$	0.07	39.40
400	34	$3.01105*10^{-4}$	0.07	39.37
600	34	$2.65964*10^{-4}$	0.10	39.36
800	34	$2.27307*10^{-4}$	0.07	39.34
1000	34	$2.19039*10^{-4}$	0.07	39.33
0	36	$3.87524*10^{-4}$	0.06	40.54
200	36	$3.73927*10^{-4}$	0.07	40.51
400	36	$3.70596*10^{-4}$	0.07	40.49
600	36	$3.32042*10^{-4}$	0.08	40.46
800	36	$3.10648*10^{-4}$	0.07	40.45
1000	36	$2.83682*10^{-4}$	0.07	40.44
0	38	$5.15892*10^{-4}$	0.06	41.62
200	38	$4.73431*10^{-4}$	0.07	41.59
400	38	$5.24545*10^{-4}$	0.07	41.57
600	38	$4.48828*10^{-4}$	0.07	41.55
800	38	$4.20189*10^{-4}$	0.07	41.53
1000	38	$4.05089*10^{-4}$	0.07	41.52
0	40	$6.86194*10^{-4}$	0.06	42.68
200	40	$6.23816*10^{-4}$	0.06	42.64
400	40	$6.76351*10^{-4}$	0.07	42.62
600	40	$6.11295*10^{-4}$	0.08	42.60
800	40	$5.42756*10^{-4}$	0.08	42.59
1000	40	$5.27373*10^{-4}$	0.07	42.57
0	42	$7.48030*10^{-4}$	0.07	43.70
200	42	$6.85187*10^{-4}$	0.07	43.67
400	42	$7.53295*10^{-4}$	0.08	43.65
600	42	$6.76752*10^{-4}$	0.08	43.63
800	42	$6.15736*10^{-4}$	0.08	43.61
1000	42	$5.91808*10^{-4}$	0.07	43.60
0	44	$7.88589*10^{-4}$	0.07	44.70
200	44	$7.10503*10^{-4}$	0.07	44.67
400	44	$7.66469*10^{-4}$	0.08	44.65
600	44	$7.35282*10^{-4}$	0.08	44.63
800	44	$6.46722*10^{-4}$	0.08	44.62
1000	44	$6.24422*10^{-4}$	0.08	44.61
0	46	$8.01264*10^{-4}$	0.08	45.68
200	46	$7.32091*10^{-4}$	0.07	45.65
400	46	$8.00221*10^{-4}$	0.09	45.63
600	46	$7.46361*10^{-4}$	0.08	45.61
800	46	$6.79557*10^{-4}$	0.09	45.60
1000	46	$6.41392*10^{-4}$	0.08	45.59
0	48	$6.85816*10^{-4}$	0.08	46.64
200	48	$6.46663*10^{-4}$	0.09	46.60
400	48	$7.29199*10^{-4}$	0.09	46.59
600	48	$6.19104*10^{-4}$	0.09	46.57
800	48	$5.67592*10^{-4}$	0.09	46.56
1000	48	$5.37600*10^{-4}$	0.08	46.55
0	50	$7.03087*10^{-4}$	0.10	47.58
200	50	$6.67829*10^{-4}$	0.10	47.55
400	50	$6.96200*10^{-4}$	0.11	47.53
600	50	$6.06543*10^{-4}$	0.11	47.52

800	50	$5.64207*10^{-4}$	0.12	47.51
1000	50	$5.51714*10^{-4}$	0.09	47.49
0	52	$5.68875*10^{-4}$	0.11	48.50
200	52	$5.22495*10^{-4}$	0.11	48.47
400	52	$5.32904*10^{-4}$	0.14	48.45
600	52	$4.74877*10^{-4}$	0.13	48.44
800	52	$4.33212*10^{-4}$	0.13	48.42
1000	52	$4.18159*10^{-4}$	0.12	48.41

Appendix II

This appendix lists the observed and theoretical masses of the copolymers analysed in Chapter 7.

Table 1 Masses of oligomers detected for Sample 1 *c.f.* figure 7.1

Number of PPG subunits (n)	Name of proposed polymer	Detected mass/ Da	Predicted mass/ Da
4	polymer A	908.2	909.2
5	polymer A	966.1	967.3
6	polymer A	1024.9	1025.4
7	polymer A	1082.6	1083.5
8	polymer A	1140.9	1141.5
9	polymer A	1198.7	1199.6
10	polymer A	1256.9	1257.7
11	polymer A	1315.5	1315.8
12	polymer A	1373.3	1373.9
13	polymer A	1431.2	1431.9
14	polymer A	1489.2	1490.0
15	polymer A	1547.2	1548.1
16	polymer A	1605.1	1606.2
17	polymer A	1664.2	1664.3
18	polymer A	1721.9	1722.3
19	polymer A	1779.4	1780.4
20	polymer A	1837.8	1838.5
21	polymer A	1895.9	1896.6
22	polymer A	1954.9	1954.7
10	polymer B	1498.0	1498.0
11	polymer B	1556.2	1556.1
12	polymer B	1614.3	1614.2
13	polymer B	1671.2	1672.2
14	polymer B	1730.2	1730.3
15	polymer B	1787.8	1788.4
16	polymer B	1846.4	1846.5
17	polymer B	1904.6	1904.6
18	polymer B	1962.5	1962.6
19	polymer B	2020.0	2020.7
20	polymer B	2078.3	2078.8
21	polymer B	2136.0	2136.9
22	polymer B	2194.6	2195.0
23	polymer B	2252.6	2253.0
24	polymer B	2311.4	2311.1
25	polymer B	2369.5	2369.2
26	polymer B	2427.0	2427.3
27	polymer B	2485.1	2485.4
28	polymer B	2541.0	2543.4
5	polymer C	1162.3	1161.6
6	polymer C	1220.6	1219.7
7	polymer C	1279.4	1277.7
8	polymer C	1337.4	1335.8
9	polymer C	1395.6	1394.0

Table 2 Masses of oligomers detected for Sample 2 *c.f.* figure 7.2

Number of PPG subunits (n)	Name of proposed polymer	Detected mass/ Da	Predicted mass/ Da
4	polymer A	908.0	909.2
5	polymer A	966.1	967.3
6	polymer A	1024.9	1025.4
7	polymer A	1082.7	1083.5
8	polymer A	1141.1	1141.5
9	polymer A	1199.0	1199.6
10	polymer A	1257.3	1257.7
11	polymer A	1314.9	1315.8
12	polymer A	1373.8	1373.9
13	polymer A	1431.8	1431.9
14	polymer A	1489.9	1490.0
15	polymer A	1548.0	1548.1
16	polymer A	1606.0	1606.2
17	polymer A	1664.0	1664.3
18	polymer A	1721.8	1722.3
19	polymer A	1780.5	1780.4
20	polymer A	1837.8	1838.5
21	polymer A	1896.0	1896.6
9	polymer B	1439.4	1439.9
10	polymer B	1497.6	1498.0
11	polymer B	1555.9	1556.1
12	polymer B	1614.1	1614.2
13	polymer B	1672.2	1672.2
14	polymer B	1730.1	1730.3
15	polymer B	1789.0	1788.4
16	polymer B	1846.5	1846.5
17	polymer B	1904.8	1904.6
18	polymer B	1962.7	1962.6
19	polymer B	2021.6	2020.7
20	polymer B	2078.7	2078.8
21	polymer B	2136.5	2136.9
22	polymer B	2195.2	2195.0
23	polymer B	2253.3	2253.0
24	polymer B	2312.1	2311.1
25	polymer B	2369.0	2369.2
26	polymer B	2426.5	2427.3
27	polymer B	2486.1	2485.4
28	polymer B	2543.5	2543.4
29	polymer B	2601.7	2601.6
30	polymer B	2660.4	2659.7
5	polymer C	1163.5	1161.6
6	polymer C	1220.9	1219.7
7	polymer C	1279.8	1277.7
8	polymer C	1337.9	1335.8
9	polymer C	1396.2	1394.0

Table 3 Masses of oligomers detected for Sample 3 *c.f.* figure 7.4

Number of PPG subunits (n)	Name of proposed polymer	Detected mass/ Da	Predicted mass/ Da
3	polymer A	850.8	851.1
4	polymer A	909.2	909.2
5	polymer A	966.7	967.3
6	polymer A	1025.1	1025.4
7	polymer A	1083.3	1083.5
8	polymer A	1141.1	1141.5
9	polymer A	1199.3	1199.6
10	polymer A	1257.9	1257.7
11	polymer A	1315.8	1315.8
13	polymer A	1431.2	1431.9
14	polymer A	1490.6	1490.0
15	polymer A	1547.8	1548.1
16	polymer A	1606.1	1606.2
17	polymer A	1664.3	1664.3
18	polymer A	1722.3	1722.3
19	polymer A	1781.3	1780.4
4	polymer D	801.6	802.1
5	polymer D	859.2	860.1
6	polymer D	917.9	918.2
7	polymer D	975.8	976.3
8	polymer D	1034.4	1034.4
9	polymer D	1092.8	1092.5
10	polymer D	1150.8	1150.5
11	polymer D	1208.3	1208.6
12	polymer D	1267.1	1266.7
13	polymer D	1324.2	1324.8
14	polymer D	1382.5	1382.9
15	polymer D	1441.0	1440.9
16	polymer D	1499.5	1499.0
17	polymer D	1556.9	1557.1
18	polymer D	1615.4	1615.2
19	polymer D	1673.7	1673.3
20	polymer D	1730.7	1731.3
21	polymer D	1789.8	1789.4
5	polymer E	752.3	753.0
6	polymer E	810.7	811.1
7	polymer E	868.6	869.2
8	polymer E	926.7	927.2
9	polymer E	984.8	985.3
10	polymer E	1042.8	1043.4
11	polymer E	1100.5	1101.5
12	polymer E	1158.7	1159.6
13	polymer E	1217.3	1217.6
14	polymer E	1275.4	1275.7
15	polymer E	1332.6	1333.8
16	polymer E	1392.2	1391.9
17	polymer E	1449.7	1450.0
18	polymer E	1507.3	1508.0
19	polymer E	1566.0	1566.1
20	polymer E	1623.5	1624.2
21	polymer E	1681.9	1682.3
22	polymer E	1739.1	1740.4
23	polymer E	1797.1	1798.4

Table 4 Masses of oligomers detected for Sample 4 *c.f.* figure 7.5

Number of PPG subunits (n)	Name of proposed polymer	Detected mass/ Da	Predicted mass/ Da
4	polymer A	908.8	909.2
5	polymer A	966.6	967.3
6	polymer A	1025.2	1025.4
7	polymer A	1082.8	1083.5
8	polymer A	1140.9	1141.5
9	polymer A	1199.6	1199.6
10	polymer A	1257.7	1257.7
11	polymer A	1316.2	1315.8
12	polymer A	1373.8	1373.9
13	polymer A	1432.7	1431.9
14	polymer A	1490.6	1490.0
15	polymer A	1548.5	1548.1
16	polymer A	1606.3	1606.2
17	polymer A	1665.2	1664.3
18	polymer A	1722.8	1722.3
19	polymer A	1780.2	1780.4
20	polymer A	1839.7	1838.5
21	polymer A	1897.8	1896.6
4	polymer D	801.7	802.1
5	polymer D	859.4	860.1
6	polymer D	917.4	918.2
7	polymer D	975.5	976.3
8	polymer D	1034.4	1034.4
9	polymer D	1092.2	1092.5
10	polymer D	1150.6	1150.5
11	polymer D	1208.5	1208.6
12	polymer D	1266.9	1266.7
13	polymer D	1324.5	1324.8
14	polymer D	1383.4	1382.9
15	polymer D	1441.3	1440.9
16	polymer D	1499.4	1499.0
17	polymer D	1557.5	1557.1
18	polymer D	1615.5	1615.2
19	polymer D	1673.4	1673.3
20	polymer D	1732.3	1731.3
21	polymer D	1789.9	1789.4
22	polymer D	1848.3	1847.5
23	polymer D	1905.2	1905.6
5	polymer E	752.2	753.0
6	polymer E	810.6	811.1
7	polymer E	868.7	869.2
8	polymer E	927.0	927.2
9	polymer E	984.4	985.3
10	polymer E	1042.7	1043.4
11	polymer E	1100.7	1101.5
12	polymer E	1159.4	1159.6
13	polymer E	1217.5	1217.6
14	polymer E	1275.0	1275.7
15	polymer E	1333.9	1333.8
16	polymer E	1391.9	1391.9
17	polymer E	1450.0	1450.0
18	polymer E	1508.3	1508.0
19	polymer E	1566.5	1566.1
20	polymer E	1623.5	1624.2
21	polymer E	1682.8	1682.3
22	polymer E	1740.7	1740.4
23	polymer E	1798.3	1798.4
24	polymer E	1855.7	1856.5

Table 5 Masses of oligomers detected for Sample 5 *c.f.* figure 7.6

Number of PPG subunits (n)	Name of proposed polymer	Detected mass/ Da	Predicted mass/ Da
5	polymer F	531.2	530.7
6	polymer F	589.2	588.8
7	polymer F	647.2	646.9
8	polymer F	705.5	704.9
9	polymer F	763.2	763.0
10	polymer F	821.5	821.1
11	polymer F	879.3	879.2
12	polymer F	937.3	937.3
13	polymer F	996.3	995.3
14	polymer F	1054.3	1053.4
15	polymer F	1111.9	1111.5
16	polymer F	1170.1	1169.6
17	polymer F	1227.8	1227.7
18	polymer F	1286.8	1285.7
19	polymer F	1345.1	1343.8
3	polymer G	669.3	668.9
4	polymer G	727.9	727.0
5	polymer G	785.6	785.0
6	polymer G	843.9	843.1
7	polymer G	901.6	901.2
8	polymer G	960.4	959.3
9	polymer G	1018.2	1017.4
10	polymer G	1075.8	1075.4
11	polymer G	1135.0	1133.5
12	polymer G	1192.8	1191.6
13	polymer G	1252.0	1249.7
14	polymer G	1309.6	1307.8
15	polymer G	1367.3	1365.8
16	polymer G	1425.2	1423.9
17	polymer G	1483.2	1482.0
18	polymer G	1542.4	1540.1

Table 6 Masses of oligomers detected for Sample 6 *c.f.* figure 7.7

Number of PPG subunits (n)	Name of proposed polymer	Detected mass/ Da	Predicted mass/ Da
5	polymer F	530.6	530.7
6	polymer F	589.2	588.8
7	polymer F	647.2	646.9
8	polymer F	705.5	704.9
9	polymer F	763.2	763.0
10	polymer F	821.5	821.1
11	polymer F	879.3	879.2
12	polymer F	937.3	937.3
13	polymer F	995.4	995.3
14	polymer F	1053.3	1053.4
15	polymer F	1111.9	1111.5
16	polymer F	1170.1	1169.6
17	polymer F	1227.8	1227.7
18	polymer F	1285.8	1285.7
19	polymer F	1344.1	1343.8
20	polymer F	1402.6	1401.9
21	polymer F	1460.1	1460.0
6	polymer G	843.9	843.1
7	polymer G	901.6	901.2
8	polymer G	959.5	959.3
9	polymer G	1018.2	1017.4